Computation of Normally Hyperbolic Invariant Manifolds

Marta Canadell Cano

Computation of Normally Hyperbolic Invariant Manifolds

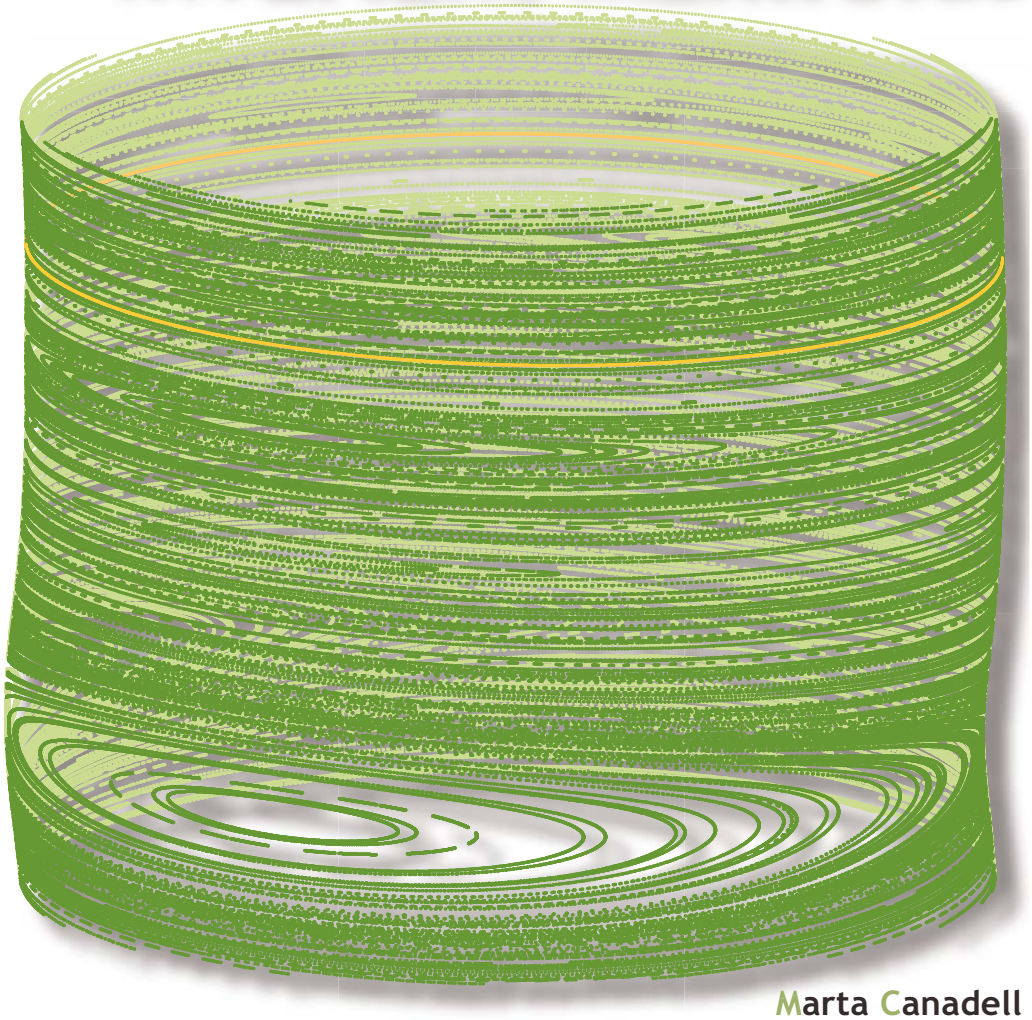

Marta Canadell
Universitat de Barcelona, 2014

Thesis Advisor: Àlex Haro

Computation of Normally Hyperbolic Invariant Manifolds

Marta Canadell Cano

A Thesis submitted
for the degree of Doctor of Mathematics
in the Universitat de Barcelona

Thesis Advisor: **Àlex Haro**

Programa de Doctorat de Matemàtiques.
Departament de Matemàtica aplicada i Anàlisi,
Universitat de Barcelona

Barcelona, Juny 2014

Marta Canadell Cano
Dept. de Matemàtica Aplicada i Anàlisi
Universitat de Barcelona
Gran Via, 585.
08007 Barcelona, Catalonia
<marta@maia.ub.es>

Certifico que la present memòria ha estat
realitzada per Marta Canadell Cano
en el Departament de Matemàtica
Aplicada i Anàlisi sota la meva direcció.
Juny de 2014, Barcelona.

Àlex Haro Provinciale

Al meu pare

Agraïments

Aquesta tesi que aquí presento se'm va presentar fa poc més de quatre anys, quan només era un "projecte de tesi" en el paper d'una FPI ("idees" de l'Àlex) i quan encara deliberava si en finalitzar el màster continuava a la universitat, o m'endinsava en el nou món de l'empresa. Fa exactament 3 anys i 8 mesos, vaig començar el camí cap al càlcul de varietats normalment hiperbòliques, ja que el càlcul de *punts hiperbòlics (tipus sella), però "grossos"*, amb paraules textuals en el primer mail que vaig rebre del que seria el meu futur director de tesi, va ser prou atraient per mi. Així que en primer lloc, vull agrair al meu director de tesi, Àlex Haro, tot el suport, guia i recolzament que m'ha donat durant aquests gairebé quatre anys. La seva paciència, esperant que el meu modest cervellet tragués els nous càlculs, les seves idees lluminoses per ajudar a accelerar-los, la gran il·lusió per la investigació que ha posat en cadascuna de les seves explicacions i el sempre present toc d'humor, han fet d'aquesta tesi una gran experiència. Espero sincerament que molts més futurs estudiants puguin gaudir d'una tesi sota la seva direcció. Gràcies Àlex, m'has fet sentir una *padawan* molt afortunada.

Agrair també tot el suport i calidesa que he rebut dels companys del Departament de Matemàtica Aplicada i Anàlisi, on hi vaig entrar amb més por que confiança i me'n en vaig amb un gran record. Mencionar especialment en Carles, pels seus consells i comentaris sempre interessants i productius, a l'Àngel, que a part de donar-me l'oportunitat de poder assistir a tots els congressos que he anat al llarg d'aquests anys, sempre ha mostrat un gran interès en com anava la meva "ciència", a l'Arturo, que ha passat de ser el meu "profe de càlcul" a ser un dels meus "profes de doctorat" entre cafès, a l'Alejandro, pels seus comentaris i correccions del *mamotreto*, a en Jordi Lluís pels seus primers consells com a germà gran i a l'Elona per fer la meva transició cap al departament de forma tant fàcil i agradable. No deixar-me, per suposat, de nombrar a la Ino, que des l'altre costat de la porta del despatx

i sempre amb un somriure a la boca, ha fet que els sempre desagradables temes burocràtics hagin estat un pèl més dolços. Agrair també al grup de Sistemes Dinàmics UB-UPC tots els coneixements que n'he tret al llarg dels incomptables seminaris i cursos que he assistit, especialment als *UPCs* Tere i Amadeu, que sempre han mostrat un gran interès en el que feia. Mencionar també als membres del DANCE, els quals a través de tots els RTNS, DDAYS i trobades varies m'han transmès tant, especialment al grup de Sevilla que des del primer moment em van acollir com a una més.

Gràcies a l'estada breu a Georgia Tech que em va ser possible realitzar l'any passat (però dir que no pas gràcies a la beca de l'estada breu, la qual em va dur més maldecaps que cap altra cosa) vaig tenir l'oportunitat de treballar durant 5 mesos amb en Rafael de la Llave, una font inacabable d'idees. Gràcies Rafa per tot el temps que em vas dedicar, i que m'has continuat dedicant posteriorment. I gràcies també per la immensa confiança que has dipositat en mi en aquesta nova etapa que començaré l'any que ve, sempre te n'estaré molt agraïda. També haig de mencionar al meu company de despatx durant aquells 5 mesos, en Renato, que tant pels seus consells a nivell científic com per la seva amistat van fer que aquells cinc mesos tant lluny de casa passessin volant i de forma infinitament agradable.

No me'n vull oblidar d'agrair a les meves primeres dues mentores del gremi, les meves professores de matemàtiques de l'institut Maite i Maria Teresa, per la passió que em van transmetre vers les matemàtiques. Elles van ser les que em van guiar cap a aquest camí que encara avui segueixo.

També vull agrair als joves del departament (i no-departament), als *MAIA Snapchateros* Ari, Dani, Narcís, Canela, Marc, Roc, Carlos, Giulia, Tomamaso, Simone, Eloi, Meri, Nadia, Maya, Estefania, totes les estones de "mates", ja sigui al *Simba* o als diferents congressos/cursos/seminaris, i les fantàstiques estones de "no-mates", començant pels *Simbeer* i acabant per les *Simbactivities*, que m'heu donat. Gràcies sobretot per aquest últim any aquí la universitat. Tot i la feinada que suposa un final de tesi, puc assegurar que ha estat el millor en diferència dels quatre, i vosaltres hi heu ajudat molt. Us trobaré a faltar moltíssim a la nova universitat.

Sense allunyar-me del tot de l'entorn matemàtic, agrair a les *nenes de la uni*, Meri, Eva, Laura i Cris, amb qui vaig començar la vida com a matemàtica, i per extensió als *Nyus*, Àlex, Dani, Juan, Rubén, Marta, Manel, Yashin, Marc i Àngela, tots els genials moments de desconnexió, des dels viatges del febrer a les canya-tapa dels dijous, que m'heu ofert tots aquests anys. Especialment a l'Eva, que em va insistir (i molt) en què demanés aquesta beca de doctorat (*total, no hi tens res a perdre*, va dir), a la Meri, amb qui

a part de compartir tots els anys de carrera he pogut compartir quatre anys més les penes i alegries corresponents entre les mateixes quatre parets de la universitat, i a la Cris, per tots els incomptables moments d'hotels de cinc estrelles amb piscina que hem passat juntes.

Allunyant-me ja del tot del món de les matemàtiques vull agrair especialment a les meves *petxines*, Helena, Maria, Collado, Teia, Martina i Laura, a la resta de *ganxons* mascles i femelles, i a també a la Neus, Violeta i Natàlia, haver pogut compartir aquesta experiència amb tots vosaltres al meu costat. La vostra amistat i punts de vista sempre tan diversos m'han acompanyat en tot moment. Heu sigut un pilar clar i estable a la meva vida que ha validat que no tot és la feina, i que sempre hi ha d'haver un equilibri entra aquesta i la resta de coses.

Agrair finalment tot el suport incondicional que he rebut de la meva família. El vostre gran interès i il·lusió que heu mostrat en tot moment cap a mi i cap a la meva feina realitzada m'ha donat una gran fortalesa per a seguir endavant sense defallir. Tot i que sabia que en molts moments no enteníeu res de res del que us explicava, en cap moment m'he sentit desemparada per part vostra. En particular, agrair a la Lourdes, la Laura i la Laia formar part de la meva família i deixar-me formar part de la seva. Sou unes grans companyes de viatge. A l'àvia, per tots els seus savis consells, per escoltar-me sempre i per haver-me criat com si fos una mare. Gràcies a tu he crescut. I especialment al meu pare, per creure sempre en mi, recolzar-me en tot moment i estar sempre al meu costat. Sé que per arribar on he arribat, ha estat en part gràcies a tots els teus esforços que has realitzat.

A tots vosaltres, un cop més, GRÀCIES PER TOT!! :)

Marta.

Barcelona, 4 de Juny de 2014.

Contents

Resum

L'objecte d'estudi dels Sistemes Dinàmics és l'evolució dels sistemes respecte del temps. Per aquesta raó, els Sistemes Dinàmics presenten moltes aplicacions en altres àrees de la Ciència, com ara la Física, Biologia, Economia, etc. i tenen nombroses interaccions amb altres parts de les Matemàtiques.

Els objectes invariants organitzen el comportament global d'un sistema dinàmic, els més simples dels quals són els punts fixos i les òrbites periòdiques (així com les seves corresponents varietats invariants). Les *Varietats Invariants Normalment Hiperbòliques* (NHIM forma abreviada provinent de l'anglès) són alguns d'aquests objectes invariants. Aquests objectes posseeixen la propietat de persistir sota petites pertorbacions del sistema. Les NHIM estan caracteritzades pel fet que les direccions en els punts de la varietat presenten una divisió en components tangent, estable i inestable. L'índex de creixement de les direccions estables (per les quals la iteració endavant del sistema tendeix cap a zero) i inestables (per les quals la iteració enrere del sistema tendeix cap a zero) domina l'índex de creixement de les direccions tangents. La robustesa de les varietats invariants normalment hiperbòliques les fa de gran utilitat a l'hora d'estudiar la dinàmica global. Per aquesta raó, tant la teoria com el càlcul d'aquests objectes sós molt importants per al coneixement general d'un sistema dinàmic.

L'objectiu principal d'aquesta tesi és desenvolupar algoritmes eficients pel càlcul de varietats invariants normalment hiperbòliques, donar-ne resultats teòrics rigorosos i implementar-los per a explorar nous fenòmens matemàtics.

Per simplicitat, considerarem el problema per a sistemes dinàmics discrets, ja que és ben conegut que el cas discret implica el cas continu usant operadors d'evolució. Considerem així difeomorfismes donats per $F : \mathbb{R}^m \to \mathbb{R}^m$ i un d-tor F-invariant parametritzat per $K : \mathbb{T}^d \to \mathbb{R}^m$. És a dir, existeix un

difeomorfisme $f : \mathbb{T}^d \to \mathbb{T}^d$ (la dinàmica interna) tal que satisfà l'equació

$$F \circ K = K \circ f, \tag{0.1}$$

anomenada *equació d'invariància.*

La nostra finalitat és solucionar aquesta equació d'invariància considerant dos possibles escenaris: un en el qual no coneixem quina és la dinàmica interna del tor (on K i f són les nostres incògnites), veure Capítol 4, i un altre en el qual imposem que la dinàmica interna sigui una rotació rígida amb freqüència quasi-periòdica (on K és una incògnita i f és la rotació rígida), pel qual necessitarem, a més a més, afegir un paràmetre ajustador a l'equació (0.1), veure Capítols 2 i 3. En ambdós casos també estarem interessats en el càlcul dels fibrats invariants tangent i normals.

A la literatura, molts dels mètodes per a resoldre l'equació d'invariancia consisteixen en escollir un algun mètode de discretització per a representar funcions i discretitzar l'equació (0.1) en un sistema, que pot ser de grans dimensions, d'equacions no lineals pels coeficients de la representació. Un cop escollit el mètode de discretització, la solució del "large system" està donada per algun mètode iteratiu. Aquest punt de vista el coneixem com a "large matrix method", i depèn fortament del mètode de discretització escollit, sent adient per a un nombre petit de coeficients de la representació, com ara 10^3. Un altra punt de vista està basat en l'anomenada "graph transform", que permet calcular les varietats estable i inestable de l'objecte invariant, i obtenir l'objecte amb la intersecció d'aquestes dues varietats.

L'algoritme que nosaltres usem pel càlcul de varietats invariants normalment hiperbòliques està basat en el conegut *mètode de la parametrització*, en el qual usem algun tipus de reductibilitat (veure Capítol 1). Aquest mètode consisteix en resoldre l'equació d'invariancia (0.1) usant un mètode "tipus-Newton" pel qual fem servir un sistema de coordenades adaptat a la dinàmica i geometria de la varietat invariant, resolent així de forma més eficient cada pas de Newton. Concretament, utilitzem un sistema adaptat definit per les direccions tangents del tor (que vénen donades per la derivada de la parametrització, $\mathrm{D}K$) i les seves direccions normals complementàries. Això ens dóna un sistema adaptat a la descomposició hiperbòlica del fibrat normal invariant. Escrivint l'equació invariant linealitzada

$$\mathrm{D}F \circ K \; \Delta K - \Delta K \circ f - \Delta K \circ f \; \Delta f = -E \tag{0.2}$$

en termes d'aquest sistema adaptat, l'equació es converteix en un sistema triangular a blocs amb el qual evitem resoldre un sistema lineal de grans dimensions en cada pas de Newton. D'aquesta manera, la correcció del tor,

ΔK, es produeix en les direccions normals del sistema adaptat, i la correcció de la dinàmica interna, Δf, es fa en la direcció tangent. Aquest punt de vista geomètric per a representar les funcions condueix a algoritmes eficients i ràpids pel càlcul d'aquests objectes invariants. Repetirem aquest pas de Newton fins que la nova solució tingui un error suficientment petit en funció de la tolerància que hem imposat al mètode.

També considerem el problema de calcular tors invariants normalment hiperbòlics amb dinàmica quasi-periòdica, així com el càlcul dels seus fibrats invariants. En aquest cas, el mètode implica tant tècniques KAM com tècniques NHIM. En particular, treballem amb famílies d-paramètriques de difeomorfismes analítics. El mètode està basat en un esquema KAM per a calcular la parametrització del tor amb freqüència fixada (una freqüència Diofàntica), on hem d'ajustar paràmetres del model per a mantenir fixa la freqüència (les incògnites són en aquest cas la parametrització del tor i aquests nous paràmetres). Aquest és un mètode constructiu que ens permet elaborar un teorema de validació. Hem desenvolupat un teorema tipus-KAM en un format "a posteriori", Teorema 2.21, per a provar l'existència d'aquests tors quasi-periòdics normalment hiperbòlics: si tenim una bona aproximació inicial d'un tor quasi-periòdic amb una freqüència Diofàntica fixada, aleshores, sota certes condicions de hiperbolicitat, no-degeneració i no-ressonància, existeix un tor invariant vertader proper a l'inicial per a un cert valor del paràmetre. Emfatitzem que els tors quasi-periòdics obtinguts pel nostre teorema són analítics, en contrast amb els què s'obtenen amb la teoria general de varietats normalment hiperbòliques.

Ja hem implementat ambdós algoritmes per tors de dimensió 1 (és a dir, cercles invariants) en sistemes dinàmics discrets de dimensió 2 i 3, i en el cas de l'algoritme general, elaborat per a tors amb dinàmica desconeguda, també pel càlcul d'un cilindre normalment invariant en un sistema dinàmic discret de dimensió 4. Tots aquests algoritmes han estat implementats per a la continuació respecte paràmetres de tors (i cilindres) invariants. En el cas de la continuació de tors quasi-periòdic s'ha fet la continuació per un tor amb freqüència fixada, mentre que en el cas general s'ha realitzat independentment de la dinàmica interna del tor, permetent-nos així creuar ressonàncies. Els nostres objectes invariants, ja siguin els tors (o cilindre) o els fibrats, vénen donats per funcions periòdiques. En aquesta tesi hem utilitzat mètodes d'interpolació Lagrangiana (a trossos) i sèries de Fourier per a aproximar aquestes funcions. Hem observat que, donat l'elevat nombre de càlculs necessaris per a la composició de dues funcions periòdiques, pel cas en què tenim el tor amb dinàmica desconeguda (on hem de composar repetidament dues funcions periòdiques) és molt millor prendre una aproximació usant interpo-

lació, i per tant produir tots els càlculs sobre un mallat de punts. D'altra banda, l'aproximació amb sèries de Fourier s'adapten perfectament als casos amb dinàmica quasi-periòdica, i són extremadament eficients quan es combinen amb mètodes de "Fast Fourier Transform".

Els mètodes d'aquesta tesi són de gran utilitat per a l'estudi de propietats dinàmiques dels sistemes dinàmics. Per exemple, atès que un tor normalment hiperbòlic és robust sota petites pertorbacions, un dels nostres interessos ha estat estudiar-ne la seva persistència sota pertorbacions i investigar-ne els diferents tipus de trencaments, és a dir, investigar com es perd la hiperbolicitat normal de l'objecte. Hem vist diferents escenaris de trencament:

- Per a tors quasi-periòdics normalment hiperbòlics, el trencament és degut a col·lisions no uniformes entre els fibrats, mentre que els multiplicadors de Lyapunov es mantenen separats els uns dels altres en el moment de la col·lisió. La pèrdua de la hiperbolicitat és deguda a la complicada geometria dels fibrats, la qual esdevé molt complexa a causa de la col·lisió "no-suau" dels fibrats. Hi ha molts contextos en els quals es produeixen aquestes col·lisions "no-suaus", referides sovint com a *bundle merging scenario*. En aquesta tesi, hem descrit exemples en els quals el fibrat tangent i el fibrat normal col·lisionen, moment en què es perd la hiperbolicitat normal i el tor es trenca. En particular, en una aplicació que preserva volum i que a més a més presenta certes simetries, com ara reversibilitat, hi hem observat un trencament degut a una triple col·lisió de fibrats entre el fibrat estable, inestable i tangent.
- Per a tors normalment hiperbòlics amb dinàmica desconeguda, hem observat alguns mecanismes globals de trencament de tors deguts a tangències entre la foliació estable i el tor invariant.

Resumint, hem desenvolupat diverses eines per al càlcul i la validació de tors invariants normalment hiperbòlics per a sistemes dinàmics discrets i les hem portat al límit de la seva validesa.

- En el **Capítol 2**, hem elaborat un teorema tipus-KAM en un format "a-posteriori" per a l'existència de tors quasi-periòdics normalment invariants en famílies de sistemes dinàmics discrets, Teorema 2.21, el qual és nou en aquest context (teoremes tipus-KAM en formats pertorbatius són àmpliament coneguts a la literatura). Aquest teorema ens dóna un suport rigorós per l'elaboració d'algoritmes numèrics de càlcul de tors invariants quasi-periòdics. Aquests algoritmes numèrics estan desenvolupats en el Capítol 3.

- En el **Capítol 3** hem considerat diversos mètodes per al càlcul de tors quasi-periòdics. El primer mètode està adaptat a tors completament reductibles, és a dir, a tors en els quals la dinàmica linealitzada pot ser reduïda a coeficients constants i diagonals (veure Subsecció 3.2.3). El segon mètode és adient per a tors reductibles (però no completament reductibles), és a dir, per a tors en els quals la dinàmica linealitzada pot ser reduïda a coeficients constants (veure Subsecció 3.2.2). Finalment, considerem un tercer mètode general en el qual no demanem cap condició de reductibilitat al tor (veure Subsecció 3.2.1). De cara a provar la generalitat dels nostres algoritmes, els hem implementat per al càlcul de tors (reductibles) tipus sella, tors reductibles atractors (tors "node" i tors "focus") i tors atractors no reductibles. Les implementacions d'aquests algoritmes, veure Subseccions 3.4, 3.5, 3.6, 3.7 i 3.8, milloren en gran mesura els resultats donats en treballs anteriors, aprofitant el fet que esquiven la immensa quantitat de càlculs necessaris per resoldre un mètode tipus "large matrix" i que eviten també un punt de vista pertorbatiu, la qual cosa ens permet apropar-nos molt al trencament de l'objecte. Part d'aquests resultats apareixen a [19].

- En el **Capítol 4**, hem desenvolupat un mètode per al càlcul de varietats invariants normalment hiperbòliques i la seva dinàmica interna. Hem implementat aquest mètode per al càlcul de tors atractors i tors tipus sella en exemples ja tractats a la literatura. En particular, ens permeten obtenir resultats més acurats i apropar-nos molt més als paràmetres crítics de trencament. Això ens ha permès refutar algun dels mecanismes de trencament proposats a la literatura, i donar soport a d'altres. A més a més, hem implementat el mètode per al càlcul d'un cilindre invariant normalment hiperbòlic en una aplicació 4-dimensional. Aquest és el primer cop que un objecte d'aquest tipus es calcula, i ens obre una nova línia d'investigació futura dirigida, per exemple, a estudiar la difusió d'Arnold. El contingut d'aquest capítol de la tesi apareix en el capítol 5 de la monografia [53].

Abstract

The subject of the theory of Dynamical Systems is the evolution of systems with respect to time. Hence, it has many applications to other areas of science, such as Physics, Biology, Economics, etc. and it also has interactions with other parts of Mathematics.

The global behavior of a dynamical system is organized by its invariant objects, the simplest ones are equilibria and periodic orbits (and related invariant manifolds). *Normally hyperbolic invariant manifolds* (NHIM for short) are some of these invariant objects. They have the property to persist under small perturbations of the system. These NHIM are characterized by the fact that the directions on the points of the manifold split into stable, unstable and tangent components. The growth rate of stable directions (for which forward evolution of the system goes to zero) and unstable directions (for which backward evolution goes to zero) dominate the growth rate of the tangent directions. The robustness of normally hyperbolic invariant manifolds makes them very useful to understand the global dynamics. Both the theory and the computation of these objects are important for the general understanding of a dynamical system.

The main goal of my thesis is to develop efficient algorithms for the computation of normally hyperbolic invariant manifolds, give a rigorous mathematical theory and implement them to explore new mathematical phenomena.

For simplicity, we consider the problem for discrete dynamical systems, since it is known that the discrete case implies the continuous case using time one flow. We consider a diffeomorphism $F : \mathbb{R}^m \to \mathbb{R}^m$ and a d-torus parameterized by $K : \mathbb{T}^d \to \mathbb{R}^m$ which is invariant under F. This means that there exists a diffeomorphism $f : \mathbb{T}^d \to \mathbb{T}^d$ (the internal dynamics) such that it satisfies

$$F \circ K = K \circ f, \tag{0.3}$$

called the *invariance equation*.

Our goal is to solve this invariance equation considering two different scenarios: one in which we do not know the internal dynamics of the invariant torus (where K and f are our unknowns), see Chapter 4, and the other in which we impose that the internal dynamics is a rigid rotation with a quasi-periodic frequency (where K is the unknown and f is the rigid rotation), for which we also need to add an adjusting parameter to equation (0.3), see Chapters 2 and 3. Additionally, in both cases we are also interested in computing the invariant tangent and normal bundles.

In the literature, many of the algorithms to solve the invariance equation consist in choosing some method of representation of functions and discretizing (0.3) into a "large system" of non-linear equations for the coefficients of the representation. The solution of such a system is done by some iterative method. This approach, referred to as *large matrix method*, is very dependent of the discretization method, and only suitable when the number of coefficients of the representation is small, say 10^3. Another family of methods are settled in the graph transform method, and compute the invariant manifolds as the intersection of its stable and unstable manifolds.

The algorithm we use to compute normally hyperbolic invariant tori is based on the so called *parameterization method* in which we use some sort of reducibility of the linearized dynamics to a simpler form (see Chapter 1). It consists in solving functional equation (0.3) using a Newton-like method but we choose an appropriate frame adapted to the dynamics and the geometry of the invariant manifold in order to efficiently solve each Newton step. Namely, we use an adapted frame defined by the tangent directions (given by the derivative of the parameterization, $\mathrm{D}K$) and the complementary normal directions to the torus. This gives us a global frame for the hyperbolic splitting of the invariant normal bundle. Writing the linearized invariance equation

$$\mathrm{D}F \circ K \; \Delta K - \Delta K \circ f - \Delta K \circ f \; \Delta f = -E \tag{0.4}$$

in terms of this frame, it is converted to a block triangular system which avoids solving a large linear system at each Newton step. That is, the correction of the torus, ΔK, is made in the normal directions of the adapted frame and the correction of the dynamics, Δf, is made in the tangent direction. Hence, this geometrical point of view to represent the functions leads to efficient and really fast algorithms to compute these invariant objects. We repeated the Newton step until the new solution has a small enough error for the tolerance we imposed to the method. We have implemented this method in several contexts and applied the algorithm to situations in which

the number of coefficients of the objects is around 10^6.

We also consider the problem of computing quasi-periodic normally hyperbolic invariant tori, as well as their invariant bundles. In this case, the problem involves tools of KAM theory together with NHIM theory. In particular, we work with a d-parameter family of diffeomorphisms. The method is based on a KAM scheme to compute the parameterization of the torus with a fixed frequency fixed (a Diophantine frequency), where we have to adjust parameters of the model to keep the desired frequency (the unknowns are the torus K and these parameters). This is a constructive method which allows us to formulate a validation theorem. We develop a KAM-like theorem in "a posteriori" format, Theorem 2.21, to prove the existence of this quasi-periodic normally hyperbolic invariant torus: if we have a good enough approximation of an invariant torus with a fixed Diophantine frequency, then, under certain hyperbolicity, non-degeneracy and non-resonance conditions, there exists a true invariant torus near the computed one for a particular vale of the parameter. We emphasize that, quasi-periodic tori we obtain through our theorem are analytic, in contrast with the ones obtained through the general theory of normally hyperbolic invariant manifolds.

We have already implemented both algorithms for one dimensional tori (which are normally hyperbolic invariant circles) in 2 and 3 dimensional discrete dynamical systems. We also implemented the general algorithm for a normally hyperbolic invariant cylinder in a 4 dimensional discrete dynamical system. We implement the algorithms for the continuations of invariant tori (and cylinder) with respect to parameters. In the quasi-periodic case we do the continuation for tori with a fixed frequency, whereas in the general case we do the continuation regardless its dynamics. Hence, the general method is able to cross resonances in the internal dynamics. Our invariant objects, tori (and cylinder) and bundles, are given by periodic functions. We have used both piecewise Lagrangian interpolation and Fourier series to discretize periodic functions. We observe that due to the large number of operations needed for the composition of two periodic functions, for the case where the dynamics is an unknown (where we need to compose two periodic functions several times) it is better to use interpolation, thus make all the computations using grids. On the other hand, Fourier methods are tailored to the case of quasi-periodic motion, and are highly efficient when combined with Fast Fourier Transform methods.

So far the methods of this thesis are useful to study dynamical properties of dynamical systems. For instance, since normally hyperbolic invariant manifolds are robust under small perturbations, one of our interests is to

see how tori persist under perturbations and investigate their mechanisms of breakdown, that is, investigate how normal hyperbolicity is lost. We have seen different scenarios of breakdown:

- For quasi-periodic NHIT the breakdown is often due to a bundle collision between bundles of different stability type. An interesting thing about this collision is that Lyapunov multipliers are away from each other at the moment of the collision, and the loss of the hyperbolicity is only because the geometry of the bundles gets more complicated since the bundles collide non-smoothly. There are several contexts in which bundles collide non-smoothly, referred to as *bundle merging scenarios*. In this thesis we describe examples in which the tangent bundle collides with the stable bundle, and at this moment the torus loses its normal hyperbolicity, and it is broken. In a volume preserving case with some extra symmetries on the system (namely reversibility), we observed a breakdown due to a triple collision between the stable, unstable and tangent bundles.
- For a NHIT with unknown internal dynamics, we have observed some global mechanisms of destruction of invariant curves produced by tangencies between the stable foliation and the invariant curve.

Summarizing, we develop several general tools to compute and validate normally hyperbolic invariant manifolds for discrete dynamical systems.

- In **Chapter 2**, we elaborate a KAM-like theorem in "a-posteriori" format for the existence of quasi-periodic normally hyperbolic tori in families of dynamical systems, Theorem 2.21, which is new in this context (KAM-like theorems in a-perturbative format are well-known in the literature). This theorem give us a rigorous support for numerical algorithms of continuation of quasi-periodic tori. These numerical algorithms are widely developed in Chapter 3.
- In **Chapter 3**, we consider several methods for computing quasi-periodic tori. The first method is tailored for completely reducible tori, that is, tori for which the linearized dynamics can be reduced to diagonal constant coefficients (see Subsection 3.2.3). The second one is appropriate for reducible (but not completely) tori, that is tori for which the linearized dynamics can be reduced to constant coefficients (see Subsection 3.2.2). Finally, the third method is a general one in which we do not impose any reducibility on the tori (see Subsection 3.2.1). In their implementations, we compute (reducible) saddle

tori, reducible attractors (node tori and focus tori) and non-reducible attractors, in order to test the generality of our algorithms. Implementations of these algorithms, see Sections 3.4, 3.5, 3.6, 3.7 and 3.8, largely improve the results given in previous works, by taking advantage of the avoidance of the massive number of computations needed to solve in a large system method and the avoidance of a perturbative setting, which allows us to get closer to the breakdown. Part of these results appear in [19].

- In **Chapter 4**, we develop a new method to compute normally hyperbolic invariant tori as well as its internal dynamics. We implement it to compute attracting and saddle tori for examples already treated in the literature, for which we improve the results. Furthermore, we also implement it to compute a two dimensional normally hyperbolic invariant cylinder and its internal dynamics in a 4 dimensional map. This is the first time this object is computed, and opens a line of further research, for instance in Arnold diffusion. The contents of this chapter appears in Chapter 5 of the monograph [53].

Chapter 1

Introduction

The long-term behavior of a dynamical system is organized by its invariant objects. Hence, it is important to understand which invariant objects persist under perturbations of the system. It has been known for a long time that the persistence of an invariant object is related to its hyperbolicity properties. Roughly speaking, an invariant manifold is normally hyperbolic if the growth rate of vectors transverse to the manifold dominates the growth rate of vectors tangent to the manifold. The celebrated theorems of Fenichel [43] and Hirsch, Pugh and Shub [63] state that a compact invariant manifold persists under all C^1 small changes in the map if it is normally hyperbolic [43, 63]. The fact that this condition is also necessary for C^1 persistence was proved by Mañé [79]. The monograph [91] revisits the main results of the theory of normally hyperbolic invariant manifolds. References [6, 41] deal with non-compact normally hyperbolic manifolds in Banach manifolds.

The previous mentioned results on persistence of normally hyperbolic invariant manifolds were proved by using the graph transform method of Hadamard and, notably, lead to numerical algorithms for computing and continuing with respect to parameters the invariant manifolds regardless of the internal dynamics [11, 8, 37, 93]. As far as we now, [11] is the first reference about computation of normally hyperbolic invariant manifolds of saddle type (in particular, invariant circles), i.e. manifolds for which the normal dynamics exhibits both contraction and expansion. A drawback of the graph transform method is that the derived algorithm computes the stable and the unstable manifolds, and then the invariant manifold is computed by intersecting them. Hence, if one is interested only on the normally hyperbolic invariant manifold, one has to deal with higher dimensional objects. Of course, if one wants to compute also the stable/unstable manifolds, this is not a drawback.

Another important problem in dynamical systems is the persistence of quasi-periodic motion. This problem involve the management of the distinguished KAM Theory. First references to dive into the problem, treated from the classical Hamiltonian point of view, deal with a perturbative setting in the sense that the problem is written as a perturbation of an "integrable" map by using action-angle variables providing from the unperturbed system. This appears in the groundbreaking work of A.N. Kolmogorov, V.I. Arnold and J.K. Moser [4, 5, 75, 86, 88, 87]. Later on, the problem has been treated in a general case, referred as *dissipative context*, where it appears the usage of extra parameters to proof the existence of quasi-periodic tori, also in a perturbative sense [7, 9, 89]. Beside of that, most of the references to the numerical computation of quasi-periodic invariant tori deals with the necessity to solve a large system without using a perturbative methodology [23, 97, 90], or by using a parameterization method to rewrite the system to solve by taking advantage of its dynamics and geometrical properties [52, 57, 16, 47].

In this thesis, we present several Newton-like methods for solving the invariance equations arising from a parameterization method formulated in [54] for computing normally hyperbolic invariant manifolds. We focus on normally hyperbolic invariant manifolds modeled by the standard torus, to which we will refer to as normally hyperbolic invariant tori (NHIT for short), whereas also a normally hyperbolic invariant cylinder (NHIC for short) has been computed. These invariant manifolds has been computed both in the case in which their internal dynamics is an unknown of our computations, or it is fixed, as a rigid rotation, and there is the necessity to add adjusting parameters.

1.1 On the numerical computation of normally hyperbolic invariant manifolds

As we mention at the beginning of this chapter, even though the main theoretical results on normally hyperbolic invariant manifolds appeared in the seventies [43, 63, 79], the first numerical methods for computing these objects were not presented until the eighties. Most of these incipient methods dealt with attracting invariant circles [2, 102], and computing either higher dimensional invariant tori or "truly" hyperbolic invariant tori (i.e. with stable and unstable manifolds) were considered a challenging problem. Since then, a large variety of methods have been designed and implemented to deal with such a problem.

Most often in the literature the invariant manifold is represented as a graph of a function over a set of variables, and one considers an equation for such function expressing that its graph is invariant. In the case of invariant tori, the function is periodic. For discrete dynamical systems, described by diffeomorphisms, the invariance equation is a functional equation, and for continuous dynamical systems, described by vector fields, the invariance equation is formulated as a (multidimensional) quasi-linear first order partial differential equation. For this reason, these strategies are usually referred to as the Functional Equation (FE) approach and the Partial Differential Equation (PDE) approach, respectively. The ways these equations are numerically solved give rise to many different methods.

The most straightforward way of solving the invariance equations essentially consist in choosing a method of representation of functions and then discretizing the invariance equation into a large system of nonlinear equations for the coefficients of the representation. We refer to these methods as *large matrix methods*, as in [57]. The solution of such a system is usually made by using a Newton method. The way the linear system is solved at each step of Newton method, taking advantage of its structure and (possible) sparseness, adds another characteristic to a large system method.

In this circle of ideas, the Functional Equation (FE) approach was implemented in [2] to compute invariant circles using grid interpolation methods. See also [77] and [64] for methods to solve the corresponding linearized equations, either using grid interpolation methods or Fourier methods, respectively. The PDE approach to compute invariant tori for flows was introduced in [38]. This method consists in solving numerically a partial differential equation subject to periodic boundary conditions, since the unknown is a periodic function. For instance, finite-difference and orthogonal collocation methods for PDE are derived from grid polynomial interpolation of periodic functions [35, 36, 38, 40], and spectral methods for PDE are derived from Fourier approximations of periodic functions [50, 101]. A modification of the PDE approach is considered in [85, 92], in which the invariant torus is considered as a graph in a tubular neighborhood of a given reference torus embedded in phase space (considering a normal bundle to the torus). Again, the discretized PDE gives rise to a large system of nonlinear equations that is solved using a Newton method. Once more, different strategies for solving the linear systems arising from the Newton method are applied, depending on the structure of the matrices. Even if these methods are intended to compute normally hyperbolic invariant tori, all the examples considered in these references are attracting tori. We do not claim that the list of methods given above is complete. A plethora of large system methods can be generated by

changing the method of representation, the way the discretized invariance equation is solved or the method used to solve the linearized equation arising from Newton method. Large system methods have also been profusely applied in computation of invariant tori with quasi-periodic dynamics, using Fourier discretizations [23, 39, 69, 82, 83, 98]. In these examples, the linearized equations possess full (i.e. non-sparse) matrices. So far in all the previous references only invariant tori (of dimensions 1 or 2) has been considered in the examples. More recently, [62] describes a large system method to compute normally hyperbolic invariant manifolds for flows via flow box tilings, based on the "fat trajectories" introduced in [61]. The algorithm is not limited to a particular dimension or topology, and [62] illustrates an example of a 2D torus in a 4D space and an attracting 2D sphere in a 3D space. But one has to keep in mind that large matrix methods suffer from the curse of dimensionality.

Another strategy for computing invariant manifolds is using the graph transform. While the large system methods mentioned above are, say, "purely numerical", the *graph transform methods* are more geometrical, and can be regarded as implementations of proofs of theorems of existence of normally hyperbolic invariant manifolds (see [43, 63] for the theoretical results). The graph transform computes both the stable and the unstable manifolds of the normally hyperbolic invariant manifold, using contractions in appropriate spaces, and then the invariant manifold is the result of their intersection. A primitive version of an algorithm based on the graph transform appeared in [102], in which simple iteration is used to compute an attracting invariant curve, using a FE discretization. Later on, [37, 93] implemented methods based on discretizations of the graph transform for computing attracting invariant tori for flows, that is, in the PDE approach. To the best of our knowledge, the first examples of computation of saddle-type invariant circles appeared in [11] (see also [8]). These were made by using implementations of the graph transform by adapting coordinates for computing the stable and unstable manifolds, and then using a separate algorithm for intersecting them.

Due to the robustness of normally hyperbolic invariant manifolds, all these methods allow us to continue an invariant torus with respect to parameters, regardless of its dynamics. For instance, the methods allow us to continue an invariant circle through resonance tongues in which the internal dynamics on the circle possesses periodic orbits, and cross non-resonant hairs in which the internal dynamics have irrational rotation numbers. This was already a main motivation for developing numerical algorithms to calculate invariant circles in the pioneering paper [2]. We emphasize that the internal dynamics on an

invariant torus is implicitly derived from these methods, but in the above mentioned references, the explicit computation of the internal dynamics is not carried out.

We can design specific methods according to the properties of the internal dynamics on the invariant manifold. For example, we can compute a resonant invariant circle simply by computing the invariant manifolds of the internal periodic orbits (see e.g. [12], and Figure 4.6 in Section 4.4), although this can be a difficult task if the periodic orbits have a very high period. In addition, we can design a specific method to compute non-resonant invariant circles, computing a parameterization of the invariant circle in which the internal dynamics is an irrational rotation. The unknowns are both the parameterization and the rotation. Such a parameterization method was already implemented in [24] for the discrete case and using Fourier methods and, much more recently, in [97, 98] for the case of flows, using grid methods and Fourier methods, respectively. Notice however that, in a continuation setting, these methods fail to converge when crossing "strong" resonances, but are able to cross weak resonances. A suitable way of avoiding that problem is fixing the irrational rotation and adjusting parameters of the system which enter now in the equations as unknowns [90]. A proper justification of this strategy, using a parameterization method and adjusting parameters, enters into the realm of KAM theory [9, 19, 31, 89], and leads to reducibility methods that avoid solving large linear systems (see Chapters 3 and 2 of this thesis).

The object of Chapter 4 is to design general purpose *parameterization methods* for computing normally hyperbolic invariant tori for diffeomorphisms, avoiding the restrictions mentioned in the previous paragraph. A similar methodology can be developed for the case of flows, or one can use an appropriate Poincaré map for leading to the FE approach and reduce the dimension of the tori and the phase space by one. The algorithms in Chapter 4 are intended to compute the invariant torus and its internal dynamics using a Newton-like method, as well as the stable and the unstable bundles. In principle, one can use *any* method of approximation for the periodic functions describing the tori without changing the framework, in contrast with the purely numerical methods that dramatically depend on such choice, e.g. as happens in large matrix methods. For example, we have tested local interpolation methods in grids and Fourier methods, but other methods can also be easily implemented (e.g., spline interpolation methods) preserving most of the codes. We should emphasize that the choice of the method of approximation for the periodic functions is at the lower level of the method, in such a way that can be easily changed according to our goal. In a continuation

setting, we can monitor some dynamical observables, such as Lyapunov multipliers (the growth rates of the linearized dynamics) and the minimum angle between the tangent, stable and unstable bundles, in order to measure the quality of the normal hyperbolicity. In continuing invariant circles, we can compute the rotation number of the internal dynamics, in order to detect resonance crossings. We illustrate the application of the parameterization method for the computation of normally hyperbolic invariant circles, and in particular to the examples in [8, 11, 12]. We do not consider here the computation of the stable and the unstable manifolds, but we mention that the parameterization method in [13, 14, 15] is also appropriate to accomplish this task (see [57, 58, 59] for rigorous, algorithmic and numerical results on the parameterization method for invariant tori and their whiskers in quasi-periodic maps). Besides that, we compute the linearized foliations of the torus, which are given by the stable and unstable bundles. The last example of Chapter 4, see section 4.6, illustrates the algorithms in the challenging problem of computing a 2 dimensional object for a higher dimensional map; the object is a normally hyperbolic invariant cylinder and the map is a 4 dimensional symplectic map. Normally hyperbolic invariant cylinders are very important in recent rigorous studies of Arnold diffusion [32, 33]. We think of this example as a first step to apply these techniques to Arnold diffusion.

Finally, we mention that the possibility of implementing computer assisted proofs of existence of invariant objects is also a feature of the parameterization method. The theorems in [54] on the parameterization method for normally hyperbolic invariant manifolds are intended to validate the numerical computations. Notice however that validating an invariant object is independent of the specific discretization method to compute the invariant object, so these validation theorems could validate the numerical computations performed in this thesis. Other validation theorems can be found in [20, 21, 22], based on a topological approach, using cone conditions and covering relations.

1.2 On the computation of quasi-periodic normally hyperbolic invariant tori

In the previous section we have introduced the significance of normally hyperbolic invariant manifolds. Here, we are focused on normally hyperbolic invariant manifolds with a specific internal dynamics: normally hyperbolic invariant tori with internal dynamics conjugated to a (Diophantine) rotation. The study of these objects involve *KAM techniques*, which appears firstly in

the celebrated *KAM theory*, named after its founders A.N. Kolmogorov [75], V.I. Arnold [4, 5], and J.K. Moser [86, 88, 87]), which originally dealt with persistence of quasi-periodic motion in Hamiltonian systems.

It is well known that classical KAM theory deals with the effect of small perturbations in integrable Hamiltonian dynamical systems, and it is remarkable that these systems allow invariant tori carrying quasi-periodic motion. The importance of these quasi-periodic invariant tori deals with the fact that, under sufficiently small perturbations on the system, KAM theory state that "most" of the previous invariant tori will persist, even though they can be slightly deformed. We have to recall that in these perturbation analysis of quasi-periodic tori, we have a torus with a prescribed frequency and we *follow* it through the perturbation. Nowadays, KAM techniques have expanded their range and are applied in many contexts. We think of KAM theory as the study of persistence of quasi-periodic motion in (families of) dynamical systems. Otherwise, we think of "a-posteriori" KAM theory as the study of the existence of quasi-periodic motion in (families of) dynamical systems.

In the literature, this problem has been treated from many points of view.

From the theoretical point of view, classical (Hamiltonian) KAM methods for studying persistence of quasi-periodic objects, with a prescribed fixed frequency are based on the use of canonical changes of coordinates to simplify the expression of the map. These methods typically deal with a perturbative setting in the sense that the problem is written as a perturbation of an "integrable" map (in which "everything" is known) and then it take advantage of the existence of action-angle-like coordinates for the unperturbed problem. In this classical Hamiltonian context, the fixed frequency vector of the torus can be treated as the parameters of the system and explained by these action-angle variables. On the other hand, in the context of general systems where no structure at all is present, also referred as a "dissipative context", we find attracting quasi-periodic tori which are isolated in the phase space. With the goal of studying the persistence of quasi-periodic solutions in families of dynamical systems (preserving or not some kind of geometric structure), hence without action angle variables, the necessity of explicit external parameters to adjust the frequencies is considered in order to prove the existence of quasi-periodic orbits. This first work with external parameters appears in the work of Moser [89], where the "counterterms" are introduced as the use of extra parameters in the system to proof the existence of a quasi-periodic torus, with the same frequency vector that the unperturbed one. Later on, the work with extra parameters has been performed in [9], where they consider, in particular, the reducible case, referred by them as

"Floquet torus". However, these results have a perturbative nature and are hardly applicable in numerical computations far from perturbative regime, in the meaning that, even that in some cases it is possible to identify an integrable approximation of a given system, the remaining part cannot be considered as an arbitrarily small, so a perturbative argument is difficult to implement.

From the numerical point of view, there are many references that consider the numerical computation of quasi-periodic invariant tori. As we argue in the previous paragraph, handling a perturbative argument leads to difficult algorithms to compute quasi-periodic tori. Certainly, the more usual numerical methods for computing invariant tori with quasi periodic dynamics are based on solving a large system of non-linear equations arising from a Fourier discretization of the invariance equation, referred, as in previous section 1.1, *large matrix method*. This big system is usually solved by using a Newton Method, see e.g. [23, 39, 68, 69, 82, 83, 98] for several examples. Reference [97] uses continuation methods without adjusting parameters but having the frequency as an unknown, but the method fails when it crosses strong resonances. On the other side, [90] adjusts parameters, but the use of a large matrix method runs into troubles when approaching breakdown because of the colossal computation time and the memory needed to store the large matrices arising from the straightforward application of a Newton method.

To avoid the massive number of computations needed to solve the large system and to avoid a perturbative setting, we use a parameterization method (also explained in previous section 1.1 for a normally hyperbolic invariant tori with general dynamics) for a quasi-periodic motion adapted to a KAM setting. In this particular case, the parameterization method in KAM theory avoids the use of transformations by adding a small function to the previous approximation of the torus and an adjusting parameter. This added function is obtained by approximately solving the linearized equation around the approximated torus, which leads to a Newton-like iterative method to solve the invariance equation. Such kind of approach, which takes advantage of the geometry of the problem, also referred to as KAM theory without action-angle variables in a Hamiltonian context, was first suggested in [29], and a complete proof for the existence of quasi-periodic invariant tori without using neither action-angle variables nor a perturbative setting was presented in [30]. Using this methodology in our dissipative case and adding parameters as in [9, 89], we are able to prove the convergence of the algorithms which deals to a validation theorem in an a posteriori format. We show that if there is an approximate solution of the invariance equation that satisfies some non-

degeneracy conditions, then there is a true solution nearby. The proofs of the existence of quasi-periodic solutions in this context consists of the following steps: start from an approximate solution of a suitable invariance equation, apply a Newton's method to get a better approximate solution, provide estimates for the norms of the different objects and quantities involved, show that the process can be iterated and finally that it converges. There are other several works following this strategy, for instance for non-twist tori [52], for skew-products with frequency given by an external forcing [57, 58, 59] (there are also computer assisted proofs in [45, 44]), for whiskered tori in symplectic maps [66], for the computation of limit cycles and their isochrons [65], or for attracting tori in conformally symplectic systems [16]. Notice that to solve the invariance equation with the prescribed fixed frequency (in particular [16]) it considers families depending on some extra parameters, where the idea goes back to [9, 89].

In this thesis, we also consider the need of external parameters to keep the frequency fixed, as in [9, 16, 89]. From the theoretical point of view, we present a KAM-like Theorem (Theorem 2.21) based on the parameterization method for quasi-periodic normally hyperbolic invariant tori for smooth families of real analytic maps (see Chapter 2). The convergence of the algorithm enters in the realm of KAM theory, and the proof of the result is constructive and leads to an efficient numerical method to compute quasi-periodic invariant tori (see Chapter 3). In addition, the hypotheses of the Theorem 2.21 depend explicitly on the different objects involved and it is not required to perform transformations nor normal forms. Thus we can obtain a suitable scheme to perform computer assisted proofs in particular problems. We plan to come back to computer assisted proofs in a near future. On the other hand, we emphasize that Theorem 2.21 leads us to efficient algorithms to compute invariant tori and their adjusting parameters. Therefore, from the numerical point of view, we consider the problem of numerically computing normally hyperbolic invariant tori with a fixed rotation of Diophantine frequency as well as its invariant bundles, which are the stable and unstable (linearized) foliations, where we needed to adjust parameters to keep the frequency fixed (see Chapter 3). In particular, we will explain different efficient algorithms, ones based on the reducibility of the normal dynamics, and so leading to very efficient and fast algorithms to compute the torus, and another for a general non-reducible case, in which we only need conditions of hyperbolicity on the system. For that reason, our algorithms allows us to obtain accurate results up to parameter values even very close to the torus breakdown, where we can use computations with even 10^6 terms to approximate the objects. We should mention that our

implementations for quasi-periodic tori are done for one dimensional torus, whereas the algorithms are formulated for d-dimensional tori and any d.

Finally, we remark that these quasi-periodic tori with a fixed frequency are isolated in the phase space, for an specific adjusting parameter, but that nearby (in parameter space) there are other normally hyperbolic invariant tori with other internal dynamics, which could be quasi-periodic or not. Then, if we modify one parameter we will obtain another normally hyperbolic invariant torus, which can have a quasi-periodic dynamics or another general dynamics. Then, we can follow this new torus by using the general method explained in Section 1.1 (see Chapter 4) or by using again the method for a quasi-periodic dynamics explained in this section (see also Chapter 2 and 3). Therefore, we can cover the search of normally hyperbolic invariant tori in the whole phase space for whatever the internal dynamics is.

1.3 Introducing the general setting

We start by reviewing some general definitions.

Let $\mathcal{A}$ be a m-dimensional Finslered manifold, i.e. assume that the fibers of the tangent bundle $\mathrm{T}\mathcal{A}$ are endowed with a norm that depends continuously with respect to the state variable in $\mathcal{A}$. We refer to $\mathcal{A}$ as the *ambient space*. Let $F : \mathcal{A} \to \mathcal{A}$ be a diffeomorphism generating a discrete dynamical system in $\mathcal{A}$. Let Θ be a d-dimensional manifold referred to as the *model manifold*.

Definition 1.1 *Let $\mathcal{K}$ be a (parameterized) submanifold of $\mathcal{A}$ modeled by Θ, that is $\mathcal{K} = K(\Theta)$ where $K : \Theta \to \mathcal{A}$ is an injective immersion (also referred to as an* embedding*). Let $f : \Theta \to \Theta$ be a diffeomorphism.*

We say that $\mathcal{K} = K(\Theta)$ is F-invariant, with internal dynamics *f, if its parameterization K and f meet the invariance equation:*

$$F \circ K = K \circ f. \tag{1.1}$$

Notice that a point $z = K(\theta)$ of $\mathcal{K}$, parameterized by $\theta \in \Theta$, is mapped to a point of $\mathcal{K}$, parameterized by $f(\theta) \in \Theta$, since

$$F(K(\theta)) = K(f(\theta)), \tag{1.2}$$

We can think of K as a semiconjugacy, and f as a subsystem of F. The map f is the *internal dynamics* in the model manifold Θ. We can see a pictorial representation in Figure 1.1.

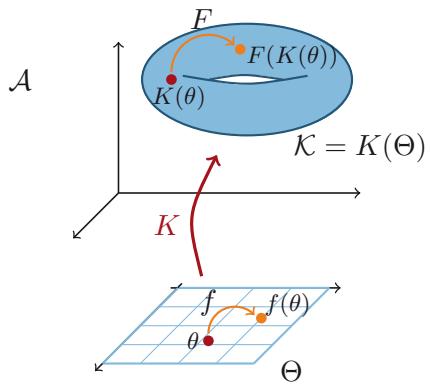

FIGURE 1.1: Pictorial representation of an F-invariant manifold parameterized by K, with internal dynamics f.

The invariance condition (1.1) lifts to the corresponding tangent maps, $\mathrm{T}F : \mathrm{T}\mathcal{A} \to \mathrm{T}\mathcal{A}$, $\mathrm{T}K : \mathrm{T}\Theta \to \mathrm{T}\mathcal{A}$, $\mathrm{T}f : \mathrm{T}\Theta \to \mathrm{T}\Theta$, so that,

$$\mathrm{T}F \circ \mathrm{T}K = \mathrm{T}K \circ \mathrm{T}f.$$

That is, the tangent bundle $\mathrm{T}\mathcal{K}$, parameterized by $\mathrm{T}K$, is $\mathrm{T}F$-invariant with internal dynamics $\mathrm{T}f$. In coordinates the previous equation is expressed by the relation

$$\mathrm{D}F(K(\theta))\mathrm{D}K(\theta) = \mathrm{D}K(f(\theta))\mathrm{D}f(\theta).$$

The key point in the robustness of $\mathcal{K}$ under (bounded) C^1-perturbations of F is that the linearized dynamics, given by the tangent map $\mathrm{T}F$, possesses hyperbolicity properties. Heuristically, this means that there exist a normal bundle $\mathrm{N}\mathcal{K}$ that dominates the dynamics on the tangent bundle $\mathrm{T}\mathcal{K}$: $\mathrm{N}\mathcal{K}$ splits in two invariant subbundles $\mathrm{N}^S\mathcal{K}$ and $\mathrm{N}^U\mathcal{K}$ such that $\mathrm{T}F$ contracts $\mathrm{N}^S\mathcal{K}$ more sharply than $\mathrm{T}\mathcal{K}$ and $\mathrm{T}F$ expands $\mathrm{N}^U\mathcal{K}$ more sharply than $\mathrm{T}\mathcal{K}$. This is the concept of normal hyperbolicity.

Definition 1.2 *We say that the manifold $\mathcal{K}$ is a* Normally Hyperbolic Invariant Manifold *(NHIM for short) of F if it is F-invariant and the linearized dynamics $\mathrm{T}F$ is uniformly exponentially trichotomic, i.e., the tangent bundle $\mathrm{T}_{\mathcal{K}}\mathcal{A}$, splits into three continuous invariant subbundles*

$$\mathrm{T}_{\mathcal{K}}\mathcal{A} = \mathrm{N}^S\mathcal{K} \oplus \mathrm{T}\mathcal{K} \oplus \mathrm{N}^U\mathcal{K} \tag{1.3}$$

that are characterized by the spectral gap conditions

$$0 < \rho_S < \rho_{L,-} \leq 1 \leq \rho_{L,+} < \rho_U, \tag{1.4}$$

in such a way that the following uniform rates of growth hold:

$$v \in \mathrm{N}^S\mathcal{K} \Leftrightarrow \forall k > 0, |\mathrm{T}F^k v| \leq C\rho_S^k |v|,$$
$$v \in \mathrm{N}^U\mathcal{K} \Leftrightarrow \forall k < 0, |\mathrm{T}F^k v| \leq C\rho_U^k |v|,$$
$$v \in \mathrm{T}\mathcal{K} \Leftrightarrow \begin{cases} \forall k > 0, |\mathrm{T}F^k v| \leq C\rho_{L,+}^k |v|, \\ \forall k < 0, |\mathrm{T}F^k v| \leq C\rho_{L,-}^k |v|, \end{cases}$$

where $C > 0$. Bundles $\mathrm{N}^S\mathcal{K}$ and $\mathrm{N}^U\mathcal{K}$ are referred to as the stable and the unstable subbundles of $\mathcal{K}$, respectively. The tangent bundle $\mathrm{T}\mathcal{K}$ is also referred to as the center bundle.

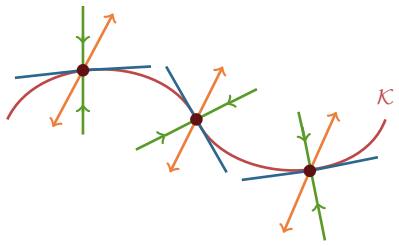

FIGURE 1.2: Pictorial representation of a normally hyperbolic manifold parameterized by K, with normal bundles in green and orange, and tangent bundle in blue.

Remark 1.3 *Notice that, for $v \in \mathrm{T}\mathcal{K}$, there exists $u \in \mathrm{T}\Theta$ so that $v = \mathrm{T}Ku$. Hence, the growth rate condition on the center bundle can be rephrased on the tangent bundle of model manifold by using that $\mathrm{T}F^k v = \mathrm{T}K \circ \mathrm{T}f^k u$.*

Remark 1.4 *Higher regularity of the normally hyperbolic invariant manifold follows from stronger spectral gap conditions. In particular, if we substitute* (1.4) *in Definition 1.2 by*

$$0 < \rho_S < \rho_{L,-}^r \leq 1 \leq \rho_{L,+}^r < \rho_U, \tag{1.5}$$

where $r \geq 1$ and F is of class C^r, then there is a bootstrap on the regularity of the normally hyperbolic invariant manifold $\mathcal{K}$ and it is also of class C^r. We say that $\mathcal{K}$ is a r-normally hyperbolic invariant manifold.

Remark 1.5 *The definition of normal hyperbolicity can be stated in functional terms, by considering the transfer operator $\mathcal{T}$ acting, in a natural way, on continuous sections $\nu : \mathcal{A} \to \mathrm{T}_{\mathcal{K}}\mathcal{A}$ of the bundle $\mathrm{T}_{\mathcal{K}}\mathcal{A}$, that is,*

$$\mathcal{T}\nu(\theta) = \mathrm{D}F(K(f^{-1}(\theta)))\nu(f^{-1}(\theta)).$$

In this setting, Definition (1.2) *is rephrased as saying that the spectrum of the transfer operator splits in three components: the stable component corresponding to the spectral values smaller than ρ_S, the unstable component corresponding to the spectral values larger than ρ_U, and the central component corresponding to the spectral values between $\rho_{L,-}$ and $\rho_{L,+}$. The corresponding spectral projections are linked with the corresponding bundle projections onto the stable, unstable and tangent subbundles. In particular, the central bundle is the tangent bundle $\mathrm{T}\mathcal{K}$. The relations between functional analysis of transfer operators and dynamics of linear skew-products have been successfully exploited since Mather's work on characterization of Anosov diffeomorphisms [80]. We refer to [100] for spectral characterizations of normal hyperbolicity. Interestingly, dynamical phenomena of collapse of invariant bundles leading to breakdown of invariant tori can be explained by a sudden growth of spectra of transfer operators [57, 59].*

In this thesis, we consider that the ambient space is a m-dimensional annulus $\mathcal{A} \subset \mathbb{T}^d \times \mathbb{R}^{m-d}$, endowed with coordinates $z = (x, y)$, with $x \in \mathbb{T}^d$ and $y \in \mathbb{R}^{m-d}$. From now on, we consider a discrete dynamical system generated by a diffeomorphism $F : \mathcal{A} \to \mathcal{A}$ of the form

$$F\begin{pmatrix} x \\ y \end{pmatrix} = \begin{pmatrix} Ax \\ 0 \end{pmatrix} + F_p\begin{pmatrix} x \\ y \end{pmatrix}, \tag{1.6}$$

where $A \in \mathrm{GL}_d(\mathbb{Z})$ and $F_p : \mathcal{A} \to \mathbb{R}^m$ is 1-periodic in x, that is, $F_p(x + e, y) = F_p(x, y)$ for all $e \in \mathbb{Z}^d$. Notice that matrix the A gives the homotopy class of F. Our interest is finding an invariant rotational torus $\mathcal{K}$, that is a d-dimensional manifold modeled on the d-dimensional torus $\Theta = \mathbb{T}^d$, and parameterized by an immersion $K : \mathbb{T}^d \to \mathcal{A}$ of the form

$$K(\theta) = \begin{pmatrix} \theta \\ 0 \end{pmatrix} + K_p(\theta), \tag{1.7}$$

where $K_p : \mathbb{T}^d \to \mathbb{R}^m$ is 1-periodic in θ, that is $K_p(\theta + e) = K_p(\theta)$ for all $e \in \mathbb{Z}^d$. Notice that, if K satisfies

$$F \circ K - K \circ f = 0,$$

then f has to be of the form

$$f(\theta) = A\theta + f_p(\theta), \tag{1.8}$$

where $f_p : \mathbb{T}^d \to \mathbb{R}^d$ is 1-periodic in θ. This is just a consequence of the topological assumptions, chosen for the sake of concreteness. The point is that the homotopy classes of F, K and f have to match.

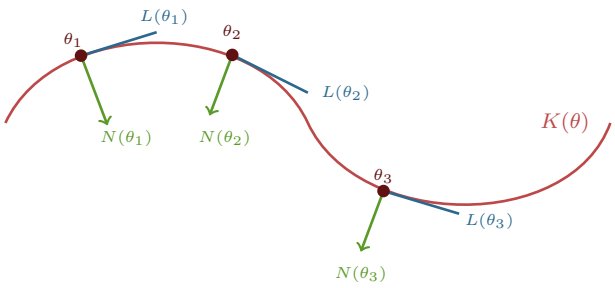

FIGURE 1.3: Pictorial representation of the adapted frame, with normal bundle in green and tangent bundle in blue.

Remark 1.6 *Recall that for any d-dimensional torus embedded in a m-dimensional ambient manifold, we have a tubular neighborhood of the torus, that is an open set around it resembling a neighborhood of the zero section in the normal bundle. Therefore, one can introduce coordinates* $x \in \mathbb{T}^d$ *and* $y \in \mathbb{R}^n$ *around the torus in where they adopt the form of tubular coordinates. In this tubular coordinates, the ambient space is an annulus* $\mathcal{A}$*, and* F*,* K *have the form* (1.6) *and* (1.7)*, respectively.*

Remark 1.7 *In applications, finding tubular coordinates can be a difficult-expensive task. The point is writing invariance equation*

$$F \circ K = K \circ f$$

in such a way that the homotopy classes of F*,* K *and* f *match.*

The tangent bundle $\mathrm{T}\mathcal{K}$ of the parameterized torus $\mathcal{K}$ is trivial. In particular, the d column vectors of the matrix map $L : \mathbb{T}^d \to \mathbb{R}^{m\times d}$, where $L(\theta) = \mathrm{D}K(\theta)$, provide a global frame for the tangent bundle. Here, it is important that $\mathcal{K}$ is a parallelizable manifold. In fact, it is important in the sequel that a normal bundle $\mathrm{N}\mathcal{K}$ is also trivial, that is, it is generated by the $n = m - d$ column vectors of a matrix map $N : \mathbb{T}^d \to \mathbb{R}^{n\times d}$. In this case, we say that $\mathcal{K}$ is a framed manifold. The columns of the matrix map $P : \mathbb{T}^d \to \mathbb{R}^{m\times m}$, obtained by juxtaposing the matrix valued maps L and N so that

$$P(\theta) = (L(\theta) \;\; N(\theta)),$$

provide an adapted frame around $\mathcal{K}$.

Assume now that $\mathcal{K}$, parameterized by K, is F-invariant with internal dynamics f. By differentiating the invariance equation of the parameterization K, (1.2) we obtain the invariance equation of the linearization $L(\theta) =$

$\mathrm{D}K(\theta)$,

$$\mathrm{D}F(K(\theta))\mathrm{D}K(\theta) - \mathrm{D}K(f(\theta))\mathrm{D}f(\theta) = 0. \tag{1.9}$$

This is just a manifestation of the $\mathrm{T}F$-invariance of the tangent bundle $\mathrm{T}\mathcal{K}$. We will write $\Lambda_{_L}(\theta) = \mathrm{D}f(\theta)$, which is the internal dynamics on $\mathrm{T}\mathcal{K}$. Hence, the linearized dynamics $\mathrm{D}F$ around $\mathcal{K}$ in the frame provided by P is given by a block triangular linear skew-product $(\Lambda, f) : \mathbb{R}^m \times \mathbb{T}^d \to \mathbb{R}^m \times \mathbb{T}^d$. Specifically, the matrix valued map $\Lambda : \mathbb{T}^d \to \mathbb{R}^{m\times m}$ is defined by the linearized equation

$$\Lambda(\theta) = P(f(\theta))^{-1}\mathrm{D}F(K(\theta))P(\theta), \tag{1.10}$$

which, employing the form of the tangent bundle given by equation (1.9), Λ has a particular form given by

$$\Lambda(\theta) = \begin{pmatrix} \Lambda_{_L}(\theta) & T(\theta) \\ 0 & \Lambda_{_N}(\theta) \end{pmatrix}, \tag{1.11}$$

where $T : \mathbb{T}^d \to \mathbb{R}^{d\times n}$ and $\Lambda_{_N} : \mathbb{T}^d \to \mathbb{R}^{n\times n}$ are matrix valued maps.

Notice that equation (1.10) splits into a tangent and a normal components, and the system can be simplified, in general to

$$\mathrm{D}K(f(\theta))\Lambda_{_L}(\theta) = \mathrm{D}F(K(\theta))\mathrm{D}K(\theta), \tag{1.12}$$

$$\mathrm{D}K(f(\theta))T(\theta) + N(f(\theta))\Lambda_{_N}(\theta) = \mathrm{D}F(K(\theta))N(\theta), \tag{1.13}$$

where we multiplied equation (1.10) by $P(f(\theta))$.

Remark 1.8 *Notice that the normal bundle, given in equation* (1.13)*, is not assumed to be invariant, since $T(\theta)$ is not necessary zero.*

Until this moment, we have introduced a general description of the needed equations involving the parameterization method for the case of normally hyperbolic invariant manifolds:

- one equation for the invariant torus (1.2),
- one equation for the bundles of the torus (1.10), whereas only the part of the normal bundle (1.13) has to be considered, since (1.12) is always given for free from the derivative of (1.2),

where the unknowns are f and K for equation (1.2) and N and $\Lambda_{_N}$ for equation (1.13).

Along this thesis, we will deal with several different situations involving normally hyperbolic invariant tori, where equations (1.2) and (1.13) has to be solved and treated in a different way.

In chapters 2 and 3, we consider the particular case in which we deal with a *quasi-periodic invariant torus*. In that case, the internal dynamics is prescribed by a *rigid rotation* of frequency $\omega \in \mathbb{R}^d$,

$$f(\theta) = \theta + \omega,$$

so that equation (1.2) is now

$$F(K(\theta)) - K(\theta + \omega) = 0.$$

We should remark that as we have fixed the internal dynamics, we have lost the unknown f of equation (1.2), which is now already given. To avoid this overdeterminacy, we have to add some extra parameters to equation (1.2) in order to fix the frequency and obtain a solvable system. Then, equation (1.2) is turned into

$$F_a(K(\theta)) - K(\theta + \omega) = 0, \tag{1.14}$$

where the unknowns are now K and a parameter $a \in \mathbb{R}^d$. Notice that the dimension of parameter a has to meet with the dimension of the fixed frequency ω.

This particular internal dynamics implies an internal dynamics on $\mathrm{T}\mathcal{K}$ given by the identity $\Lambda_L(\theta) = \mathrm{Id}$. Then, we get that the matrix valued map $\Lambda(\theta)$, given by equation (1.11), is a block-triangular matrix with the identity in the top-left corner

$$\Lambda(\theta) = \begin{pmatrix} \mathrm{Id} & T(\theta) \\ 0 & \Lambda_N(\theta) \end{pmatrix}.$$

To get a quasi-periodic normally hyperbolic invariant torus, so that it is a solution of (1.14), the only restriction in the matrix valued map $\Lambda(\theta)$ is that the cocycle (Λ_N, R_ω) has to be hyperbolic. This is the assumption we use in Chapter 2, where in particular, the dynamics on the normal bundle is written as

$$H(\theta) := \Lambda_N(\theta).$$

Moreover, using this assumption, some non-degeneracy conditions and a KAM strategy, we prove the existence of the solution of (1.14), which is the goal of Chapter 2. We present there a KAM-like theorem (Theorem 2.21) in *a posteriori* format for the existence and local uniqueness of quasi-periodic normally hyperbolic tori in families of dynamical systems. This theorem shows

that a computed approximation (K, a) of the invariance equation (1.14), satisfying appropriated non-degeneracy and hyperbolicity conditions, implies the existence of a true solution (K_*, a_*) of equation (1.14). The proof of Theorem 2.21, gives us an efficient algorithm to compute a quasi-periodic normally hyperbolic invariant torus and the adjusting parameter, which is the goal of Chapter 3.

Remark 1.9 *To validate a numerical computation we should check that the computed approximation verifies the hypotheses of our Theorem 2.21. Even if in some close to "integrable" examples these checks could be made by hand, far from this integrable cases, this could be made with the aid of computers, leading to* computer assisted proofs.

Apart from computing the invariant torus, we will also compute the invariant normal bundle and its splitting into stable and unstable bundles. For that reason, we will require the invariance on the normal bundle by assuming $T(\theta) = 0$,

$$\mathrm{D}F_a(K(\theta))N(\theta) - N(\theta + \omega)\Lambda_N(\theta) = 0, \tag{1.15}$$

so that the matrix valued map $\Lambda(\theta)$ has a block diagonal form

$$\Lambda(\theta) = \mathrm{blockdiag}(\mathrm{Id}, \Lambda_N(\theta)),$$

and the system to solve is turned into

$$\begin{aligned} F_a(K(\theta)) - K(\theta + \omega) &= 0, \\ \mathrm{D}F_a(K(\theta))N(\theta) - N(\theta + \omega)\Lambda_N(\theta) &= 0, \end{aligned}$$

given by (1.14) and (1.15).

In a general (non-reducible) setting, we solve that system without imposing reducibility on the torus, so that the only requirement is the hyperbolicity on $\Lambda_N(\theta)$. In that case, the hyperbolicity condition allows us to solve equation (1.15) as a fixed point problem, by using contractions which are given by Λ_N.

We can impose some restrictions on the system, by imposing *reducibility (to constants)* on the torus, to speed up the method. This means that, there exists a matrix $M : \mathbb{T}^d \to \mathbb{R}^{m\times m}$ and a constant matrix $\Lambda \in \mathbb{R}^{m\times m}$ such that

$$\mathrm{D}F_a(K(\theta))M(\theta) - M(\theta + \omega)\Lambda = 0,$$

where $M(\theta) = P(\theta)$ in our case. This reducibility can be understood as a change of variables in the total tangent space $\mathrm{T}_{K(\theta)}\mathcal{M}$ in such a way

that $\mathrm{D}F(K(\theta))$ corresponds to a constant linear cocycle. Then, by the new expression of Λ, given by

$$\Lambda = \begin{pmatrix} \mathrm{Id} & 0 \\ 0 & \Lambda_N \end{pmatrix},$$

we can express equation (1.15), which now reads as

$$\mathrm{D}F_a(K(\theta))N(\theta) - N(\theta+\omega)\Lambda_N = 0, \tag{1.16}$$

in a Fourier basis. Equation (1.16) can be solved fast when it is discretized.

In particular, we will consider two reducible cases: one in which the constant matrix Λ_N is diagonalizable (referred as *completely reducible method*) and another in which we do not require it (referred as *non-completely reducible method*). The particularity of the completely reducible method is that we can split completely equation (1.16) into n subequations, so that the computations can be done with a linear cost (with respect to the number of Fourier coefficients), and they become extremely fast. The non-completely reducible method is also linear, but the factor grows as n^2 (instead of n with the method for completely reducible tori). Of course, these two methods fail when the assumptions, that is reducibility properties, does not hold, but we can switch to the other general non-reducible method and so cover the computation of quasi-periodic tori regardless the reducibility property. We should emphasize that by using the reducible methods we obtain, directly, more information about the torus, whereas using the non-reducible one we need to produce more extra computations to get the information.

We emphasize that neither in the rigorous results nor in the general algorithm explained here, we use hypothesis of reducibility of the cocycle $(\Lambda_N, \mathcal{R}_\omega)$ to a constant cocycle (using a so called Floquet transformation), which is a rather standard assumption in the area (see e.g. [9, 89]).

Finally, in Chapter 4 we present a general method for the computation of normally hyperbolic invariant manifolds, in which the dynamics can be anything and not given. As it is useful to compute the torus and the stable and unstable bundles, we use a restriction in equation (1.13) by imposing that the normal bundle has to be invariant, so that we take again $T(\theta) = 0$, and the system to solve is now

$$\begin{aligned} F(K(\theta)) - K(f(\theta)) &= 0, \\ \mathrm{D}F(K(\theta))N(\theta) - N(f(\theta))\Lambda_N(\theta) &= 0. \end{aligned}$$

We should remark that this restriction is not mandatory to compute the torus, since we could implement the algorithm without imposing this condition. Besides of that, we consider more interesting to compute stable and unstable invariant bundles.

In the numerical computations one has to choose a method of approximation of periodic functions, in order to approximate the parameterizations of the torus. It is well known that Fourier series are very specialized for quasi-periodic dynamics, since they leads to a fast and efficiently computations to solve the cohomological equations providing from the invariance equation. But in the general normally hyperbolic case, due to the hard cost of the composition of two periodic functions in the computation, for instance the composition of the parameterization K with the internal dynamics f, $K(f(\theta))$, other (local) interpolation from grid points, splines, simplicial approximations, has to be considered. In Chapter 4, we choose a Lagrangian local interpolation.

Remark 1.10 *In this thesis we develop the methods for the computation of normally hyperbolic invariant manifolds for a discrete dynamical system, but a similar methodology can be developed for the case of flows.*

Chapter 2

A KAM-like theorem for Quasi-Periodic Normally Hyperbolic Invariant Tori

In this chapter, we present a KAM-like theorem in *a posteriori* format for the existence of quasi-periodic normally hyperbolic tori in families of dynamical systems. It is based on a KAM scheme to find the parameterization of a torus with fixed Diophantine frequency and adjusting of parameters of the family. This is a constructive method which allow us to formulate a theorem to prove the existence of an invariant normally hyperbolic invariant torus carrying quasi-periodic dynamics.

The proof of this theorem gives us an efficient algorithm to compute the torus and the adjusting parameter (see Chapter 3 for related algorithms and implementations). To give a brief idea of the method, under normal hyperbolicity and additional non-degeneracy conditions on an approximate invariant torus and on the adjusting parameter a, if the error estimates are small enough (in suitable Banach spaces of real-analytic periodic functions), the theorem ensures that there is a true invariant torus and an adapting parameter nearby.

2.1 The setting

Consider the phase space an annulus $\mathcal{A}$, that is an open set $\mathcal{A} \subset \mathbb{T}^d \times \mathbb{R}^n = \{z = (x, y) \mid x \in \mathbb{T}^d,\ y \in \mathbb{R}^n\}$ that is homotopic to $\mathbb{T}^d \times \mathcal{V}$, where $\mathcal{V} \subset \mathbb{R}^n$ is open. Let $F : \mathcal{A} \times \mathcal{U} \to \mathbb{T}^d \times \mathbb{R}^n$ be a family of smooth maps, where $\mathcal{U} \subset \mathbb{R}^d$

is the open set of parameters. We will assume that for each parameter $a \in \mathcal{U}$, $F_a : \mathcal{A} \to \mathbb{T}^d \times \mathbb{R}^n$, defined by $F_a(z) = F(z, a)$ is *homotopic to the identity*:

$$F_a(z) = \begin{pmatrix} x \\ 0 \end{pmatrix} + F_p(z, a) \tag{2.1}$$

where $F_p(z; a) = F_p((x, y), a)$ is 1-periodic in x. To avoid an abuse of notation, we will denote by $\mathrm{D}F_a$ the derivative of F_a with respect to z, we will denote $\frac{\partial F_a}{\partial a}$ the derivative of F_a with respect to the parameter a and by $\mathrm{D}F$ the derivative of F with respect the variables z and a. For instance, $\mathrm{D}F_a(z) = \mathrm{D}_z F(z, a)$ and $\frac{\partial F_a}{\partial a}(z) = \frac{\partial F}{\partial a}(z, a)$.

Let $\mathcal{K}$ be a (parameterized) submanifold of $\mathbb{T}^d \times \mathbb{R}^n$ modeled by $\mathbb{T}^d$, that is $\mathcal{K} = K(\mathbb{T}^d)$ where $K : \mathbb{T}^d \to \mathbb{T}^d \times \mathbb{R}^n$ is an injective immersion (also referred to as an *embedding*). This embedding is assumed to be homotopic to the zero section of $\mathbb{T}^d \times \mathbb{R}^n$:

$$K(\theta) = \begin{pmatrix} \theta \\ 0 \end{pmatrix} + K_p(\theta) \tag{2.2}$$

where $K_p(\theta)$ is 1-periodic in θ.

Definition 2.1 *We say that the torus parameterized by K, $\mathcal{K}$, is F_a-***invariant** *with a* quasi-periodic *motion given by the frequency $\omega \in \mathbb{R}^d$ if K satisfies the invariance equation:*

$$F_a \circ K(\theta) = K(\theta + \omega). \tag{2.3}$$

Note that (2.3) is an equation for (K, a) given the family F.

Remark 2.2 *Notice that the dimension of the parameter space equals the dimension of the torus, d. This is to fix the dynamics on an invariant torus as a d-dimensional rotation.*

Remark 2.3 *Notice that $K_\alpha(\theta) = K(\theta + \alpha)$ is also a solution of* (2.3)*. In order to avoid this non-uniqueness, we can fix an initial phase on the torus by imposing the following condition:*

$$\langle K^x(\theta) - \theta \rangle = 0 \tag{2.4}$$

where the superindex x represents the projection on the angle variables. In that case, in order to get this zero average, we select $\alpha = -\langle K_p^x(\theta) \rangle$.

The purpose of this chapter is, then, solving the system of equations

$$\begin{aligned} F_a(K(\theta)) - K(\theta+\omega) &= 0, \\ \langle K^x(\theta) - \theta \rangle &= 0, \end{aligned} \tag{2.5}$$

in appropriate functional spaces. Note that we assume ω given and that the unknowns are the embedding K and the adjusting parameter a.

Let us consider $\mathcal{K}$ invariant with a quasi periodic internal dynamics $R_\omega : \mathbb{T}^d \to \mathbb{T}^d$ given by $R_\omega(\theta) = \theta + \omega$. An immediate consequence is that the tangent bundle of $\mathcal{K}$, $\mathrm{T}\mathcal{K}$, is invariant under the tangent map. That is, the matrix-valued function $\mathrm{D}K : \mathbb{T}^d \to \mathbb{R}^{(d+n)\times d}$ provides a global frame of the tangent bundle and satisfies:

$$\mathrm{D}F_a \circ K(\theta) = \mathrm{D}K(\theta+\omega), \tag{2.6}$$

which is just the derivative of equation (2.3).

The key point in proving the robustness of an invariant manifold under perturbations of F_a, is that there exists a normal bundle $\mathrm{N}\mathcal{K}$ that dominates the linearized dynamics given by $\mathrm{D}F_a$. More specifically, $\mathrm{N}\mathcal{K}$ splits in two invariant subbundles $\mathrm{N}^s\mathcal{K}$ and $\mathrm{N}^u\mathcal{K}$ such that $\mathrm{D}F_a$ contracts $\mathrm{N}^s\mathcal{K}$ more sharply than $\mathrm{T}\mathcal{K}$ and $\mathrm{D}F_a$ expands $\mathrm{N}^u\mathcal{K}$ more sharply than $\mathrm{T}\mathcal{K}$. This is the concept of normal hyperbolicity.

Then, a normal bundle $N\mathcal{K}$ will be generated by a matrix valued map $N^0 : \mathbb{T}^d \to \mathbb{R}^{(d+n)\times n}$ such that for each $\theta \in \mathbb{T}^d$, the column vectors of $\mathrm{D}K(\theta)$ join with the column vectors of $N^0(\theta)$ form a basis of $\mathrm{T}_{K(\theta)}\mathcal{A} \simeq \mathbb{R}^{n+d}$. In other words, the matrix valued map $P : \mathbb{T}^d \to \mathbb{R}^{(d+n)\times(d+n)}$, obtained by juxtaposing the matrix valued $\mathrm{D}K$ and N^0 so that

$$P(\theta) = \begin{pmatrix} \mathrm{D}K(\theta) & N^0(\theta) \end{pmatrix}, \tag{2.7}$$

provides an adapted frame around the torus.

In these coordinates, the linearized dynamics around the torus is given by the matrix valued map $\Lambda : \mathbb{T}^d \to \mathbb{R}^{(d+n)\times(d+n)}$ given by

$$\Lambda(\theta) = P(\theta+\omega)^{-1}\mathrm{D}F_a(K(\theta))P(\theta). \tag{2.8}$$

From the invariance of the tangent bundle and equation (2.6), we obtain that Λ is a block-triangular matrix with the identity in the top-left corner

$$\Lambda(\theta) = \begin{pmatrix} \mathrm{Id} & T(\theta) \\ 0 & H(\theta) \end{pmatrix},$$

where $T(\theta)$ is a $d \times n$ matrix and $H(\theta)$ is a $n \times n$ matrix. We emphasize that the normal bundle is not assumed to be invariant, since $T(\theta)$ is not necessary zero. On the other hand, the normal bundle is not invariant but fixed, which in fact is transported by $\mathrm{D}F_a$ as:

$$\begin{aligned} \mathrm{D}F_a(K(\theta))N^0(\theta) &= \mathrm{D}K(\theta+\omega)T(\theta) + N^0(\theta+\omega)H(\theta) \\ &= P(\theta+\omega)\begin{pmatrix} T(\theta) \\ H(\theta) \end{pmatrix}. \end{aligned} \tag{2.9}$$

So, we have explicitly defined both matrix T and H as

$$\begin{pmatrix} T(\theta) \\ H(\theta) \end{pmatrix} = P(\theta+\omega)^{-1}\mathrm{D}F_a(K(\theta))N^0(\theta). \tag{2.10}$$

The hypothesis of normal hyperbolicity is formulated in terms of the hyperbolicity of the cocycle (H, R_ω), as we will see in the following section.

Our goal in this chapter is to show that if there is an approximate quasi-periodic invariant normally hyperbolic torus, K, for a given F_a, then under some specific conditions there exists a true invariant torus K_∞ near it for F_{a_∞} near F_a.

2.2 Preliminary definitions and results

Let us introduce the functional analytical tools that we will use in the proofs of this chapter.

We will denote a *complex strip of* $\mathbb{T}^d$ *of width* $\rho > 0$ by

$$\mathbb{T}^d_\rho = \{\theta \in \mathbb{T}^d_{\mathbb{C}} : \mathrm{Im}|\theta_i| < \rho,\ i = 1, \dots, d\},$$

where $\mathbb{T}^d_{\mathbb{C}} = \mathbb{T}^d + \mathbf{i}\mathbb{R}^d$ is the complex d-dimensional torus. We consider A_ρ the Banach space of functions $f : \bar{\mathbb{T}}^d_\rho \to \mathbb{C}$ that are continuous in $\bar{\mathbb{T}}^d_\rho$, holomorphic in $\mathbb{T}^d_\rho$ and such that $f(\mathbb{T}^d) \subset \mathbb{R}$, endowed with the norm

$$||f||_\rho = \sup_{\theta \in \mathbb{T}^d_\rho} |f(\theta)|.$$

We will also denote by A^1_ρ the Banach space of functions $f : \bar{\mathbb{T}}^d_\rho \to \mathbb{C}$ that are continuous in $\bar{\mathbb{T}}^d_\rho$, holomorphic in $\mathbb{T}^d_\rho$, such that $f(\mathbb{T}^d) \subset \mathbb{R}$, and that also their derivatives $\frac{\partial f}{\partial \theta_i}$, $i = 1, \dots, d$, are continuously extended to the boundary of $\mathbb{T}^d_\rho$, endowed with the norm

$$||f||_{\rho,C^1} = \sup_{\theta \in \mathbb{T}^d_\rho} \max\left(|f(\theta)|, \left|\frac{\partial f}{\partial \theta_1}(\theta)\right|, \dots, \left|\frac{\partial f}{\partial \theta_d}(\theta)\right|\right).$$

Remark 2.4 *The previous definitions extend component wise to functions* $f : \mathbb{T}^d_\rho \to \mathbb{C}^m$. *In particular, for* $f \in (A_\rho)^m$ *we consider the norm*

$$||f||_\rho = \sup_{\theta \in \mathbb{T}^d_\rho} |f(\theta)|,$$

where $|\cdot|$ *is the maximum norm in* $\mathbb{C}^m$.

We will denote the norm of a pair of objects (f, a), where $f \in (A_\rho)^m$ and $a \in \mathbb{R}^d$, by $||(f, a)||_\rho$ defined as

$$||(f, a)||_\rho := \max\{||f||_\rho, |a|\}.$$

Lemma 2.5 (Cauchy estimates) *Given* $\rho > 0$, *let* $f \in A_\rho$. *Then, for any* $0 < \delta < \rho$, $f \in A^1_{\rho-\delta}$, *so then* $\frac{\partial f}{\partial \theta_i} \in A_{\rho-\delta}$, *for* $i = 1, \ldots, d$, *and the partial derivatives satisfy inequalities*

$$\left\| \frac{\partial f}{\partial \theta_i} \right\|_{\rho-\delta} \leq \frac{1}{\delta} ||f||_\delta. \tag{2.11}$$

In particular,

$$||\mathrm{D}f||_{\rho-\delta} = \sum_{i=0}^{d} \left\| \frac{\partial f}{\partial \theta_i} \right\|_{\rho-\delta} \leq \frac{d}{\delta} ||f||_\rho. \tag{2.12}$$

Remark 2.6 *Estimate* (2.12) *is extended to vector functions* $f \in (A_\rho)^m$ *as follows*

$$||\mathrm{D}f||_{\rho-\delta} = \max_{j=1,\ldots,m} \sum_{i=0}^{d} \left\| \frac{\partial f_j}{\partial \theta_i} \right\|_{\rho-\delta} \leq \frac{d}{\delta} ||f||_\rho. \tag{2.13}$$

In the meaning of distances, given A, B subsets of a metric space X, we will denote by $\mathrm{dist}(A, B)$ the distance between two subspaces A and B as

$$\mathrm{dist}(A, B) = \inf\{d(x, y) \ : \ x \in A, \ y \in B\},$$

where $d(\cdot, \cdot)$ is the distance in X.

The following definitions and classical results are important in KAM theory. See the tutorial [29] and papers [95, 94] for completeness.

Definition 2.7 *We say that* $\omega \in \mathbb{R}^d$ *is* ergodic *if*

$$|\omega \cdot q - p| > 0, \ q \in \mathbb{Z}^d \setminus \{0\}, \ p \in \mathbb{Z}. \tag{2.14}$$

Lemma 2.8 *Let $\eta : \mathbb{T}^d \to \mathbb{R}$ continuous and ω ergodic. If there exists a continuous zero-average solution $\xi : \mathbb{T}^d \to \mathbb{R}$ of*

$$\xi(\theta) - \xi(\theta + \omega) = \eta(\theta) - \langle \eta \rangle, \tag{2.15}$$

called tangent cohomological equation*, where*

$$\langle \eta \rangle = \int_{\mathbb{T}^d} \eta(\theta) \, \mathrm{d}\theta$$

is the average of η, then it is unique.

In such a case, we will denote by $\mathcal{R}_\omega \eta$ the only zero-average solution ξ of the equation (2.15)*.*

Definition 2.9 *We say that $\omega \in \mathbb{R}^d$ satisfies the* Diophantine condition *of type (γ, τ), denoted by $\omega \in \mathcal{D}(\gamma, \tau)$, if*

$$|\omega \cdot q - p| \geq \gamma |q|_1^{-\tau}, \ q \in \mathbb{Z}^d \setminus \{0\}, \ p \in \mathbb{Z}, \tag{2.16}$$

where $|q|_1 = |q_1| + \cdots + |q_d|$.

The following lemma gives us sufficient conditions for the existence of the solution of equation (2.15).

Lemma 2.10 (Russmann Estimates) *Let ω be a Diophantine number of type (γ, τ), $\gamma > 0$, $\tau \geq d$. Then, there exists a constant $c_R > 0$, such that for any $\eta \in A_\rho$, there exists an unique zero-average solution ξ of the equation*

$$\xi(\theta) - \xi(\theta + \omega) = \eta(\theta) - \langle \eta \rangle,$$

such that, for any $0 < \delta < \rho$, $\xi \in A_{\rho - \delta}$ and satisfies

$$||\xi||_{\rho - \delta} \leq \frac{c_R}{\gamma \delta^\tau} ||\eta||_\rho. \tag{2.17}$$

The following definitions and results deals with the hyperbolicity properties.

Let $H : \bar{\mathbb{T}}^d_\rho \to \mathbb{C}^{n \times n}$ be a matrix valued map whose components are in A_ρ. Let $\omega \in \mathbb{R}^d$ be a rotation vector, and denote by $R_\omega : \bar{\mathbb{T}}^d_\rho \to \bar{\mathbb{T}}^d_\rho$ the map

$$R_\omega(\theta) = \theta + \omega.$$

Let $(H, R_\omega) : \mathbb{C}^n \times \bar{\mathbb{T}}^d_\rho \to \mathbb{C}^n \times \bar{\mathbb{T}}^d_\rho$ be the corresponding cocycle defined by

$$(H, \omega)(v, \theta) = (H(\theta)v, \theta + \omega).$$

The cocycle (H, R_ω) induces a *transfer operator* $\mathcal{H}$ acting on sections of the (trivial) bundle $\mathbb{C}^n \times \bar{\mathbb{T}}^d_\rho$, which are identified with functions $\xi : \bar{\mathbb{T}}^d_\rho \to \mathbb{C}^n$, defined by the formula

$$\mathcal{H}\xi(\theta) = H(\theta - \omega)\xi(\theta - \omega).$$

We can consider $\mathcal{H}$ defined on spaces of functions with different regularities. In particular, we will consider the spaces

$$(B_\rho)^n = \{\xi : \bar{\mathbb{T}}^d_\rho \to \mathbb{C}^n \text{ bounded }\},$$

$$(A_\rho)^n = \{\xi : \bar{\mathbb{T}}^d_\rho \to \mathbb{C}^n \text{ continuous, holomorphic in } \mathbb{T}^d_\rho\},$$

endowed with the supremum norm. Notice that, $(A_\rho)^n \subset (B_\rho)^n$ and the inclusion is closed.

The arguments in [55] leads to the following results.

Lemma 2.11 *Let (H, R_ω) be a cocycle where $H \in (A_\rho)^{n\times n}$ and $\omega \in \mathbb{R}^d$. Assume that the transfer operator $\mathcal{H}$ is hyperbolic in the space of bounded sections, $(B_\rho)^n$. Then, there exists $c_H > 0$ such that for any $0 < \rho' \leq \rho$, for any $\eta \in (A_{\rho'})^n$, there exists an unique solution ξ of the* normal cohomological equation

$$H(\theta)\xi(\theta) - \xi(\theta + \omega) = \eta(\theta), \tag{2.18}$$

such that $\xi \in (A_{\rho'})^n$ and satisfies

$$||\xi||_{\rho'} \leq c_H ||\eta||_{\rho'}. \tag{2.19}$$

We will denote by $\mathcal{R}_H\eta$ the unique solution ξ of (2.18). Notice that

$$\mathcal{R}_H\eta(\theta) = (\mathcal{H} - \mathrm{Id})^{-1}\eta(\theta + \omega).$$

The constant c_H in the previous lemma is

$$c_H = ||\mathcal{R}_H||_\rho = ||(\mathcal{H} - \mathrm{Id})^{-1}||_\rho$$

where $||\cdot||_\rho$ is the operator norm in $(B_\rho)^n$.

Bootstrap arguments, also lead to the following lemma.

Lemma 2.12 *Let (H, R_ω) be a cocycle, where $H \in (A_\rho)^{n\times n}$ and $\omega \in \mathbb{R}^d$, and $\mathcal{H}$ the corresponding transfer operator. Assume that $\mathcal{H}$ is hyperbolic in $(B_0)^n$. Then, for ρ small enough, $\mathcal{H}$ is hyperbolic in $(B_\rho)^n$ and hence $\mathcal{H}$ is hyperbolic in $(A_\rho)^n$.*

Remark 2.13 *We emphasize that in previous results of this section, the hypothesis of quasi-periodic dynamics is essential for the proofs.*

2.3 Approximately invariant torus: a Newton step

In this section, we will give an iterative scheme to solve invariance equation (2.5) for (K, a), based on a Newton Method. We will describe an step formally, without considering the estimates when solving the cohomological equations. This will be the bulk of the difficulties when proving the convergence of Theorem 2.21 in section 2.4.

Along this chapter, we will say that F_a is real analytic if

$$F_a(x, y) - \begin{pmatrix} x \\ 0 \end{pmatrix}$$

is real analytic. In the same way, we will say that K is real analytic if

$$K(\theta) - \begin{pmatrix} \theta \\ 0 \end{pmatrix}$$

is real analytic.

Consider we have an approximately F_a-invariant torus $\mathcal{K}$ parameterized by $K : \mathbb{T}^d \to \mathbb{T}^d \times \mathbb{R}^n$ of frequency ω for a given parameter a and such that $\langle K^x(\theta) - \theta \rangle = 0$. That is, we assume that the error

$$E(\theta) = F_a(K(\theta)) - K(\theta + \omega), \tag{2.20}$$

is small (in an appropriate norm).

Our interest is to improve this approximation. So, we will look for a new approximation $(\bar{K}, \bar{a})$ from (K, a) of the form

$$\begin{aligned} \bar{K}(\theta) &= K(\theta) + \Delta K(\theta), \\ \bar{a} &= a + \Delta a, \end{aligned}$$

where the corrections ΔK and Δa are the solutions of the linearized invariance equation

$$\mathrm{D}F_a(K(\theta))\Delta K(\theta) - \Delta K(\theta + \omega) + \frac{\partial F_a}{\partial a}(K(\theta))\Delta a = -E(\theta). \tag{2.21}$$

Rewriting the correction of the torus in terms of the adapted frame P and $\Delta K(\theta) = P(\theta)\xi(\theta)$, we obtain

$$\mathrm{D}F_a(K(\theta))P(\theta)\xi(\theta) - P(\theta + \omega)\xi(\theta + \omega) + \frac{\partial F_a}{\partial a}(K(\theta))\Delta a = -E(\theta). \tag{2.22}$$

Remark 2.14 *Note that, from the error on the invariance equation of the torus* (2.20)*, we obtain the error on the invariance of the tangent bundle directly from its derivative:*

$$\mathrm{D}F_a(K(\theta))\mathrm{D}K(\theta) - \mathrm{D}K(\theta+\omega) = \mathrm{D}E(\theta). \tag{2.23}$$

Then, using (2.9) *and* (2.23)*, the error of the linearized equation is, in fact, the derivative of the error on the invariance equation:*

$$E_{\mathrm{red}}(\theta) = \mathrm{D}F_a(K(\theta))P(\theta) - P(\theta+\omega)\Lambda(\theta) = (\ \mathrm{D}E(\theta) \mid 0\ ). \tag{2.24}$$

By multiplying equation (2.25) by $P(\theta+\omega)^{-1}$, we get a block-triangular system:

$$\begin{aligned}\Lambda(\theta)\xi(\theta) - \xi(\theta+\omega) + P(\theta+\omega)^{-1}E_{red}(\theta)\xi(\theta)\\ + P(\theta+\omega)^{-1}\frac{\partial F_a}{\partial a}(K(\theta))\Delta a = -P(\theta+\omega)^{-1}E(\theta),\end{aligned} \tag{2.25}$$

which by neglecting quadratic order therms is simplified to:

$$\Lambda(\theta)\xi(\theta) - \xi(\theta+\omega) + B(\theta)\Delta a = \eta(\theta), \tag{2.26}$$

where $\eta(\theta) = -P(\theta+\omega)^{-1}E(\theta)$ and $B(\theta) = P(\theta+\omega)^{-1}\frac{\partial F_a}{\partial a}(K(\theta))$.
Our immediate goal is to solve equation (2.26). Note that if we obtain a solution of (2.26), it is in fact an approximate solution of (2.25), which is equivalent to (2.22). We can solve (2.26) by using the following Lemma 2.15.

Lemma 2.15 (Cohomological Equations) *Consider a real analytic vector valued map* $\eta = \begin{pmatrix}\eta^L\\ \eta^N\end{pmatrix} : \mathbb{T}^d \to \mathbb{R}^{d+n}$*, and real analytic matrix valued maps* $B : \mathbb{T}^d \to \mathbb{R}^{(d+n)\times d}$*,* $H : \mathbb{T}^d \to \mathbb{R}^{n\times n}$*,* $T : \mathbb{T}^d \to \mathbb{R}^{d\times n}$*. Assume that:*

H1) the cocycle (H, R_ω) *is hyperbolic,*

H2) $\omega \in \mathbb{R}^d$ *is Diophantine of type* (γ, τ)*,*

H3) $\langle B^L(\theta) - T(\theta)\mathcal{R}_H(B^N(\theta))\rangle$ *is invertible.*

Then, every solution of the system

$$\begin{pmatrix}\mathrm{Id} & T(\theta)\\ 0 & H(\theta)\end{pmatrix}\begin{pmatrix}\xi^L(\theta)\\ \xi^N(\theta)\end{pmatrix} - \begin{pmatrix}\xi^L(\theta+\omega)\\ \xi^N(\theta+\omega)\end{pmatrix} + \begin{pmatrix}B^L(\theta)\\ B^N(\theta)\end{pmatrix}\Delta a = \begin{pmatrix}\eta^L(\theta)\\ \eta^N(\theta)\end{pmatrix} \tag{2.27}$$

is given by

$$\begin{aligned} \Delta a &= \langle B^L(\theta) - T(\theta)\mathcal{R}_H B^N(\theta)\rangle^{-1}\langle \eta^L(\theta) - T(\theta)\mathcal{R}_H\eta^N(\theta)\rangle & \text{(2.28a)}\\ \xi^N(\theta) &= \mathcal{R}_H\eta^N(\theta) - \mathcal{R}_H B^N(\theta)\Delta a & \text{(2.28b)}\\ \xi^L(\theta) &= \bar{\xi^L}(\theta) + \xi_0^L & \text{(2.28c)} \end{aligned}$$

where

$$\xi^L(\theta) = \mathcal{R}_\omega(\eta^L(\theta) - B^L(\theta)\Delta a - T(\theta)\xi^N(\theta)),$$

and $\xi_0^L \in \mathbb{R}^d$.

PROOF: Observe that (2.27) is a triangular system, so we start by solving

$$H(\theta)\xi^N(\theta) - \xi^N(\theta+\omega) = \eta^N(\theta) - B^N(\theta)\Delta a, \tag{2.29}$$

for any $\Delta a \in \mathbb{R}^d$. From the hyperbolicity condition *H1*, the normal cohomological equation (2.29) has a solution

$$\xi^N(\theta) = \mathcal{R}_H\eta^N(\theta) - \mathcal{R}_H\mathrm{B}^N(\theta)\Delta a. \tag{2.30}$$

Now, we have solve the tangent cohomological equation by substituting the value of ξ^N on:

$$\xi^L(\theta) - \xi^L(\theta+\omega) = \eta^L(\theta) - B^L(\theta)\Delta a - \mathrm{T}(\theta)\xi^N(\theta). \tag{2.31}$$

We first fix the value of Δa in order to get the average of the right hand side of equation (2.31) equal to zero:

$$\langle\eta^L(\theta)\rangle - \langle B^L(\theta)\rangle\Delta a - \langle\mathrm{T}(\theta)\mathcal{R}_H\eta^N(\theta)\rangle - \langle\mathrm{T}(\theta)\mathrm{B}^N(\theta)\rangle\Delta a = 0.$$

So then,

$$\Delta a = \langle B^L(\theta) - T(\theta)\mathrm{B}^N(\theta)\rangle^{-1}\langle\eta^L(\theta) - T(\theta)\mathcal{R}_H\eta^N(\theta)\rangle,$$

where the invertibility of $\langle B^L(\theta) - T(\theta)\mathrm{B}^N(\theta)\rangle$ is in fact the non-degeneracy condition of hypothesis *H3*. This choice of Δa fixes the value o ξ^N.

Thanks to hypothesis *H2*, we have an unique solution of (2.31) with zero average given by

$$\bar{\xi^L}(\theta) := \mathcal{R}_\omega(\eta^L(\theta) - B^L(\theta)\Delta a - T(\theta)\xi^N(\theta)). \tag{2.32}$$

Then, the general solution of this tangent cohomological equation has the form

$$\xi^L(\theta) = \bar{\xi^L}(\theta) + \xi_0^L, \tag{2.33}$$

with average $\langle\xi^L\rangle = \xi_0^L$. □

We apply Lemma 2.15 to our case by using $\eta(\theta) = -P(\theta+\omega)^{-1}E(\theta)$ and we fix value ξ_0^L to ensure the condition $\langle K^x(\theta) - \theta\rangle = 0$, the uniqueness of the torus. Note that by assuming this condition, we need the same zero average for the form of the correction of the torus,

$$\langle \Pi_x(K(\theta) + P(\theta)\xi(\theta)) - \theta\rangle = \langle \Pi_x(P(\theta)\xi(\theta)\rangle = 0.$$

Using the notation

$$\bar{\xi}(\theta) = \begin{pmatrix} \bar{\xi^L}(\theta) \\ \xi^N(\theta) \end{pmatrix},$$

where $\bar{\xi^L}$ is given in equation(2.32), we find conditions for ξ_0^L:

$$\begin{aligned} 0 &= \langle \Pi_x(P(\theta)(\begin{pmatrix} \xi_0^L \\ 0 \end{pmatrix} + \bar{\xi}(\theta))\rangle = \langle \mathrm{D}K^x(\theta)\xi_0^L + \Pi_x(P(\theta)\bar{\xi}(\theta))\rangle \\ &= \xi_0^L\langle \mathrm{D}K^x(\theta)\rangle + \langle \Pi_x(P(\theta)\bar{\xi}(\theta))\rangle \end{aligned}$$

Recall that K is homotopic to the zero section of $\mathbb{T}^d\times\mathbb{R}^n$ and K_p is 1-periodic in θ, so that $\langle \mathrm{D}K^x\rangle = \langle \mathrm{Id} + \mathrm{D}K_p^x\rangle = \mathrm{Id} + \langle \mathrm{D}K_p^x\rangle = \mathrm{Id}$, and value ξ_0^L will be given by

$$\begin{aligned} \xi_0^L &= -\langle \Pi_x(P(\theta)\bar{\xi}(\theta))\rangle = -\langle \Pi_x(\mathrm{D}K(\theta)\bar{\xi^L}(\theta)) + \Pi_x(N^0(\theta)\xi^N(\theta))\rangle \\ &= -\langle \mathrm{D}K^x(\theta)\bar{\xi^L}(\theta) + N^{0,x}(\theta)\xi^N(\theta)\rangle. \end{aligned} \tag{2.34}$$

The following lemma summarizes the main results of this section and it is an immediate consequence of Lemma 2.15.

Lemma 2.16 *Let $F : \mathcal{A}\times\mathcal{U} \to \mathbb{T}^d\times\mathbb{R}^n$ be a smooth family of real analytic homotopic to the identity maps and $N^0 : \mathbb{T}^d \to \mathbb{R}^{(d+n)\times n}$ real analytic. Let $K : \mathbb{T}^d \to \mathbb{T}^d\times\mathbb{R}^n$ be a real analytic homotopic to the zero section parameterization and $a \in \mathbb{R}^d$. Define $E : \mathbb{T}^d \to \mathbb{R}^{d+n}$ by $E(\theta) = F_a(K(\theta)) - K(\theta+\omega)$. Let $e : \mathbb{T}^d \to \mathbb{R}^{d+n}$ real analytic. Let $H : \mathbb{T}^d \to \mathbb{R}^{n\times n}$ and $T : \mathbb{T}^d \to \mathbb{R}^{d\times n}$, given by equation (2.10), where we assume that $P : \mathbb{T}^d \to \mathbb{R}^{(d+n)\times(d+n)}$, given by (2.7), is invertible for any $\theta \in \mathbb{T}^d$ in order to construct the adapted frame. Assume that H1), H2), H3) of Lemma 2.15 are satisfied with*

$$B(\theta) = P(\theta+\omega)^{-1}\frac{\partial F_a}{\partial a}(K(\theta)).$$

Then, the only solution of

$$\begin{aligned} \mathrm{D}F_a(K(\theta))\Delta K(\theta) - \Delta K(\theta+\omega) + \frac{\partial F_a}{\partial a}(K(\theta))\Delta a + e(\theta) &= \mathrm{D}E(\theta)\xi^L(\theta), \\ \langle \Delta K^x(\theta)\rangle &= 0, \end{aligned} \tag{2.35}$$

is given by $(\Delta K(\theta) = P(\theta)\xi(\theta), \Delta a)$ *where we get* ξ *and* Δa *as the solutions given by Lemma 2.15 for this particular case, which corresponds to*

$$\Delta a = \langle B^L(\theta) - T(\theta)\mathcal{R}_H B^N(\theta)\rangle^{-1}\langle \eta^L(\theta) - T(\theta)\mathcal{R}_H\eta^N(\theta)\rangle \quad (2.36a)$$

$$\xi^N(\theta) = \mathcal{R}_H\eta^N(\theta) - \mathcal{R}_H B^N(\theta)\Delta a \quad (2.36b)$$

$$\xi^L(\theta) = \bar{\xi^L}(\theta) + \xi_0^L \quad (2.36c)$$

with

$$\bar{\xi^L}(\theta) = \mathcal{R}_\omega(\eta^L(\theta) - B^L(\theta)\Delta a - T(\theta)\xi^N(\theta)),$$
$$\xi_0^L = -\langle \mathrm{D}K^x(\theta)\bar{\xi^L}(\theta) + N^{0,x}(\theta)\xi^N(\theta)\rangle$$

and

$$\eta(\theta) = -P(\theta+\omega)^{-1}e(\theta).$$

PROOF: We write the corrections in terms of $P(\theta)$, and then the proof is immediate:

$$\begin{aligned}\mathrm{D}F_a(K(\theta))P(\theta)\xi(\theta) - P(\theta+\omega)\xi(\theta+\omega) + e(\theta) + \frac{\partial F_a}{\partial a}(K(\theta))\Delta a&\\ =(E_{\mathrm{red}}(\theta) + P(\theta+\omega)\Lambda(\theta))\xi(\theta) - P(\theta+\omega)\xi(\theta+\omega)&\\ \quad - P(\theta+\omega)\eta(\theta) + P(\theta+\omega)B(\theta)&\\ =E_{\mathrm{red}}(\theta)\xi(\theta)&\\ =\mathrm{D}E(\theta)\xi^L(\theta).&\end{aligned}$$

□

Remark 2.17 *In the Newton step,* $e(\theta) = E(\theta)$ *is assumed to be small, and then the error in the solution of the linearized equation* (2.21) *is quadratically small.*

Then, after one Newton step, we have a new error associated to the new solution, which is quadratically small from the previous error, given by the following lemma.

Lemma 2.18 *Let* $\bar{K}(\theta) = K(\theta) + \Delta K(\theta)$ *and* $\bar{a} = a + \Delta a$ *the new approximate solution. Then, the new error of the invariance equation associated to this new solution is of the form*

$$\bar{E}(\theta) = \mathrm{D}E(\theta)\xi^L(\theta) + \int_0^1 (1-t)\mathrm{D}^2F(K(\theta)+t\Delta K(\theta), a+t\Delta a)(\Delta K(\theta), \Delta a)^{\otimes 2}\mathrm{d}t \quad (2.37)$$

Proof: By using the definition of the new solutions and first order Taylor expansions with the integral error formula, the new error is defined as

$$\begin{aligned}\bar{E}(\theta) &= F_{\bar{a}}(\bar{K}(\theta)) - \bar{K}(\theta+\omega)\\ &= F_{a+\Delta a}(K(\theta)+\Delta K(\theta)) - K(\theta+\omega) - \Delta K(\theta+\omega)\\ &= E(\theta) + \mathrm{D}F_a(K(\theta))\Delta K(\theta) + \frac{\partial F_a}{\partial a}(K(\theta))\Delta a - \Delta K(\theta+\omega)\\ &\quad + \int_0^1 (1-t)\mathrm{D}^2F(K(\theta)+t\Delta K(\theta), a+t\Delta a)(\Delta K(\theta),\Delta a)^{\otimes 2}\mathrm{d}t,\end{aligned}$$

and by using Lemma 2.16, it reads as equation (2.37), where D^2F is the second derivative with respect all the variables. □

Summarizing, we can construct an iterative process to compute these invariant tori by using the corrections obtained in previous lemmas.

Algorithm 2.19 (Iterative Scheme) *Let $F : \mathcal{A}\times\mathcal{U} \to \mathbb{T}^d\times\mathbb{R}^n$, $N^0 : \mathbb{T}^d \to \mathbb{R}^{(d+n)\times n}$ and $\omega\in\mathbb{R}^d$ given. Given $K_0 : \mathbb{T}^d \to \mathcal{A}$ and $a_0\in\mathbb{R}^d$, then the iterative scheme has the following form, for $i\geq 0$:*

1) *$E_i(\theta) = F_a(K_i(\theta)) - K_i(\theta+\omega)$,*
2) *Define the frame $P_i(\theta) = (\mathrm{D}K_i(\theta)\ N^0(\theta))$ and compute*

$$\eta_i(\theta) = -P(\theta+\omega)^{-1}E_i(\theta),\quad B_i(\theta) = P(\theta+\omega)^{-1}\frac{\partial F_a}{\partial a}(K_i(\theta))$$

and

$$\begin{pmatrix} T_i(\theta)\\ H_i(\theta)\end{pmatrix} = P_i(\theta+\omega)^{-1}\mathrm{D}F_{a_i}(K_i(\theta))N^0(\theta).$$

3) *Construct the correction of the torus ξ_i and the adjustment of the parameter Δa_i as in equations (2.36) given in Lemma 2.16, with $e(\theta) = E_i(\theta)$:*
   - $\Delta a_i = \langle B_i^L(\theta) - T_i(\theta)\mathcal{R}_{H_i}B_i^N(\theta)\rangle^{-1}\langle\eta_i^L(\theta) - T_i(\theta)\mathcal{R}_{H_i}\eta_i^N(\theta)\rangle$,
   - $\xi_i^N(\theta) = \mathcal{R}_{H_i}\eta_i^N(\theta) - \mathcal{R}_{H_i}B_i^N(\theta)\Delta a_i$,
   - $\xi_i^L(\theta) = \bar{\xi_i^L}(\theta)+\xi_0^L$, *with* $\bar{\xi_i^L}(\theta) = \mathcal{R}_\omega(\eta_i^L(\theta) - B_i^L(\theta)\Delta a_i - T_i(\theta)\xi_i^N(\theta))$ *and* $\xi_0^L = -\langle \mathrm{D}K_i^x(\theta)\bar{\xi_i^L}(\theta) + N^{0,x}(\theta)\xi_i^N(\theta)\rangle$.
4) *Correct the torus and adjust the parameter*
   - $K_{i+1} = K_i + \Delta K_i$,

· $a_{i+1} = a_i + \Delta a_i$.

Remark 2.20 *The procedure leads to efficient algorithms for computing invariant tori. Chapter 3 describes several variants of the algorithm and details of several numerical implementations.*

2.4 The KAM theorem

With these lemmas, we can now introduce our KAM theorem. The convergence of the iterative scheme 2.19 is stated in our KAM-like theorem.

Theorem 2.21 (KAM theorem for NHIT) *Let $\mathcal{B} \subset \mathbb{T}^d_{\mathbb{C}} \times \mathbb{C}^n$ be a complex strip of the annulus $\mathcal{A}$ and $\mathbb{T}^d_\rho$ a complex strip of the torus $\mathbb{T}^d$. Let $F : \mathcal{B} \times \mathcal{U} \to \mathbb{T}^d_{\mathbb{C}} \times \mathbb{C}^n$ be a C^2-family of homotopic to the identity holomorphic maps such that $F(\mathcal{A} \times \mathcal{U}) \subset \mathbb{T}^d \times \mathbb{R}^n$, with $F_a(z) = F(a, z)$.*

Let $N^0 : \bar{\mathbb{T}}^d_\rho \to \mathbb{C}^{(d+n)\times n}$ be a matrix valued map such that $N^0(\mathbb{T}^d) \subset \mathbb{R}^{(d+n)\times n}$ and $N^0 \in (A_\rho)^{(d+n)\times n}$.

Let $K : \bar{\mathbb{T}}^d_\rho \to \mathcal{B} \subset \mathbb{T}^d_{\mathbb{C}} \times \mathbb{C}^n$ be an homotopic to the zero section embedding such that $K(\mathbb{T}^d) \subset \mathcal{A} \subset \mathbb{T}^d \times \mathbb{R}^n$ and that

$$K_p(\theta) = K(\theta) - \begin{pmatrix} \theta \\ 0 \end{pmatrix} \in (A^1_\rho)^{d+n}$$

and assume that $\langle K^x(\theta) - \theta \rangle = 0$. Notice that $\operatorname{dist}(K(\bar{\mathbb{T}}^d_\rho), \partial\mathcal{B}) > 0$. Let $a \in \mathcal{U} \subset \mathbb{R}^d$ be a parameter value. Obviously, $\operatorname{dist}(a, \partial\mathcal{U}) > 0$.

Let $\omega \in \mathbb{R}^d$ be a fixed frequency vector.

Assume that there exists constants:

H1) $c_{F,1,z}$, $c_{F,1,a}$, $c_{F,2}$, c_N *such that*

$$||\mathrm{D}_z F||_{\mathcal{B}\times\mathcal{U}} < c_{F,1,z},\ ||\mathrm{D}_a F||_{\mathcal{B}\times\mathcal{U}} < c_{F,1,a},\ ||\mathrm{D}^2 F||_{\mathcal{B}\times\mathcal{U}} < c_{F,2},$$

and

$$||N^0||_\rho < c_N;$$

H2) σ_L *such that* $||\mathrm{D}K||_\rho < \sigma_L$*;*

H3) (Transversality condition) σ_P *such that* $P = (\mathrm{D}K \mid N^0)$ *is invertible with* $||P^{-1}||_\rho < \sigma_P$*;*

H4) (Hyperbolicity condition) σ_H *such that the cocycle* (H,ω) *is hyperbolic with* $||\mathcal{R}_H||_\rho < \sigma_H$, *where* H *is given by* (2.10)*;*

H5) (Non-degeneracy condition) σ_D *such that the matrix* $\langle B^L - T\mathcal{R}_H B^N\rangle$ *is invertible with*

$$|\langle B^L - T\mathcal{R}_H B^N\rangle^{-1}| < \sigma_D,$$

where T *is given by* (2.10) *and* $B(\theta) = P(\theta+\omega)^{-1}\frac{\partial F_a}{\partial a}(K(\theta))$*;*

H6) (Diophantine condition) γ, τ *such that* $|\omega\cdot q - p| \geq \gamma|q|_1^{-\tau}$, $q \in \mathbb{Z}^d\setminus\{0\}$ *and* $p \in \mathbb{Z}$.

Define $E(\theta) = F_a(K(\theta)) - K(\theta+\omega)$.

Then, for any $0 < \delta < \frac{\rho}{2}$ *and* $0 < \rho_\infty < \rho - 2\delta$, *there exists constants* $\hat{C}_*$, $\hat{C}_{**}$ *and* $\hat{C}_{***}$ *(depending explicitly on initial data,* δ *and* ρ_∞*) such that:*

T1) Existence*: If the following condition holds*

$$\frac{\hat{C}_*||E||_\rho}{\gamma^2\rho^{2\tau}} < 1, \tag{2.38}$$

then, there exists a couple (K_∞, a_∞), *with* $K_\infty : \bar{\mathbb{T}}^d_{\rho_\infty} \to \mathcal{B} \subset \mathbb{T}^d_{\mathbb{C}} \times \mathbb{C}^n$ *such that*

$$K_\infty(\theta) - \begin{pmatrix}\theta\\ 0\end{pmatrix} \in (A^1_{\rho_\infty})^n,$$

and $a_\infty \in \mathcal{U}$ *, such that*

$$\begin{aligned} F_{a_\infty}(K_\infty(\theta)) &= K_\infty(\theta+\omega),\\ \langle K^x_\infty(\theta) - \theta\rangle &= 0. \end{aligned}$$

That is, $\mathcal{K}_\infty = K_\infty(\mathbb{T}^d)$ *is a QP-NHIT for* F_{a_∞} *with frequency* ω. *Moreover,* K_∞ *satisfies hypothesis H2-H5.*

T2) Closeness*: The torus* $\mathcal{K}_\infty$ *is close to the original approximation, in the sense that*

$$||(K_\infty - K, a_\infty - a)||_{\rho_\infty} \leq \frac{\hat{C}_{**}}{\gamma\rho^\tau}||E||_\rho. \tag{2.39}$$

T3) Local Uniqueness*: If the following condition holds*

$$\frac{\hat{C}_{***}}{\gamma^2\rho_\infty^\tau\rho^\tau}||E||_\rho < 1, \tag{2.40}$$

then, if (K'_∞, a'_∞) *satisfies*

$$F_{a'_\infty}(K'_\infty(\theta)) = K'_\infty(\theta+\omega),$$
$$\langle K'^x_\infty(\theta) - \theta\rangle = 0.$$

and

$$||(K'_\infty - K, a'_\infty - a)||_{\rho_\infty} < \hat{C}_{**}\left(\frac{\gamma\rho_\infty^\tau}{\hat{C}_{***}} - \frac{1}{\gamma\rho^\tau}||E||_\rho\right), \tag{2.41}$$

then, $(K'_\infty, a'_\infty) = (K_\infty, a_\infty)$.

The proof consist in proving that the iterative scheme of Algorithm 2.19 converges to a solution of the invariance equation. Notice that at each iterative step, we have to be careful with the analicity properties of new objects in order to well construct the new approximately invariant torus and parameter. In particular, at each Newton step i, it is reduced the analicity strip of the objects. It is proved in the following Lemma.

Remark 2.22 *The constants* $\hat{C}_*$, $\hat{C}_{**}$ *and* $\hat{C}_{***}$ *depend explicitly on the initial data. Concretely, they depend polynomially on* $c_{F,1,z}$, $c_{F,1,a}$, $c_{F,2}$, c_N *and on* $(\sigma_L - ||\mathrm{D}K||_\rho)^{-1}$, $(\sigma_P - ||P^{-1}||_\rho)^{-1}$, $(\sigma_D - |\langle B^L - T\mathcal{R}_H(B^N)\rangle^{-1}|)^{-1}$, $(\sigma_H - ||\mathcal{R}_H||_{\rho'})^{-1}$, $\mathrm{dist}(K(\mathbb{T}^d_\rho), \partial\mathcal{B})^{-1}$ *and* $\mathrm{dist}(a, \partial\mathcal{U})^{-1}$. *They also depend polynomially on the estimates given by the definition of the objects,* σ_L, σ_P, σ_H *and* σ_D. *If we fix the constant* c_R *in Lemma 2.10 (that depends on* τ *in a non-polynomial way) then* $\hat{C}_*$, $\hat{C}_{**}$ *and* $\hat{C}_{***}$ *depend also polynomially on the dimension* d, c_R, γ *and on powers of the initial bite of the width of analycity* δ.

Lemma 2.23 (Iterative Lemma) *Under the same hypothesis H1-H6 of Theorem 2.21, for any* $0 < \delta < \frac{\rho}{2}$, *there exists constants* $\hat{C}_1$, $\hat{C}_2$, $\hat{C}_3$, $\hat{C}_4$, $\hat{C}_5$, $\hat{C}_6$, $\hat{C}_7$, *depending explicitly on constants defined in the hypothesis and on* δ, *such that if*

$$\frac{\hat{C}_1}{\gamma\delta^{\tau+1}}||E||_\rho < 1, \tag{2.42}$$

then there exists an approximately invariant torus $\bar{K} = K + \Delta K$ *of frequency* ω *for some* $\bar{a} = a + \Delta a$, *in the sense that the new error* $\bar{E}(\theta) = F_{\bar{a}}(\bar{K}(\theta)) - \bar{K}(\theta+\omega)$ *will satisfy*

$$||\bar{E}||_{\rho-\delta} < \frac{\hat{C}_7}{\gamma^2\delta^{2\tau}}||E||^2_\rho. \tag{2.43}$$

In particular, this new torus will define new objects $\bar{P}$, $\bar{T}$, $\bar{H}$ such that satisfies the conditions of Theorem 2.21

$$||\mathrm{D}\bar{K}||_{\rho-2\delta} < \sigma_L, \qquad ||\bar{P}^{-1}||_{\rho-2\delta} < \sigma_P, \tag{2.44}$$

$$||\mathcal{R}_{\bar{H}}||_{\rho} < \sigma_H, \qquad |\langle \bar{B}^L - \bar{T}\mathcal{R}_{\bar{H}}\bar{B}^N\rangle^{-1}| < \sigma_D, \tag{2.45}$$

$$\mathrm{dist}(\bar{K}(\mathbb{T}^d_{\rho-\delta}), \partial\mathcal{B}) > 0, \qquad \mathrm{dist}(\bar{a}, \partial\mathcal{U}) > 0, \tag{2.46}$$

and

$$||\bar{K} - K||_{\rho-\delta} < \frac{\hat{C}_2}{\gamma\delta^\tau}||E||_\rho, \qquad |\bar{a} - a| < \hat{C}_3||E||_\rho, \tag{2.47}$$

$$||\bar{P}^{-1} - P^{-1}||_{\rho-2\delta} < \frac{\hat{C}_4}{\gamma\delta^{\tau+1}}||E||_\rho, \tag{2.48}$$

$$||\mathcal{R}_{\bar{H}} - \mathcal{R}_H||_{\rho'} < \frac{\hat{C}_5}{\gamma\delta^{\tau+1}}||E||_\rho, \text{ for all } \rho' \le \rho - 2\delta, \tag{2.49}$$

$$|\langle \bar{B}^L - \bar{T}\mathcal{R}_{\bar{H}}\bar{B}^N\rangle^{-1} - \langle B^L - T\mathcal{R}_H B^N\rangle^{-1}| < \frac{\hat{C}_6}{\gamma\delta^{\tau+1}}||E||_\rho. \tag{2.50}$$

Remark 2.24 *The explicit form of the constants, discussed on remark 2.22, will appear during the proof of the Theorem. These are useful for implementation on computer assisted proofs.*

The scheme of the proofs of this section follows the same KAM-like strategy used in the proof of the Theorem 4.22 of Chapter 4 of [53] and it is intended to lead to computer assisted proofs.

Proof: From the definition of the reducibility error $||E_{\mathrm{red}}||$ in (2.24) and from Cauchy estimates (2.12), we obtain directly

$$||E_{\mathrm{red}}||_{\rho-\delta} = ||\mathrm{D}E||_{\rho-\delta} \le \frac{d}{\delta}||E||_\rho \tag{2.51}$$

Now, we can proceed to bound the corrections we get during a Newton step, given by equations (2.28c) and (2.28b) of Lemma 2.15.

Let us start with the normal cohomological equation, which has solution (2.28b). Observe that by (2.19) for $\eta(\theta) = -P(\theta+\omega)^{-1}E(\theta)$, we control operator $\mathcal{R}_H$ by

$$||\mathcal{R}_H(\eta^N(\theta))||_\rho < \sigma_H\sigma_P||E||_\rho$$
$$||\mathcal{R}_H(B^N(\theta))||_\rho < \sigma_H\sigma_P c_{F,1,a}$$

and the correction of the parameter a by

$$\begin{aligned} |\Delta a| &< \sigma_D(|\langle \eta^L(\theta)\rangle| + |\langle T(\theta)\mathcal{R}_H(\eta^N(\theta))\rangle|) \\ &< \sigma_D(\sigma_P||E||_\rho + \sigma_P\sigma_{F,1,z}c_N\sigma_H\sigma_P||E||_\rho) < \sigma_D\sigma_P C_1||E||_\rho, \end{aligned} \tag{2.52}$$

where

$$C_1 := 1 + \sigma_H\sigma_P c_N c_{F,1,z}.$$

Then, we get an estimate for the normal correction of the torus by

$$||\xi^N||_\rho < ||\mathcal{R}_H(\eta^N(\theta))||_\rho + ||\mathcal{R}_H(B^N(\theta))||\Delta a| < \sigma_H\sigma_P C_2||E||_\rho, \tag{2.53}$$

where

$$C_2 := 1 + \sigma_P\sigma_D c_{F,1,a}C_1.$$

On the other side, the tangent component has solution (2.28b), and by Russmann estimates (2.17) applied to $v(\theta) = \eta^L(\theta) - B^L(\theta)\Delta a - T(\theta)\xi^N(\theta)$, we obtain the inequality

$$\begin{aligned} ||\bar{\xi^L}||_{\rho-\delta} &\leq \frac{c_R}{\gamma\delta^\tau}||v||_\rho < \frac{c_R}{\gamma\delta^\tau}(\sigma_P||E||_\rho + \sigma_P c_{F,1,a}|\Delta a| + \sigma_P c_N c_{F,1,z}||\xi^N||_\rho) \\ &< \frac{c_R}{\gamma\delta^\tau}\sigma_P C_1 C_2||E||_\rho. \end{aligned}$$

We consider the term ξ_0^L defined in equation (2.34), and we rewrite last inequality as

$$\begin{aligned} ||\xi^L||_{\rho-\delta} &\leq |\xi_0^L| + ||\bar{\xi^L}||_{\rho-\delta} \leq \sigma_L||\bar{\xi^L}||_{\rho-\delta} + c_N||\xi^N||_{\rho-\delta} + ||\bar{\xi^L}||_{\rho-\delta} \\ &< \frac{1}{\gamma\delta^\tau}(\underbrace{(\sigma_L+1)c_R\sigma_P C_1 C_2 + c_N\sigma_H\sigma_P C_2\gamma\delta^\tau}_{C_3})||E||_\rho. \end{aligned} \tag{2.54}$$

As has been said, the correction of the torus is of the form $\Delta K(\theta) = P(\theta)\xi(\theta)$. Then, the first estimate of (2.47) follows directly from (2.53) and (2.54) in the following way

$$\begin{aligned} ||\bar{K} - K||_{\rho-\delta} &= ||\Delta K||_{\rho-\delta} = ||\mathrm{D}K(\theta)\xi^L(\theta) + N(\theta)\xi^N(\theta)||_{\rho-\delta} \\ &< \left(\sigma_L\frac{C_3}{\gamma\delta^\tau} + C_N\sigma_H\sigma_P C_2\right)||E||_\rho := \frac{\hat{C}_2}{\gamma\delta^\tau}||E||_\rho. \end{aligned} \tag{2.55}$$

Using expression (2.55) and Cauchy estimates (2.12) , we obtain the first estimate on (2.44):

$$||\mathrm{D}\bar{K}||_{\rho-2\delta} \leq ||\mathrm{D}\bar{K}||_\rho + ||\mathrm{D}\Delta K||_{\rho-2\delta} < ||\mathrm{D}\bar{K}||_\rho + \frac{d}{\delta}\frac{\hat{C}_2}{\gamma\delta^\tau}||E||_\rho < \sigma_L, \tag{2.56}$$

where last inequality is imposed in order to satisfy inequality (2.42) of the hypothesis, so then

$$\frac{d\hat{C}_2}{\sigma_L - ||\mathrm{D}K||_\rho} \frac{1}{\gamma\delta^{\tau+1}} ||E||_\rho < 1, \tag{2.57}$$

which is included in the definition of $\hat{C}_1$.

Note that the second estimate of (2.47) has been already computed in equation (2.52), since

$$|\bar{a} - a| = |\Delta a| < \hat{C}_3 ||E||_\rho, \tag{2.58}$$

with

$$\hat{C}_3 := \sigma_D \sigma_P C_1.$$

In particular, we will define $\hat{C}_{2,3}$ as

$$\hat{C}_{2,3} := \max(\hat{C}_2, \hat{C}_3 \gamma \delta^\tau).$$

Observe that, to get conditions (2.46) of the hypothesis of the lemma satisfied, we need

$$\begin{aligned} \operatorname{dist}(\bar{K}(\bar{\mathbb{T}}^d_{\rho-\delta}), \partial\mathcal{B}) &\geq \operatorname{dist}(K(\bar{\mathbb{T}}^d_\rho), \partial\mathcal{B}) - ||\Delta K||_{\rho-\delta} \\ &\geq \operatorname{dist}(K(\bar{\mathbb{T}}^d_\rho), \partial\mathcal{B}) - \frac{\hat{C}_2}{\gamma\delta^\tau} ||E||_\rho > 0, \end{aligned}$$

and

$$\operatorname{dist}(\bar{a}, \partial\mathcal{U}) \geq \operatorname{dist}(a, \partial\mathcal{U}) - |\Delta a| \geq \operatorname{dist}(a, \partial\mathcal{U}) - \hat{C}_3 ||E||_\rho > 0,$$

so that $\bar{K}(\bar{\mathbb{T}}^d_{\rho-\delta}) \subset \partial\mathcal{B}$ and $\bar{a} \in \mathcal{U}$. Notice that these inequalities are satisfied if

$$\frac{\hat{C}_2}{\gamma\delta^\tau \operatorname{dist}(K(\mathbb{T}^d_\rho), \partial\mathcal{B})} ||E||_\rho < 1 \tag{2.59}$$

and

$$\frac{\hat{C}_3}{\operatorname{dist}(a, \partial\mathcal{U})} ||E||_\rho < 1. \tag{2.60}$$

These two last conditions (2.59) and (2.60) are included in the definition of $\hat{C}_1$.

To control the computations that involves inverses, such as $||\bar{P}^{-1} - P^{-1}||$, $||\mathcal{R}_{\bar{H}} - \mathcal{R}_H||$ and $|\langle \bar{B}^L - \bar{T}\mathcal{R}_{\bar{H}} \bar{B}^N \rangle^{-1} - \langle B^L - T\mathcal{R}_H B^N \rangle^{-1}|$, we use the following statement: for any pair of matrices X and Y, with X invertible, we can express the inverse of Y, provided that Y is close enough to X, by

$$Y^{-1} = (I + X^{-1}(Y - X))^{-1} X^{-1}.$$

Then, using Neumann series, we can use the following inequality

$$||Y^{-1} - X^{-1}|| \leq \frac{||X^{-1}||^2||Y - X||}{1 - ||X^{-1}||||Y - X||}. \tag{2.61}$$

First, we use expression (2.61) for $X = P$ and $Y = \bar{P}$ satisfying

$$\begin{aligned} ||\bar{P}^{-1} - P^{-1}||_{\rho-2\delta} &\leq \frac{||P^{-1}||^2_{\rho-2\delta}||\bar{P} - P||_{\rho-2\delta}}{1 - ||P^{-1}||_{\rho-2\delta}||\bar{P} - P||_{\rho-2\delta}} \\ &< \frac{\sigma_P^2||\bar{P} - P||_{\rho-2\delta}}{1 - \sigma_P||\bar{P} - P||_{\rho-2\delta}}, \end{aligned} \tag{2.62}$$

where it is assumed that $\sigma_P||\bar{P} - P||_{\rho-2\delta} < 1$.

Recall that the normal bundle is fixed during the Newton iteration. Then, using computations in (2.56) we obtain

$$\begin{aligned} ||\bar{P} - P||_{\rho-2\delta} &= ||(\mathrm{D}\bar{K} \mid N^0) - (\mathrm{D}K \mid N^0)||_{\rho-2\delta} = ||(\mathrm{D}\bar{K} - \mathrm{D}K \mid 0)||_{\rho-2\delta} \\ &= ||\mathrm{D}\Delta K||_{\rho-2\delta} < \frac{d\hat{C}_2}{\gamma\delta^{\tau+1}}||E||_\rho. \end{aligned} \tag{2.63}$$

To satisfy $\sigma_P||\bar{P} - P||_{\rho-2\delta} < 1$, we in fact impose

$$\sigma_P||\bar{P} - P||_{\rho-2\delta} < \sigma_P\frac{d\hat{C}_2}{\gamma\delta^{\tau+1}}||E||_\rho < \frac{1}{2}. \tag{2.64}$$

Using (2.63) and (2.64) in (2.62), we obtain estimate (2.48)

$$||\bar{P}^{-1} - P^{-1}||_{\rho-2\delta} < \frac{2\sigma_P^2 d\hat{C}_2}{\gamma\delta^{\tau+1}}||E||_\rho := \frac{\hat{C}_4}{\gamma\delta^{\tau+1}}||E||_\rho, \tag{2.65}$$

and writing $\bar{P}^{-1}$ as $\bar{P}^{-1} = P^{-1} + (\bar{P}^{-1} - P^{-1})$ we obtain the second estimate on (2.44)

$$||\bar{P}^{-1}||_{\rho-2\delta} < ||P^{-1}||_{\rho-2\delta} + \frac{\hat{C}_4}{\gamma\delta^{\tau+1}}||E||_\rho < \sigma_P \tag{2.66}$$

where last inequality is obtained by imposing

$$\frac{\hat{C}_4}{\sigma_P - ||P^{-1}||_\rho}\frac{1}{\gamma\delta^{\tau+1}}||E||_\rho < 1, \tag{2.67}$$

that has to be included in the computation of $\hat{C}_1$. Notice that (2.67) implies (2.64).

To obtain the inequality (2.49), we will use again Neumann series, using now that $\mathcal{R}_H = (\mathcal{H} - \mathrm{Id})^{-1}$

$$||\mathcal{R}_{\bar{H}} - \mathcal{R}_H||_{\rho'} = ||(\bar{\mathcal{H}} - \mathrm{Id})^{-1} - (\mathcal{H} - \mathrm{Id})^{-1}||_{\rho'}$$

$$\leq \frac{||(\mathcal{H} - \mathrm{Id})^{-1}||^2_{\rho'} ||\mathcal{H} - \mathcal{H}||^2_{\rho'}}{1 - ||(\mathcal{H} - \mathrm{Id})^{-1}||_{\rho'} ||\mathcal{H} - \mathcal{H}||_{\rho'}}, \tag{2.68}$$

where

$$||\bar{\mathcal{H}} - \mathcal{H}||_{\rho'} = ||\bar{H} - H||_{\rho'} \leq ||\bar{H} - H||_{\rho - 2\delta},$$

for any $\rho' \leq \rho - 2\delta$.

Observe that,

$$\begin{aligned} ||\mathrm{D}_z F(\bar{K}(\theta),\bar{a}) - \mathrm{D}_z F(K(\theta), a)||_{\rho-\delta} = \\ =&|| \int_0^1 \frac{\mathrm{d}}{\mathrm{d}t} \left(\mathrm{D}_z F(K(\theta) + t\Delta K(\theta), a + t\Delta a)\right) \mathrm{d}t||_{\rho-\delta} \\ =&|| \int_0^1 \left(\mathrm{D}_{zz} F(K(\theta) + t\Delta K(\theta), a + t\Delta a)\Delta K(\theta)\right. \\ &\left. + \mathrm{D}_{za} F(K(\theta) + t\Delta K(\theta), a + t\Delta a)\Delta a\right) \mathrm{d}t||_{\rho-\delta} \\ \leq& ||\mathrm{D}^2 F||_{\rho-\delta} ||(\Delta K, \Delta a)||_{\rho-\delta}. \end{aligned} \tag{2.69}$$

Note that to control $||\bar{H} - H||_{\rho-2\delta}$, we have to control the matrix map

$$\left\| \begin{pmatrix} \bar{T} \\ \bar{H} \end{pmatrix} - \begin{pmatrix} T \\ H \end{pmatrix} \right\|_{\rho-2\delta}$$

which comes directly from the definition (2.10) and from estimates (2.65),

(2.55) and (2.69). Then, it reads as

$$\begin{aligned}
&\left|\left|\begin{pmatrix}\bar{T}\\ \bar{H}\end{pmatrix}-\begin{pmatrix}T\\ H\end{pmatrix}\right|\right|_{\rho-2\delta}\\
&\quad\leq||\bar{P}(\theta+\omega)^{-1}\mathrm{D}F_{\bar{a}}(\bar{K}(\theta))-P(\theta+\omega)^{-1}\mathrm{D}F_a(K(\theta))||_{\rho-2\delta}||N^0(\theta)||_{\rho-2\delta}\\
&\quad< c_N\Big(||\bar{P}(\theta+\omega)^{-1}||_{\rho-2\delta}||\mathrm{D}F_{\bar{a}}(\bar{K}(\theta))-\mathrm{D}F_a(K(\theta))||_{\rho-2\delta}\\
&\qquad+||\bar{P}(\theta+\omega)^{-1}-P(\theta+\omega)^{-1}||_{\rho-2\delta}||\mathrm{D}F(K(\theta))||_{\rho-2\delta}\Big)\\
&\quad< c_N\Big(\sigma_P||\mathrm{D}^2F||_{\mathcal{B}\times\mathcal{U}}||(\Delta K,\Delta a)||_{\rho-2\delta}+||\bar{P}^{-1}-P^{-1}||_{\rho-2\delta}||\mathrm{D}F_a||_{\mathcal{B}\times\mathcal{U}}\Big)\\
&\quad<\underbrace{c_N\Big(\sigma_P c_{F,2}\hat{C}_{2,3}\delta+c_{F,1,z}\hat{C}_4\Big)}_{C_4}\frac{||E||_\rho}{\gamma\delta^{\tau+1}}.
\end{aligned}\tag{2.70}$$

So, if we assume

$$\sigma_H||\bar{H}-H||_{\rho-2\delta}<\sigma_H C_4\frac{||E||_\rho}{\gamma\delta^{\tau+1}}<\frac{1}{2}\tag{2.71}$$

then, inequality (2.68) becomes

$$||\mathcal{R}_{\bar{H}}-\mathcal{R}_H||_{\rho'}<\frac{2\sigma_H^2C_4}{\gamma\delta^{\tau+1}}||E||_\rho:=\hat{C}_5\frac{||E||_\rho}{\gamma\delta^{\tau+1}}\tag{2.72}$$

and using $\mathcal{R}_{\bar{H}}=\mathcal{R}_H+(\mathcal{R}_{\bar{H}}-\mathcal{R}_H)$ we obtain the first estimate on (2.45)

$$||\mathcal{R}_{\bar{H}}||_{\rho'}<||\mathcal{R}_H||_{\rho'}+\frac{\hat{C}_5}{\gamma\delta^{\tau+1}}||E||_\rho<\sigma_H\tag{2.73}$$

by imposing last inequality, for all $\rho'\leq\rho-2\delta$. Then

$$\frac{\hat{C}_5}{\sigma_H-||\mathcal{R}_H||_{\rho'}}\frac{1}{\gamma\delta^{\tau+1}}||E||_\rho<1,\tag{2.74}$$

which as before, we have to introduce in the definition of $\hat{C}_1$.

From the definition of B and estimates (2.55), (2.58), (2.65) and (2.69) , we

obtain

$$\begin{aligned}
&||\bar{B}(\theta)-B(\theta)||_{\rho-2\delta}\\
&\quad=||\bar{P}(\theta+\omega)^{-1}\frac{\partial F_{\bar{a}}}{\partial a}(\bar{K}(\theta))-P(\theta+\omega)^{-1}\frac{\partial F_a}{\partial a}(K(\theta))||_{\rho-2\delta}\\
&\quad\leq||(\bar{P}(\theta+\omega)^{-1}-P(\theta+\omega)^{-1})\frac{\partial F_{\bar{a}}}{\partial a}(\bar{K}(\theta))||_{\rho-2\delta}\\
&\qquad+||P(\theta+\omega)^{-1}\left(\frac{\partial F_{\bar{a}}}{\partial a}(\bar{K}(\theta))-\frac{\partial F_a}{\partial a}(K(\theta))\right)||_{\rho-2\delta}\\
&\quad\leq\frac{\hat{C}_4}{\gamma\delta^{\tau+1}}||E||_\rho c_{F,1,a}+\sigma_P c_{F,2}||(\Delta K,\Delta a)||_{\rho-2\delta}||E||_\rho\\
&\quad\leq\left(\hat{C}_4 c_{F,1,a}+\sigma_P c_{F,2}\hat{C}_{2,3}\delta\right)\frac{1}{\gamma\delta^{\tau+1}}||E||_\rho\\
&\quad:=\frac{C_5}{\gamma\delta^{\tau+1}}||E||_\rho.
\end{aligned}\tag{2.75}$$

Otherwise, from the definition of B, T and $\mathcal{R}_H$ and inequalities (2.75), (2.70) and (2.72) we obtain

$$\begin{aligned}
&|\langle\bar{B}^L-\bar{T}\mathcal{R}_{\bar{H}}(\bar{B}^N)\rangle-\langle B^L-T\mathcal{R}_H(B^N)\rangle|\\
&\quad\leq|\langle\bar{B}^L-B^L\rangle|+|\langle(T-\bar{T})\mathcal{R}_{\bar{H}}(\bar{B}^N)\rangle|+|\langle T\mathcal{R}_H(\bar{B}^N-B^N)\rangle|\\
&\qquad+|\langle T(\mathcal{R}_H-\mathcal{R}_{\bar{H}})(\bar{B}^N)\rangle|\\
&\quad\leq\frac{C_5}{\gamma\delta^{\tau+1}}||E||_\rho+\frac{C_4}{\gamma\delta^{\tau+1}}||E||_\rho\sigma_H\sigma_P c_{F,1,a}+\sigma_P c_{F,1,z}c_N\sigma_H\frac{C_5}{\gamma\delta^{\tau+1}}||E||_\rho\\
&\qquad+\sigma_P c_{F,1,z}c_N\frac{\hat{C}_5}{\gamma\delta^{\tau+1}}||E||_\rho\sigma_P c_{F,1,a}:=\frac{C_6}{\gamma\delta^{\tau+1}}||E||_\rho.
\end{aligned}\tag{2.76}$$

To find the inequality (2.50) we use again Neumann series as follows

$$\begin{aligned}
&|\langle\bar{B}^L-\bar{T}\mathcal{R}_{\bar{H}}(\bar{B}^N)\rangle^{-1}-\langle B^L-T\mathcal{R}_H(B^N)\rangle^{-1}|\\
&\leq\frac{|\langle B^L-T\mathcal{R}_H(B^N)\rangle^{-1}|^2|\langle\bar{B}^L-\bar{T}\mathcal{R}_{\bar{H}}(\bar{B}^N)\rangle-\langle B^L-T\mathcal{R}_H(B^N)\rangle|}{1-|\langle B^L-T\mathcal{R}_H(B^N)\rangle^{-1}||\langle\bar{B}^L-\bar{T}\mathcal{R}_{\bar{H}}(\bar{B}^N)\rangle-\langle B^L-T\mathcal{R}_H(B^N)\rangle|}
\end{aligned}\tag{2.77}$$

If we assume

$$\sigma_D|\langle\bar{B}^L-\bar{T}\mathcal{R}_{\bar{H}}(\bar{B}^N)\rangle-\langle B^L-T\mathcal{R}_H(B^N)\rangle|<\frac{C_6}{\gamma\delta^{\tau+1}}||E||_\rho<\frac{1}{2}\tag{2.78}$$

then, inequality (2.77) becomes

$$|\langle \bar{B}^L - \bar{T}\mathcal{R}_{\bar{H}}(\bar{B}^N)\rangle^{-1} - \langle B^L - T\mathcal{R}_H(B^N)\rangle^{-1}|$$

$$< 2\sigma_D^2 \frac{C_6}{\gamma\delta^{\tau+1}}||E||_\rho := \frac{\hat{C}_6}{\gamma\delta^{\tau+1}}||E||_\rho \tag{2.79}$$

and we obtain second estimate on (2.45)

$$\begin{aligned}
&|\langle \bar{B}^L - \bar{T}\mathcal{R}_{\bar{H}}(\bar{B}^N)\rangle^{-1}| \\
&\quad \leq |\langle B^L - T\mathcal{R}_H(B^N)\rangle^{-1}| + |\langle \bar{B}^L - \bar{T}\mathcal{R}_{\bar{H}}(\bar{B}^N)\rangle^{-1} - \langle B^L - T\mathcal{R}_H(B^N)\rangle^{-1}| \\
&\quad < |\langle B^L - T\mathcal{R}_H(B^N)\rangle^{-1}| + \frac{\hat{C}_6}{\gamma\delta^{\tau+1}}||E||_\rho < \sigma_D,
\end{aligned} \tag{2.80}$$

by imposing the last inequality, and then we get

$$\frac{\hat{C}_6}{\sigma_D - |\langle B^L - T\mathcal{R}_H(B^N)\rangle^{-1}|}\frac{1}{\gamma\delta^{\tau+1}}||E||_\rho < 1, \tag{2.81}$$

which will be included in the definition of $\hat{C}_1$.

Finally, we need to proof that the new error $\bar{E}$ is quadratically small in E. Observe first, that, by Lemma 2.18, the error $\bar{E}$ can be expressed as:

$$\bar{E}(\theta) = \mathrm{D}E(\theta)\xi^L(\theta) + \int_0^1 (1-t)\mathrm{D}^2F(K(\theta)+t\Delta K(\theta), a+t\Delta a)(\Delta K(\theta), \Delta a)^{\otimes 2}\mathrm{d}t.$$

Then, using (2.54), (2.55), (2.58) and Cauchy estimates (2.12) we get

$$\begin{aligned}
||\bar{E}||_{\rho-\delta} &\leq \frac{d}{\delta}||E||_\rho \frac{c_R C_3}{\gamma\delta^\tau}||E||_\rho + \frac{1}{2}c_{F,2}||(\Delta K, \Delta a)||^2_{\rho-\delta} \\
&\leq \left(\frac{dc_R C_3}{\gamma\delta^{\tau+1}} + \frac{1}{2}\frac{c_{F,2}\hat{C}_{2,3}^2}{\gamma^2\delta^{2\tau}}\right)||E||^2_\rho \\
&:= \frac{\hat{C}_7}{\gamma^2\delta^{2\tau}}||E||^2_\rho,
\end{aligned} \tag{2.82}$$

which proves the lemma.

But even more, we can obtain explicitly the value $\hat{C}_1$ of the hypothesis, assuming that it has to satisfy all conditions (2.57), (2.67), (2.74), (2.81),

(2.59) and (2.60) we have imposed during the proof of the lemma. So, we can define $\hat{C}_1$ as the maximum of all these constants of all previous inequalities:

$$\hat{C}_1 := \max\left\{ \frac{d\hat{C}_2}{\sigma_L - ||\mathrm{D}K||_\rho}, \frac{\hat{C}_4}{\sigma_P - ||P^{-1}||_\rho}, \frac{\hat{C}_5}{\sigma_H - ||\mathcal{R}_H||_{\rho'}}, \right. \\ \left. \frac{\hat{C}_6}{\sigma_D - |\langle B^L - T\mathcal{R}_H(B^N)\rangle^{-1}|}, \frac{\hat{C}_2\delta}{\mathrm{dist}(K(\mathbb{T}^d_\rho), \partial\mathcal{B})}, \frac{\hat{C}_3\delta^{\tau+1}\gamma}{\mathrm{dist}(a, \partial\mathcal{U})} \right\} \tag{2.83}$$

□

This previous iterative lemma has covered all the analycity aspects on one Newton step. We can prove Theorem 2.21, in which we will prove the convergence (so the existence) using the results of previous Lemma 2.23 and the local uniqueness.

PROOF: [Proof of *T1)* in Theorem 2.21: *Existence*]
Let $K_0 = K$ and $a_0 = a$, an approximate solution with error $E_0 = F_{a_0}(K_0(\theta)) - K_0(\theta + \omega)$, for an adapted frame $P_0 = (\mathrm{D}K_0 \mid N^0)$, with N^0 fixed along the iterative process.

By the Iterative Lemma 2.23, we know that at each Newton step the domain of analycity of the objects is reduced. Given $0 < \delta_0 < \frac{\rho}{2}$ and $0 < \rho_\infty < \rho - 2\delta_0$, we define $a_3 = \frac{\rho_0}{\delta_0} > 2$, $a_2 = \frac{\rho_0}{\rho_\infty} > 1$ and

$$a_1 = \frac{\rho_0 - \rho_\infty}{\rho_0 - 2\delta_0 - \rho_\infty} > 1.$$

Constants a_1, a_2 and a_3 satisfy

$$a_3 = 2\frac{a_1}{a_1 - 1}\frac{a_2}{a_2 - 1} > 2.$$

Then, the sequence of widths

$$\rho_0 = \rho,$$
$$\rho_s = \rho_{s-1} - 2\delta_{s-1},$$

where $\delta_s = \frac{\delta_0}{a_1^s}$, converges to the final width of the analycity strip

$$\rho_0 - 2\delta_0 \sum_{s=0}^{\infty} \frac{1}{a_1^s} = \rho_\infty.$$

Remark 2.25 *This generality is suitable for finding "applicable" values of a_1, a_2 and a_3, or equivalently δ_0, ρ_0 and ρ_∞, for computer assisted proofs, in the spirit of Chapter 3 of [53].*

Denote by K_s, a_s, E_s, T_s, H_s, B_s the objects at the s-step. Notice that, at each Newton step, the condition (2.42) is required to be satisfied, but in this case, the construction is performed in such a way that we have to control objects, at each step, with respect to ρ_s. In particular, the constants $\hat{C}_i$, $i = 1, \dots, 7$, that appear in the Iterative Lemma 2.23 can be taken to be the same for all steps by considering the worst value of δ_s, that is, δ_0.

Now, we proceed by induction. We suppose that we have applied s times the Iterative Lemma 2.23, so we have to verify that it can be applied again. We first need to compute the error E_s in terms of E_0. Observe that E_s reads in terms of E_{s-1} in the following way

$$||E_s||_{\rho_s} < \frac{\hat{C}_7}{\gamma^2 \delta_{s-1}^{2\tau}} ||E_{s-1}||^2_{\rho_{s-1}} = \frac{\hat{C}_7}{\gamma^2 \delta_0^{2\tau}} a_1^{2\tau(s-1)} ||E_{s-1}||^2_{\rho_{s-1}},$$

so then, by iterating the process until E_0 and using that $1 + 2 + \cdots + 2^{s-1} = 2^s - 1$ and $1(s-1) + 2(s-2) + \cdots + 2^{s-2}1 = 2^s - s - 1$, we obtain

$$||E_s||_{\rho_s} < \left(\frac{\hat{C}_7}{\gamma^2 \delta_0^{2\tau}} a_1^{2\tau} ||E_0||_{\rho_0} \right)^{2^s - 1} a_1^{-2\tau s} ||E_0||_{\rho_0}, \tag{2.84}$$

Notice that, to obtain a decreasing sequence of the error, it suffices to assume that

$$\frac{\hat{C}_7}{\gamma^2 \delta_0^{2\tau}} a_1^{2\tau} ||E_0||_{\rho_0} < 1, \tag{2.85}$$

and then we get

$$||E_s||_{\rho_s} < a_1^{-2\tau s} ||E_0||_{\rho_0}. \tag{2.86}$$

This condition (2.85) has to be imposed in the definition of $\hat{C}_*$ in (2.38).

Now, we have to verify all conditions included on (2.42). For instance, equation (2.42)

$$\begin{aligned} ||\mathrm{D}K_s||_{\rho_s} + \frac{d\hat{C}_2}{\gamma \delta_s^{\tau+1}} ||E_s||_{\rho_s} &< ||\mathrm{D}K_0||_{\rho_0} + \sum_{j=0}^{s} \frac{d\hat{C}_2}{\gamma \delta_j^{\tau+1}} ||E_j||_{\rho_j} \\ &< ||\mathrm{D}K_0||_{\rho_0} + \frac{d\hat{C}_2}{\gamma \delta_0^{\tau+1}} ||E_0||_{\rho_0} \sum_{j=0}^{\infty} a_1^{(1-\tau)j} \\ &= ||\mathrm{D}K_0||_{\rho_0} + \frac{d\hat{C}_2}{\gamma \delta_0^{\tau+1}} \frac{1}{1 - a_1^{1-\tau}} ||E_0||_{\rho_0} < \sigma_L, \end{aligned} \tag{2.87}$$

where last inequality is included in (2.38). In the same way, we obtain the following inequalities to guarantee all conditions involved on (2.42), which reads as follows:

$$\begin{aligned}\operatorname{dist}(K_s(\mathbb{T}^d_{\rho_s}),\partial\mathcal{B}) - \frac{\hat{C}_2}{\gamma\delta_s^\tau}||E_s||_{\rho_s} \\ > \operatorname{dist}(K_0(\mathbb{T}^d_{\rho_0}),\partial\mathcal{B}) - \frac{\hat{C}_2}{\gamma\delta_0^\tau}\frac{1}{1-a_1^{-\tau}}||E_0||_{\rho_0} > 0,\end{aligned} \tag{2.88}$$

$$\operatorname{dist}(a_s,\partial\mathcal{U}) - \hat{C}_3||E_s||_{\rho_s} > \operatorname{dist}(a_0,\partial\mathcal{U}) - \hat{C}_3\frac{1}{1-a_1^{-2\tau}}||E_0||_{\rho_0} > 0, \tag{2.89}$$

$$||P_s^{-1}||_{\rho_s} + \frac{\hat{C}_4}{\gamma\delta_s^{\tau+1}}||E_s||_{\rho_s} < ||P_0^{-1}||_{\rho_0} + \frac{\hat{C}_4}{\gamma\delta_0^{\tau+1}}\frac{1}{1-a_1^{1-\tau}}||E_0||_{\rho_0} < \sigma_P, \tag{2.90}$$

$$||\mathcal{R}_{H_s}||_{\rho_s} + \frac{\hat{C}_5}{\gamma\delta_s^{\tau+1}}||E_s||_{\rho_s} < ||\mathcal{R}_{H_0}||_{\rho_0} + \frac{\hat{C}_5}{\gamma\delta_0^{\tau+1}}\frac{1}{1-a_1^{1-\tau}}||E_0||_{\rho_0} < \sigma_H, \tag{2.91}$$

$$\begin{aligned}|\langle B_s^L - T_s\mathcal{R}_{H_s}(B_s^N)\rangle^{-1}| + \frac{\hat{C}_6}{\gamma\delta_s^{\tau+1}}||E_s||_{\rho_s} \\ < |\langle B_s^L - T_s\mathcal{R}_{H_s}(B_s^N)\rangle^{-1}| + \frac{\hat{C}_6}{\gamma\delta_0^{\tau+1}}\frac{1}{1-a_1^{1-\tau}}||E_0||_{\rho_0} < \sigma_D,\end{aligned} \tag{2.92}$$

where constants $\hat{C}_2,\ldots,\hat{C}_6$ are evaluated at δ_0.

Then, we obtain that the condition that we have to ask to E_0 is

$$\frac{\hat{C}_8}{\gamma\delta_0^{\tau+1}}||E_0||_{\rho_0} < 1, \tag{2.93}$$

where

$$\begin{aligned}\hat{C}_8 := \max\Bigg\{ &\frac{d\hat{C}_2}{\sigma_L - ||\mathrm{D}K_0||_{\rho_0}}\frac{1}{1-a_1^{1-\tau}}, \frac{\hat{C}_4}{\sigma_P - ||P_0^{-1}||_{\rho_0}}\frac{1}{1-a_1^{1-\tau}}, \\ &\frac{\hat{C}_5}{\sigma_H - ||\mathcal{R}_{H_0}||_{\rho_0}}\frac{1}{1-a_1^{1-\tau}}, \\ &\frac{\hat{C}_6}{\sigma_D - |\langle B_0^L - T_0\mathcal{R}_{H_0}(B_0^N)\rangle^{-1}|}\frac{1}{1-a_1^{1-\tau}}, \\ &\frac{\hat{C}_2\delta_0}{\operatorname{dist}(K_0(\mathbb{T}^d_{\rho_0}),\partial\mathcal{B})}\frac{1}{1-a_1^{-\tau}}, \frac{\hat{C}_3\delta_0^{\tau+1}\gamma}{\operatorname{dist}(a_0,\partial\mathcal{U})}\frac{1}{1-a_1^{-2\tau}}\Bigg\}\end{aligned} \tag{2.94}$$

Notice that condition (2.93) implies the hypothesis of the Iterative Lemma in equation (2.42), so we can apply, again, the Iterative Lemma. Note also that the sequence $||E_s||_{\rho_s} \to 0$ when $s \to \infty$, such that it satisfies equation (2.84) with (2.85). Then, the iterative scheme converges to a true quasi-periodic F_{a_∞}-invariant torus K_∞, defined in $\mathbb{T}^d_{\rho_\infty}$ for a certain a_{a_∞}.

In particular, the conditions required in this proof, (2.85) and (2.93), can be expressed in terms of ρ_0, a_1, a_3 as

$$\hat{C}_7(a_1a_3)^{2\tau}\frac{||E_0||_{\rho_0}}{\gamma^2\rho_0^{2\tau}} < 1,$$
$$\hat{C}_8 a_3^{\tau+1}\gamma\rho_0^{\tau-1}\frac{||E_0||_{\rho_0}}{\gamma^2\rho_0^{2\tau}} < 1,$$

where $\hat{C}_7$ is given in (2.82) and $\hat{C}_8$ in (2.94). So then, previous conditions correspond to the hypothesis *T1* of Theorem 2.21 with

$$C_* := \max\left\{\hat{C}_7(a_1a_3)^{2\tau}, \hat{C}_8 a_3^{\tau+1}\gamma\rho_0^{\tau-1}\right\}. \tag{2.95}$$

□

Remark 2.26 *A possible choice is selecting a_1 so that, for a fixed $a_2 > 1$,*

$$a_1a_3 = 2\frac{a_1^2}{a_1-1}\frac{a_2}{a_2-1},$$

attains its minimum value. This is for $a_1 = 2$, so that $a_3 = 4\frac{a_2}{a_2-1}$.

PROOF: [Proof of *T2)* in Theorem 2.21: *Closeness*]
We need to prove now that the final torus (K_∞, a_∞) is close to the initial approximation (K, a). In equation (2.55) appears how close is one torus from the other in one Newton step. By iteration, we get how close is the final torus (K_∞, a_∞) to the initial one (K, a). Computing separately estimates for K and a we get estimates

$$\begin{aligned}||K_\infty - K||_{\rho_\infty} &< \sum_{j=0}^{\infty}\frac{\hat{C}_2}{\gamma\delta_j^\tau}||E_j||_{\rho_j}\\ &< \frac{\hat{C}_2}{\gamma\delta_0^\tau}\sum_{j=0}^{\infty}a_1^{-\tau j}||E_0||_{\rho_0} = \frac{\hat{C}_2}{\gamma\delta_0^\tau}\frac{1}{1-a_1^{-\tau}}||E_0||_{\rho_0},\\ |a_\infty - a| &< \sum_{j=0}^{\infty}\hat{C}_3||E_j||_{\rho_j} < \hat{C}_3\sum_{j=0}^{\infty}a_1^{-2\tau j}||E_0||_{\rho_0} = \frac{\hat{C}_3}{1-a_1^{-2\tau}}||E_0||_{\rho_0}\end{aligned}$$

Finally, using that $\delta_0 = \frac{\rho_0}{a_3}$, we obtain thesis T2 of the theorem, i.e. inequality (2.39):

$$\begin{aligned}||(K_\infty - K, a_\infty - a)||_{\rho_\infty} &\leq \max\left\{\frac{\hat{C}_2 a_3^\tau}{1-a_1^{-\tau}}, \frac{\hat{C}_3\gamma\rho_0^\tau}{1-a_1^{-2\tau}}\right\}\frac{||E_0||_{\rho_0}}{\gamma\rho_0^\tau}\\ &\leq \frac{a_3^\tau}{1-a_1^{-\tau}}\frac{\hat{C}_{2,3}}{\gamma\rho_0^\tau}||E_0||_{\rho_0}\\ &:= \frac{\hat{C}_{**}}{\gamma\rho_0^\tau}||E_0||_{\rho_0}.\end{aligned}$$

□

PROOF: [Proof of *T3)* in Theorem 2.21: *Local uniqueness.*]
Let us assume that there are two quasi-periodic invariant tori (K_1, a_1) and (K_2, a_2) in $\mathbb{T}^d_{\bar{\rho}_0}$, for some $\bar{\rho}_0$, which satisfy $\langle K_i^x(\theta) - \theta\rangle = 0$. Then, we will see that they are the same as long as the are close enough, say $\bar{\rho}_0$ small.

Consider (K_1, a_1) a solution of the system (2.5) and (K_2, a_2) another solution. We can write $F_{a_2}(K_2(\theta))$ in terms of $(K_1(\theta), a_1)$ using Taylor expansions up to first order term, which reads as

$$\begin{aligned}F_{a_2}(K_2(\theta)) =& F_{a_1}(K_1(\theta)) + \mathrm{D}F_{a_1}(K_1(\theta))\Delta K(\theta) + \frac{\partial F_{a_1}}{\partial a}(K_1(\theta))\Delta a\\ &+ \int_0^1 (1-t)\mathrm{D}^2F(K_1(\theta) + t\Delta K(\theta), a_1 + t\Delta a)(\Delta K(\theta), \Delta a)^{\otimes 2}\mathrm{d}t,\end{aligned} \tag{2.96}$$

where $\Delta K(\theta) = K_2(\theta) - K_1(\theta)$ and $\Delta a = a_2 - a_1$. As (K_1, a_1) is solution of the invariance equation (2.3), then $\mathrm{D}E(\theta) = 0$. If we take

$$e(\theta) = \int_0^1 (1-t)\mathrm{D}^2F(K_1(\theta) + t\Delta K(\theta), a_1 + t\Delta a)(\Delta K(\theta), \Delta a)^{\otimes 2}\mathrm{d}t,$$

it is controlled by

$$||e||_{\bar{\rho}_0} \leq \frac{1}{2}c_{F,2}||\Delta K, \Delta a||^2_{\bar{\rho}_0}.$$

Using that both (K_1, a_1) and (K_2, a_2) are solutions of (2.5), so in particular of (2.3), previous equation (2.96) reads as

$$\begin{aligned}\mathrm{D}F_{a_1}(K_1(\theta))\Delta K(\theta) - \Delta K(\theta+\omega) + \frac{\partial F_{a_1}}{\partial a}(K_1(\theta))\Delta a - e(\theta) = 0,\\ \langle \Delta K^x\rangle = 0.\end{aligned}$$

Lemma 2.16 gives explicit formulas for $(\Delta K, \Delta a)$, from where we get an estimate for $||(\Delta K, \Delta a)||_{\bar{\rho}_0-\bar{\delta}_0}$ given by expressions (2.36a), (2.36b) and (2.36c). So then, for any $\bar{\delta}_0 < \bar{\rho}_0$, the norm $||(\Delta K, \Delta a)||_{\bar{\rho}_0-\bar{\delta}_0}$ is controlled by

$$||\Delta K(\theta)||_{\bar{\rho}_0-\bar{\delta}_0} < \frac{\hat{C}_2}{\gamma\bar{\delta}_0^\tau}||e||_{\bar{\rho}_0} < \frac{\hat{C}_2}{\gamma\delta_0^\tau}\frac{1}{2}c_{F,2}||\Delta K, \Delta a||^2_{\bar{\rho}_0}$$

and

$$|\Delta a| < \hat{C}_3||e||_{\bar{\rho}_0} < \hat{C}_3\frac{1}{2}c_{F,2}||\Delta K, \Delta a||^2_{\bar{\rho}_0},$$

so collecting both estimates we get

$$\begin{aligned} ||(\Delta K, \Delta a)||_{\bar{\rho}_0-\bar{\delta}_0} <& \hat{C}_{2,3}\frac{1}{2}\frac{c_{F,2}}{\gamma\bar{\delta}_0^\tau}||(\Delta K, \Delta a)||^2_{\bar{\rho}_0} \\ :=& \frac{\tilde{C}}{\gamma\bar{\delta}_0^\tau}||(\Delta K, \Delta a)||^2_{\bar{\rho}_0}, \end{aligned} \tag{2.97}$$

where $\hat{C}_{2,3}$ depends now on $\bar{\delta}_0$.

Consider now $0 < \bar{\rho}_\infty < \bar{\rho}_0$. We define $\bar{a}_2 = \frac{\bar{\rho}_0}{\bar{\rho}_\infty}$. For any $\bar{a}_1 > 1$ we define

$$\bar{a}_3 = \frac{\bar{a}_1}{\bar{a}_1 - 1}\frac{\bar{a}_2}{\bar{a}_2 - 1}$$

so that the sequence of widths

$$\bar{\rho}_0 = \bar{\rho}_0,$$

$$\bar{\rho}_s = \bar{\rho}_{s-1} - \bar{\delta}_{s-1},$$

where $\bar{\delta}_s = \frac{\bar{\delta}_0}{\bar{a}_1^s}$ and $\delta_0 = \frac{\bar{\rho}_0}{\bar{a}_3}$, converges to the final width of the analycity strip

$$\bar{\rho}_\infty = \bar{\rho}_0 - \bar{\delta}_0\frac{1}{1-\frac{1}{\bar{a}_1}} = \frac{\bar{\rho}_0}{\bar{a}_2}.$$

Now, we proceed by induction. We suppose that we have applied s times estimate (2.97), so we have estimates for $||(\Delta K, \Delta a)||_{\rho_s}$, which reads in terms of $||(\Delta K, \Delta a)||_{\rho_{s-1}}$ in the following way

$$||(\Delta K, \Delta a)||_{\rho_s} \leq \frac{\tilde{C}}{\gamma\delta_{s-1}^\tau}||(\Delta K, \Delta a)||^2_{\rho_{s-1}} = \frac{\tilde{C}}{\gamma\bar{\delta}_0^\tau}\bar{a}_1^{\tau(s-1)}||(\Delta K, \Delta a)||^2_{\rho_{s-1}},$$

so then, by iterating the process until $||(\Delta K, \Delta a)||_{\bar{\rho}_0}$ and using that $1+2+\cdots+2^{s-1} = 2^s - 1$ and $1(s-1)+2(s-2)+\cdots+2^{s-2}1 = 2^s - s - 1$, we obtain

$$||(\Delta K, \Delta a)||_{\rho_s} < \left(\frac{\tilde{C}}{\gamma \delta_0^\tau} \bar{a}_1^\tau ||(\Delta K, \Delta a)||_{\bar{\rho}_0}\right)^{2^s-1} \bar{a}_1^{-\tau s} ||(\Delta K, \Delta a)||_{\bar{\rho}_0}. \quad (2.98)$$

Notice that, in order to obtain a decreasing sequence of the norms of the increments, it suffices to assume that

$$\frac{\tilde{C}}{\gamma \bar{\delta}_0^\tau} \bar{a}_1^\tau ||(\Delta K, \Delta a)||_{\bar{\rho}_0} < 1,$$

which in terms of $\bar{\delta}_0 = \frac{\bar{\rho}_0}{\bar{a}_3}$ reads as

$$\frac{\tilde{C}}{\gamma \bar{\rho}_0^\tau} (\bar{a}_1 \bar{a}_3)^\tau ||(\Delta K, \Delta a)||_{\bar{\rho}_0} < 1. \quad (2.99)$$

An optimal choice is, for a fixed $\bar{a}_2$, choose an $\bar{a}_1$ in such a way that the product $\bar{a}_1 \bar{a}_3$ attains its minimum value. This is for $\bar{a}_1 = 2$, so that

$$\bar{a}_3 = \lim_{\bar{a}_2 \to \infty} \frac{\bar{a}_1}{\bar{a}_1 - 1} \frac{\bar{a}_2}{\bar{a}_2 - 1} = 2,$$

and $\bar{a}_1 \bar{a}_3 = 4$. Then, equation (2.99) reads as

$$\frac{\tilde{C}}{\gamma \bar{\rho}_0^\tau} 4^\tau ||(\Delta K, \Delta a)||_{\bar{\rho}_0} < 1. \quad (2.100)$$

Moreover, for any $\bar{a}_2 \gg 1$, so $0 < \bar{\rho}_\infty \ll \bar{\rho}_0$, condition (2.100) also holds for $\bar{a}_3 = 2\frac{\bar{a}_2}{\bar{a}_2 - 1}$, and we get

$$\lim_{s \to \infty} ||(\Delta K, \Delta a)||_{\bar{\rho}_s} = 0,$$

so then $(K_1, a_1) = (K_2, a_2)$ in $\mathbb{T}^d_{\bar{\rho}_\infty}$. Moreover, by the Identity Theorem of Holomorphic functions in several complex variables, $(K_1, a_1) = (K_2, a_2)$ in $\mathbb{T}^d_{\bar{\rho}_0}$.

Assume now we start in an analycity strip of width $\bar{\rho}_0 = \rho_\infty$, where ρ_∞ comes from the *existence-closeness* part of the proof, and $(K_1, a_1) = (K_\infty, a_\infty)$. Our goal is to see that, if (K_2, a_2) is another solution of (2.5) in $\mathbb{T}^d_{\rho_\infty}$, and it is close to (K, a), then it is, in fact, the same as (K_1, a_1). Assuming then

that $(K_1, a_1) = (K_\infty, a_\infty)$ (satisfying condition (2.39) of *T2)* and (K_2, a_2) is another solution of (2.5) in $\mathbb{T}^d_{\rho_\infty}$, we can write the following inequality

$$\begin{aligned}
&\frac{4^\tau \tilde{C}}{\gamma \rho_\infty^\tau} ||(K_2 - K_1, a_2 - a_1)||_{\rho_\infty} \\
&\qquad \leq \frac{4^\tau \tilde{C}}{\gamma \rho_\infty^\tau} \left(||(K_2 - K, a_2 - a)||_{\rho_\infty} + ||(K - K_\infty, a - a_\infty)||_{\rho_\infty} \right) \\
&\qquad \leq \frac{4^\tau \tilde{C}}{\gamma \rho_\infty^\tau} \left(||(K_2 - K, a_2 - a)||_{\rho_\infty} + \frac{\hat{C}_{**}}{\gamma \rho_0^\tau} ||E_0||_{\rho_0} \right) < 1,
\end{aligned}$$

where we impose last inequality in order to get (2.100) for $\rho_\infty = \bar{\rho}_0$, $\Delta K = K_2 - K_1$ and $\Delta a = a_2 - a_1$. This assumption on the last inequality also reads as

$$||(K_2 - K, a_2 - a)||_{\rho_\infty} < \frac{\gamma \rho_\infty^\tau}{4^\tau \tilde{C}} - \frac{\hat{C}_{**}}{\gamma \rho_0^\tau} ||E_0||_{\rho_0}$$

and we obtain the condition in (K_2, a_2) in which there is uniqueness of the solution by requiring the right hand side to be positive

$$\frac{\hat{C}_{**}}{\gamma \rho_0^\tau} ||E_0||_{\rho_0} < \frac{\gamma \rho_\infty^\tau}{4^\tau \tilde{C}}.$$

In other words, we need get satisfied the inequality

$$\frac{\hat{C}_{***}}{\gamma^2 \rho_0^\tau \rho_\infty^\tau} ||E_0||_{\rho_0} < 1,$$

for

$$\hat{C}_{***} := 4^\tau \tilde{C} \hat{C}_{**}.$$

So then,

$$||(K_2 - K, a_2 - a)||_{\rho_\infty} < \hat{C}_{**} \left(\frac{\gamma \rho_\infty^\tau}{\hat{C}_{***}} - \frac{1}{\gamma \rho^\tau} ||E||_\rho \right),$$

is the required condition for the uniqueness. □

Chapter 3

Newton-like methods for computing Quasi-Periodic Normally Hyperbolic Invariant Tori

In this chapter, we consider the problem of numerically computing quasi-periodic normally hyperbolic invariant tori (NHIT) with fixed frequency as well as their invariant bundles. The algorithms are based on a KAM scheme (see Chapter 2) to find the parameterization of a torus with fixed Diophantine frequency (by adjusting parameters of the model) and the stable and unstable bundles.

We start by considering a general algorithm for quasi-periodic normally hyperbolic invariant tori. Furthermore, several algorithms for computing reducible quasi-periodic tori, i.e., tori for which the linearized dynamics can be reduced to constant coefficients, are already treated. These are the cases in which linearized dynamics is more understandable.

We implement these methods to continue curves of quasi-periodic NHIT of a perturbed dynamical system. Our interest here, is to explore the different mechanism of breakdown of these invariant tori. Several observables, such as C^r and Sobolev norms, Lyapunov multipliers and the distance between bundles, are computed in order to justify the breakdown tori and to predict the critical parameter value of torus breakdown.

3.1 The setting

Consider the ambient manifold $\mathbb{T}^d \times \mathbb{R}^n = \{(x, y) \mid x \in \mathbb{T}^d,\ y \in \mathbb{R}^n\}$. Let $F_a : \mathbb{T}^d \times \mathbb{R}^n \to \mathbb{T}^d \times \mathbb{R}^n$ be a family of diffeomorphisms parameterized by $a \in \mathbb{R}^d$. For each parameter $a \in \mathbb{R}^d$, we assume that F_a is homotopic to the identity:

$$F_a \begin{pmatrix} x \\ y \end{pmatrix} = \begin{pmatrix} x \\ 0 \end{pmatrix} + F_{a,p} \begin{pmatrix} x \\ y \end{pmatrix},$$

where $F_{a,p}$ is 1-periodic in x.

Given $\omega \in \mathbb{R}^d$, let $\mathcal{K} = K(\mathbb{T}^d)$ be a d-dimensional F_a-**invariant** torus with a *quasi-periodic* motion of frequency ω, parameterized by $K : \mathbb{T}^d \to \mathbb{T}^d \times \mathbb{R}^n$. Then, see Definition 2.1, it satisfies equation

$$F_a \circ K(\theta) = K(\theta + \omega). \tag{3.1}$$

Note that (3.1) is an equation for K and a given the family F_a.

It is clear that the homotopy classes of F and K has to match. This means that in particular, we look for invariant tori $\mathcal{K}$ parameterized by K that are homotopic to the zero-section of $\mathbb{T}^d \times \mathbb{R}^n$, $\mathbb{T}^d \times \{0\}$, that is

$$K(\theta) = \begin{pmatrix} \theta \\ 0 \end{pmatrix} + K_p(\theta),$$

where $K_p : \mathbb{T}^d \to \mathbb{R}^d \times \mathbb{R}^n$ is 1-periodic in the θ-variables.

As it has been seen in some previous works, see e.g. [57], we find very useful to compute the torus and the bundles at the same time by using a Newton method.

The tangent bundle $\mathrm{T}\mathcal{K}$ of the parameterized torus $\mathcal{K}$ is trivial. In particular, for each $\theta \in \mathbb{T}^d$, the d column vectors of the $(d+n)\times d$ matrix $\mathrm{D}K(\theta)$ provides a basis of the fiber $\mathrm{T}_{K(\theta)}\mathcal{K}$ of the tangent bundle. Hence, the matrix-valued map $L : \mathbb{T}^d \to \mathbb{R}^{(d+n)\times d}$ defined as $L(\theta) = \mathrm{D}K(\theta)$, provides a global frame for the tangent bundle. Moreover, the normal bundle $\mathrm{N}\mathcal{K}$ is defined by a matrix-valued map $N : \mathbb{T}^d \to \mathbb{R}^{(d+n)\times n}$ generated by n vectors linearly independents to $L(\theta)$ for each $\theta \in \mathbb{T}^d$, so that the column vectors of $L(\theta)$ joined with the column vectors of $N(\theta)$ form a basis of $\mathrm{T}_{K(\theta)}\mathbb{T}^d \times \mathbb{R}^n \simeq \mathbb{R}^{d+n}$. In other words, the matrix valued map $P : \mathbb{T}^d \to \mathbb{R}^{(d+n)\times(d+n)}$, obtained by juxtaposing L and N so that $P(\theta) = \begin{pmatrix} L(\theta) & N(\theta) \end{pmatrix}$, provides an adapted frame around the torus. It is said that $\mathcal{K}$ is a framed manifold.

Assume now that $\mathcal{K}$, parameterized by K, is F_a-invariant with a fixed frequency ω. From the definition of the invariance equation, by differentiating (3.1), we get the invariance equation of the linearization $L(\theta) = \mathrm{D}K(\theta)$,

$$\mathrm{D}F_a(K(\theta))L(\theta) - L(\theta + \omega) = 0, \tag{3.2}$$

which means the invariance of the tangent bundle $\mathrm{T}\mathcal{K}$.

Notice that the linearized dynamics $\mathrm{D}F$ around $\mathcal{K}$ in the adapted frame P is given by a block triangular matrix valued map, $\Lambda : \mathbb{T}^d \to \mathbb{R}^{(d+n)\times(d+n)}$, defined as

$$\Lambda(\theta) = P(\theta + \omega)^{-1}\mathrm{D}F_a(K(\theta))P(\theta). \tag{3.3}$$

so it is of the form

$$\Lambda(\theta) = \begin{pmatrix} \mathrm{Id} & T(\theta) \\ O & \Lambda_N(\theta) \end{pmatrix}, \tag{3.4}$$

where $\Lambda_N : \mathbb{T}^d \to \mathbb{R}^{n\times n}$ is the dynamics on the normal bundles and $T : \mathbb{T}^d \to \mathbb{R}^{d\times n}$ is the torsion of the system. It is also desirable to work with a normal bundle $\mathrm{N}\mathcal{K}$ which is also invariant. Using global frames, this reads as

$$\mathrm{D}F_a(K(\theta))N(\theta) - N(\theta + \omega)\Lambda_N(\theta) = 0. \tag{3.5}$$

Notice that this invariance condition on the normal bundle is equivalent to say $T(\theta) = 0$. In such a case, the adapted frame P introduced above reduces the linearized dynamics to a block diagonal matrix Λ,

$$\Lambda(\theta) = \mathrm{blockdiag}(\mathrm{Id}, \Lambda_N(\theta)).$$

From now on, we assume the normal bundle invariant. Moreover, under normal hyperbolicity properties, the invariant normal bundle decomposes into stable and unstable subbundles, that we will also assume to be trivial. So, the normal bundle has the form

$$N(\theta) = \begin{pmatrix} N^S(\theta) & N^U(\theta) \end{pmatrix} \tag{3.6}$$

where $N^S : \mathbb{T}^d \to \mathbb{R}^{(d+n)\times n_s}$ and $N^U : \mathbb{T}^d \to \mathbb{R}^{(d+n)\times n_u}$, with $n_s + n_u = n$, provides a global frame for the stable and unstable bundles, respectively. Then, the linearized normal dynamics is given by

$$\Lambda_N(\theta) = \mathrm{blockdiag}(\Lambda_S(\theta), \Lambda_U(\theta)),$$

with Λ_S contracting and Λ_U expanding, that is: $||\Lambda_S|| < 1$ and $||(\Lambda_U)^{-1}|| < 1$ (for adapted Finsler norms).

Remark 3.1 *The property of triviality of stable and unstable bundles is an extra hypothesis in our setting. There are cases in which non-trivial (non-orientable) bundles are easily trivialized by using a double covering trick. That is, we can consider the frame P defined from $\tilde{\mathbb{T}}^d = (\mathbb{R}/2\mathbb{Z})^d$ instead of $\mathbb{T}^d$ by using a double covering trick, see e.g. [59]. There are also cases in higher dimensional bundles in which there are other topological obstructions (characteristic classes).*

3.2 Specification of three Newton-like methods

Given a family $F_a : \mathbb{T}^d \times \mathbb{R}^n \to \mathbb{T}^d \times \mathbb{R}^n$ and $\omega \in \mathbb{R}^d$ Diophantine, our goal is to compute a parameterization K of a quasi-periodic normally hyperbolic invariant torus and its adjusting parameter, as well as their invariant normal bundles. In the following, we explain how to perform one step of a Newton-like method to solve invariance equations (3.1) and (3.5) above, in different contexts. Starting with an approximate parameterization of a quasi-periodic NHIT, K, and a parameter, a, an approximate invariant normal bundle, N, and its linearized dynamics, Λ_N, the aim of one step of Newton method is to compute their corresponding corrections $\Delta K, \Delta a, \Delta N, \Delta\Lambda_N$ in such a way that the error estimates of the new approximations $\bar{K} = K + \Delta K, \bar{a} = a + \Delta a, \bar{N} = N + \Delta N, \bar{\Lambda}_N = \Lambda_N + \Delta\Lambda_N$, are quadratically small with respect to the starting error estimates. To do so, the parameter a is adjusted in order to keep fixed the frequency ω. The procedure is repeated until we achieve the desired error-tolerance.

Remark 3.2 *The framework of this algorithm is based on KAM techniques, detailed in Chapter 2. Remarkably, the method for proving the theorem is similar to the algorithms presented here.*

Remark 3.3 *Notice that, the fact of impose an invariant normal bundle, so using $T(\theta) = 0$, is not a compulsory condition if we do not require reducibility on the torus. We can use a fix normal bundle, as we have done in Chapter 2, and proceed to compute a new torus and its adjusting parameter.*

Since we are dealing with periodic functions to represent the torus K and the adapted frame P and the internal dynamics is a rotation R_ω, it is natural to represent them in Fourier series. For a periodic function f, we denote by

$$f(\theta) = \sum_{k \in \mathbb{Z}^d} f_k e^{2\pi \mathbf{i} k\theta} \tag{3.7}$$

its Fourier series. The average of f is defined as

$$\langle f \rangle = f_0 = \int_{\mathbb{T}^d} f(\theta)\ \mathrm{d}\theta.$$

3.2.1 A general algorithm

This algorithm is an adaptation of the method of proof of our KAM-like theorem (Theorem 2.21) in Chapter 2.

Substep 1: Correction of the torus K and parameter a

Let $E : \mathbb{T}^d \to \mathbb{R}^{d+n}$ be the error in the invariance equation of the torus,

$$E(\theta) = F_a(K(\theta)) - K(\theta + \omega), \tag{3.8}$$

which is "small".

Recall that the adapted frame P, defined by juxtaposing $L = \mathrm{D}K$ and N is approximately invariant. Indeed, the error of reducibility, $E_{\mathrm{red}} : \mathbb{T}^d \to \mathbb{R}^{(d+n)\times(d+n)}$, is of the form

$$E_{\mathrm{red}}(\theta) = P(\theta + \omega)^{-1}\mathrm{D}F_a(K(\theta))P(\theta) - \Lambda(\theta), \tag{3.9}$$

and it satisfies $E_{\mathrm{red}}(\theta) = \begin{pmatrix} P(\theta+\omega)^{-1}\mathrm{D}E(\theta) & E^N_{\mathrm{red}}(\theta) \end{pmatrix}$, where

$$E^N_{\mathrm{red}}(\theta) = P(\theta + \omega)^{-1}\mathrm{D}F_a(K(\theta))N(\theta) - \begin{pmatrix} 0 \\ \Lambda_N(\theta) \end{pmatrix}, \tag{3.10}$$

so E_{red} is assumed to be "small".

We consider the correction of the torus of the form $\Delta K(\theta) = P(\theta)\xi(\theta)$, being $\xi : \mathbb{T}^d \to \mathbb{R}^{d+n}$ a periodic function. Note that the correction preserve the homotopy class of the torus. The adjustment of a is given by Δa, $\bar{a} = a + \Delta a$. Then, by substituting new approximations $\bar{K} = K + P\xi$ and $\bar{a} = a + \Delta a$ in (3.1) and using first order Taylor expansion, we obtain

$$\begin{aligned} 0 &= F_a(K(\theta) + P(\theta)\xi(\theta)) - K(\theta + \omega) - P(\theta + \omega)\xi(\theta + \omega) \\ &= F_a(K(\theta)) + \mathrm{D}F_a(K(\theta))P(\theta)\xi(\theta) + \frac{\partial F_a}{\partial a}(K(\theta))\Delta a \\ &\quad - K(\theta + \omega) - P(\theta + \omega)\xi(\theta + \omega) + \mathcal{O}_2 \\ &= E(\theta) + \frac{\partial F_a}{\partial a}(K(\theta))\Delta a + P(\theta + \omega)\Lambda(\theta)\xi(\theta) - P(\theta + \omega)\xi(\theta + \omega) + \mathcal{O}_2, \end{aligned} \tag{3.11}$$

where we apply definitions (3.9) and (3.10) above, and $\mathcal{O}_2$ collect the quadratically small terms. Multiplying (3.11) by $P(\theta+\omega)^{-1}$ and neglecting quadratically small terms, we obtain the cohomological equation

$$\eta(\theta) = \Lambda(\theta)\xi(\theta) - \xi(\theta+\omega) + B(\theta)\Delta a, \tag{3.12}$$

where

$$\eta(\theta) = -P(\theta+\omega)^{-1}E(\theta) \tag{3.13}$$

is the error of the approximate solution in the adapted frame and $B(\theta) = P(\theta+\omega)^{-1}\frac{\partial F_a}{\partial a}(K(\theta))$. Finally, splitting (3.12) into tangent and normal components, we realize that a Newton step reduces our equation to the block diagonal system

$$\begin{aligned} \eta^L(\theta) &= \xi^L(\theta) - \xi^L(\theta+\omega) + B^L(\theta)\Delta a, & (3.14)\\ \eta^N(\theta) &= \Lambda_N(\theta)\xi^N(\theta) - \xi^N(\theta+\omega) + B^N(\theta)\Delta a. & (3.15) \end{aligned}$$

which can be solved separately.

Tangent component. We have to solve the cohomological equation (3.14):

$$\xi^L(\theta) - \xi^L(\theta+\omega) = \eta^L(\theta) - B^L(\theta)\Delta a.$$

To be able to solve this cohomological equation, we need the right hand side to be zero averaged. Then, to ensure $\eta^L(\theta) - B^L(\theta)\Delta a$ has zero average, we have to choose the correction Δa as

$$\Delta a = - < B^L >^{-1} < \eta^L > . \tag{3.16}$$

From this condition, we obtain a non-degeneracy condition over the system: it is needed that $< B^L(\theta) >$ be invertible. Notice that this condition corresponds to the hypothesis *H5)*, the non-degeneracy condition. Since ω satisfies Diophantine conditions and $\langle \eta^L(\theta) - B^L(\theta)\Delta a \rangle = 0$, we can solve (3.14). Notice that, equation (3.14) splits into d equations corresponding to its d tangent directions:

$$\xi^i(\theta) - \xi^i(\theta+\omega) = \eta^i(\theta) - B^i(\theta)\Delta a, \tag{3.17}$$

for $i = 1, \ldots, d$.

The solution is obtained by solving (3.17) order by order in terms of Fourier modes:

$$\xi^i_k = \frac{\eta^i_k - B^i_k \Delta a}{1 - e^{2\pi i k\omega}},\ k \neq 0, \tag{3.18}$$

for each $i = 1, \ldots, d$, which corresponds to each tangent direction. Notice that ξ^i_0 is free. In particular, we choose $\xi^i_0 = 0$, for all i.

Remark 3.4 *As ω is Diophantine, we do not have resonances in* (3.18).

Normal component. From normal hyperbolicity, and matrix Λ_N being block diagonal, equation (3.15) splits into stable and unstable components:

$$\begin{aligned} \eta^S(\theta) - B^S(\theta)\Delta a &= \Lambda_S(\theta)\xi^S(\theta) - \xi^S(\theta+\omega), && (3.19)\\ \eta^U(\theta) - B^U(\theta)\Delta a &= \Lambda_U(\theta)\xi^U(\theta) - \xi^U(\theta+\omega), && (3.20) \end{aligned}$$

where the left hand side is already known, since we first solved the tangent component, and so that Δa. Hence, we can solve both equations by simple iteration using the contracting principle, which will converge to the solutions ξ^S and ξ^U we wanted. In particular, ξ^S and ξ^U solve the fixed point equations

$$\begin{aligned} \xi^S(\theta) &= \Lambda_S(\theta-\omega)\xi^S(\theta-\omega) - \eta^S(\theta-\omega) + B^S(\theta-\omega)\Delta a,\\ \xi^U(\theta) &= (\Lambda_U(\theta))^{-1}\left(\xi^U(\theta+\omega) + \eta^U(\theta) - B^U(\theta)\Delta a\right), \end{aligned}$$

respectively, that can be solved by iteration.

At this step, we have gained new approximations $\bar K$ and $\bar a$ for which the new error $\bar E(\theta) = F_{\bar a}(\bar K(\theta)) - \bar K(\theta+\omega)$ is quadratically small with respect to $E(\theta)$. Additionally, we obtain a new approximation for the tangent bundle $\bar L = \mathrm{D}\bar K$.

Substep 2: Correction of the normal bundles

We redefine the error in the invariance equation of the adapted frame for the new $\bar K$ (so that for $\bar P = (\mathrm{D}\bar K\ N)$) and $\bar a$ as

$$\bar E_{\mathrm{red}}(\theta) = \bar P(\theta+\omega)^{-1}\mathrm{D}F_{\bar a}(\bar K(\theta))\bar P(\theta) - \Lambda(\theta)$$

which is close to the previous $E_{\mathrm{red}}(\theta)$. For the sake of concreteness, we redefine $K = \bar K$, $P = \bar P$, $a = \bar a$ and $E_{\mathrm{red}} = \bar E_{\mathrm{red}}$.

We consider the corrections of the normal bundle, $\bar N = N + \Delta N$, and its linearized dynamics, $\bar\Lambda_N = \Lambda_N + \Delta\Lambda_N$ of the form:

$$\begin{aligned} \Delta N(\theta) &= P(\theta)Q^N(\theta),\\ \Delta\Lambda_N(\theta) &= \mathrm{blockdiag}(\Delta\Lambda_S(\theta), \Delta\Lambda_U(\theta)), \end{aligned}$$

where $Q^N : \mathbb{T}^d \to \mathbb{R}^{(d+n)\times n}$ is a periodic matrix map. Then, we obtain

$$\begin{aligned}
0 &= \mathrm{D}F(K(\theta))\bar{N}(\theta) - \bar{N}(\theta+\omega)\bar{\Lambda}_N(\theta) \\
&= \mathrm{D}F(K(\theta))\left(N(\theta) + P(\theta)Q^N(\theta)\right) - \\
&\quad - \left(N(\theta+\omega) + P(\theta+\omega)Q^N(\theta+\omega)\right)\left(\Lambda_N(\theta) + \Delta_N(\theta)\right) \\
&= P(\theta+\omega)E^N_{\mathrm{red}}(\theta) + \left(P(\theta+\omega)\Lambda(\theta) + P(\theta+\omega)E_{\mathrm{red}}(\theta)\right)Q^N(\theta) - \\
&\quad - P(\theta+\omega)Q^N(\theta+\omega)\Lambda_N(\theta) - N(\theta+\omega)\Delta_N(\theta) \\
&\quad - P(\theta+\omega)Q^N(f(\theta))\Delta_N(\theta).
\end{aligned}$$

Hence, by multiplying both sides of the equation by $P(\theta+\omega)^{-1}$ and by neglecting quadratically small terms, in the same way we proceed with the tangent component, we obtain the following cohomological equation:

$$-E^N_{\mathrm{red}}(\theta) = \Lambda(\theta)Q^N(\theta) - Q^N(\theta+\omega)\Lambda_N(\theta) - \begin{pmatrix} O \\ \Delta_N(\theta) \end{pmatrix}. \tag{3.21}$$

The corrections of the (approximate) stable and unstable bundles are performed in the complementary directions. That is, the correction matrix Q^N is chosen of the form

$$Q^N(\theta) = \begin{pmatrix} Q^{LS}(\theta) & Q^{LU}(\theta) \\ O & Q^{SU}(\theta) \\ Q^{US}(\theta) & O \end{pmatrix}, \tag{3.22}$$

so that the "missing" blocks Q^{SS} and Q^{UU} are taken to be zero. Hence, Equation (3.21) corresponds to the following block equations, where we use super-indices to indicate the blocks, just as in (3.22):

$$\begin{aligned}
-E^{LS}_{\mathrm{red}}(\theta) &= Q^{LS}(\theta) - Q^{LS}(\theta+\omega)\Lambda_S(\theta), && \text{(3.23a)} \\
-E^{LU}_{\mathrm{red}}(\theta) &= Q^{LU}(\theta) - Q^{LU}(\theta+\omega)\Lambda_U(\theta), && \text{(3.23b)} \\
-E^{US}_{\mathrm{red}}(\theta) &= \Lambda_U(\theta)Q^{US}(\theta) - Q^{US}(\theta+\omega)\Lambda_S(\theta), && \text{(3.23c)} \\
-E^{SU}_{\mathrm{red}}(\theta) &= \Lambda_S(\theta)Q^{SU}(\theta) - Q^{SU}(\theta+\omega)\Lambda_U(\theta), && \text{(3.23d)} \\
-E^{SS}_{\mathrm{red}}(\theta) &= -\Delta\Lambda_S(\theta), && \text{(3.23e)} \\
-E^{UU}_{\mathrm{red}}(\theta) &= -\Delta\Lambda_U(\theta). && \text{(3.23f)}
\end{aligned}$$

We obtain directly the correction of the linearized normal dynamics from equations (3.23e) and (3.23f). The other 4 equations give us the components of the correction of the normal bundle, Q^N in (3.22), and can be solved by the contraction mapping, as all of them are contractions or expansions by

NHIM hypothesis (Λ_S contractive and Λ_U expansive). The corresponding fixed point equations are

$$Q^{LS}(\theta) = Q^{LS}(\theta+\omega)\Lambda_S(\theta) - E^{LS}_{\text{red}}(\theta), \tag{3.24a}$$
$$Q^{LU}(\theta) = (Q^{LU}(\theta-\omega) + E^{LU}_{\text{red}}(\theta-\omega))\,(\Lambda_U(\theta-\omega))^{-1}, \tag{3.24b}$$
$$Q^{US}(\theta) = (\Lambda_U(\theta))^{-1}\,(Q^{US}(\theta+\omega)\Lambda_S(\theta) - E^{US}_{\text{red}}(\theta))\,, \tag{3.24c}$$
$$Q^{SU}(\theta) = (\Lambda_S(\theta-\omega)Q^{SU}(\theta-\omega) + E^{SU}_{\text{red}}(\theta-\omega))\,(\Lambda_U(\theta-\omega))^{-1}, \tag{3.24d}$$

that can be solved by iteration.

Summarizing, we obtain the following new approximations of the invariant normal bundle, $\bar{N}$,

$$\begin{aligned}\bar{N}^S(\theta) &= N^S(\theta) + L(\theta)Q^{LS}(\theta) + N^U(\theta)Q^{US}(\theta),\\ \bar{N}^U(\theta) &= N^U(\theta) + L(\theta)Q^{LU}(\theta) + N^S(\theta)Q^{SU}(\theta),\end{aligned}$$

and of the corresponding linearized dynamics $\bar{\Lambda}_N = \text{diag}(\bar{\Lambda}_S, \bar{\Lambda}_U)$,

$$\begin{aligned}\bar{\Lambda}_S(\theta) &= \Lambda_S(\theta) + E^{SS}_{\text{red}}(\theta),\\ \bar{\Lambda}_U(\theta) &= \Lambda_U(\theta) + E^{UU}_{\text{red}}(\theta).\end{aligned}$$

That is, we obtain a new adapted frame $\bar{P}(\theta) = \begin{pmatrix}\bar{L}(\theta) & \bar{N}(\theta)\end{pmatrix}$, and a new linearized dynamics $\bar{\Lambda}(\theta) = \text{diag}(\text{Id}, \bar{\Lambda}_N(\theta))$, that improves the error $E_{\text{red}}(\theta)$. We have to repeat substeps 1 and 2 until we reach the desired error tolerance.

Remark 3.5 *Fast iterative methods for solving cohomology equations* (3.19), (3.20),(3.24a), (3.24b), (3.24c) *and* (3.24d) *have been designed in [66, 67], reducing n iterations of simple iteration method to* $\log_2 n$. *These methods have been adapted to work with cohomological equations over general dynamics instead of rotations for the computations of normally hyperbolic invariant manifolds performed in Chapter 4.*

3.2.2 An algorithm based on reducibility

Sometimes, it is possible to choose a frame in such a way that the linearization becomes a constant matrix. When this happens, we say that our system is reducible. When it is possible, the Newton step is extremely fast and accurate when using Fourier series, since we have the equations completely uncoupled. Moreover, reducibility is a geometrically important property, since it gives full information about the linearization, see [42, 70, 71]. Unfortunately, the property of reducibility is not always satisfied, as we will detect in many examples of this chapter.

Definition 3.6 *We say that the invariant torus is* reducible *if and only if there exists* $P : \tilde{\mathbb{T}}^d = (\mathbb{R}/2\mathbb{Z})^d \to \mathbb{R}^{(d+n)\times(d+n)}$ *and* $\Lambda \in \mathbb{R}^{(d+n)\times(d+n)}$ *constant such that:*

$$P^{-1}(\theta+\omega)\mathrm{D}F_a(K(\theta))P(\theta) - \Lambda = 0. \tag{3.25}$$

Notice that the Floquet transformation is assumed to be 2-periodic, instead of being 1- periodic, in order to include non-orientable bundles in the definition.

We will consider here the reducible case. We will redefine in this subsection the Newton step for the reducible case.

Substep 1: Correction of the torus K and parameter a

We proceed in the same way as we did in the general algorithm, but taking into account that now the error of reducibility, $E_{\mathrm{red}} : \mathbb{T}^d \to \mathbb{R}^{(d+n)\times(d+n)}$, is of the form

$$E_{\mathrm{red}}(\theta) = P(\theta+\omega)^{-1}\mathrm{D}F_a(K(\theta))P(\theta) - \Lambda, \tag{3.26}$$

with Λ constant, so that

$$E^N_{\mathrm{red}}(\theta) = P(\theta+\omega)^{-1}\mathrm{D}F_a(K(\theta))N(\theta) - \begin{pmatrix} 0 \\ \Lambda_N \end{pmatrix}. \tag{3.27}$$

Consider the errors E and E_{red}, defined by (3.8) and (3.26) respectively, "small". Consider, again, the correction of the torus $\bar{K} = K + \Delta K$ of the form $\Delta K(\theta) = P(\theta)\xi(\theta)$, being $\xi : \mathbb{T}^d \to \mathbb{R}^{d+n}$ a periodic function, and the adjustment of a given by Δa, $\bar{a} = a + \Delta a$. Then, by substituting new approximations $\bar{K} = K + P\xi$ and $\bar{a} = a + \Delta a$ in (3.1) and using first order Taylor expansion, we obtain

$$-E(\theta) = \frac{\partial F_a}{\partial a}(K(\theta))\Delta a + P(\theta+\omega)\Lambda\xi(\theta) - P(\theta+\omega)\xi(\theta+\omega) + \mathcal{O}_2, \tag{3.28}$$

where we apply definitions (3.26) and (3.27) above, and $\mathcal{O}_2$ collect the quadratically small terms. Multiplying last equation (3.28) by $P(\theta+\omega)^{-1}$ and neglecting quadratically small terms, we obtain the cohomological equation

$$\eta(\theta) = \Lambda\xi(\theta) - \xi(\theta+\omega) + B(\theta)\Delta a, \tag{3.29}$$

where

$$\eta(\theta) = -P(\theta+\omega)^{-1}E(\theta) \tag{3.30}$$

is the error of the approximate solution in the adapted frame and $B(\theta) = P(\theta+\omega)^{-1}\frac{\partial F_a}{\partial a}(K(\theta))$. Finally, splitting (3.29) into tangent and normal components, we realize that a Newton step reduces our equation to the block diagonal system

$$\eta^L(\theta) = \xi^L(\theta) - \xi^L(\theta+\omega) + B^L(\theta)\Delta a, \tag{3.31}$$
$$\eta^N(\theta) = \Lambda_N\xi^N(\theta) - \xi^N(\theta+\omega) + B^N(\theta)\Delta a. \tag{3.32}$$

which can be solved separately.

Tangent component. Observe that equation (3.31) is exactly the same as in the non-reducible case, (3.14), so that the solution is the same as well. Then, the correction over the tangent component of the torus is given by (3.18) as:

$$\xi_k^i = \frac{\eta_k^i - B_k^i\Delta a}{1-e^{2\pi i k\omega}},\ k\neq 0,$$

for each $i = 1,\dots,d$, with ξ_0^i free (in particular we take $\xi_0^i = 0$, for all i), and the adjustment of the parameter a is of the form (3.16)

$$\Delta a = - < B^L >^{-1} < \eta^L > .$$

Normal component. At this point, Δa is a known value, so then we can redefine

$$\tilde{\eta}^N(\theta) = \eta^N(\theta) - B^N(\theta)\Delta a. \tag{3.33}$$

With this new notation, we write equation (3.32) in terms of Fourier

$$\tilde{\eta}_k^N = \Lambda_N\xi_k^N - \xi_k^N e^{2\pi \mathbf{i} k\omega}. \tag{3.34}$$

Notice that by normal hyperbolicity, the term $(\Lambda_N\xi_k^N - e^{2\pi\mathbf{i}k\omega}\mathrm{Id})$ is invertible for all k. Then, we get immediately the solution of (3.34) by isolating the term ξ_k^N, and the solution is of the form

$$\xi_k^N = (\Lambda_N - e^{2\pi\mathbf{i}k\omega}\mathrm{Id})^{-1}\tilde{\eta}_k^N, \tag{3.35}$$

for all k.

At this step, we have gained new approximations $\bar{K}$ and $\bar{a}$ for which the new error $\bar{E}(\theta) = F_{\bar{a}}(\bar{K}(\theta)) - \bar{K}(\theta+\omega)$ is, hopefully, quadratically small with respect to $E(\theta)$. Additionally, we obtain a new approximation for the tangent bundle $\bar{L} = \mathrm{D}\bar{K}$.

Remark 3.7 *Notice that, compared with the general algorithm, instead of solving* (3.32) *by using by using iteration, we solve it term by term in Fourier modes. This update leads to a faster algorithm, as long as the torus is reducible. Analogous improvements will be detailed in other substeps of the algorithm.*

Substep 2: Correction of the Floquet transformations

We redefine the error in the invariance equation of the adapted frame for the new $\bar{K}$ (so that for $\bar{P} = (\mathrm{D}\bar{K}\ N)$) and $\bar{a}$ as

$$\bar{E}_{\mathrm{red}}(\theta) = \bar{P}(\theta+\omega)^{-1}\mathrm{D}F_{\bar{a}}(\bar{K}(\theta))\bar{P}(\theta) - \Lambda \tag{3.36}$$

which is close to the previous $E_{\mathrm{red}}(\theta)$. For the sake of concreteness, we redefine $K = \bar{K}$, $a = \bar{a}$ and $P = \bar{P}$.

We consider the corrections of the normal bundle, $\bar{N} = N + \Delta N$, and its linearized dynamics, $\bar{\Lambda}_N = \Lambda_N + \Delta\Lambda_N$, where $Q^N : \mathbb{T}^d \to \mathbb{R}^{(d+n)\times n}$ is a periodic matrix map and Λ_N a constant $n \times n$ matrix, so that $\Lambda = \mathrm{blockdiag}(\mathrm{Id}, \Lambda_N)$. Doing similar computations on equation

$$\mathrm{D}F(K(\theta))\bar{N}(\theta) - \bar{N}(\theta+\omega)\bar{\Lambda}_N = 0 \tag{3.37}$$

as in the substep 2 of the general algorithm, we obtain the cohomological equation:

$$-E^N_{\mathrm{red}}(\theta) = \Lambda Q^N(\theta) - Q^N(\theta+\omega)\Lambda_N - \begin{pmatrix} O \\ \Delta\Lambda_N \end{pmatrix}. \tag{3.38}$$

As Λ is blockdiagonal, we can split equation (3.38) in two different equations

$$-E^{LN}_{\mathrm{red}}(\theta) = Q^{LN}(\theta) - Q^{LN}(\theta+\omega)\Lambda_N, \tag{3.39}$$

$$-E^{NN}_{\mathrm{red}}(\theta) = \Lambda_N Q^{NN}(\theta) - Q^{NN}(\theta+\omega)\Lambda_N + \Delta\Lambda_N, \tag{3.40}$$

and solve them separately.

Note that equation (3.39) is similar to (3.32). In that case, if the matrix $(\mathrm{Id} - e^{2\pi \mathbf{i} k\omega}\Lambda_N)$ is invertible then we can solve equation (3.39), again in terms of Fourier, by isolating Q^{LN}_k. Then, the solution is

$$Q^{LN}_k = -E^{LN}_{\mathrm{red}\,k}(\mathrm{Id} - e^{2\pi \mathbf{i} k\omega}\Lambda_N)^{-1}, \tag{3.41}$$

for all k. The condition for the matrix $(\mathrm{Id} - e^{2\pi \mathbf{i} k\omega}\Lambda_N)$ to be invertible, that is

$$1 - e^{2\pi \mathbf{i} k\omega}\lambda \neq 0, \tag{3.42}$$

where $\lambda \in \mathrm{Spec}(\Lambda_N)$, is a *first Melnikov condition*. See Remark 3.10 in the following subsection.

The second equation (3.40) is not immediate, since Λ_N is a complete matrix $n \times n$. Notice that, in terms of Fourier it reads as

$$-E^{NN}_{\mathrm{red}\,0} = \Lambda_N Q^{NN}_0 - Q^{NN}_0\Lambda_N - \Delta\Lambda_N, \qquad k = 0, \tag{3.43}$$

$$-E^{NN}_{\mathrm{red}\,k} = \Lambda_N Q^{NN}_k - Q^{NN}_k e^{2\pi \mathbf{i} k\omega}\Lambda_N, \qquad k \neq 0. \tag{3.44}$$

By choosing $Q_0^{NN} = 0$ in the first equation, which corresponds to the constant Fourier term, we obtain directly the correction of the dynamics on the bundles, which is of the form

$$\Delta\Lambda_N = E^{NN}_{\text{red }0}. \tag{3.45}$$

To obtain the other $k \neq 0$ Fourier terms of Q^{NN}, we just have to solve equation (3.44) as an n^2-dimensional linear system by using some numerical method. The hypothesis for solvability of these equations is a *second Melnikov condition*

$$\lambda_i - e^{2\pi \mathbf{i} k\omega}\lambda_j \neq 0, \tag{3.46}$$

where $\lambda_i, \lambda_j \in \text{Spec}(\Lambda_N)$. In particular, the Floquet multipliers are the eigenvalues of the matrix, and both real and complex Floquet multipliers can appear in this reducible case.

Summarizing, we have obtained new better approximations $\bar{K} = K + P\xi$, $\bar{a} = a + \Delta a$ and $\bar{N} = N + PQ^N$ and $\bar{\Lambda}_N = \Lambda_N + \Delta\Lambda_N$, such that improves the errors E and E_{red}. We have to repeat substeps 1 and 2 until we reach the desired error tolerance.

3.2.3 An algorithm based on complete reducibility

Furthermore, sometimes it is possible to chose a frame in such a way that the linearization becomes a constant, and also diagonal, matrix.

Definition 3.8 *We say that the invariant torus is* completely reducible *if and only if there exists* $P : \tilde{\mathbb{T}}^d = (\mathbb{R}/2\mathbb{Z})^d \to \mathbb{R}^{(d+n)\times(d+n)}$ *and* $\Lambda \in \mathbb{R}^{(d+n)\times(d+n)}$ *constant such that:*

$$P^{-1}(\theta + \omega)\mathrm{D}F_a(K(\theta))P(\theta) - \Lambda = 0, \tag{3.47}$$

where Λ *is a diagonal matrix.*

This is the case, for instance, if we are under Diophantine conditions on ω and the invariant normal bundle decomposes into n one dimensional subbundles. In such a case, the normal dynamics is reduced to a diagonal constant matrix

$$\Lambda_N = \text{diag}(\lambda_{d+1}, \ldots, \lambda_{d+n}),$$

with real entries $|\lambda_j| \neq 1$, which we will denote as the *eigenvalues* of the torus. Notice that in that case, the correction of the dynamics of the bundles Λ_N is also a diagonal matrix

$$\Delta\Lambda_N = \text{diag}(\delta_{d+1}, \ldots, \delta_{d+n}),$$

which in fact its components are the Floquet multipliers. When it is possible to completely reduce the system, each step in the Newton-like method becomes very fast, see e.g. [59].

The essential idea of the completely reducible method is that we can consider both the invariance equation (3.1) and the reducibility equation for the normal bundle (3.49), in such a way that at each step of the Newton method, the linear equation to be solved is, in some sense, diagonalized. Lets see now the reformulation of the Newton step for the completely reducible case.

Substep 1: Correction of the torus K and parameter a

We proceed in the same way as we done in the non-reducible case, but taking into account that now the error of reducibility, $E_{\text{red}} : \mathbb{T}^d \to \mathbb{R}^{(d+n)\times(d+n)}$, is of the form

$$E_{\text{red}}(\theta) = P(\theta+\omega)^{-1}\mathrm{D}F_a(K(\theta))P(\theta) - \Lambda, \tag{3.48}$$

with Λ diagonal and constant, so that

$$E^N_{\text{red}}(\theta) = P(\theta+\omega)^{-1}\mathrm{D}F_a(K(\theta))N(\theta) - \begin{pmatrix} 0 \\ \Lambda_N \end{pmatrix}. \tag{3.49}$$

Consider the errors E and E_{red}, defined by (3.8) and (3.48) respectively, "small", so that we have an approximate invariant torus K for some parameter a with his normal invariant bundle N, which has a reduced constant diagonal dynamics Λ_N. In order to improve the approximation K, N and Λ_N, we consider the correction of the torus of the form $\Delta K(\theta) = P(\theta)\xi(\theta)$, being $\xi : \mathbb{T}^d \to \mathbb{R}^{d+n}$ a periodic function, and the adjustment of a given by Δa, so that we have new better approximations given by $\bar{K} = K + \Delta K$ and $\bar{a} = a + \Delta a$. Then, by substituting new approximations $\bar{K} = K + P\xi$ and $\bar{a} = a + \Delta a$ in (3.1) and using first order Taylor expansion, we obtain

$$-E(\theta) = \frac{\partial F_a}{\partial a}(K(\theta))\delta + P(\theta+\omega)\Lambda\xi(\theta) - P(\theta+\omega)\xi(\theta+\omega) + \mathcal{O}_2, \tag{3.50}$$

where we apply definitions (3.48) and (3.49) above, and $\mathcal{O}_2$ collect the quadratically small terms. Multiplying (3.50) by $P(\theta+\omega)^{-1}$ and neglecting quadratically small terms, we obtain the cohomological equation

$$\eta(\theta) = \Lambda\xi(\theta) - \xi(\theta+\omega) + B(\theta)\Delta a, \tag{3.51}$$

where

$$\eta(\theta) = -P(\theta+\omega)^{-1}E(\theta) \tag{3.52}$$

is the error of the approximate solution in the adapted frame and $B(\theta) = P(\theta+\omega)^{-1}\frac{\partial F_a}{\partial a}(K(\theta))$. Finally, splitting (3.51) into tangent and normal components, we realize that a Newton step reduces our equation to the block diagonal system

$$\eta^L(\theta) = \xi^L(\theta) - \xi^L(\theta+\omega) + B^L(\theta)\Delta a, \tag{3.53}$$
$$\eta^N(\theta) = \Lambda_N\xi^N(\theta) - \xi^N(\theta+\omega) + B^N(\theta)\Delta a. \tag{3.54}$$

which can be solved separately.

Tangent component. Observe that equation (3.53) is exactly the same as in the non-reducible case, (3.14), so that the solution is the same as well. Then, the correction over the tangent component of the torus is given by (3.18) as:

$$\xi^i_k = \frac{\eta^i_k - B^i_k\Delta a}{1-e^{2\pi ik\omega}},\ k\neq 0,$$

for each $i = 1,\dots,d$, with ξ^i_0 free (in particular $\xi^i_0 = 0$, for all i), and the adjustment of the parameter a is of the form (3.16)

$$\Delta a = -<B^L>^{-1}<\eta^L>.$$

Normal component. As Λ_N is now diagonal, in this case equation (3.54) splits into n equations, corresponding to their n normal components.

$$\eta^i(\theta) - B^i(\theta)\Delta a = \lambda_i\xi^i(\theta) - \xi^i(\theta+\omega) \tag{3.55}$$

for $i = d+1,\dots,d+n$. Notice that now, these equations are diagonal in Fourier space, so that the solution is obtained by solving (3.55) term by term in Fourier modes:

$$\xi^i_k = \frac{\eta^i_k - B^i_k\Delta a}{\lambda_i - e^{2\pi \mathbf{i}k\omega}}, \tag{3.56}$$

for all k. In particular, in this case we could have small divisors if the denominator becomes zero, that is

$$\lambda_i - e^{2\pi\mathbf{i}k\omega} = 0.$$

Since, by assumption, we are computing normally hyperbolic tori, this means $|\lambda_i| \neq 1$ for all i, there are no resonances in (3.56).

Remark 3.9 *The absence of resonances in* (3.56) *is known as* first Melnikov condition. *This is also important for dealing with complex eigenvalues of modulus 1, i.e. elliptic eigenvalues.*

At this step, we have gained new approximations $\bar{K}$ and $\bar{a}$ for which the new error $\bar{E}(\theta) = F_{\bar{a}}(\bar{K}(\theta)) - \bar{K}(\theta+\omega)$ is, hopefully, quadratically small with respect to $E(\theta)$. Additionally, we obtain a new approximation for the tangent bundle $\bar{L} = \mathrm{D}\bar{K}$.

Substep 2: Correction of the Floquet transformations

We redefine the error in the invariance equation of the adapted frame for the new $\bar{K}$ (so that for $\bar{P} = (\mathrm{D}\bar{K}\ N)$) and $\bar{a}$ as

$$\bar{E}_{\mathrm{red}}(\theta) = \bar{P}(\theta+\omega)^{-1}\mathrm{D}F_{\bar{a}}(\bar{K}(\theta))\bar{P}(\theta) - \Lambda \tag{3.57}$$

which is close to the previous $E_{\mathrm{red}}(\theta)$. For the sake of concreteness, we redefine $K = \bar{K}$, $a = \bar{a}$ and $P = \bar{P}$.

We consider the corrections of the normal bundle, $\bar{N} = N + \Delta N$, and its linearized dynamics, $\bar{\Lambda}_N = \Lambda_N + \Delta\Lambda_N$, of the form:

$$\begin{aligned} \Delta N(\theta) &= P(\theta)Q^N(\theta), \\ \Delta_N &= \mathrm{diag}(\delta_{d+1}, \ldots, \delta_{d+n}), \end{aligned}$$

where $Q^N : \mathbb{T}^d \to \mathbb{R}^{(d+n)\times n}$ is a periodic matrix map. Doing similar computations on equation

$$\mathrm{D}F(K(\theta))\bar{N}(\theta) - \bar{N}(\theta+\omega)\bar{\Lambda}_N = 0 \tag{3.58}$$

as in the substep 1, we obtain the cohomological equation:

$$-E^N_{\mathrm{red}}(\theta) = \Lambda Q^N(\theta) - Q^N(\theta+\omega)\Lambda_N - \begin{pmatrix} O \\ \Delta_N \end{pmatrix}. \tag{3.59}$$

Notice that now, this cohomological equation is diagonal in Fourier space. Then, using the matrix notation

$$Q^N(\theta) = (Q^{i,j}(\theta)),$$

for $i = 1, \ldots, n+d$, $j = d+1, \ldots, d+n$, equation (3.59) splits into $(d+n)\times n$ equations, which can be classified in three different equation types:

$$i \le d,\ i \ne j: \quad -E^{i,j}_{\mathrm{red}}(\theta) = Q^{i,j}(\theta) - Q^{i,j}(\theta+\omega)\lambda_j, \tag{3.60a}$$

$$i > d,\ i \ne j: \quad -E^{i,j}_{\mathrm{red}}(\theta) = \lambda_i Q^{i,j}(\theta) - Q^{i,j}(\theta+\omega)\lambda_j, \tag{3.60b}$$

$$i > d,\ i = j: \quad -E^{i,i}_{\mathrm{red}}(\theta) = \lambda_i Q^{i,i}(\theta) - Q^{i,i}(\theta+\omega)\lambda_i - \delta^i, \tag{3.60c}$$

for $j = d+1, \ldots, d+n$. We solve each of these three equations in terms of Fourier modes, in the same way we have done in the previous cases, and we obtain the following solutions

$$i \leq d,\ i \neq j \quad : \quad Q_k^{i,j} = \frac{(E_{\text{red}}^{i,j})_k}{\lambda_j e^{2\pi \mathbf{i} k\omega} - 1},\ \forall k. \tag{3.61a}$$

$$i > d,\ i \neq j \quad : \quad Q_k^{i,j} = \frac{(E_{\text{red}}^{i,j})_k}{\lambda_j e^{2\pi \mathbf{i} k\omega} - \lambda_i},\ \forall k. \tag{3.61b}$$

$$i > d,\ i = j \quad : \quad Q_k^{i,i} = \begin{cases} \frac{(E_{\text{red}}^{i,i})_k}{\lambda_i (e^{2\pi \mathbf{i} k\omega} - 1)}, & k \neq 0, \\ 0, & k = 0, \end{cases} \tag{3.61c}$$

$$\delta_i = (E_{\text{red}}^{i,i})_0.$$

Note that, there are no resonances in any of these equations, provided that we are considering $|\lambda_i| \neq |\lambda_j| \neq 1$. More concretely, we can have resonances in (3.61a) if $|\lambda_j| = 1$ and we can have resonances in (3.61b) if $|\lambda_j| = |\lambda_i|$. Notice that the absence of resonances in (3.61c) is granted by the Diophantine condition.

Remark 3.10 *The absence of resonances in* (3.61a) *is known as the* First Melnikov condition *and the absence of resonances in* (3.61b) *is known as the* Second Melnikov condition. *Notice that the absence of resonances in* (3.61a) *correspond to the condition* (3.42) *and the absence of resonances in* (3.61b) *correspond to the condition* (3.46)*, for the (non-diagonal) reducible case.*

Summarizing, we have obtained new better approximations $\bar{K} = K + P\xi$, $\bar{a} = a + \Delta a$ and $\bar{N} = N + PQ^N$ and $\bar{\Lambda}_N = \Lambda_N + \Delta\Lambda_N$, such that improves the errors E and E_{red}. We have to repeat substeps 1 and 2 until we reach the desired error tolerance.

Remark 3.11 *In order to prove the convergence of algorithms based on reducibility (both diagonal and non-diagonal), Melnikov conditions have to be strengthened in appropriate Diophantine conditions, such as*

$$|\lambda_j e^{2\pi \mathbf{i} k\omega} - \lambda_i| \geq \frac{\gamma}{|k|^\tau},$$

for $k \neq 0$.

3.3 Some guidelines for the implementation

In this section, we are going to implement the algorithms explained in this chapter, and how we can mix them in order to get more efficiency on the

computations.

Even that the main objective of this chapter is how to compute quasi-periodic normally hyperbolic invariant tori, our general interest is to study dynamical systems and determine, as well as possible, their global behavior. Indeed, due to the important role of invariant manifolds and how they organize the phase space of a dynamical system, we are very interested on their continuation along with the different mechanisms of breakdown it appears.

Recall from Section 1.3, that the definition of normally hyperbolic invariant manifold, see Definition 1.2 in which $\rho_{L,\pm} = 1$ for the quasi-periodic case, gives us two measures for the quality of the normal hyperbolicity property: one measures the asymptotic rate of growth (given by ρ_S and ρ_U in (1.4)) and the other measures how long you take to observe this asymptotic rate of growth, given by C in Definition 1.2. In the literature, several different kind of breakdowns for quasi-periodic normally hyperbolic invariant tori has been seen. One of the most frequent scenarios is the loss of the hyperbolicity due to the degeneracy of the rates of growth, in which either ρ_S or ρ_U goes to $1(=\rho_{L,\pm})$, which concerns the known *quasi-periodic bifurcation theory*, see e.g. [10, 25, 26]. Besides of that, the loss of hyperbolicity due to the incapacity to bound the factor C of Definition 1.2 is also possible, which is related to the collision of the invariant bundles of the torus, in which we cannot have the splitting into tangent, stable and unstable directions of equation (1.3), independently of the rates of growth, which can be different from 1 or not. This kind of behaviour has been profusely studied in [44, 57, 59]. In particular, in [57, 59] the authors describe two different *bundle merging scenarios* on skew-products over rotations. In the first scenario there appears a collision between stable and unstable bundles, which leads to an immediate breakdown of the torus, although their corresponding Lyapunov multipliers remain different and far from 1. In the second one, there appears a collision between stable bundles (slow and fast) leading to the loss of the reducibility of the torus but not to its immediate breakdown (the breakdown becomes later). More recently, a different bundle merging scenario has been observed for a quasi-periodic attractor torus in the dissipative standard map, in which the breakdown is due to the collision of the tangent and the stable bundle, see [18]. Notice that the above mentioned families of dynamical systems have some extra geometrical structure. In particular, [57, 59] deal with skew-products over rotations (for which the normal bundle is invariant) and [18] deals with conformally symplectic maps. In this chapter, we will observe similar scenarios in the more general families we consider.

3.3.1 Fourier series

It is well known that Fourier series are very specialized for rotational and periodic dynamics, so that for our particular case of this chapter. Notice that our method manipulates periodic objects $g(\theta)$ of the same dimension as the torus, so that $\theta \in \mathbb{T}^d$ and g defined by $g : \mathbb{T}^d \to \mathbb{R}^{d+n}$. Since the examples we will consider are defined modulus 2π, for the numerical implementation we use real (truncated) Fourier series, of the form

$$g(\theta) = c_0 + \sum_{k=1}^{\mathrm{N_F}} c_k \cos(k\theta) + s_k \sin(k\theta),$$

where s_k, c_k are the real Fourier modes, and $\mathrm{N_F}$ is the needed number of Fourier modes for a good representation of the function. In fact, during the computations we will store these s_k and c_k coefficients.

The norm we have used in these implementation is defined as

$$||g|| = |a_0| + \sum_{k=1}^{\mathrm{N_F}} \sqrt{s_k^2 + c_k^2} \geq ||g||_\infty,$$

where the numbers $\sqrt{s_k^2 + c_k^2}$ are called the amplitudes of the Fourier modes. In particular, for periodic matrix $M(\theta) = (M_{i,j}(\theta))$ or periodic vectors $V(\theta) = (V_i(\theta))$, we denote theirs norms by

$$||M|| = \max_{ij} ||M_{i,j}||$$

and

$$||V|| = \max_{i} ||V_i||,$$

respectively. Notice that the objects we compute are smooth, or even analytic, so the last terms of the expansions decrease faster than powers. We consider that we have a good representation of a periodic function g if the norm of the tail of the Fourier expansion (meaning, for instance, of the last 10 Fourier modes) is smaller than a desired tolerance. For that reason, in order to compute an invariant torus, we should take care not only on the error estimates of the invariance equations, E and E_{red}, but also on the accuracy of the approximations, that is of the tail of the Fourier series.

Recall that the parameterization method to compute quasi-periodic invariant tori consists in a Newton method to solve the invariance equation (3.1), and then to use there a Fourier discretization to solve their corresponding

N_F	Completely Red.	Red.	Non-Red.
64	2.12500e-01	2.15000e-01	4.10000e-01
128	9.00000e-02	8.60000e-02	1.70000e-01
256	2.25000e-01	2.25000e-01	4.47500e-01
512	2.95000e-01	3.13333e-01	5.44000e-01
1024	6.77500e-01	7.15000e-01	1.27500e+00
2048	7.32500e-01	7.35000e-01	1.38750e+00
4096	1.33750e+00	1.37000e+00	2.55250e+00
8192	1.93500e+00	2.04000e+00	3.81250e+00
16384	5.27500e+00	5.96250e+00	1.02050e+01
32768	1.16475e+01	1.19700e+01	2.44850e+01
65536	2.10425e+01	2.10575e+01	4.39350e+01
131072	5.13425e+01	5.07920e+01	1.04690e+02
262144	7.92025e+01	7.57500e+01	1.51110e+02
524288	1.40776e+02	1.70220e+02	2.74075e+02
1048576	3.46405e+02	4.06400e+02	6.64240e+02

TABLE 3.1: Computation time of one Newton step for the different algorithms of this chapter by using an usual laptop.

linear invariance equation. In reducible cases, the algorithm reduces to steps that are diagonal in the Fourier space, so then becoming really faster. In particular, we need $O(2N_F+1)$ storage space and $O((2N_F+1)\log(2N_F+1))$ operations in order to perform a Newton step combined with FFT routines. See Table 3.1 for the computation time (in seconds) of a Newton step for all three methods explained in this chapter.

3.3.2 Observables

In order to monitor and measure the quality of the normal hyperbolicity property, we analyze the following observables:

- Lyapunov multipliers,
- Minimum angle between invariant bundles.

Otherwise, in order to measure the quality of the regularity of the torus, and so a better understanding of its breakdown, we analyze:

- the blow up of the Sobolev norms,
- the blow up of the C^r-norms.

Dynamical Observables

First natural observables to compute are the *Lyapunov multipliers*, which give us information about the linearized dynamics. Notice that, in the reducible case they correspond to the absolute values of the eigenvalues of the reduced matrix Λ, in which we have d multipliers equal to 1, corresponding to the tangent dynamics, and n hyperbolic eigenvalues corresponding to the normal dynamics. Otherwise, when we are not dealing with a completely reducible torus, we can compute them from the hyperbolic cocycle (Λ_N, ω), given by

$$\begin{aligned} \bar{v} &= \Lambda_N(\theta)v \\ \bar{\theta} &= \theta + \omega \end{aligned}$$

by using usual methods to compute Lyapunov multipliers over cocycles. But even more, using our methods, during the continuations quasi-periodic tori we obtain the concrete parameters (a, ε) for which the diffeomorphism $F_{a,\varepsilon}$ has a quasi-periodic invariant torus, so then we can compute the Lyapunov multipliers, direct from the diffeomorphism $F_{a,\varepsilon}$, by using an usual QR-method to compute Lyapunov multipliers. Notice that, in the non-completely reducible case (and also for the non-reducible), the Lyapunov multipliers could have the same value, that is, the invariant torus is of a focus type. In particular, as long as the Lyapunov multipliers are far from 1, the non-completely reducible and the non-reducible methods will work.

Hence, following [56, 59], we consider as another suitable observable the *minimum angle between bundles*. Using this observable, we are able to detect the mechanism of the "bundle merging scenario", in which the Lyapunov multipliers of the cocycle of the torus remain different but the bundles corresponding to them approach each other, in a non-smooth way, leading to the destruction of the torus. We will denote by α the minimum angle between two sections $v_1, v_2 : \mathbb{T}^1 \to \mathbb{R}^{n+d}$,

$$\alpha(v_1, v_2) = \min_{\theta \in \mathbb{T}} \alpha(v_1(\theta), v_2(\theta)).$$

Certainly, these values α are related to the value C on Definition 1.2, and the breakdown in the bundle merging scenario is due to the impossibility of the splitting into tangent, stable and unstable directions around the torus, so that we lose the reducibility of the torus. Moreover, we can approach the critical ε value for the breakdown by extrapolating this minimum angle. As it has been seen in [18, 56, 59], for skew products and symplectic maps, the minimum angle between bundles in this scenario has a lineal decay close to

the breakdown. Then, we formulate the following conjecture, to be verified in our more general class of problems.

Conjecture 3.12 *Let $F_{a,\varepsilon}$ be a family of real analytic functions, where ε represents the continuation parameter. Let $(K_\varepsilon, a_\varepsilon)$ be the family of quasi-periodic normally hyperbolic invariant tori and their adjusting parameters for this family $F_{a,\varepsilon}$. In a bundle merging scenario, the minimum angle between bundles satisfies a linear decay close to the breakdown of the torus, given by*

$$\alpha(\varepsilon) \sim A(\varepsilon_c - \varepsilon),$$

when $\varepsilon \to \varepsilon_c$.

Remark 3.13 *In the bundle merging scenario, the bundles involved have different Lyapunov multipliers.*

Otherwise, we can also use this observable on other scenarios with a smooth collision between bundles, which do not lead to the breakdown of the torus. For instance, we can observe a smooth collision of the bundles, where the minimum angle between bundles goes to zero, uniformly, in a square root way

$$\alpha(\varepsilon) \sim A(\varepsilon_c - \varepsilon)^{\frac{1}{2}},$$

but moreover the Lyapunov multipliers collide. In this scenario, there is a transition from a *node* torus to a *focus* torus. In that moment, the torus loses the complete reducibility property, but not the non-completely one, so that the torus persists as a *focus invariant torus* with complex eigenvalues. This has been seen in many works of bifurcation theory, see e.g.[10, 25, 26].

Summarizing, the torus loses the complete reducibility property at the time of a bundle collision, due to the loss of the splitting into tangent, stable and unstable directions, but depending on how smooth this collision is, the torus will be destroyed or not.

Functional Observables

Following [17, 31] we consider the *Sobolev norms* of the torus in order to measure the quality of the regularity of the parameterization. We add to the game the computation of the *C^r-norms*. We are also interested in the regularity of the torus at the breakdown.

We focus here with univariate functions. For a real-analytic periodic function $f : \mathbb{T}^d \to \mathbb{C}$, we can define a fractional derivative $f^{(r)} : \mathbb{T} \to \mathbb{C}$, for any $r \geq 0$,

through the Fourier expansions. Hence, if the Fourier expansion is expressed in the complex way by

$$f(\theta) = \sum_{k\in\mathbb{Z}} \hat{f}_k e^{\mathbf{i}k\theta},$$

we define its derivative by

$$f^{(r)}(\theta) = \sum_{k\in\mathbb{Z}} |k|^r e^{\frac{\pi}{2} r \mathrm{sg}(k)\mathbf{i}} \hat{f}_k e^{\mathbf{i}k\theta}.$$

Hence, we can define a C^r semi-norm

$$||f||_{C^r} = ||f^{(r)}||_\infty = \max_{\theta\in\mathbb{T}} |f^{(r)}(\theta)| \tag{3.62}$$

and $W^{s,p}$ semi-norms defined by

$$||f||^p_{W^{s,p}} = \sum_{k\in\mathbb{Z}} |k|^{sp} |f_k|^p, \tag{3.63}$$

but we will mainly consider the $H^s = W^{s,2}$ semi-norm, the *Sobolev semi norm*. Notice that, from Holder inequality, with $\frac{1}{q} + \frac{1}{p} = 1$,

$$||f||_{C^r} \leq ||f||_{W^{r,1}} \leq \left(\sum_{k\in\mathbb{Z}} |k|^{(r-s)q} \right)^{\frac{1}{q}} ||f||_{W^{s,p}},$$

as long as $r < s - \frac{1}{q}$. Then, there is the inclusion $W^{s,p} \subset W^{r,1}$, which is closed with the "norm"

$$\left(\sum_{k\in\mathbb{Z}} |k|^{(r-s)q} \right)^{\frac{1}{q}}.$$

In the study of PDE's, this type of results are used to prove the existence of weak solutions (in Sobolev sense), and bootstrap their C^r regularity. Here we use this type of results in the opposite way: if the C^r semi-norm of a parameterization explodes, then the H^s semi-norm, with $s > \frac{1}{2} + r$ explodes.

In our applications,we will consider the blow up of the C^r and H^r semi-norms in order to detect and to study the destruction of invariant torus (in connection with renormalization group theory).

Conjecture 3.14 *Let $K_{p,\varepsilon} : \mathbb{T} \to \mathbb{R}^{d+n}$ be the periodic part of*

$$K_\varepsilon(\theta) = \begin{pmatrix} \theta \\ 0 \end{pmatrix} + K_{p,\varepsilon}(\theta),$$

where K is F_{a_ε}-invariant, for a fixed ϵ value of the continuation process and a_ε its adjusting parameter. In particular, we will consider norms defined as

$$||K_{p,\varepsilon}||_* := \max_{i=1,\dots,d+n} ||K^i_{p,\varepsilon}||_*,$$

where $* = H^r, C^r$.

Then, in a bundle merging scenario at a critical value ε_c, the Sobolev and C^r regularities of the torus are r_c and $\hat{r}_c$, respectively. Moreover, near the breakdown, for $\varepsilon < \varepsilon_c$:

- *For $r > r_c$ the H^r semi-norm blows up as*

$$||K_{p,\varepsilon} - K_{p,\varepsilon_c}||_{H^r} \sim \frac{A_r}{(\varepsilon_c - \varepsilon)^{B_r}}, \tag{3.64}$$

  when $\varepsilon \to \varepsilon_c$, with a critical exponent $B_r = a + br$, in such a way that the critical Sobolev regularity is given by

$$r_c = -\frac{a}{b}.$$

- *For $r > \hat{r}_c$ the C^r semi-norm blows up as*

$$||K_{p,\varepsilon} - K_{p,\varepsilon_c}||_{C^r} \sim \frac{\hat{A}_r}{(\varepsilon_c - \varepsilon)^{\hat{B}_r}}, \tag{3.65}$$

  when $\varepsilon \to \varepsilon_c$, with a critical exponent $\hat{B}_r = \hat{a} + \hat{b}r$, in such a way that the critical regularity is given by

$$\hat{r}_c = -\frac{\hat{a}}{\hat{b}}.$$

Remark 3.15 *These constants a, b, $\hat{a}$, $\hat{b}$ of the critical exponents B_r and $\hat{B}_r$ are, possibly, universal for every "class of breakdown".*

Remark 3.16 *From Sobolev inequalities, the critical regularities are related by*

$$\hat{r}_c \geq r_c - \frac{1}{2}.$$

In particular, in our implementations we will estimate the critical values ε_c by extrapolating the semi-norms H^2 and C^1 and we will also reproduce fits for the critical regularity in terms of the critical exponent B_r and $\hat{B}_r$ of H^r and C^r, respectively. By using these observables in different examples, we want to *discover* new classes of universality, that is different breakdown types.

3.3.3 Our particular examples

For the implementation of the algorithm, we restrict ourselves to the computation of torus of dimension 1, which means that in fact, we are computing normally hyperbolic invariant circles. We continue curves of NHIT in parameter space (a, ε) with respect to ε with the same fixed frequency $\omega = (\sqrt{5}-1)\pi$, which corresponds to the Golden mean value, up to a critical value. For each ε-value, we compute its normally hyperbolic invariant torus, its adjusting parameter, its normal bundles and their dynamics (which in the completely reducible case coincides with the absolute value of the Lyapunov multipliers). Moreover, we also compute the observables discussed in this section, that is Sobolev and C^r norms, angle between bundles and Lyapunov multipliers. Also, in the non-reducible case, we compute the *index* of the bundles, which gives us information about the orientability of the fibers of the torus.

Our computations has been done by demanding an error tolerance $||E|| < 10^{-10}$. When we apply our Newton-like methods, if the Newton process do not converge, we decrease the step size $\Delta\varepsilon$ by a factor of $\frac{1}{2}$ with respect to the previous parameter ε. Furthermore, we also require to the algorithm to double the number of Fourier modes if the method does not converge for three consecutive steps, as well as if the tail of our torus is greater than 10^{-10}, which means that our objects are not well approximated. In particular, our algorithm is imposed to stop when the torus reaches $2^{20} = 1048576$ Fourier nodes, which we consider that is large enough for a critical value, with a continuation step size of the order $\Delta\varepsilon = 10^{-7}$. We should remark that we can produce a continuation till breakdown because we use an efficient method which allows us to do computations using a large number of Fourier modes. The breakdown of the computation happens when the dynamical properties of the torus deteriorate, which happens just before the breakdown of the object is engendered.

In our first four examples, we consider as a toy example the 3D-*Fattened Arnold Family*, also used in [11], given by $F_{a,\varepsilon} : \mathbb{R}/2\pi\mathbb{Z} \times \mathbb{R}^2 \to \mathbb{R}/2\pi\mathbb{Z} \times \mathbb{R}^2$ defined as:

$$F_{a,\varepsilon}\begin{pmatrix} x \\ y \\ z \end{pmatrix} = \begin{pmatrix} x + a + \varepsilon(\sin(x) + y + z/2) \\ b(\sin(x) + y) \\ c(\sin(x) + y + z) \end{pmatrix} \tag{3.66}$$

where b, c are fixed parameters, $a \in \mathbb{R}$ is the adjusting parameter and $\varepsilon \in \mathbb{R}$ is the continuation parameter. This system has a constant determinant of the Jacobian $\det(\mathrm{D}F_{a,\varepsilon}) = bc$, so we can choose different parameters b and c

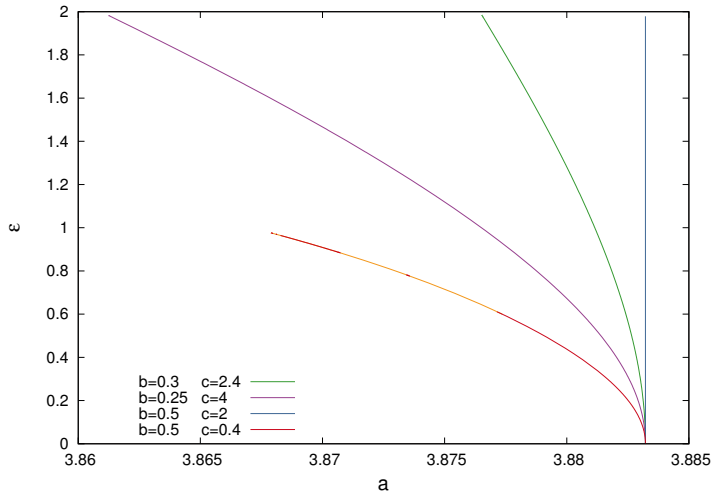

FIGURE 3.1: Curves of quasi-periodic NHIT in the parameter plane (a, ε) for the Fattened Arnold Family in Examples 1, 2, 3 and 4. In particular the red-orange curve represent the parameters in the continuation of Example 4, where tori are either completely reducible (red) or non-completely reducible (orange).

in order to explore different examples of normally hyperbolic invariant tori. In particular, in Examples 1, 2, and 3 we compute quasi-periodic saddle tori, for some fixed values $b < 1$ and $c > 1$, in which the first one is for a dissipative map ($bc < 1$) and the other two are both for a conservative map ($bc = 1$), and in Example 4 we compute attracting tori for some values $b, c < 1$. Figure 3.1 shows the continuation parameter plane (a, ε) for examples based on the Fattened Arnold Family.

In Example 5, we consider as a toy example a 3D-*Fattened Hénon Family*, given by $F_{a,\varepsilon} : \mathbb{R}/2\pi\mathbb{Z} \times \mathbb{R}^2 \to \mathbb{R}/2\pi\mathbb{Z} \times \mathbb{R}^2$ defined as:

$$F_{a,\varepsilon}\begin{pmatrix} x \\ y \\ z \end{pmatrix} = \begin{pmatrix} x + a + d\varepsilon(\cos(x) + z) \\ 1 + z - by^2 + \varepsilon\cos(x) \\ cy \end{pmatrix} \tag{3.67}$$

where b, c, d are fixed parameters, $a \in \mathbb{R}$ is the adjusting parameter and $\varepsilon \in \mathbb{R}$ is the continuation parameter. This system has a determinant of the Jacobian $\det(\mathrm{D}F_{a,\varepsilon}(x)) = -c(\varepsilon\sin(x)(1+\varepsilon) + 1)$. In particular, this family is an extension of the *rotating Hénon Family*, studied in [59], for which they have fixed $d = 0$. In this case, we use the same fixed parameters as in [59], $b = 0.68$ and $c = 0.1$, in which a saddle torus bifurcates into an attracting "node-torus", either for the skew-product case, $d = 0$, and for the coupled case, $d = 1$. In particular, for $d = 0$ we will reproduce the results in [59].

Figure 3.2 shows the continuation on the parameter plane (a, ε) for examples based on the Fattened Hénon Family.

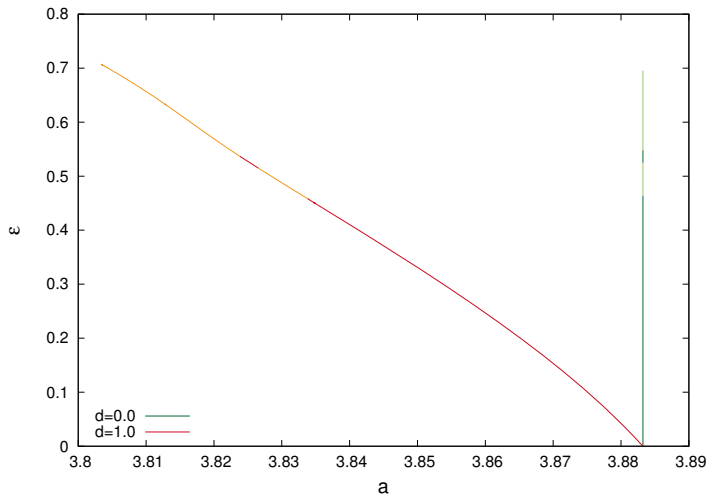

FIGURE 3.2: Curves of quasi-periodic NHIT in the parameter plane (a, ε) for the Fattened Hénon Family of Example 5, for the skew-product case $d = 0$ (red-orange) and the coupled case $d = 1$ (green-light green). We distinct in orange (and light green, respectively) the ε parameter values in which we do not have reducibility on the torus.

All of these examples are continued till the torus breaks, using any of the three methods explained in this chapter according the requirement of each particular example. Since in Examples 1, 2 and 3 we continue saddle tori, it is natural to use the completely reducible method. In these examples, the breakdown of the torus is due to a bundle merging scenario (particularly, between tangent and stable bundles in Examples 1 and 2, and with a triple collision in Example 3). In Example 4, we continue an attracting torus, which has a 2-dimensional stable bundle. In this example, we observe several transitions from node to focus torus (also viceversa), in which the torus loses the complete reducibility property at the concrete point in which the Lyapunov multipliers collide and the slow and fast bundles also collide, but in a smooth way. In that example, we have test all the three methods. The torus finally breaks due to a bundle collision between the tangent and the 2-dimensional stable bundle, after all these node-focus transitions.

Finally, in Example 5 we observe similar transitions as in [56, 59], both for the skew-product $d = 0$ and coupled case $d = 1$. We deal with a saddle torus, for small values of ε, which is turned to an attracting-node type torus via a period-halving bifurcation. The torus loses its reducibility due to a non-smooth bundle collision of the slow and fast bundles, whereas its Lyapunov

multipliers remains separated and remain far from 1, so the torus does not break. For a large ε parameter, the method (which is, of course, necessary to be the non-reducible method) stops due to a possible "fractalization" of the torus. This mechanism deserves further study.

3.4 Example 1: Continuation of a saddle torus in a dissipative system

This example deals with a continuation of a saddle torus for a dissipative Fattened Arnold family with parameters $0 < b < 1$, $c > 1$ and $bc < 1$. In the first place, we consider the particular case $b = 0.3$ and $c = 2.4$ ($bc = 0.72$).

Look first what does happen for the unperturbed case $\varepsilon = 0$. In that case, the system (3.66) is a skew product over a rotation $\theta + a$, and in fact, we can explicitly compute the invariant torus with rotation number a for $\varepsilon = 0$ (we will take $a = \omega$). In order to get an initial approximation of the torus, we ask for a parameterization of it which has to meet the invariance equation for $\varepsilon = 0$,

$$F_{a,0}(K_{a,0}(\theta)) = K_{a,0}(\theta + a).$$

From this equation, we get that $K_{a,0}$ has to be a graph of the form

$$K_{a,0}(\theta) = \begin{pmatrix} \theta \\ \varphi_a(\theta) \\ \psi_a(\theta) \end{pmatrix}, \tag{3.68}$$

where

$$\begin{aligned} \varphi_a(\theta) &= \sum_{k=1}^{\infty} b^k \sin(\theta - ka), \\ \psi_a(\theta) &= -\sum_{k=0}^{\infty} c^{-k} \left(\sin(\theta + ka) + \varphi_a(\theta + ka)\right). \end{aligned} \tag{3.69}$$

By defining

$$C(a,b) = \frac{1 - b\cos(a)}{1 - 2b\cos(a) + b^2}, \; S(a,b) = \frac{b\sin(a)}{1 - 2b\cos(a) + b^2},$$

we can sum the series (3.69), and we get

$$\begin{aligned} \varphi_a(\theta) &= S(a,b)\ \cos(\theta) + (C(a,b) - 1)\ \sin(\theta), \\ \psi_a(\theta) &= \frac{c}{b}\left(S(a,b)(C(-a,c^{-1}) - 1) + (C(a,b) - 1)S(-a,c^{-1})\right)\cos(\theta) \\ &\quad - \frac{c}{b}\left((C(a,b) - 1)(C(-a,c^{-1}) - 1) - S(a,b)S(-a,c^{-1})\right)\sin(\theta). \end{aligned}$$

Remark 3.17 *Notice that formulae above work for any* $b \neq \pm 1, 0$ *and* $c \neq 0$.

Moreover, from the linearized equation

$$P_{a,0}(\theta + a)^{-1} \mathrm{D}F_{a,0}(K_{a,0}(\theta)) P_{a,0}(\theta) = \Lambda_{a,0}(\theta),$$

we get the values of the initial $P_{a,0}$ and $\Lambda_{a,0}$,

$$P_{a,0}(\theta) = \begin{pmatrix} 1 & 0 & 0 \\ \varphi_a'(\theta) & 1 & 0 \\ \psi_a'(\theta) & \frac{c}{b-c} & 1 \end{pmatrix} \tag{3.70}$$

and

$$\Lambda_{a,0} = \begin{pmatrix} 1 & 0 & 0 \\ 0 & b & 0 \\ 0 & 0 & c \end{pmatrix}.$$

Remark 3.18 *Notice that formulae above work for any* $b \neq c$.

In this example, from $P_{a,0}(\theta)$, we get the parameterization of stable and unstable bundles,

$$N^S_{a,0}(\theta) = \begin{pmatrix} 0 \\ 1 \\ \frac{c}{b-c} \end{pmatrix}, \; N^U_{a,0}(\theta) = \begin{pmatrix} 0 \\ 0 \\ 1 \end{pmatrix},$$

respectively, which are its last two columns.

During the continuation of this torus with respect to ε, we observe how the tangent and stable bundles approach each other till finally collide, see Figure 3.3 (top-right). Notice that N^U remains far from L and N^S. Near the breakdown, there is a linear decay to zero of the angle between tangent and stable bundle, $\alpha_{L,S} = \alpha(L, N^S)$, given by

$$\alpha_{L,S}(\varepsilon) \simeq 1.06010644 - 0.53398534\ \varepsilon.$$

See Figure 3.3 bottom-right to see this fit over the values of the continuation, supporting Conjecture 3.12. With this fit, we can get a first approximation of the critical value ε_c given by the intersection of $\alpha_{L,S}(\varepsilon)$ with zero, so that

$$\varepsilon_{c_\alpha} \simeq 1.9852725710.$$

At this value, the torus is destroyed. Despite that, the Lyapunov multipliers Λ_L and Λ_S are moving away from each other, see Table 3.3, when the torus is destroyed. We are, in fact, in a *bundle merging scenario* which cause the destruction of the torus.

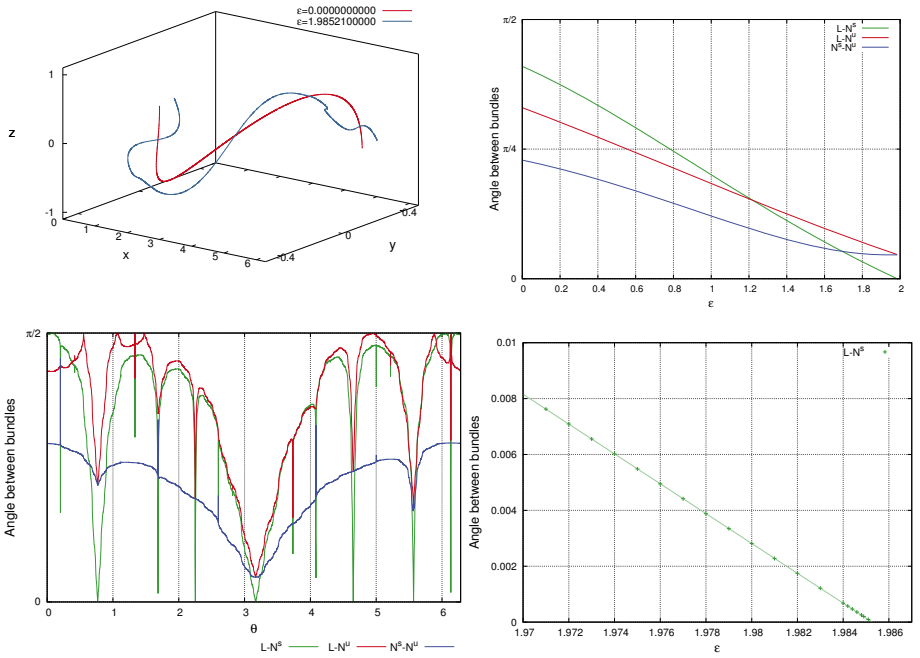

FIGURE 3.3: Results for the dissipative system with $b = 0.3$ and $c = 2.4$ in Example 1. Left: First (red) and last (blue) tori we compute during the continuation (top) and minimum angles between bundles for the last torus we compute (bottom). Right: Minimum angles between bundles for all ε values of the continuation (top) and linear fit of $\alpha_{L,S} = \alpha(L, N^S)$ (bottom).

In order to get another indicator of the breakdown of the torus, we show the blow up of the H^2 and C^1 semi-norms when we approach the critical value, see Table 3.2 and Figure 3.4 (left). We can check in Figure 3.4 (left) how expressions of Conjecture 3.14 given by equations (3.64) and (3.65) fit very well the semi-norms of the parameterization of the invariant tori for the last parameters ε of the continuation and how they grow up when ε approaches the critical value (labeled with a blue vertical line). In particular, the H^2 and C^1 semi-norms of this example are given by expressions

$$\begin{aligned} H^2(\varepsilon) &\simeq \frac{1.25256702}{(1.98528019-\varepsilon)^{1.04030871}}, \\ C^1(\varepsilon) &\simeq \frac{2.35258564}{(1.98528553-\varepsilon)^{0.46438943}}. \end{aligned}$$

Concretely, for these H^2 and C^1 semi-norms we obtain the critical breakdown

values

$$\begin{aligned} \varepsilon_{c_{H^2}} &\simeq 1.9852801944, \\ \varepsilon_{c_{C^1}} &\simeq 1.9852855326, \end{aligned}$$

which coincides up to five significant digits with ε_{c_α}. Another indicator of how close to the breakdown we are, is the necessity to increase a lot the number of the Fourier modes, $\mathrm{N_F}$, in order to approximate the torus, see Table 3.2.

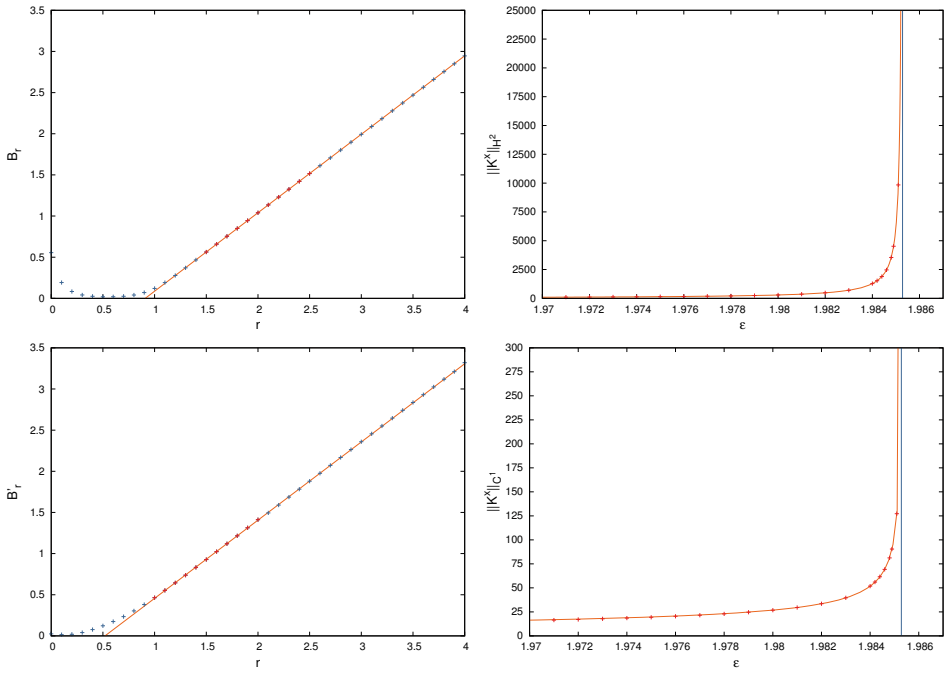

FIGURE 3.4: Blow up at the critical value of the H^2 (top-right) and C^1 (bottom-right) seminorms, where the critical value is drawn with an straight blue line. In the left, it appears the fit for the affine expression of the critical exponent which match with expressions (3.64) and (3.65) of Conjecture 3.14, that is B_r and $\hat{B}_r$ (B'_r in this picture), respectively.

We also compute the blow up for different Sobolev and C^r norms, obtaining the corresponding estimates of the critical parameter of breakdown. See Table 3.4. Concretely, the critical exponents B_r and $\hat{B}_r$ satisfy the linear expressions

$$\begin{aligned} B_r &\simeq -0.86694475 + 0.95349421\ r, \\ \hat{B}_r &\simeq -0.49407515 + 0.95017818\ r, \end{aligned}$$

supporting Conjecture 3.14. From this expressions, we get the critical regularities of the torus in the breakdown, which are $r \simeq 0.9092291712$ and $\hat{r} \simeq 0.5199815828$, respectively. We obtain these values by fitting expressions (3.64) and (3.65) using the last 10 well equispaced ε values. See Figure 3.4 (left).

In order to test the universality of this mechanism of breakdown, we have done the continuation for another saddle torus in a dissipative system. In this new case, we choose $b = 0.4$ and $c = 2.8$. We observe again a breakdown due to the bundle collision of tangent and stable bundle, with a separately Lyapunov multipliers. The linear fit of the decay of the minimum angle, given by

$$\alpha_{L,S}(\varepsilon) \simeq 1.03781398 - 0.52392610\ \varepsilon,$$

gives us a critical breakdown value

$$\varepsilon_{c_\alpha} \simeq 1.9808403980.$$

In that case, the H^2 and C^2 semi-norms are given, respectively by

$$\begin{aligned} H^2(\varepsilon) &\simeq \frac{0.63574332}{(1.98084535-\varepsilon)^{1.03892062}}, \\ C^1(\varepsilon) &\simeq \frac{1.68323296}{(1.98085685-\varepsilon)^{0.47005532}}, \end{aligned}$$

so the critical breakdown values are

$$\begin{aligned} \varepsilon_{c_{H^2}} &\simeq 1.9808453525, \\ \varepsilon_{c_{C^1}} &\simeq 1.9808568502, \end{aligned}$$

respectively. In particular, the general asymptotic expression of the critical exponents are given by

$$\begin{aligned} B_r &\simeq -0.86314089 + 0.95072600\ r, \\ \hat{B}_r &\simeq -0.47728414 + 0.93883642\ r, \end{aligned}$$

supporting Conjecture 3.14 if r is greater than $r_c \simeq 0.9078755460$ and $\hat{r}_c \simeq 0.5083783845$, respectively.

ε	a	H^2	C^1	$\mathrm{N_F}$
0.0000000000	3.8832220775	0.00000e+00	0.00000e+00	64
0.5000000000	3.8826566337	1.53973e-01	1.79450e-01	64
1.0000000000	3.8811478677	4.55716e-01	5.23489e-01	64
1.5000000000	3.8789968697	1.55869e+00	1.44720e+00	256
1.9000000000	3.8769720127	1.42373e+01	6.13174e+00	2048
1.9500000000	3.8767071001	3.83020e+01	1.02936e+01	4096
1.9800000000	3.8765473488	2.92166e+02	2.67485e+01	16384
1.9850000000	3.8765206722	6.21073e+03	1.03983e+02	262144
1.9852000000	3.8765196048	2.30904e+04	1.84828e+02	1048576
1.9852100000	3.8765195515	2.66068e+04	1.96656e+02	1048576

TABLE 3.2: Results for the continuation in the dissipative case $b = 0.3$ and $c = 2.4$ in Example 1. The table shows the H^2 Sobolev norm, the C^1 norm and the number of Fourier modes, $\mathrm{N_F}$, for each parameter value.

ε	a	Λ_L	Λ_S	Λ_U	$\alpha(L, N^S)$	$\alpha(L, N^U)$	$\alpha(N^S, N^U)$
0.0000000000	3.8832220775	1.00	0.3000000000	2.4000000000	1.28654e+00	1.03665e+00	7.18830e-01
0.5000000000	3.8826566337	1.00	0.2988625871	2.4091339337	9.83777e-01	8.11604e-01	5.68469e-01
1.0000000000	3.8811478677	1.00	0.2949374873	2.4411952732	6.30198e-01	5.76768e-01	3.80341e-01
1.9000000000	3.8769720127	1.00	0.2702183511	2.6645118550	4.62783e-02	1.80088e-01	1.45678e-01
1.9500000000	3.8767071001	1.00	0.2672472031	2.6941348369	1.89256e-02	1.60225e-01	1.45004e-01
1.9800000000	3.8765473488	1.00	0.2652737239	2.7141776027	2.81240e-03	1.48454e-01	1.44653e-01
1.9850000000	3.8765206722	1.00	0.2649259305	2.7177407607	1.47876e-04	1.46503e-01	1.44592e-01
1.9851000000	3.8765201385	1.00	0.2649188988	2.7178128976	9.46853e-05	1.46464e-01	1.44591e-01
1.9852000000	3.8765196048	1.00	0.2649118635	2.7178850753	4.14868e-05	1.46425e-01	1.44590e-01
1.9852100000	3.8765195515	1.00	0.2649111597	2.7178922954	3.61621e-05	1.46421e-01	1.44589e-01

TABLE 3.3: Results for the continuation in the dissipative case $b = 0.3$ and $c = 2.4$ in Example 1. The table shows the Λ values, corresponding to the Lyapunov multipliers, and the angle between bundles. We can observe here the decay of the angle between tangent and stable bundle, given by $\alpha(L, N^S)$.

r	ε_c	B_r	$\hat{\varepsilon}_c$	$\hat{B}_r$
0.0	2.7351644781	0.5557053222	2.0017499720	0.0241935458
0.1	2.2160544464	0.1922165988	1.9898692389	0.0149793181
0.2	2.0690625518	0.0827874948	1.9868589494	0.0192726838
0.3	2.0175747948	0.0414438527	1.9861072368	0.0405516415
0.4	1.9981289589	0.0248344053	1.9854562792	0.0767804115
0.5	1.9904984586	0.0189164398	1.9853986327	0.1229470550
0.6	1.9874202840	0.0191054657	1.9853517737	0.1743283284
0.7	1.9861571663	0.0252293694	1.9853214691	0.2343932678
0.8	1.9856313576	0.0403266642	1.9853029582	0.3035830172
0.9	1.9854123369	0.0701950851	1.9852918597	0.3807860724
1.0	1.9853239921	0.1205182897	1.9852855326	0.4643894253
1.1	1.9852913912	0.1915994375	1.9852821932	0.5527102202
1.2	1.9852814663	0.2774334407	1.9852804001	0.6441227418
1.3	1.9852795191	0.3706492223	1.9852796237	0.7375487784
1.4	1.9852796841	0.4664087573	1.9852794190	0.8322080595
1.5	1.9852800847	0.5625857314	1.9852795670	0.9276129567
1.6	1.9852803160	0.6585461139	1.9852799543	1.0234622568
1.7	1.9852803825	0.7542219041	1.9852804524	1.1195843668
1.8	1.9852803532	0.8496899819	1.9852813241	1.2161857832
1.9	1.9852802807	0.9450328975	1.9852825160	1.3132099003
2.0	1.9852801944	1.0403087109	1.9852816452	1.4120787752
2.1	1.9852801088	1.1355527234	1.9852753716	1.4941488433
2.2	1.9852800300	1.2307848258	1.9852761548	1.5896859826
2.3	1.9852799598	1.3260156103	1.9852770710	1.6862852051
2.4	1.9852798983	1.4212503656	1.9852778142	1.7829287246
2.5	1.9852798447	1.5164914574	1.9852783954	1.8794563743
2.6	1.9852797981	1.6117396876	1.9852789059	1.9759019724
2.7	1.9852797574	1.7069950523	1.9852790220	2.0716943118
2.8	1.9852797218	1.8022571599	1.9852793339	2.1678654394
2.9	1.9852796905	1.8975254593	1.9852794649	2.2636718215
3.0	1.9852796629	1.9927993637	1.9852794737	2.3592553545
3.1	1.9852796384	2.0880783156	1.9852795145	2.4548775650
3.2	1.9852796165	2.1833618214	1.9852795520	2.5505958893
3.3	1.9852795970	2.2786494658	1.9852795165	2.6460705877
3.4	1.9852795795	2.3739409157	1.9852794167	2.7413815939
3.5	1.9852795638	2.4692359158	1.9852792168	2.8363521216
3.6	1.9852795498	2.5645342775	1.9852789211	2.9309874593
3.7	1.9852795371	2.6598358630	1.9852784977	3.0250691994
3.8	1.9852795258	2.7551405641	1.9852779411	3.1185425157
3.9	1.9852795157	2.8504482783	1.9852772375	3.2113037823
4.0	1.9852795066	2.9457588819	1.9852802966	3.3196381528

TABLE 3.4: Estimates of the critical values ε_c and $\hat{\varepsilon}_c$ of the breakdown of the invariant torus in Example 1 and their corresponding critical exponent, for the Sobolev and C^r semi-norms respectively.

3.5 Example 2: Continuation of a saddle torus in a conservative system

In this example, we consider the case $b = 0.25$ and $c = 4$, in which the system is *conservative* ($bc = 1$). We can start the continuation by using the same initial approximation expression (3.68) given in the previous section.

Now, we continue a saddle invariant torus with respect to ε. Again, as in Example 1, the breakdown of the torus is due to a bundle collision between the tangent and stable subbundles. We can observe in Figure 3.5 (top-right) how the angle between tangent and stable bundle approaches zero as the parameter continuation ε increases. Near the breakdown, we observe again a linear decay to zero of the value $\alpha_{L,S}$, given in this case by expression

$$\alpha_{L,S}(\varepsilon) \simeq 0.95101870 - 0.47951222\ \varepsilon,$$

and showed in Figure 3.5 (bottom-right) with the last values of the continuation. Then, a first approximation of the critical value ε_c is given by the intersection between $\alpha_{L,S}(\varepsilon)$ and the horizontal axis, so that

$$\varepsilon_{c_\alpha} \simeq 1.9833043862.$$

At this moment, the torus is destroyed. Despite that, the Lyapunov multipliers Λ_L and Λ_S are moving away from each other, see Table 3.6, even though their product value is constant to 1, $\det(\mathrm{D}F_{a,\varepsilon}) = 1 = \Lambda_L\Lambda_S\Lambda_U$. We are, again, in a *bundle merging scenario* which cause the destruction of the torus.

As in last example, we take information about the breakdown from the semi-norms H^2 and C^1. In this case, the fits of the semi-norms H^2 and C^1 near the critical values are given by

$$\begin{aligned} H^2(\varepsilon) &\simeq \frac{0.52106152}{(1.98331250 - \varepsilon)^{1.03657369}}, \\ C^1(\varepsilon) &\simeq \frac{1.36754056}{(1.98333604 - \varepsilon)^{0.47751520}}, \end{aligned}$$

and represented in Figure 3.6 (left), where the respectively critical values are

$$\begin{aligned} \varepsilon_{c_{H^2}} &\simeq 1.9833125000, \\ \varepsilon_{c_{C^1}} &\simeq 1.9833360406, \end{aligned}$$

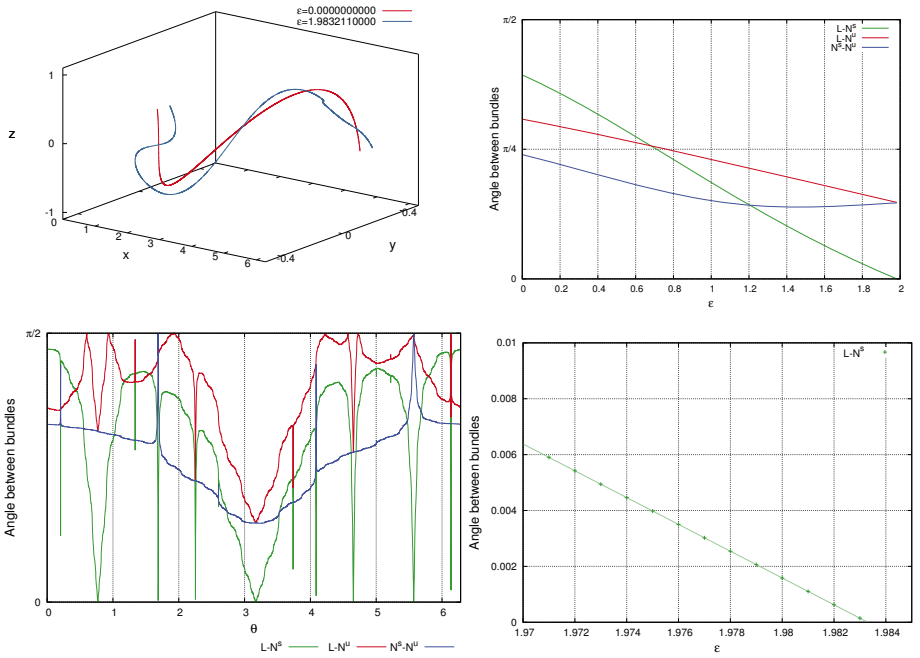

FIGURE 3.5: Results for all ε values of the continuation process for Example 2. Left: First (red) and last (blue) tori we compute (top) and minimum angles between bundles for the last torus we compute (bottom). Right: Minimum angles between bundles for all ε values (top) and linear fit of the angle $\alpha(L, N^S)$ close to the breakdown (bottom).

are represented by a blue vertical line. We can observe the blow up of these norms when ε approaches the critical value, supporting assertion on Conjecture 3.14. Notice also that, the explosion of these two norms as the ε value approaches the critical value, coincides with the increment of the number of Fourier modes needed to approximate the torus, see Table 3.5.

In the same way, we compute for a range of $r \in [0, 4]$ the critical breakdown values, ε_c and $\hat{\varepsilon}_c$, and their corresponding critical exponents, B_r and $\hat{B}_r$, see Table 3.7, which satisfy the linear expressions of Conjecture 3.14, given in this case by

$$\begin{aligned} B_r &\simeq -0.86158681 + 0.94921635\ r, \\ \hat{B}_r &\simeq -0.46503572 + 0.93164713\ r, \end{aligned}$$

which are well defined if r is greater than $r_c \simeq 0.9076822517$ and $\hat{r}_c \simeq 0.49915435$, respectively. Notice that these approximations of the critical exponents fits better, in a range $r \in [1.5, 2.5]$ for Sobolev norms and in $r \in [1, 2]$ for C^r norms, see Figure 3.6.

ε	a	H^2	C^1	$\mathrm{N_F}$
0.0000000000	3.8832220775	0.00000e+00	0.00000e+00	64
0.5000000000	3.8813974424	1.43788e-01	1.64755e-01	64
1.0000000000	3.8765074834	3.93198e-01	4.51560e-01	64
1.5000000000	3.8694737697	1.17980e+00	1.11774e+00	256
1.9000000000	3.8627251961	9.25609e+00	4.02912e+00	1024
1.9500000000	3.8618308534	2.46976e+01	6.68652e+00	2048
1.9800000000	3.8612901228	2.74229e+02	2.08560e+01	16384
1.9830000000	3.8612358919	3.16805e+03	6.23433e+01	131072
1.9832000000	3.8612322755	9.23013e+03	9.98547e+01	524288
1.9832100000	3.8612320947	1.01840e+04	1.04263e+02	1048576
1.9832110000	3.8612320766	1.02901e+04	1.04738e+02	1048576

TABLE 3.5: Results for the continuation in the conservative and non-reversible case ($b = 0.25$, $c = 4.0$) of Example 2. The table shows the H^2 Sobolev norm, the C^1 norm and number of Fourier modes $\mathrm{N_F}$ for each parameter value.

ε	a	Λ_L	Λ_S	Λ_U	$\alpha(L, N^S)$	$\alpha(L, N^U)$	$\alpha(N^S, N^U)$
0.0000000000	3.8832220775	1.00	0.2500000000	4.0000000000	1.23529e+00	9.67700e-01	7.53151e-01
0.5000000000	3.8813974424	1.00	0.2492943142	4.0113229344	9.31169e-01	8.51379e-01	6.00598e-01
1.0000000000	3.8765074834	1.00	0.2470073613	4.0484623406	5.84550e-01	7.24296e-01	4.74488e-01
1.5000000000	3.8694737697	1.00	0.2424544054	4.1244868228	2.60063e-01	5.92036e-01	4.35148e-01
1.9000000000	3.8627251961	1.00	0.2360025603	4.2372421662	4.06820e-02	4.85572e-01	4.55743e-01
1.9500000000	3.8618308534	1.00	0.2349048345	4.2570430790	1.60579e-02	4.72351e-01	4.58851e-01
1.9800000000	3.8612901228	1.00	0.2341969934	4.2699096403	1.58441e-03	4.64434e-01	4.60560e-01
1.9830000000	3.8612358919	1.00	0.2341236575	4.2712471286	1.48398e-04	4.63643e-01	4.60725e-01
1.9832000000	3.8612322755	1.00	0.2341187477	4.2713367041	5.26130e-05	4.63591e-01	4.60736e-01
1.9832100000	3.8612320947	1.00	0.2341185021	4.2713411844	4.78291e-05	4.63588e-01	4.60736e-01
1.9832110000	3.8612320766	1.00	0.2341184775	4.2713416324	4.73511e-05	4.63588e-01	4.60736e-01

TABLE 3.6: Results for the continuation in the conservative non-reversible case ($b = 0.25$, $c = 4.0$) of Example 2. The table shows the Λ values, corresponding to the Lyapunov multipliers, and the angle between bundles. We can observe here the decrease of the angle between tangent and stable bundle, given by $\alpha(L, N^S)$.

r	ε_c	B_r	$\hat{\varepsilon}_c$	$\hat{B}_r$
0.0	2.3659464613	0.2923785848	1.9990850327	0.0297868131
0.1	2.1470888074	0.1441053933	1.9942725833	0.0449380274
0.2	2.0586744062	0.0813569806	1.9861547446	0.0307922402
0.3	2.0190008373	0.0519823211	1.9846007465	0.0531485814
0.4	2.0004005665	0.0384265744	1.9837333445	0.0993803809
0.5	1.9914714224	0.0337309143	1.9835940891	0.1482622013
0.6	1.9871411293	0.0355595795	1.9834952022	0.2004862355
0.7	1.9850647712	0.0444374737	1.9834269153	0.2589178359
0.8	1.9840987055	0.0631748194	1.9833823470	0.3248803775
0.9	1.9836593710	0.0958261725	1.9833538126	0.3980653612
1.0	1.9834618324	0.1454271549	1.9833360406	0.4775151988
1.1	1.9833750554	0.2116620562	1.9833253051	0.5619829735
1.2	1.9833384372	0.2908069846	1.9833190481	0.6502075333
1.3	1.9833235897	0.3780306111	1.9833155914	0.7410890006
1.4	1.9833176436	0.4695009290	1.9833138158	0.8337511825
1.5	1.9833151573	0.5629406029	1.9833131068	0.9275761885
1.6	1.9833139955	0.6572301080	1.9833131090	1.0221473834
1.7	1.9833133634	0.7518832385	1.9833136041	1.1171863901
1.8	1.9833129682	0.8467031525	1.9833145987	1.2125264852
1.9	1.9833126969	0.9416111360	1.9833160167	1.3079337731
2.0	1.9833125000	1.0365736863	1.9833139383	1.4048686885
2.1	1.9833123524	1.1315743685	1.9833051417	1.4922947800
2.2	1.9833122392	1.2266035739	1.9833066911	1.5878751888
2.3	1.9833121510	1.3216548487	1.9833082179	1.6839561633
2.4	1.9833120811	1.4167235069	1.9833093694	1.7800335253
2.5	1.9833120249	1.5118060206	1.9833101943	1.8759803248
2.6	1.9833119793	1.6068996870	1.9833107898	1.9717868183
2.7	1.9833119416	1.7020024110	1.9833111998	2.0674691575
2.8	1.9833119103	1.7971125472	1.9833114583	2.1630388912
2.9	1.9833118839	1.8922287831	1.9833116899	2.2585826656
3.0	1.9833118614	1.9873500514	1.9833118090	2.3540487329
3.1	1.9833118421	2.0824754657	1.9833118889	2.4494840059
3.2	1.9833118254	2.1776042766	1.9833119188	2.5448764649
3.3	1.9833118107	2.2727358426	1.9833118536	2.6401706338
3.4	1.9833117977	2.3678696152	1.9833116434	2.7352870374
3.5	1.9833117862	2.4630051345	1.9833113639	2.8302412587
3.6	1.9833117758	2.5581420338	1.9833107989	2.9247764069
3.7	1.9833117665	2.6532800486	1.9833100521	3.0188834398
3.8	1.9833117582	2.7484190289	1.9833090236	3.1123520542
3.9	1.9833117507	2.8435589503	1.9833075621	3.2048662855
4.0	1.9833117441	2.9386999211	1.9833137278	3.3135418818

TABLE 3.7: Estimates of the critical value ε_c and $\hat{\varepsilon}_c$ of the breakdown of the invariant torus in Example 2 and their corresponding exponent, for the Sobolev and C^r semi-norms respectively.

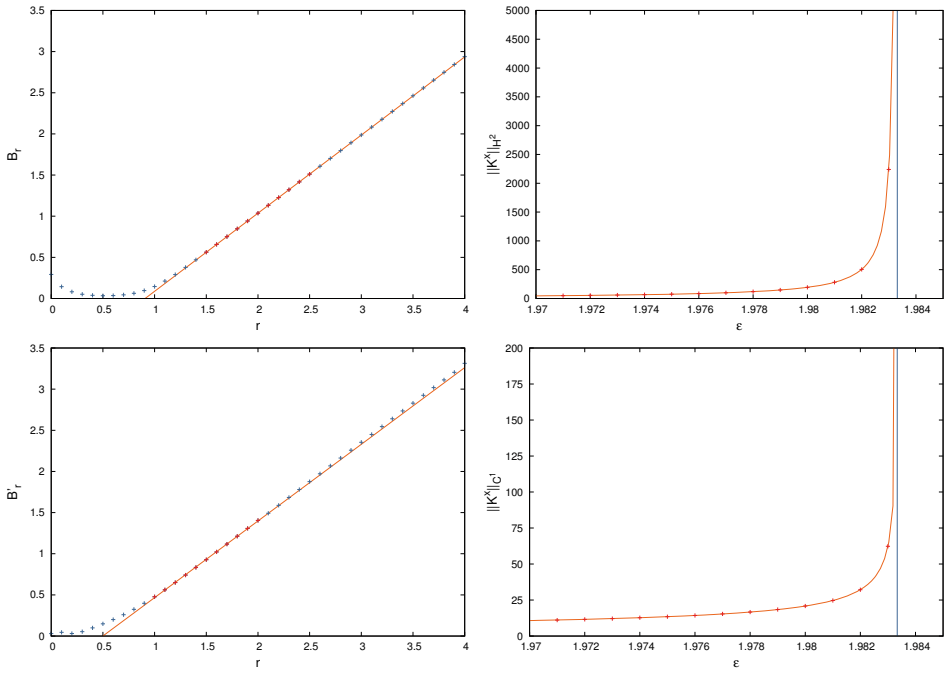

FIGURE 3.6: Blow up at the critical value of the H^2 (top-right) and C^1 (bottom-right) semi-norms, where the critical value is drawn with a blue vertical line. In the left, it appears the fit for the affine expression of the critical exponent given by expressions (3.65) and (3.64) of Conjecture 3.14, that is B_r and $\hat{B}_r$ (B'_r in this picture), respectively.

Otherwise, we also consider the continuation of another saddle torus in a conservative system, so as to prove the generality of the method. In this case, we use parameters $b = 0.2$ and $c = 5.0$, and we observe a breakdown due to the collision of the tangent and stable bundle, which has a linear decay near the breakdown given by

$$\alpha_{LS}(\varepsilon) = 0.92759921 - 0.46742319\ \varepsilon,$$

which gets us a critical value

$$\varepsilon_{c_\alpha} = 1.98449548.$$

Even that this angle goes to zero, the Lyapunov multipliers are moving away from each other. Also, we compute its H^2 and C^1 semi-norms, which has expressions

$$C^1(\varepsilon) \simeq \frac{1.34506486}{(1.98451614 - \varepsilon)^{0.47157364}}$$

and

$$H^2(\varepsilon) \simeq \frac{0.70167623}{(1.98449697 - \varepsilon)^{1.03381575}}$$

respectively, so they give us critical values

$$\varepsilon_{c_{H^2}} = 1.98449697$$

and

$$\varepsilon_{c_{C^1}} = 1.98451614.$$

In that case, we fit the corresponding critical exponents by the following linear expressions

$$B_r \simeq -0.81288669 + 0.92039181\ r$$

and

$$\hat{B}_r \simeq -0.55598388 + 1.00593990\ r.$$

3.6 Example 3: Continuation of a saddle torus in a conservative and reversible system

In previous examples, we have seen the same mechanism of breakdown, in a bundle merging scenario, by the collision of the tangent and stable bundles, whereas the Lyapunov multipliers are moving away. In the following example, we introduce some symmetries in the system by choosing parameters in which the system is not only conservative, but reversible. Then, we choose parameters $b = 0.5$ and $c = 2$ in order to deal with a *conservative*, $\det(\mathrm{D}F_{a,\varepsilon}) = bc = 1$, and *reversible* system.

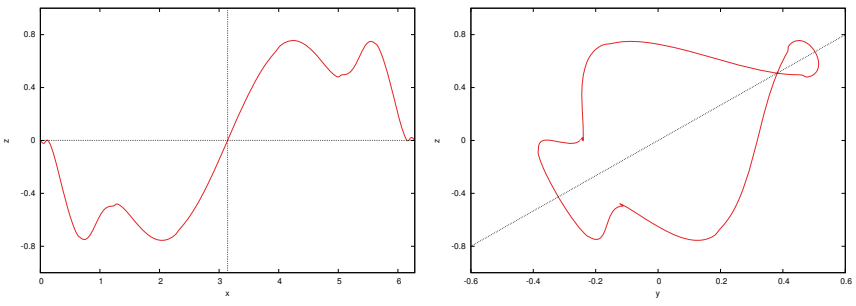

FIGURE 3.7: Symmetries on the torus for the conservative and reversible example.

The property of reversibility means that we can express our map $F_{a,\varepsilon}$ as a composition of two involutions

$$F_{a,\varepsilon} = I_1 I_0.$$

In our particular case, the involutions I_0 and I_1 are given by

$$I_0 \begin{pmatrix} x \\ y \\ z \end{pmatrix} = \begin{pmatrix} -x & + & 2\pi & \\ \sin(x) & + & y & + & \frac{3}{4}z \\ & - & z & \end{pmatrix}$$

and

$$I_1 \begin{pmatrix} x \\ y \\ z \end{pmatrix} = \begin{pmatrix} -x & + & \varepsilon y & + & \frac{\varepsilon}{4}z & + & a + 2\pi \\ & & \frac{y}{2} & + & \frac{3}{8}z & & \\ & & 2y & - & \frac{z}{2} & & \end{pmatrix}.$$

Due to the reversibility property, along the continuation with respect to ε the torus possesses two symmetries. The 0^{th}-symmetry is given by

$$\Gamma_0 = \left\{(x, y, z) \in \mathbb{R}^3 \mid (\pi, y, 0)\right\},$$

and the 1^{st}-symmetry is given by

$$\Gamma_1 = \left\{(x, y, z) \in \mathbb{R}^3 \mid \left(\frac{a}{2} + \pi + \varepsilon z, \frac{3}{4}z, z\right)\right\}.$$

These symmetries are showed in Figure 3.7 for a particular torus of the continuation process.

In this example, by the symmetries of the system, the breakdown of the torus is due to a triple bundle collision: all bundles collide together, values $\alpha_{L,S} = \alpha(L, N^S)$, $\alpha_{L,U} = \alpha(L, N^U)$ and $\alpha_{S,U} = \alpha(N^S, N^U)$ tend to zero at the same time, see Figure 3.8 (top-right). In particular, Figure 3.8 (bottom-left) shows the minimum angle between bundles for the last computed torus. We observe also that, all of these angles goes to zero in a linear way when ε approaches the critical value, see Figure 3.8 (bottom-right). This decay to zero is approximated by the linear expressions

$$\begin{aligned} \alpha_{L,S} &\simeq 1.27075384 - 0.64180240\ \varepsilon, \\ \alpha_{L,U} &\simeq 0.96088637 - 0.48530176\ \varepsilon, \\ \alpha_{S,U} &\simeq 0.60684869 - 0.30649291\ \varepsilon, \end{aligned}$$

from which, by the intersection of them with the horizontal axis, we get the three critical values

$$\begin{aligned} \varepsilon_{c_{LS}} &\simeq 1.9799767600, \\ \varepsilon_{c_{LU}} &\simeq 1.9799771064, \\ \varepsilon_{c_{SU}} &\simeq 1.9799762457, \end{aligned}$$

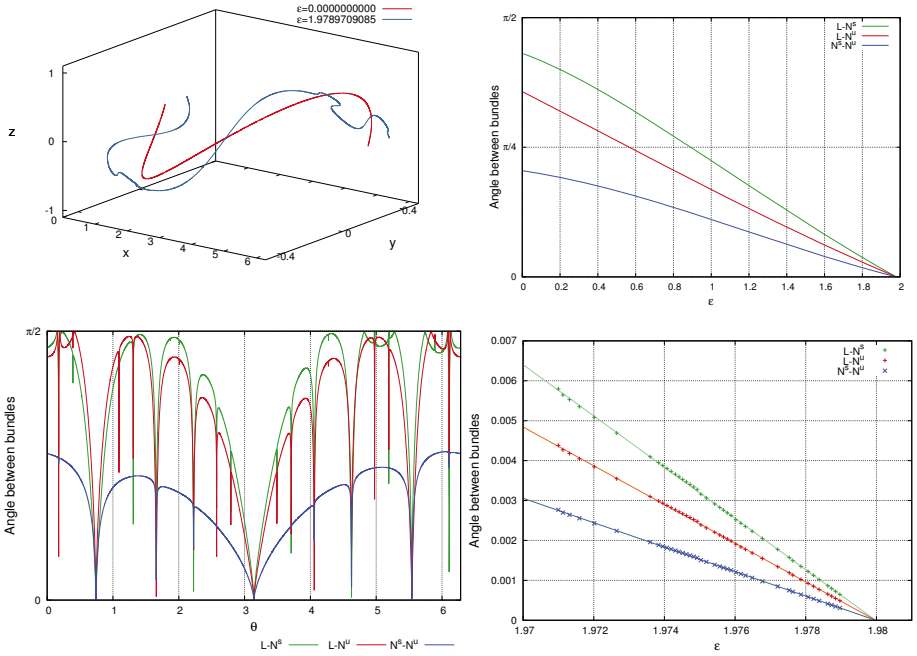

FIGURE 3.8: Results for all ε values of the continuation process in Example 3. Left: First (red) and last (blue) tori we compute (top) and minimum angles between bundles for the last torus we compute (bottom). Right: Minimum angles between bundles for all ε values (top) and linear fit of $\alpha(L, N^S)$, $\alpha(L, N^U)$ and $\alpha(N^S, N^U)$ (bottom).

which meet up to 6 significant digits. These fits support Conjecture 3.12.

In this example, we also observe the fact that even that the torus is destroyed, in particular by a triple bundle collision, the Lyapunov multipliers remains far from collide each other, see Table 3.9. Notice also that, in this case, the adjusting parameter is fixed to $a = \omega$ along the continuation, see Figure 3.1. This is due to the symmetries of the system.

In this example, in the asymptotic behavior of the semi-norms H^2 and C^1 close to the breakdown is

$$\begin{aligned} H^2(\varepsilon) &\simeq \frac{0.21964940}{(1.97998184-\varepsilon)^{1.74772558}}, \\ C^1(\varepsilon) &\simeq \frac{0.47057452}{(1.97998827-\varepsilon)^{1.00213916}}, \end{aligned}$$

when $\varepsilon \to \varepsilon_c$, and we can extrapolate the critical values by

$$\begin{aligned} \varepsilon_{c_{H^2}} &\simeq 1.9799818419, \\ \varepsilon_{c_{C^1}} &\simeq 1.9799882669, \end{aligned}$$

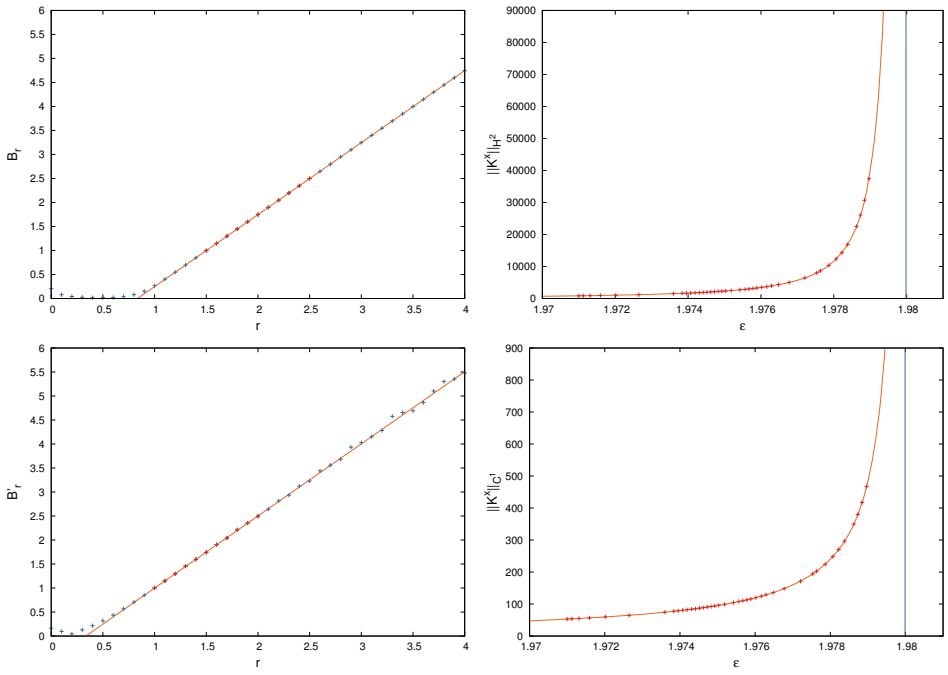

FIGURE 3.9: Blow up at the critical value of the H^2 (top-right) and C^1 (bottom-right) seminorms for Example 3, where the critical value is drawn with an straight blue line. In the left, it appears the fits for the affine expression of the exponent of expressions (3.64) and (3.65), that is B_r and $\hat{B}_r$ (B'_r in this picture) respectively.

which meet up to 6 significant digits. The blow up of these norms appears in Figure 3.9 and Table 3.8, where we can also see how the Fourier nodes increase as we approach the critical value. We also compute the critical exponents, B_r and $\hat{B}_r$ and their critical breakdown values, ε_c and $\hat{\varepsilon}_c$, for different values r in the range $[0, 4]$, see Table 3.10, which satisfy the linear expressions of Conjecture 3.14, in particular given by

$$\begin{aligned} B_r &\simeq -1.25200123 + 1.49986455r, \\ \hat{B}_r &\simeq -0.50312626 + 1.50219068r. \end{aligned}$$

In this case, we get that the critical regularities of the torus in the breakdown are $r_c \simeq 0.8347428722$ and $\hat{r}_c \simeq 0.3349283585$. Notice that, these regularity values are significantly smaller than in previous examples, supporting the fact that this breakdown mechanism belongs to another universality class.

ε	a	H^2	C^1	N_F
0.0000000000	3.8832220775	0.00000e+00	0.00000e+00	64
0.8000000000	3.8832220775	2.81522e-01	3.33102e-01	64
1.6000000000	3.8832220775	2.86960e+00	2.18468e+00	128
1.8000000000	3.8832220775	1.04273e+01	5.32462e+00	512
1.8750000000	3.8832220775	2.63196e+01	9.61127e+00	1024
1.9000000000	3.8832220775	4.20873e+01	1.28306e+01	1024
1.9710000000	3.8832220775	8.31053e+02	5.29780e+01	16384
1.9740722656	3.8832220775	1.72509e+03	8.04969e+01	32768
1.9760206354	3.8832220775	3.46879e+03	1.20065e+02	131072
1.9780678706	3.8832220775	1.23640e+04	2.48336e+02	262144
1.9787328155	3.8832220775	2.60693e+04	3.80229e+02	524288
1.9789709085	3.8832220775	3.77268e+04	4.69412e+02	1048576

TABLE 3.8: Results for the continuation in the conservative and reversible case. The table shows the H^2 Sobolev norm, the C^1 norm and the number of Fourier modes N_F for each ε parameter value.

ε	a	Λ_L	Λ_S	Λ_U	$\alpha(L, N^S)$	$\alpha(L, N^U)$	$\alpha(N^S, N^U)$
0.0000000000	3.8832220775	1.00	0.5000000000	2.0000000000	1.35380e+00	1.12244e+00	6.43501e-01
0.8000000000	3.8832220775	1.00	0.4960293703	2.0160096556	8.53835e-01	6.46182e-01	4.21770e-01
1.6000000000	3.8832220775	1.00	0.4732854745	2.1128896911	2.57675e-01	1.93476e-01	1.24632e-01
1.8000000000	3.8832220775	1.00	0.4571297413	2.1875627634	1.18118e-01	8.90142e-02	5.66872e-02
1.8750000000	3.8832220775	1.00	0.4483006678	2.2306457960	6.80124e-02	5.13315e-02	3.25626e-02
1.9000000000	3.8832220775	1.00	0.4448527617	2.2479347914	5.16573e-02	3.90081e-02	2.47141e-02
1.9710000000	3.8832220775	1.00	0.4329278856	2.3098535189	5.79599e-03	4.38281e-03	2.76782e-03
1.9740722656	3.8832220775	1.00	0.4322949602	2.3132353883	3.80362e-03	2.87635e-03	1.81625e-03
1.9760206354	3.8832220775	1.00	0.4318828798	2.3154425579	2.51950e-03	1.90531e-03	1.20300e-03
1.9780678706	3.8832220775	1.00	0.4314383141	2.3178284524	1.22170e-03	9.23918e-04	5.83306e-04
1.9787328155	3.8832220775	1.00	0.4312905751	2.3186224269	7.96833e-04	6.02615e-04	3.80445e-04
1.9789709085	3.8832220775	1.00	0.4312371565	2.3189096415	6.42944e-04	4.86248e-04	3.06950e-04

TABLE 3.9: Results for the continuation in a conservative and reversible case. The table shows the Λ values, corresponding to the Lyapunov multipliers, and the angle between bundles. We can observe here the decay of all angle between bundles at the same time, a triple bundle collision.

r	ε_c	B_r	$\hat{\varepsilon}_c$	$\hat{B}_r$
0.0	2.2746097498	0.2230123126	1.9946715877	0.0222630169
0.1	2.0978743955	0.1013872229	1.9973908734	0.0529054549
0.2	2.0328090976	0.0542050832	1.9870877972	0.0351918802
0.3	2.0058895374	0.0338958164	1.9834719159	0.0305304741
0.4	1.9941311280	0.0256519663	1.9856031683	0.1638095484
0.5	1.9887533368	0.0241564311	1.9834656155	0.1329003011
0.6	1.9861560175	0.0281080458	1.9835403200	0.1969570307
0.7	1.9848234244	0.0386228049	1.9834682198	0.2564168846
0.8	1.9841045276	0.0586856332	1.9834091603	0.3223085065
0.9	1.9837096812	0.0923148617	1.9833698435	0.3955225954
1.0	1.9834990330	0.1425960919	1.9833442815	0.4749745682
1.1	1.9833945290	0.2093861217	1.9833271099	0.5590621590
1.2	1.9833473258	0.2890537434	1.9833140597	0.6459853941
1.3	1.9833276932	0.3767096171	1.9833017046	0.7338801609
1.4	1.9833198291	0.4684576737	1.9832865567	0.8205728104
1.5	1.9833165612	0.5620315136	1.9832658052	0.9037831508
1.6	1.9833150321	0.6563623341	1.9832356959	0.9804050604
1.7	1.9833141927	0.7510097345	1.9831914298	1.0461132929
1.8	1.9833136649	0.8458039669	1.9831304107	1.0968641655
1.9	1.9833133028	0.9406785495	1.9830507121	1.1283505993
2.0	1.9833130411	1.0356039919	1.9832028014	1.3231479897
2.1	1.9833128433	1.1305637549	1.9835177519	1.6425512250
2.2	1.9833126838	1.2255449095	1.9833576783	1.6173673871
2.3	1.9833125361	1.3205317409	1.9832995592	1.6661849900
2.4	1.9833123587	1.4154951674	1.9832753666	1.7409067352
2.5	1.9833120654	1.5103677504	1.9832642206	1.8258024179
2.6	1.9833114559	1.6049811947	1.9832562845	1.9131081928
2.7	1.9833100528	1.6989103374	1.9832473455	1.9986006529
2.8	1.9833067220	1.7910898013	1.9832270602	2.0716838163
2.9	1.9832988104	1.8788985442	1.9831982202	2.1340356521
3.0	1.9832803157	1.9560950063	1.9831583460	2.1809972406
3.1	1.9832385743	2.0087418698	1.9830978882	2.2006949828
3.2	1.9831508114	2.0097695803	1.9830065117	2.1763286943
3.3	1.9829897956	1.9212149341	1.9828810580	2.0961244145
3.4	1.9827551044	1.7247591196	1.9827360284	1.9717358196
3.5	1.9825051024	1.4644095586	1.9825941548	1.8299192615
3.6	1.9823173931	1.2250532053	1.9824423457	1.6396607448
3.7	1.9822203600	1.0744997423	1.9823090751	1.4328188925
3.8	1.9821812096	1.0122913824	1.9822323624	1.2936428257
3.9	1.9821645493	0.9964339087	1.9821948306	1.2260948718
4.0	1.9821563610	1.0016733695	1.9821737256	1.1994162056

Table 3.10: Estimates of the critical value ε_c and $\hat{\varepsilon}_c$ of the breakdown of the invariant torus in Example 3 and their corresponding exponent, for the Sobolev and Cr semi-norms respectively.

3.7 Example 4: Node-Focus transitions in continuation of an attracting torus

In this example, we choose parameters $b = 0.5$ and $c = 0.4$, so for $\varepsilon = 0$ we start the continuation with an attracting invariant torus with a 2-dimensional stable bundle. Moreover, for $\varepsilon = 0$ we can use the same expression given by (3.68) and (3.70) to produce an initial approximation of the torus and its invariant bundles. In particular, the eigenvalues of Λ_N are $\lambda_{n_1} = 0.5$ and $\lambda_{n_2} = 0.4$, corresponding to the dynamics of the slow and fast stable directions, denoted by N^S and N^{SS} respectively. In the same way, we will denote by $\Lambda_S = |\lambda_{n_1}|$ and $\Lambda_{SS} = |\lambda_{n_2}|$ the corresponding Lyapunov multipliers. In that case, our invariant torus is completely reducible for the unperturbed case, so it is natural to start the continuation using the completely reducible method. When the torus is completely reducible, it is referred to as *node torus*.

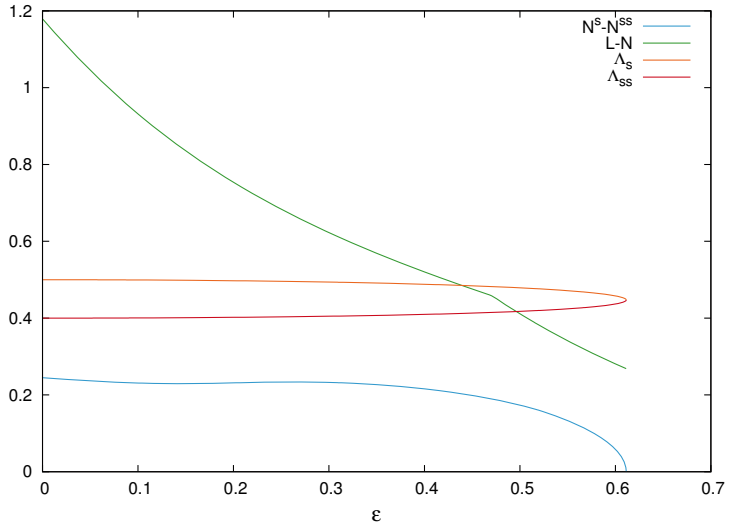

FIGURE 3.10: Continuation results for Example 4 using the completely reducible algorithm. It is shown the angle between slow and fast bundle (blue), and also the angle between the tangent and stable bundle (green), which is in fact two dimensional. Also, the Lyapunov multipliers are shown (orange and red).

During this continuation, the method stops because of a node-focus bifurcation on the torus. That is, the complete reducibility property is lost, and both real eigenvalues collide and become complex eigenvalues, so we cannot diagonalize the cocycle Λ_N to a real matrix. The completely reducible

ε	a	Λ_L	Λ_S	Λ_{SS}	$\alpha(N^S, N^{SS})$
0.0000000000	3.8832220775	1.00	0.5000000000	0.4000000000	2.44979e-01
0.1000000000	3.8830439063	1.00	0.4993691197	0.4005053418	2.31035e-01
0.2000000000	3.8825174896	1.00	0.4974087583	0.4020837925	2.31429e-01
0.3000000000	3.8816642539	1.00	0.4938786213	0.4049578001	2.32581e-01
0.4000000000	3.8805105878	1.00	0.4882077414	0.4096616727	2.15809e-01
0.5000000000	3.8790753867	1.00	0.4788999938	0.4176237264	1.73476e-01
0.6000000000	3.8773582471	1.00	0.4578897228	0.4367863921	5.83418e-02
0.6100000000	3.8771703292	1.00	0.4508313858	0.4436248363	1.98262e-02
0.6110000000	3.8771513697	1.00	0.4489395858	0.4454942403	9.47391e-03
0.6112500000	3.8771466250	1.00	0.4478913207	0.4465368947	3.72443e-03
0.6112812500	3.8771460318	1.00	0.4475940968	0.4468334169	2.09229e-03
0.6112929688	3.8771458094	1.00	0.4473786202	0.4470486303	9.10835e-04
0.6112951660	3.8771457676	1.00	0.4472821838	0.4471450174	3.79164e-04
0.6112955780	3.8771457598	1.00	0.4472355773	0.4471916146	1.23348e-04
0.6112956166	3.8771457591	1.00	0.4472200814	0.4472071096	3.67750e-05

TABLE 3.11: Continuation with respect to ε of the invariant attracting curve for the Fattened Arnold Family for $b = 0.5$ and $c = 0.4$ by using the completely reducible method. The first and second columns corresponds to the continuation and adjusting parameters, respectively. The following three columns show the Lyapunov multipliers of the torus, which corresponds with the elements of Λ. In the last column there appears the minimum angle between the slow and fast subbundles. We do not write here the minim angle between the tangent and the two dimensional stable bundle, since they remain separately during the continuation.

method detects when the torus stops being node type at

$$\varepsilon_{\mathrm{A}} \simeq 0.6112956166.$$

The collision of the eigenvalues coincides with the smooth collision between the slow and fast subbundles. Table 3.11 shows the values of the Lyapunov multipliers, which go to collision, and the minimum angle between the slow and fast subbundles, which tends to zero in a square root way. See also Figure 3.10 for the continuation curves of Λ_S, Λ_{SS} and of the angle between bundles, $\alpha_{S,SS}$ and $\alpha_{L,S}$.

Notice that after the collision, the torus is still reducible (but not completely reducible): it has only lost the "real" reducibility and persists as a reducible torus with complex eigenvalues. This type of torus will be referred to as *focus torus*. At that point, we can use the reducible method of Section 3.2.2 to follow with the continuation of that torus. In our computations using this second method, we have seen that, depending on the continuation step-size, this method continues till further or not. For instance, using a larger step size as $\Delta\varepsilon = 10^{-1}$, we continue the torus until $\varepsilon_{\mathrm{D}} \simeq 0.8835419732$, whereas using a small step size $\Delta\varepsilon = 10^{-3}$, our computations stops in $\varepsilon_{\mathrm{B}} \simeq 0.7766015964$. In fact, these two values correspond to parameter values in which the torus is again completely reducible inside a small interval of ε, see Figures 3.11 and 3.13. This means that the algorithm for the non-completely reducible case

is very sensitive to the changes in the dynamics of the system, and that even that the system continues being reducible, the method notices the change on the reducibility type. Otherwise, by using a big step size, we can "jump" over these disabilities without the necessity to stop in them. The dynamical explanation of this behavior is that the torus is node-type in an open set of parameters, while the torus is focus-type in a Cantor set of parameters strictly contained in the complementary. See e.g. [70, 71]. Moreover, in the regions corresponding to node tori the invariant bundles could be non-orientable. Hence, we could use a double covering trick to consider these cases and avoid stopping the method, see [59].

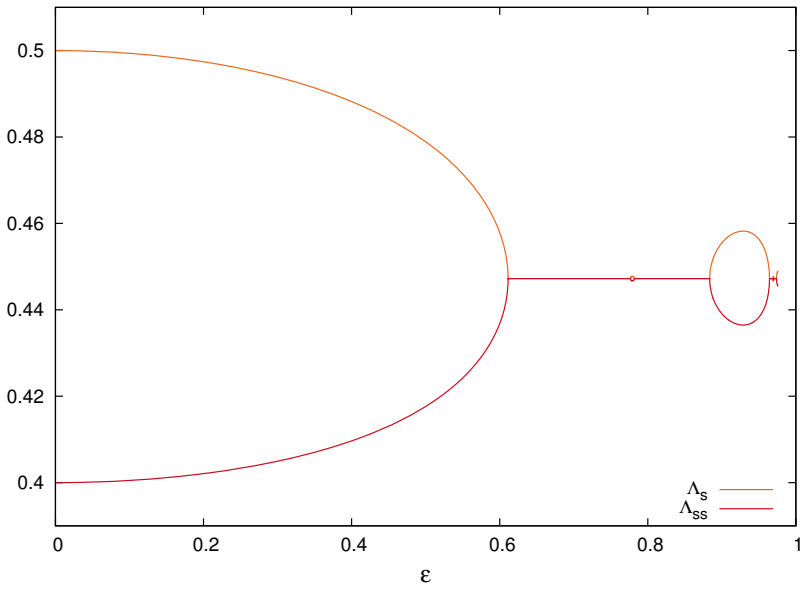

FIGURE 3.11: Lyapunov multipliers for the continuation of Example 4 by the method of non-reducible quasi-periodic tori. During the continuation several transitions from *node-torus* to *focus-torus* (with complex eigenvalues) can be seen with the Lyapunov multipliers collided.

We will use here the general method to go through the changes of the dynamical properties which produces the eventualities mentioned above. The drawback is that dynamical information as Lyapunov multipliers has to be computed apart. First notable observation we take from this example is the several transitions from node to focus tori, in which we observe how the eigenvalues collide (they become complex) and separate again, see Figure 3.11. Notice that during these node-focus transitions, the the slow and fast subbundles suffer smooth collisions, and the minimum angle between between them behaves as square root functions.

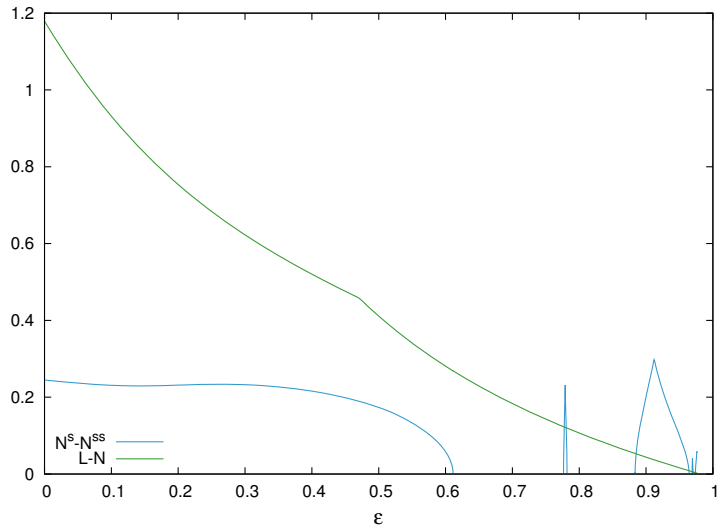

FIGURE 3.12: Continuation results for the minimum angle between bundles of Example 4 by using the non-reducible algorithm. It is shown the minimum angle between slow and fast subbundles (in blue) and minimum angle between tangent and the two dimensional stable bundle (in green).

The first value ε_{A}, corresponds to the parameter in which the first continuation, using the completely reducible method, stops. Values ε_{B} and ε_{D} corresponds to the parameters near which the non-completely reducible method stops. Another transition in $\varepsilon_{\mathrm{F}} \simeq 0.9663195313$, producing an small gap of ε values in which the torus is node type, has also been detected. See magnifications of these transitions in Figure 3.13 and see Figure 3.12 for the minimum angles between bundles along all the continuation values.

When the torus is completely reducible, we assign a sign to the Lyapunov multipliers in order to obtain the eigenvalues of the torus. To do so, we consider that the invariant subbundle inside the invariant normal bundle is, in fact, a subbundle of $\mathbb{T} \times \mathbb{R}^2$ and then can be represented as two couple of curves in $\mathbb{T} \times 1$. Then, if one of this curves is fixed under iteration of $\mathrm{D}F_{a,\varepsilon}$, we assign a positive sign to the eigenvalue. Otherwise, if the copy is 2-periodic by $\mathrm{D}F_{a,\varepsilon}$, that is it is shipped to the other copy, we consider a negative sign. Notice that in this example, see Table 3.12, the sign of the eigenvalues change from one gap to the other. We assign $\pm$ to the Lyapunov multipliers in which the method is not capable to find the sign, which is a numerical evidence of the non-complete reducibility on the torus. This change of sign is in some sense natural in this case, because in these node-focus transitions the eigenvalues collide. We will observe in the next Example 5, that this has

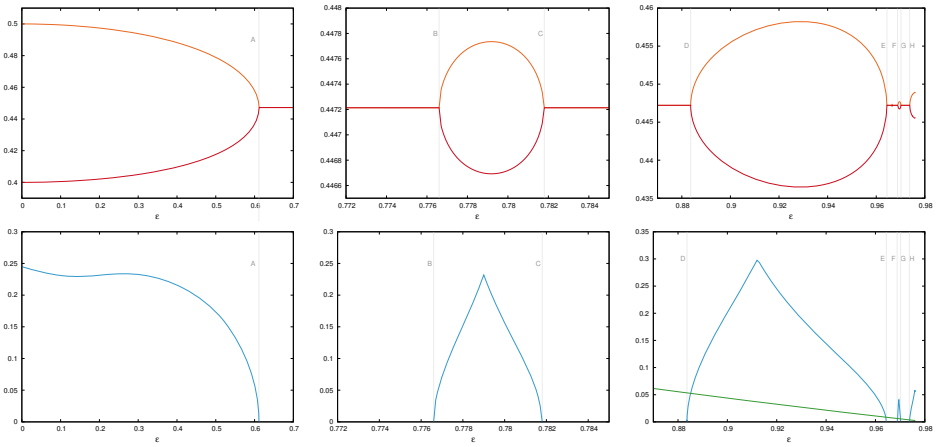

FIGURE 3.13: Magnifications of Lyapunov multipliers and minimum angle between bundles near transitions from *node-torus* to *focus-torus* in Example 4.

not always the same "natural" explanation.

Due to the possibility of a changing topology of the bundles, we find very useful to compute their indices that are the number of turns they do when θ goes from 0 to 2π. To do so, each bundle is computed by (backward and forward) iteration of the cocycle Λ_N over a grid in the interval $[0, 2\pi]$. Then, we add the angles between consecutive fibers to obtain the total angle of revolution of the bundle, β. The index is then

$$\frac{m}{2} = \frac{\beta}{2\pi}.$$

In the numerical computations, we take m as the nearest integer to $\frac{\beta}{\pi}$. In particular, if the value m is even means that the bundle is orientable. Otherwise, m is odd and it means that the bundle is non-orientable. The sign of m means in which direction the fiber rotates: from left to right $(+)$ or from right to left $(-)$.

We have detailed this information of the index in Table 3.12, where we illustrate the behavior of the bundles inside the different node-gaps mentioned above (in gray). Inside these gaps we observe evidence of orientable and non-orientable bundles. Some of these tori with their respectively bundles are shown in Figures 3.14 and 3.15.

Remark 3.19 *We should emphasize that when we have reducibility along all the continuation process, even completely or not, we can use the reducible method instead of the general one. But in this case, we should take care about*

ε	a	Λ_L	λ_{n_1}	λ_{n_2}	index×2
0.0000000000	3.8832220775	1.00	0.5000000000	0.4000000000	0
0.6000000000	3.8773582471	1.00	0.4579030644	0.4367722458	0
0.6112956166	3.8771457591	1.00	0.4472200814	0.4472071096	0
0.6500000000	3.8763877719	1.00	±0.4472137319	±0.4472134526	-
0.7000000000	3.8753378014	1.00	±0.4472137102	±0.4472134760	-
0.7780000000	3.8735326319	1.00	0.4476774260	0.4467502443	13
0.7790000000	3.8735081165	1.00	0.4477345633	0.4466932326	13
0.7800000000	3.8734835655	1.00	0.4477095796	0.4467181597	13
0.7810000000	3.8734589788	1.00	0.4475859170	0.4468415827	13
0.8000000000	3.8729849911	1.00	±0.4472137084	±0.4472134827	-
0.8700000000	3.8711212578	1.00	±0.4472137080	±0.4472134930	-
0.9000000000	3.8702618736	1.00	-0.4554795000	-0.4390977148	-8
0.9200000000	3.8696673033	1.00	-0.4579718128	-0.4367081149	-8
0.9400000000	3.8690546139	1.00	-0.4577666206	-0.4369038657	-8
0.9600000000	3.8684230069	1.00	-0.4528731098	-0.4416248197	-8
0.9650000000	3.8682620624	1.00	±0.4472138320	±0.4472133709	-
0.9660000000	3.8682297243	1.00	±0.4472137740	±0.4472134288	-
0.9664195313	3.8682161425	1.00	0.4472442872	0.4471829177	-152
0.9665195313	3.8682129039	1.00	0.4473017886	0.4471254316	-152
0.9670000000	3.8681973361	1.00	±0.4472137871	±0.4472134157	-
0.9680000000	3.8681648979	1.00	±0.4472137160	±0.4472134867	-
0.9690000000	3.8681324095	1.00	0.4473631379	0.4470641148	81
0.9696000000	3.8681128924	1.00	0.4476850163	0.4467426827	81
0.9698878174	3.8681035237	1.00	0.4476003264	0.4468272104	81
0.9700597656	3.8680979246	1.00	0.4474490260	0.4469783005	81
0.9702000000	3.8680933571	1.00	±0.4472138298	±0.4472133728	-
0.9725000000	3.8680183043	1.00	±0.4472138034	±0.4472133990	-
0.9738288651	3.8679748195	1.00	-0.4473179175	-0.4471093093	-63
0.9748679777	3.8679407539	1.00	-0.4486032989	-0.4458282085	-63
0.9758575973	3.8679082596	1.00	-0.4488862184	-0.4455472163	-63
0.9761123718	3.8678998859	1.00	-0.4489059727	-0.4455276098	-63

Table 3.12: Continuation results for the general algorithm. The first two columns show the continuation and adjusting parameters, respectively. The next three columns show the Lyapunov multipliers of the cocycle Λ and their corresponding sign. Notice that when the torus is not a node torus (in white), this sign is not defined (in present example, this corresponds to a focus torus). In the last column it appears the index of the bundles. In bold it appears the parameter values for which we show the corresponding tori and angles of the bundles in Figures 3.14 and Figure 3.15.

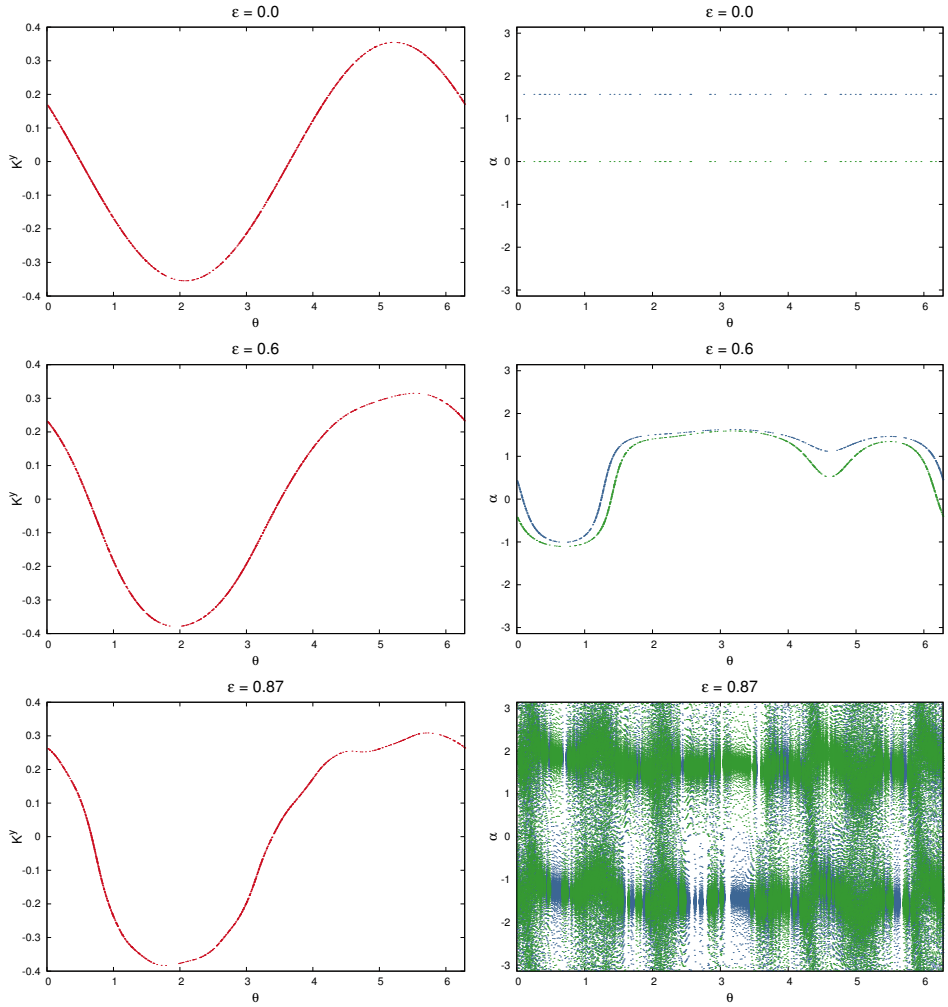

FIGURE 3.14: Tori (left) and angles of slow and fast bundles with respect to the horizontal axis (right) for parameter values $\varepsilon = 0.0$, 0.6 and 0.87, respectively. Notice that the first two rows correspond to *node tori* with orientable bundles of index 0, whereas the last one corresponds to a *focus torus*.

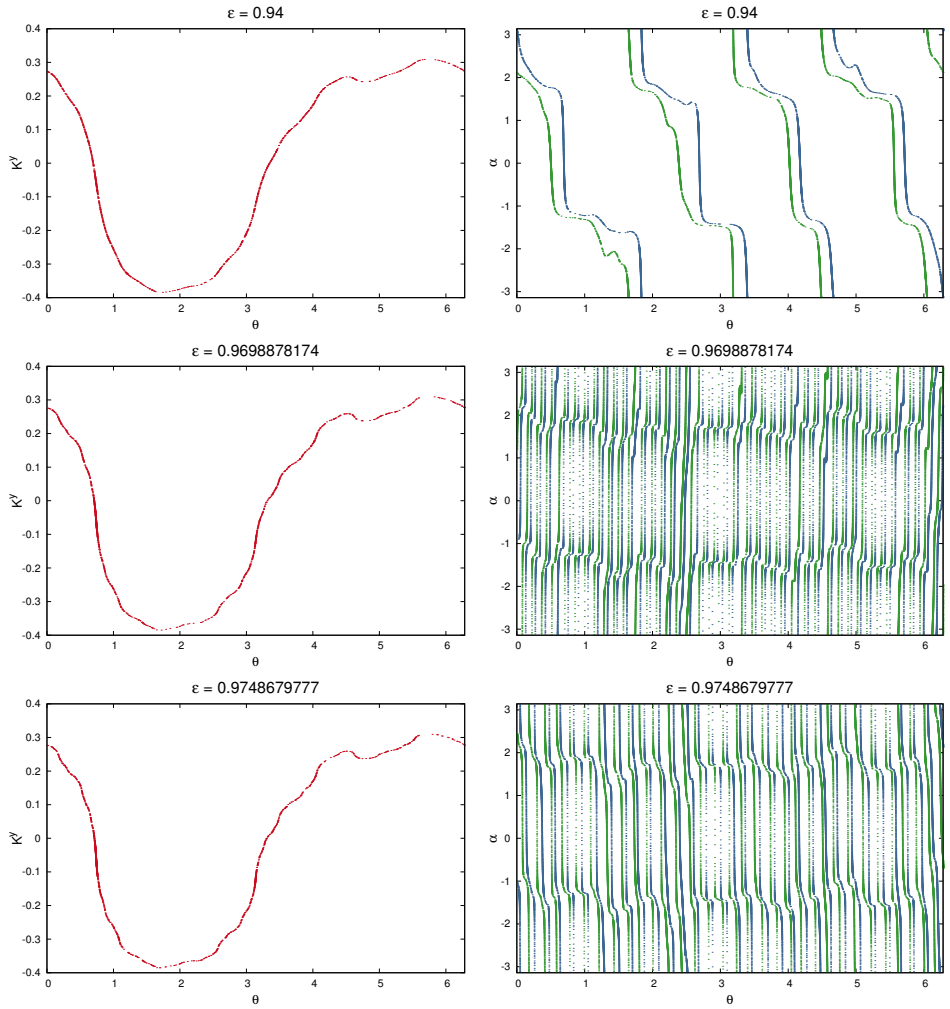

FIGURE 3.15: Tori (left) and angles of slow and fast bundles with respect to the horizontal axis (right) for parameter values $\varepsilon = 0.94$, 0.9698878174 and 0.9748679777, respectively. All of these tori are *node tori*. Notice that the first torus has orientable bundles, with index 4, whereas the other two have non-orientable bundles, with indices $\frac{81}{2}$ and $\frac{63}{2}$, respectively.

the changes in the topology, in the meaning of orientabilily of bundles, and use the "double covering trick" to pass through these changes of the topology. This has been used in [59].

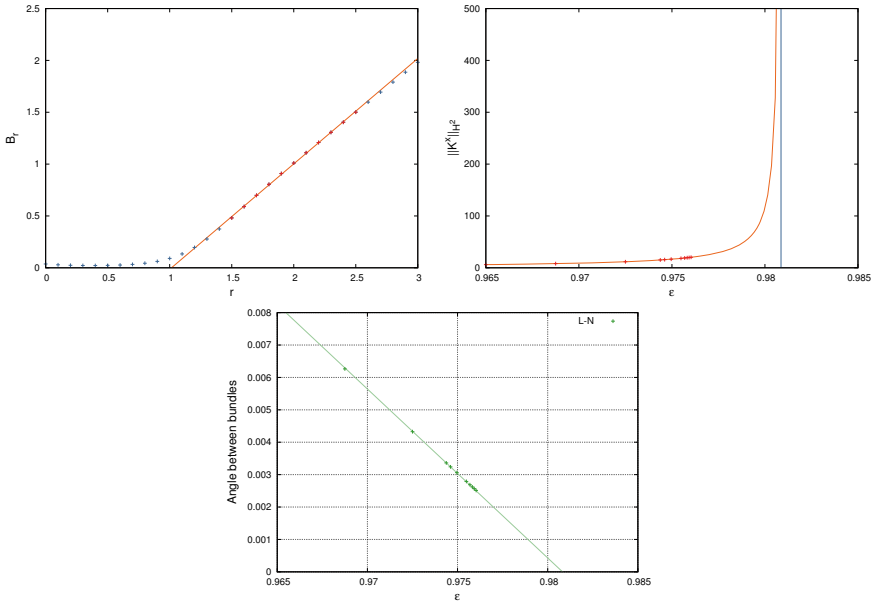

FIGURE 3.16: Extrapolations of the critical value for the continuation of Example 4, by using the H^2 semi-norm and the minimum angle between the tangent and the two dimensional stable bundles. In particular, the top-left figure show the lineal fit for the critical exponent of the Sobolev norm with respect to r.

At the end of the continuation process, we observe that the angle between the tangent and the two dimensional stable bundle tends to zero. In fact, there is a linear decay to zero given by the expression

$$\alpha_{LS}(\varepsilon) \simeq 0.51143611 - 0.52143653\ \varepsilon,$$

supporting Conjecture 3.12. This behavior indicates us that there is a collision between the tangent and the two dimensional stable bundles which destroys the invariant torus of this example, at the critical breakdown parameter

$$\varepsilon_{c_\alpha} \simeq 0.98082139.$$

Furthermore, we also compute their H^2 Sobolev norms to have a better understanding of the breakdown, which near the critical value blows up as

$$H^2(\varepsilon) \simeq \frac{0.09301440}{(0.98086341 - \varepsilon)^{1.01005287}}.$$

Notice that, even that we are not very close to the breakdown, the extrapolation of the H^2 Sobolev norm gives us a critical value

$$\varepsilon_{c_{H^2}} = 0.98086341$$

which fits very well with the one obtained before.

Remark 3.20 *This example exposes that the reducible method is very sensitive to the topology and dynamics of the system, whereas the general method offers us the possibility to explore the regions in which reducible methods has troubles or suffers changes. The situation can be more dramatic if reducibility property is lost, see next Example 5.*

Summarizing, in this example we have observed several bifurcations produced by transitions between node to focus tori, and finally there is a collision between the tangent and the two dimensional stable bundles which leads to the torus breakdown (also observed by the blow up of the Sobolev norms). This mechanism of breakdown is again in a bundle merging scenario as in previous examples, with the Lyapunov multipliers being separate, but in this case the stable bundle is two dimensional.

3.8 Example 5: Transitions to non-reducibility in continuation of an attracting torus

There is another mechanism in which an attracting node torus ceases to be completely reducible, to be non-reducible. In this case, the slow and fast bundles collide non-smoothly. In order to illustrate this scenario, we will continue quasi-periodic normally attracting invariant tori for a Fattened Hénon Family, defined by (3.67).

Look first what does happen for the unperturbed case $\varepsilon = 0$. In that case, the system (3.67) is simply a direct product of a rotation by angle a and the classical Hénon map:

$$F_{a,0}\begin{pmatrix} x \\ y \\ z \end{pmatrix} = \begin{pmatrix} x + a \\ 1 + z - by^2 \\ cy \end{pmatrix}.$$

If we are looking for a parameterization of a torus with quasi-periodic fixed frequency ω, for $\varepsilon = 0$, $K_{a,0}$ has to satisfy the invariance equation,

$$F_{a,\varepsilon}(K_{a,0}(\theta)) = K_{a,0}(\theta + \omega),$$

and so we have to adjust parameter $a = \omega$, and

$$K_{a,0}(\theta) = \begin{pmatrix} \theta \\ 0 \\ 0 \end{pmatrix} + K_{p,a,0}(\theta) = \begin{pmatrix} \theta \\ 0 \\ 0 \end{pmatrix} + \begin{pmatrix} 0 \\ y_0 \\ z_0 \end{pmatrix},$$

with

$$\begin{aligned} y_0 &= \frac{-1 + c \pm \sqrt{(1-c)^2 + 4b}}{2b}, \\ z_0 &= c y_0, \end{aligned}$$

so that the periodic part of the initial parameterization is constant and given by one of the fixed points of the Hénon map. Moreover, the invariant bundles are parameterized by the eigenvectors of these fixed points, and the initial values of Λ_N by the eigenvalues of these fixed points, respectively.

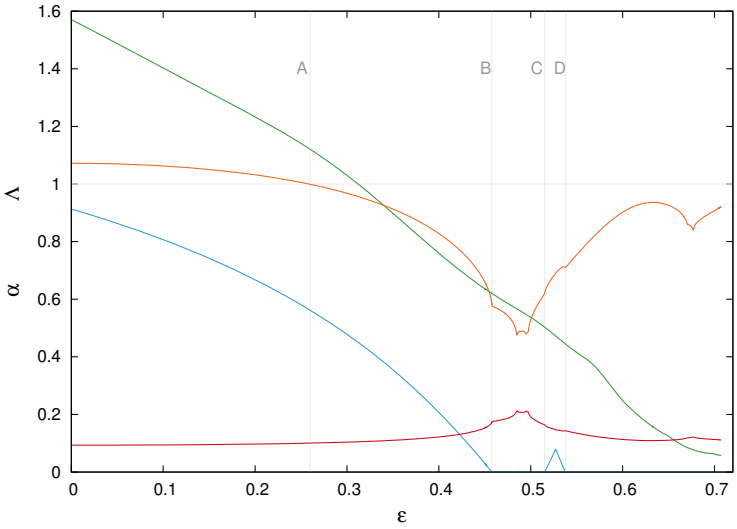

FIGURE 3.17: Continuation results with respect to ε for the minimum angle between bundles (α) and Lyapunov multipliers (Λ) in Example 5. Notice that from $\varepsilon = 0$ to $\varepsilon_{\mathrm{A}} \simeq 0.26$, the blue line represents the angle between stable and unstable bundles, since the torus is of a saddle type, and the green line represents the angle between the tangent and the total two dimensional normal bundles. On the other hand, from $\varepsilon_{\mathrm{A}} \simeq 0.26$ till the end of the continuation, the blue line represents the minimum angle between slow and fast subbundles and the green line represent the minimum angle between tangent and the stable two dimensional bundle, since in this region tori are of attracting type.

We will consider the same parameter values as in the work [59], $b = 0.68$ and $c = 0.1$, and y_0 with $+$ sign, so that the initial unperturbed torus is of a saddle type. In particular, if we also choose the parameter $d = 0$, we are doing the computations for exactly the same problem as in [59], which is in

ε	a	λ_L	λ_{n_1}	λ_{n_2}	||Tail||	N_F
0.0000000000	3.8832220775	1.00	-1.0721039594	0.0932745366	3.2e-18	64
0.0500000000	3.8793832851	1.00	-1.0698001982	0.0934778087	2.4e-17	64
0.1000000000	3.8750776341	1.00	-1.0627289651	0.0941158257	2.7e-17	64
0.1500000000	3.8703299648	1.00	-1.0503995297	0.0952617221	4.0e-17	64
0.2000000000	3.8651713720	1.00	-1.0318728888	0.0970480228	1.8e-17	64
0.2500000000	3.8596395550	1.00	-1.0054568522	0.0997164626	5.4e-17	64
0.2600000000	3.8584922585	1.00	-0.9989884645	0.1003912484	5.7e-17	64
0.3000000000	3.8537802950	1.00	-0.9679969682	0.1037438592	3.2e-17	64
0.3500000000	3.8476507902	1.00	-0.9133271092	0.1101794739	4.6e-17	64
0.4000000000	3.8413214332	1.00	-0.8282686012	0.1217897138	1.5e-14	64
0.4400000000	3.8361693482	1.00	-0.7099672326	0.1423907847	3.9e-11	64
0.4500000000	3.8348757982	1.00	-0.6598206531	0.1532988873	1.8e-11	64
0.4512695313	3.8347115462	1.00	-0.6517231472	0.1552147792	2.6e-11	64
0.4561361791	3.8340819306	1.00	-0.6104235380	0.1657621720	1.6e-17	512
0.4575522341	3.8338987545	1.00	-0.5847050004	0.1730673263	5.4e-16	8192
0.4576004767	3.8338925143	1.00	-0.5825237581	0.1737158508	7.8e-13	131072
0.4576027468	3.8338922206	1.00	-0.5824044644	0.1737514561	9.3e-13	1048576

TABLE 3.13: Continuation results with respect to ε for the reducible algorithm (both reducible algorithms match in this region) in Example 5. The first two columns show the continuation and adjusting parameters, respectively. The next three columns show the eigenvalues of the cocycle Λ, so of Λ_L and Λ_N, and their corresponding signs. The following curve shows the tail of the last 10 Fourier modes of the torus, whereas in the last column it appears the number of Fourier modes we need to use. Notice that between $\varepsilon \simeq 0.25$ and $\varepsilon \simeq 0.26$ there is a period-halving bifurcation.

a skew-product form. Our results match in this test example. From now on, we will consider the coupled case, with $d = 1$. See Figure 3.2 to see the curves of the continuation of both cases.

During the continuation with respect to ε of this example, we observe several bifurcations, such as a period-halving bifurcation and some transitions from a reducible torus to a non-reducible one.

In a leading continuation, we use both reducible algorithms to continue the torus with respect to ε. We observe the transition from a saddle torus to an attracting node one. Looking the Lyapunov multipliers, we see that between parameters $\varepsilon \simeq 0.25$ and $\varepsilon \simeq 0.26$, the eigenvalue corresponding to maximal Lyapunov multiplier crosses -1, so there is a period-halving bifurcation and the torus changes from an unstable (saddle) torus to an stable (attracting) torus. This bifurcation can be explained with tools of quasi-periodic bifurcation theory. Notice that, the method does not suffer any trouble and we can cross the bifurcation and continue the continuation in a normal way. See Table 3.13.

This continuation with both reducible algorithms stops at

$$\varepsilon_B \simeq 0.4576027468,$$

where there is a global bifurcation in which we loss the reducibility property. At this point, we cannot reduce to constant the cocycle Λ_N and both reducible algorithms, the completely and the non-completely one, stop as we approach the critical value ε_{B} of the transition. The slow and fast subbundles approach each other as we increase parameter ε, and for this parameter value ε_{B} there is a non-smooth (non-uniform) collision between them. We also fit the values of this minimum angle, and we obtain an expression as in Conjecture 3.12, see Figure 3.18, from which we get a critical value

$$\varepsilon_\alpha \simeq 0.4576780589.$$

In this case, the collision of the bundles only leads to a loss of the reducibility, but not to the destruction of the torus. Numerically, we detect this collision with a minimum angle of the order $\alpha(N^S, N^{SS}) \simeq 2.51665 \times 10^{-4}$. In this transition, there is again a bundle merging scenario, but in this example it does not lead to the breakdown of the torus, only to the lost of the reducibility.

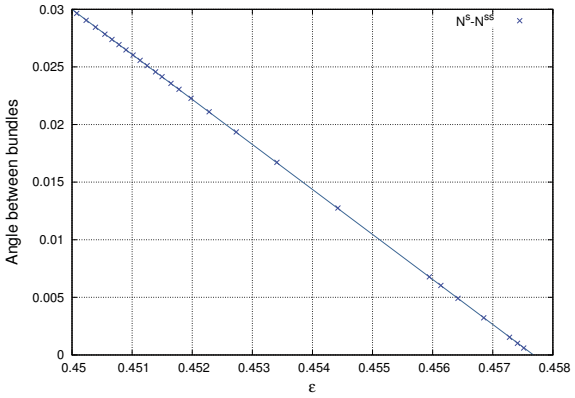

FIGURE 3.18: Fit of the minimum angle between slow and fast invariant subbundles near the transition in ε_{B}. This fits has expression $\alpha(N^S, N^{SS})(\varepsilon) \simeq 1.78786134 - 3.90637328\ \varepsilon$, and so we can extrapolate its critical value as $\varepsilon_\alpha \simeq 0.4576780589$.

Despite that, we can use the general method to perform the continuation from the point in which we do not have reducibility. Through this second continuation, we observe small gaps in which the merged subbundles become separated again, the big one from ε_{C} to ε_{D} can be easily seen in Figure 3.17. Inside these gaps, the reducibility of the torus has been recovered, and cocycle Λ_N can be diagonalized again. Notice that in these small gaps, the sign of the eigenvalues of the cocycle, which in modulus are the Lyapunov multipliers, have changed from the previous gap, see Table 3.14, even that

ε	a	λ_L	λ_{n_1}	λ_{n_2}	||TAIL||	N_F
0.4000000000	3.8413214332	1.00	-0.8282669115	0.1217898279	1.5e-14	64
0.4500000000	3.8348757982	1.00	-0.6598113298	0.1533012145	7.6e-13	64
0.4600000000	3.8335821637	1.00	±0.5728158729	±0.1766959169	1.3e-12	64
0.4850000000	3.8303568912	1.00	±0.4768072652	±0.2125670876	8.3e-12	64
0.4860000000	3.8302283997	1.00	0.4846543199	-0.2091365623	9.8e-12	64
0.4870000000	3.8300999652	1.00	0.4880126564	-0.2077106060	1.1e-11	64
0.4880000000	3.8299715897	1.00	0.4881328051	-0.2076679808	1.3e-11	64
0.4890000000	3.8298432754	1.00	±0.4881850451	±0.2076542462	1.6e-11	64
0.4900000000	3.8297150245	1.00	±0.4890045397	±0.2073141954	1.8e-11	64
0.5000000000	3.8284365048	1.00	±0.5283807452	±0.1919893945	7.9e-11	64
0.5130000000	3.8267882941	1.00	±0.6088512685	±0.1667504564	1.2e-17	128
0.5140000000	3.8266623137	1.00	±0.6135186826	±0.1654852677	1.9e-17	128
0.5150000000	3.8265364635	1.00	0.6199920977	-0.1637538925	1.8e-17	128
0.5200000000	3.8259092807	1.00	0.6580093691	-0.1543513137	2.0e-17	128
0.5250000000	3.8252858540	1.00	0.6819510891	-0.1489775089	3.3e-17	128
0.5300000000	3.8246666229	1.00	0.7001836965	-0.1451419905	6.2e-17	128
0.5350000000	3.8240520408	1.00	0.7119176806	-0.1427927736	1.6e-16	128
0.5370000000	3.8238076120	1.00	0.7107233508	-0.1430500564	2.5e-16	128
0.5380000000	3.8236857129	1.00	±0.7105751874	±0.1430877793	3.3e-16	128
0.5400000000	3.8234425628	1.00	±0.7180360168	±0.1416138372	5.1e-16	128
0.6000000000	3.8165452607	1.00	±0.9020479186	±0.1131508954	4.0e-13	256
0.6501400261	3.8108084316	1.00	±0.9258623440	±0.1105645259	1.8e-12	4096
0.6608539635	3.8095099697	1.00	±0.9067759985	± 0.1129483085	5.1e-15	8192
0.6708539635	3.8082600966	1.00	±0.8590492022	±0.1192847477	2.9e-12	8192
0.6808539635	3.8069695498	1.00	±0.8666652404	±0.1182825448	1.8e-12	8192
0.6903539635	3.8057042091	1.00	±0.8893682730	±0.1153096342	2.2e-12	8192
0.7001039635	3.8043653898	1.00	±0.9074951874	±0.1130418735	1.9e-12	8192
0.7071713019	3.8033706211	1.00	±0.9210259697	±0.1113994914	4.1e-13	1048576

Table 3.14: Continuation results with respect to ε for the non-reducible algorithm in Example 5. The first two columns show the continuation and adjusting parameters, respectively. The next three columns show the eigenvalues of the cocycles Λ_L and Λ_N with their corresponding signs. The following columns shows the tail of the last 10 Fourier modes of the torus, whereas in the last column it appears the number of Fourier modes we need to use. Notice that there are some changes of the sign of the eigenvalues, which corresponds to a different gaps in which we have the invariant subbundles separated (see Figure 3.17 to see these separations).

both Lyapunov multipliers do not collide. This is also an evidence of the lack of reducibility between the gaps.

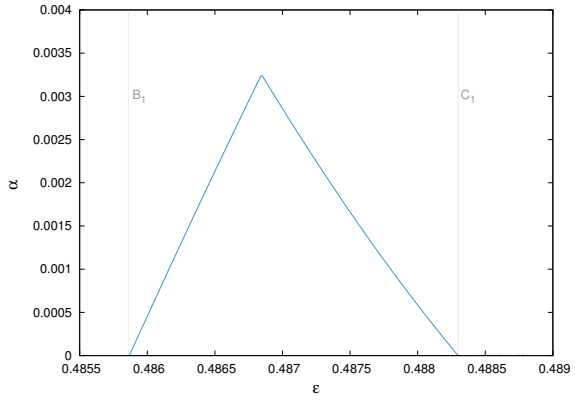

FIGURE 3.19: Minimum angle between slow and fast invariant subbundles. This is a magnification of a region between ε_{B} and ε_{C}, in which the bundles are separated again, and so the torus is reducible again.

Inside these regions of non-reducibility, we can find a lot of small gaps in which the torus is reducible again, as small as they can be. As an illustration, we find an small gap inside $[0.485, 0.489]$, see Figure 3.19. We can observe again that inside this interval the sign of the eigenvalues of the cocycle has also changed, see Table 3.14. Moreover, we can observe the angle between the slow and fast subbundles for each coordinate θ of different tori in Figure 3.21. Notice that when the torus is reducible ($\varepsilon = 0.45, 0.478, 0.525$) they do not touch each other, but they have a wild behavior because they are near a non-reducible zone.

Even that we observe several changes from reducible to non-reducible torus, the bundles are always orientable with index 0 and Lyapunov multipliers are different during the whole continuation, where the torus is analytic. In particular, the last torus we can compute is not the last normally hyperbolic invariant tori in the continuation. But as long as we increase the continuation parameter, we can see how the torus start to wrinkle, see Figure 3.20. This wildness on the slope of the torus makes harder the computations, and the method stops. This can be seen as a *fractalization mechanism* leading to the destruction of the torus, which has been observed for skew-products systems in [72, 73]. Numerical computations in [60] for a skew-product system (case $d = 0$ here) suggest that the torus persists till the maximal Lyapunov multiplier touches 1, even though the torus develops slopes of size 10^{30}. This phenomenon deserve further study.

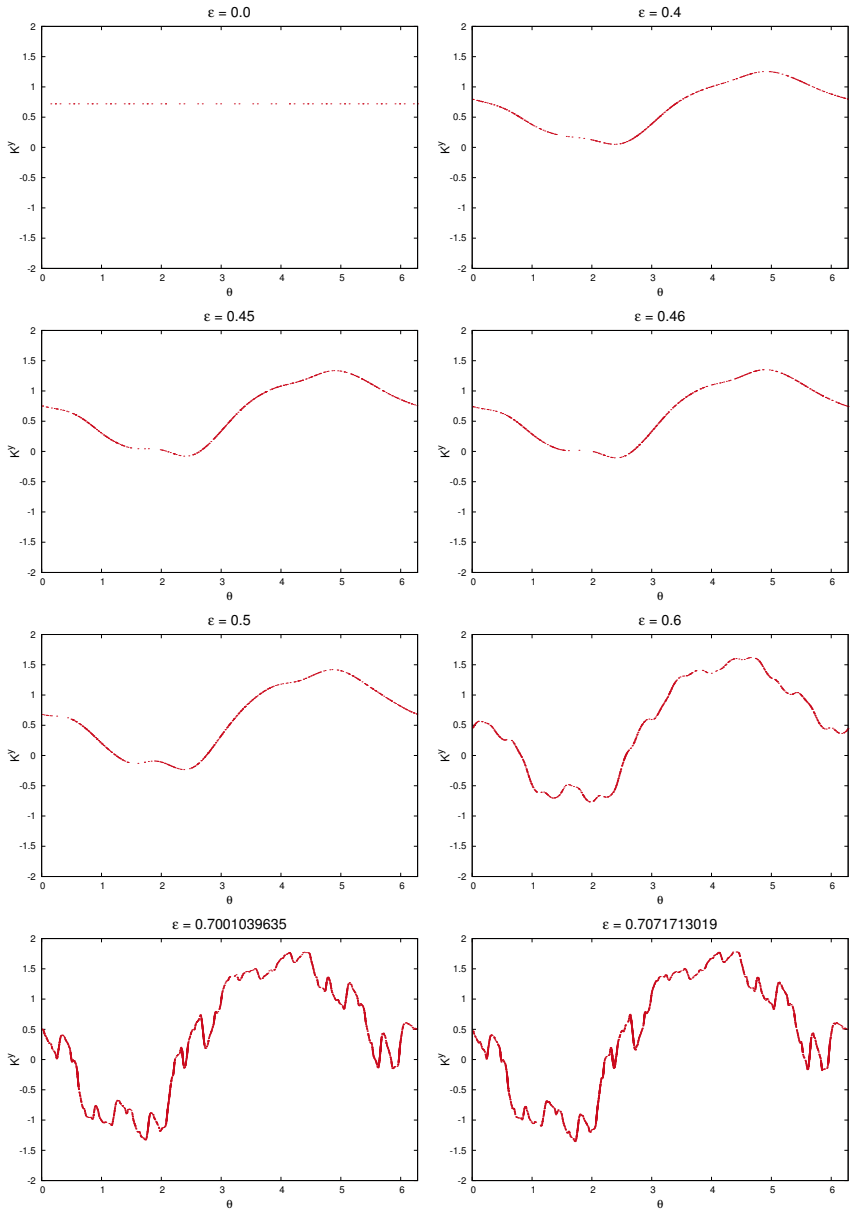

FIGURE 3.20: Quasi-periodic invariant attracting tori of Example 5 for the continuation parameter values $\varepsilon = 0.0$, 0.4, 0.45, 0.46, 0.5, 0.6, 0.7001039635 and 0.7071713019, respectively.

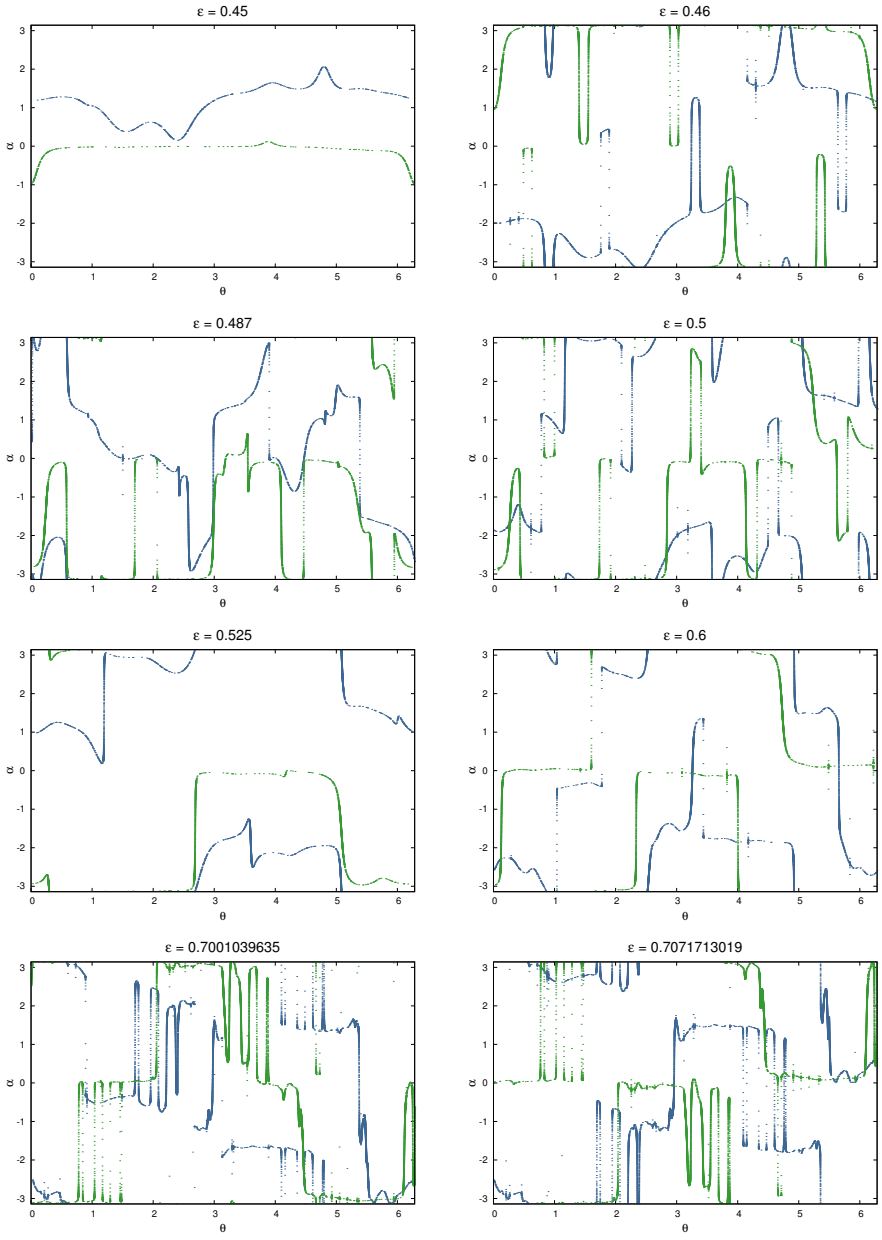

FIGURE 3.21: Angles between slow and fast bundles with respect to the horizontal axis for the continuation parameter values $\varepsilon = 0.45$, 0.46, 0.487, 0.5, 0.525, 0.6, 0.7001039635 and 0.7071713019, respectively. Notice that the ones corresponding to $\varepsilon = 0.45$, 0.487 and 0.525 has the slow and fast subbundles separated. These three parameters corresponds to regions in which the torus is reducible, whereas the others ones corresponds to regions in which it is not reducible.

Chapter 4

A Newton-like method for computing Normally Hyperbolic Invariant Tori

The aim of this chapter is to produce an algorithm to compute the parameterization of an invariant torus, the corresponding internal dynamics and the parameterizations of the associated stable and unstable bundles. Hence, we avoid the need for a separate algorithm to compute the invariant torus as the intersection of its stable and unstable manifolds.

We illustrate the empiric application of this method in several examples, starting with the computation of invariant curves in 2D and 3D "fattened" extensions of the Arnold standard circle map [12, 11, 8]. We implement the algorithm for the continuation of an invariant curve with respect to parameters, regardless of its internal dynamics. Hence, the method is able to cross resonances in the internal dynamics. Our interest is to explore the behavior of the invariant curve and its mechanisms of breakdown. The last example deal with the computation of a higher dimensional object: a normally hyperbolic cylinder for a four dimensional symplectic map. This type of object is important in recent studies of Arnold diffusion [32, 33].

4.1 The setting

We recover now the setting considered in this thesis, established in Section 1.3 of Chapter 1, adapted to a normally hyperbolic general case. We consider the ambient space an $(n+d)$-dimensional annulus $\mathcal{A} \subset \mathbb{T}^d \times \mathbb{R}^n$ and

a discrete dynamical system generated by a diffeomorphism $F : \mathcal{A} \to \mathcal{A}$ of the form

$$F\begin{pmatrix} x \\ y \end{pmatrix} = \begin{pmatrix} Ax \\ 0 \end{pmatrix} + F_p\begin{pmatrix} x \\ y \end{pmatrix},$$

where $A \in \mathrm{GL}_d(\mathbb{Z})$ and $F_p : \mathcal{A} \to \mathbb{R}^m$ is 1-periodic in x. Our interest is finding an invariant rotational torus $\mathcal{K}$, that is a d-dimensional manifold modeled on the d-dimensional torus $\Theta = \mathbb{T}^d$, and parameterized by an immersion $K : \mathbb{T}^d \to \mathcal{A}$ of the form

$$K(\theta) = \begin{pmatrix} \theta \\ 0 \end{pmatrix} + K_p(\theta),$$

where $K_p : \mathbb{T}^d \to \mathbb{R}^m$ is 1-periodic in θ. Notice that, if $\mathcal{K}$ satisfies

$$F \circ K - K \circ f = 0,$$

then f has to be of the form

$$f(\theta) = A\theta + f_p(\theta),$$

where $f_p : \mathbb{T}^d \to \mathbb{R}^d$ is 1-periodic in θ. This is just a consequence of the topological assumptions, chosen for the sake of concreteness. Recall that, the point is that the homotopy classes of F, K and f have to match.

As in previous chapters, the columns of the matrix map $P : \mathbb{T}^d \to \mathbb{R}^{n\times n}$, obtained by juxtaposing the matrix valued maps L and N so that

$$P(\theta) = (L(\theta) \;\; N(\theta)),$$

provide an adapted frame around $\mathcal{K}$.

Assume now that $\mathcal{K}$, parameterized by K, is F-invariant with internal dynamics f. By differentiating the invariance equation of the parameterization K,

$$F(K(\theta)) - f(K(\theta)) = 0, \tag{4.1}$$

we obtain the invariance equation of the linearization $L(\theta) = \mathrm{D}K(\theta)$,

$$\mathrm{D}F(K(\theta))\mathrm{D}K(\theta) - \mathrm{D}K(f(\theta))\mathrm{D}f(\theta) = 0, \tag{4.2}$$

where $\Lambda_L(\theta) = \mathrm{D}f(\theta)$ is the internal dynamics on $\mathrm{T}\mathcal{K}$. Hence, the linearized dynamics $\mathrm{D}F$ around $\mathcal{K}$ in the frame provided by P is given by a block triangular linear skew-product $(f, \Lambda) : \mathbb{T}^d \times \mathbb{R}^m \to \mathbb{T}^d \times \mathbb{R}^m$. Specifically, the matrix valued map $\Lambda : \mathbb{T}^d \to \mathbb{R}^{m\times m}$ defined as

$$\Lambda(\theta) = P(f(\theta))^{-1}\mathrm{D}F(K(\theta))P(\theta) \tag{4.3}$$

is of the form

$$\Lambda(\theta) = \begin{pmatrix} \Lambda_L(\theta) & T(\theta) \\ O & \Lambda_N(\theta) \end{pmatrix}, \tag{4.4}$$

where

$$\begin{pmatrix} T(\theta) \\ \Lambda_N(\theta) \end{pmatrix} = P(f(\theta))^{-1} \mathrm{D}F(K(\theta))N(\theta).$$

Therefore, the normal frame $N(\theta)$ is invariant if and only if $T(\theta) = 0$. This is equivalent to the invariance condition

$$\mathrm{D}F(K(\theta))N(\theta) - N(f(\theta))\Lambda_N(\theta) = 0. \tag{4.5}$$

The normal hyperbolicity of the torus $\mathcal{K}$ is characterized by the hyperbolicity of the cocycle $(f, \Lambda_N) : \mathbb{T}^d \times \mathbb{R}^n \to \mathbb{T}^d \times \mathbb{R}^n$, and the fact that this hyperbolicity dominates the dynamics of the cocycle $(f, \Lambda_L) : \mathbb{T}^d \times \mathbb{R}^d \to \mathbb{T}^d \times \mathbb{R}^d$.

From now on, we assume that the invariant normal bundle splits in trivial stable and unstable bundles, in such a way that

$$N(\theta) = (N^S(\theta)\ N^U(\theta)) \tag{4.6}$$

where $N^S : \mathbb{T}^d \to \mathbb{R}^{m \times n_s}$ and $N^U : \mathbb{T}^d \to \mathbb{R}^{m \times n_u}$ provide global frames for the stable and unstable bundles, respectively. This means that the $\Lambda_N(\theta)$ is block diagonal

$$\Lambda_N(\theta) = \begin{pmatrix} \Lambda_S(\theta) & O \\ O & \Lambda_U(\theta) \end{pmatrix} \tag{4.7}$$

where Λ_S is "contracting" and Λ_U is "expanding" (ie: $\|\Lambda_S\| < 1$, $\|(\Lambda_U)^{-1}\| < 1$ for an appropriate adapted norm) and both Λ_S and Λ_U dominate the tangent dynamics Λ_L. As we will see, these conditions will become important in the implementation of a Newton step. Of course, $n = n_s + n_u$, and either n_s or n_u can be 0 (i.e., if $n_s = 0$ then torus is repelling, and if $n_u = 0$ the torus is attracting).

Remark 4.1 *We have not considered here the parameterizations of the stable and unstable manifolds (just of their linear approximations). For example, the invariance equation for the stable bundle would be*

$$F(W(\theta, s)) = W(f(\theta), \hat{\Lambda}_S(\theta, s)).$$

This sort of parameterizations also provides parameterizations of the stable foliation. *The leave of the stable foliation at a point $K(\theta) = W(\theta, 0)$ parameterized by θ is*

$$\mathcal{W}_{K(\theta)} = \{W(\theta, s) \mid s \in \mathbb{R}^{n_s}\}. \tag{4.8}$$

Notice that $F(\mathcal{W}_{K(\theta)}) = \mathcal{W}_{F(K(\theta))}$, i.e., the stable foliation is invariant. Idem for the unstable foliation. Theoretical results and examples in a quasi-periodic context on skew products can be found in papers [57, 58, 59].

Remark 4.2 *While the topological assumptions on the ambient space and the torus are justified by the tubular neighborhood theorem, and the existence of global frames comes from the topological properties of embedded tori, the assumption of triviality of the stable and unstable bundles is a severe one. In the numerical examples considered in this chapter, the stable and unstable bundles are trivial. There are also cases in which vector bundles are easily trivializable by performing the double covering trick. We refer the reader to [59] for examples of computations of invariant tori with quasi-periodic dynamics, for which the stable an unstable bundles (and the corresponding attached manifolds) are non-orientable.*

4.2 Specification of one step of a Newton-like method

In the following, we consider the problem of computing a parameterization K of a normally hyperbolic invariant torus and its internal dynamics f, solving (4.1), as well as computing a global frame for the hyperbolic splitting of the invariant normal bundle $N = (N^S \; N^U)$, and the corresponding internal dynamics $\Lambda = \mathrm{diag}(\Lambda_S, \Lambda_U)$, solving (4.5). In particular, we explain how to perform one step of a Newton-like method to solve the invariance equations (4.1) and (4.5).

Assume that we have an approximate parameterization of a normally hyperbolic invariant torus, K, an approximate expression of the internal dynamics, f, and an approximate invariant normal bundle N and its linearized dynamics $\Lambda_N = \mathrm{diag}(\Lambda_S, \Lambda_U)$, in block diagonal form. The aim of one step of Newton method is computing the corresponding corrections $\Delta K, \Delta f, \Delta N, \Delta\Lambda_N = \mathrm{diag}(\Delta\Lambda_S, \Delta\Lambda_U)$ in such a way that the error estimates of the new approximations $\bar{K} = K + \Delta K, \bar{f} = f + \Delta f, \bar{N} = N + \Delta N, \bar{\Lambda}_N = \Lambda_N + \Delta\Lambda_N$, are quadratically small with respect to the starting error estimates.

At each step of Newton method, we first deal with the invariance of the torus, computing $\bar{K}$ and $\bar{f}$, and then we deal with the invariance of the normal bundle (and its stable and unstable subbundles), computing $\bar{N}$ and $\bar{\Lambda}_N$. In the next subsections, we will explain in detail this step.

4.2.1 Substep 1: Correction of the approximate invariant torus

Let $E : \mathbb{T}^d \to \mathbb{R}^m$ be the error in the invariance equation of the torus, that is

$$E(\theta) = F(K(\theta)) - K(f(\theta)), \tag{4.9}$$

which is "small".

The adapted frame, $P : \mathbb{T}^d \to \mathbb{R}^{m\times m}$, defined by juxtaposing $L = \mathrm{D}K$ and N as

$$P(\theta) = \begin{pmatrix} L(\theta) & N(\theta) \end{pmatrix},$$

is approximately invariant. Indeed, the error of reducibility $E_{\mathrm{red}} : \mathbb{T}^d \to \mathbb{R}^{m\times m}$ defined by

$$E_{\mathrm{red}}(\theta) = P(f(\theta))^{-1}\mathrm{D}F(K(\theta))P(\theta) - \Lambda(\theta) \tag{4.10}$$

satisfies $E_{\mathrm{red}}(\theta) = \begin{pmatrix} P(f(\theta))^{-1}\mathrm{D}E(\theta) & E^N_{\mathrm{red}}(\theta) \end{pmatrix}$, where

$$E^N_{\mathrm{red}}(\theta) = P(f(\theta))^{-1}\mathrm{D}F(K(\theta))N(\theta) - \begin{pmatrix} 0 \\ \Lambda_N(\theta) \end{pmatrix}, \tag{4.11}$$

so it is also small.

We consider the correction of the torus of the form:

$$\Delta K(\theta) = P(\theta)\xi(\theta) \tag{4.12}$$

where $\xi : \mathbb{T}^d \to \mathbb{R}^m$ is a periodic function.

Remark 4.3 *Notice that the correction terms of the torus and its internal dynamics preserve the homotopy classes of both objects.*

Then, by substituting the new approximations $\bar{K} = K + P\xi$ and $\bar{f} = f + \Delta f$ in the invariance equation (4.1), and using first order Taylor expansion, we obtain:

$$\begin{aligned}
0 =& F(K(\theta) + P(\theta)\xi(\theta)) - K(f(\theta) + \Delta f(\theta)) - P(f(\theta) + \Delta f(\theta))\xi(f(\theta) + \Delta f(\theta)) \\
=& F(K(\theta)) + \mathrm{D}F(K(\theta))P(\theta)\xi(\theta) \\
& - K(f(\theta)) - L(f(\theta))\Delta f(\theta) - P(f(\theta))\xi(f(\theta)) + \mathcal{O}_2 \\
=& E(\theta) + (P(f(\theta))\Lambda(\theta) + P(f(\theta))E_{\mathrm{red}}(\theta))\xi(\theta) \\
& - \mathrm{D}K(f(\theta))\Delta f(\theta) - P(f(\theta))\xi(f(\theta)) + \mathcal{O}_2,
\end{aligned}$$

where we apply definitions (4.9) and (4.10) above, and $\mathcal{O}_2$ collect the quadratically small terms. By multiplying the last equation by $(P(f(\theta)))^{-1}$ and neglecting quadratically small terms, we get the cohomology equation

$$\eta(\theta) = \Lambda(\theta)\xi(\theta) - \xi(f(\theta)) - \begin{pmatrix} \Delta f(\theta) \\ 0 \end{pmatrix}, \tag{4.13}$$

where

$$\eta(\theta) = -(P(f(\theta)))^{-1}E(\theta) \tag{4.14}$$

is the error of the approximate solution in the adapted frame. Hence, by splitting (4.13) in tangent and normal components we realize that Newton step corresponds, up to quadratically small terms, to consider the block diagonal system

$$\begin{aligned} \eta^L(\theta) &= \Lambda_L(\theta)\xi^L(\theta) - \xi^L(f(\theta)) - \Delta f(\theta), & (4.15)\\ \eta^N(\theta) &= \Lambda_N(\theta)\xi^N(\theta) - \xi^N(f(\theta)), & (4.16) \end{aligned}$$

that we solve in two steps.

The normal cohomology equation

From the normal hyperbolicity property, in the setting of Section 1.3, matrix $\Lambda_N = \mathrm{diag}(\Lambda_S, \Lambda_U)$ is block diagonal, and equation (4.16) splits into stable and unstable components:

$$\begin{aligned} \eta^S(\theta) &= \Lambda_S(\theta)\xi^S(\theta) - \xi^S(f(\theta)), & (4.17)\\ \eta^U(\theta) &= \Lambda_U(\theta)\xi^U(\theta) - \xi^U(f(\theta)). & (4.18) \end{aligned}$$

Hence, we can solve both equations by simple iteration using the contracting principle, which will converge to the solutions ξ^S and ξ^U we wanted. In particular, ξ^S and ξ^U solve the fixed point equations

$$\begin{aligned} \xi^S(\theta) &= \Lambda_S(f^{-1}(\theta))\xi^S(f^{-1}(\theta)) - \eta^S(f^{-1}(\theta)), & (4.19)\\ \xi^U(\theta) &= (\Lambda_U(\theta))^{-1}\left(\xi^U(f(\theta)) + \eta^U(\theta)\right), & (4.20) \end{aligned}$$

respectively, that can be solved by iteration.

Remark 4.4 *The normal hyperbolicity property implies that Equation* (4.16) *has a unique solution. But we emphasize that what it is important is solving Equation* (4.16)*, not the specific method for solving it. As a case in point, one can discretize Equation* (4.16) *into a* large linear system*, and solve it using linear algebra methods. The method we explain here avoids solving these large linear systems, but slows down when normal hyperbolicity degenerates.*

The tangent cohomology equation

Now, we want to solve (4.15). Observe that in this case we have one equation with two unknowns (ξ^L and Δf), an *underdetermined system*. The simplest choice is taking

$$\xi^L(\theta) = 0,\ \Delta f(\theta) = -\eta^L(\theta). \tag{4.21}$$

Geometrically, it means that we modify the torus in the normal directions, and the correction of the dynamics is achieved as a byproduct. This is a *graph style* of parameterization (in the adapted coordinates).

Remark 4.5 *The choice of ξ^L, the correction of the torus in the tangent directions, determines Δf, the correction of the internal dynamics on the torus. By taking other ξ^L, we reparameterize the torus and the corresponding internal dynamics.*

Summarizing, we gain new approximations $\bar{K}$ and $\bar{f}$, of the form

$$\bar{K}(\theta) = K(\theta) + N(\theta)\xi^N(\theta), \tag{4.22}$$
$$\bar{f}(\theta) = f(\theta) - \eta^L(\theta), \tag{4.23}$$

for which the new error $\bar{E}(\theta) = F(\bar{K}(\theta)) - \bar{K}(\bar{f}(\theta))$ is, hopefully, quadratically small with respect to $E(\theta)$. Additionally, we obtain new approximations for the tangent bundle $\bar{L} = \mathrm{D}\bar{K}$ and its linearized dynamics $\bar{\Lambda}_L = \mathrm{D}\bar{f}$.

4.2.2 Substep 2: Correction of the stable and unstable subbundles

We start the correction of N and Λ_N by redefining the error in the invariance equation of the adapted frame P, since K, f, L and Λ_L have been improved to $\bar{K}$, $\bar{f}$, $\bar{L}$ and $\bar{\Lambda}_L$ respectively.

We consider E_{red} defined with the new approaches $\bar{K}$, $\bar{f}$, $\bar{L}$ and $\bar{\Lambda}_L$. To avoid stodgy notation, from now on we redefine $K := \bar{K}$, $f := \bar{f}$, $L := \bar{L}$ and $\Lambda_L := \bar{\Lambda}_L$. (This is in fact what we do in implementing the algorithm).

We consider the corrections of the normal bundle, N, and its linearized dynamics, $\Lambda_N = \mathrm{diag}(\Lambda_S, \Lambda_U)$, of the form:

$$\Delta N(\theta) = P(\theta)Q^N(\theta),\ \Delta\Lambda_N(\theta) = \Delta_N(\theta), \tag{4.24}$$

where $Q^N : \mathbb{T}^d \to \mathbb{R}^{m\times n}$ and $\Delta_N = \operatorname{diag}(\Delta_S, \Delta_U) : \mathbb{T}^d \to \mathbb{R}^{n\times n}$ are periodic matrix-valued functions. Then, we obtain:

$$\begin{aligned}
0 &= \mathrm{D}F(K(\theta))\bar{N}(\theta) - \bar{N}(f(\theta))\bar{\Lambda}_N(\theta) \\
&= \mathrm{D}F(K(\theta))\left(N(\theta) + P(\theta)Q^N(\theta)\right) \\
&\quad - \left(N(f(\theta)) + P(f(\theta))Q^N(f(\theta))\right)\left(\Lambda_N(\theta) + \Delta_N(\theta)\right) \\
&= P(f(\theta))E^N_{\mathrm{red}}(\theta) + \left(P(f(\theta))\Lambda(\theta) + P(f(\theta))E_{\mathrm{red}}(\theta)\right)Q^N(\theta) - \\
&\quad - P(f(\theta))Q^N(f(\theta))\Lambda_N(\theta) - N(f(\theta))\Delta_N(\theta) - P(f(\theta))Q^N(f(\theta))\Delta_N(\theta).
\end{aligned}$$

Hence, by multiplying both sides of the equation by $P(f(\theta))^{-1}$ and by neglecting quadratically small terms we obtain the following cohomological equation:

$$-E^N_{\mathrm{red}}(\theta) = \Lambda(\theta)Q^N(\theta) - Q^N(f(\theta))\Lambda_N(\theta) - \begin{pmatrix} O \\ \Delta_N(\theta) \end{pmatrix}. \tag{4.25}$$

The corrections of the (approximate) stable and unstable bundles are performed in the complementary directions. That is, the correction matrix Q^N is chosen of the form

$$Q^N(\theta) = \begin{pmatrix} Q^{LS}(\theta) & Q^{LU}(\theta) \\ O & Q^{SU}(\theta) \\ Q^{US}(\theta) & O \end{pmatrix}, \tag{4.26}$$

so that the "missing" blocks Q^{SS} and Q^{UU} are taken to be zero. Hence, Equation (4.25) corresponds to the following block equations, where we use super-indices to indicate the blocks, just as in (4.26):

$$\begin{aligned}
-E^{LS}_{\mathrm{red}}(\theta) &= \Lambda_L(\theta)Q^{LS}(\theta) - Q^{LS}(f(\theta))\Lambda_S(\theta), && \text{(4.27a)} \\
-E^{LU}_{\mathrm{red}}(\theta) &= \Lambda_L(\theta)Q^{LU}(\theta) - Q^{LU}(f(\theta))\Lambda_U(\theta), && \text{(4.27b)} \\
-E^{US}_{\mathrm{red}}(\theta) &= \Lambda_U(\theta)Q^{US}(\theta) - Q^{US}(f(\theta))\Lambda_S(\theta), && \text{(4.27c)} \\
-E^{SU}_{\mathrm{red}}(\theta) &= \Lambda_S(\theta)Q^{SU}(\theta) - Q^{SU}(f(\theta))\Lambda_U(\theta), && \text{(4.27d)} \\
-E^{SS}_{\mathrm{red}}(\theta) &= -\Delta_S(\theta), && \text{(4.27e)} \\
-E^{UU}_{\mathrm{red}}(\theta) &= -\Delta_U(\theta). && \text{(4.27f)}
\end{aligned}$$

We obtain directly the correction of the linearized normal dynamics from equations (4.27e) and (4.27f). The other 4 equations give us the components of the correction of the normal bundle, Q^N in (4.26), and can be solved by the contracting principle, as all of them are contractions or expansions by

NHIM hypothesis (Λ_S contractive and Λ_U expansive, both dominating Λ_L). The corresponding fixed point equations are

$$Q^{LS}(\theta) = (\Lambda_L(\theta))^{-1} \left(Q^{LS}(f(\theta))\Lambda_S(\theta) - E^{LS}_{\rm red}(\theta)\right), \tag{4.28a}$$
$$Q^{LU}(\theta) = \left(\Lambda_L(f^{-1}(\theta))Q^{LU}(f^{-1}(\theta)) + E^{LU}_{\rm red}(f^{-1}(\theta))\right)(\Lambda_U(f^{-1}(\theta)))^{-1}, \tag{4.28b}$$
$$Q^{US}(\theta) = (\Lambda_U(\theta))^{-1} \left(Q^{US}(f(\theta))\Lambda_S(\theta) - E^{US}_{\rm red}(\theta)\right), \tag{4.28c}$$
$$Q^{SU}(\theta) = \left(\Lambda_S(f^{-1}(\theta))Q^{SU}(f^{-1}(\theta)) + E^{SU}_{\rm red}(f^{-1}(\theta))\right)(\Lambda_U(f^{-1}(\theta)))^{-1}, \tag{4.28d}$$

that can be solved by iteration.

Remark 4.6 *Fast iterative methods for solving cohomology equations similar to* (4.17)*,* (4.18)*,* (4.28a)*,* (4.28b)*,* (4.28c)*, and* (4.28d) *have been described in [66, 67] in a KAM context (f being a rotation), reducing n iterations of simple iteration method to* $\log_2 n$*. We have extended and implemented them for a general f.*

Summarizing, we obtain the following new approximations of the invariant normal bundle, $\bar N$,

$$\begin{aligned} \bar N^S(\theta) &= N^S(\theta) + L(\theta)Q^{LS}(\theta) + N^U(\theta)Q^{US}(\theta), \\ \bar N^U(\theta) &= N^U(\theta) + L(\theta)Q^{LU}(\theta) + N^S(\theta)Q^{SU}(\theta), \end{aligned}$$

and of the corresponding linearized dynamics $\bar\Lambda_N = \mathrm{diag}(\bar\Lambda_S, \bar\Lambda_U)$,

$$\begin{aligned} \bar\Lambda_S(\theta) &= \Lambda_S(\theta) + E^{SS}_{\rm red}(\theta), \\ \bar\Lambda_U(\theta) &= \Lambda_U(\theta) + E^{UU}_{\rm red}(\theta). \end{aligned}$$

That is, we obtain a new adapted frame $\bar P(\theta) = \begin{pmatrix} \bar L(\theta) & \bar N(\theta) \end{pmatrix}$, and a new linearized dynamics $\bar\Lambda(\theta) = \mathrm{diag}(\bar\Lambda_L(\theta), \bar\Lambda_N(\theta))$.

4.2.3 Substep 3: Computation of approximate inverses

The previous substeps involve the computation of inverses of matrix valued maps such as P^{-1} in (4.14) and (4.11), Λ_U^{-1} in (4.20) and (4.28b), (4.28d), Λ_L^{-1} in (4.28a), and the computation of the inverse of the torus diffeomorphisms f, f^{-1}, see (4.19) and (4.28b), (4.28d). In computer implementations, these inverses can be performed by using specialized routines to manipulate discretized periodic functions, see Section 4.3. Here, we explain how to include additional equations for these objects, to be included in the Newton step. Besides the unknowns K, f, N and Λ_U, we consider the unknowns

P^-, Λ_U^-, Λ_L^- and f^-, corresponding to P^{-1}, Λ_U^{-1}, Λ_L^{-1} and f^{-1}, respectively. The equations for these new unknowns are

$$P^-(\theta)P(\theta) - I = 0,\ \Lambda_U^-(\theta)\Lambda_U(\theta) - I = 0,\ \Lambda_L^-(\theta)\Lambda_L(\theta) - I = 0$$

and

$$f^- \circ f(\theta) - \theta = 0.$$

Therefore, starting the step of Newton method we have the approximations K, f, N, Λ_U and P^-, Λ_U^-, Λ_L^- and f^-. Hence, in the computations of substep 1, we have just to substitute the occurrences of P^{-1}, Λ_U^{-1} and f^{-1} by P^-, Λ_U^- and f^-, respectively.

After completing substep 1, we perform an improvement of f^-, $\bar{f}^-$, since this is going to be used in substep 2 in place of $\bar{f}^{-1}$. From the error estimate $e : \mathbb{T}^d \to \mathbb{R}^d$, given by

$$e(\theta) = f^-(\bar{f}(\theta)) - \theta,$$

we accomplish that a correction term $\Delta f : \mathbb{T}^d \to \mathbb{R}^d$ of f^-, such that $\bar{f}^- = f^- + \psi$, should satisfy $e(\theta) + \Delta f(\bar{f}(\theta)) = 0$, up to quadratically small terms with respect to $e(\theta)$. The choice

$$\Delta f(\theta) = -e(f^-(\theta))$$

makes the job, so that we compute

$$\bar{f}^-(\theta) = f^-(\theta) - e(f^-(\theta)). \tag{4.29}$$

Hence, in the formulae of substep 2, we have to substitute the occurrences of P^{-1}, Λ_U^{-1} and Λ_L^{-1} by P^-, Λ_U^- and Λ_L^-, respectively, and the occurrences of $\bar{f}^{-1}$ by $\bar{f}^-$.

After completing substep 2, it is the moment of recomputing P^-, Λ_U^- and Λ_L^- to produce $\bar{P}^-$, $\bar{\Lambda}_U^-$ and $\bar{\Lambda}_L^-$. From the error estimate $E : \mathbb{T}^d \to \mathbb{R}^{m\times m}$, given by

$$E_{\text{inv}}(\theta) = P^-(\theta)\bar{P}(\theta) - \mathrm{I},$$

we obtain

$$\bar{P}^-(\theta) = P^-(\theta) - E_{\text{inv}}(\theta)P^-(\theta). \tag{4.30}$$

Analogous computation can be performed to obtain $\bar{\Lambda}_U^-$ and $\bar{\Lambda}_L^-$.

4.2.4 A continuation method

In parameter dependent problems, we use a continuation method (see e.g. [99, 76]). In order to obtain accurate seeds as starting approximations in the Newton method, one can use expansions of the solutions with respect to the parameters. Here we use first order expansions.

Let $F_\varepsilon : \mathbb{T}^d \times \mathbb{R}^n \to \mathbb{T}^d \times \mathbb{R}^n$ a parameter family of diffeomorphisms, parameterized by the 1D parameter $\varepsilon \in \mathbb{R}$. Then aim is solving the equations:

$$F_\varepsilon(K_\varepsilon(\theta)) - K_\varepsilon(f_\varepsilon(\theta)) = 0, \tag{4.31}$$

$$\mathrm{D}F_\varepsilon(K_\varepsilon(\theta))N_\varepsilon(\theta) - N_\varepsilon(f_\varepsilon(\theta))\Lambda_{N\varepsilon}(\theta) = 0, \tag{4.32}$$

for K_ε, f_ε, N_ε and $\Lambda_{N\varepsilon}$, with respect to ε, starting from the solutions for a given parameter, say $\varepsilon = 0$.

Assume we have computed the solutions for a given ε, K_ε, f_ε, N_ε and $\Lambda_{N\varepsilon}$, and we want to compute the corresponding solutions for $\varepsilon + h$. We can take as seeds of Newton method the first order approximations of $K_{\varepsilon+h}$ and $f_{\varepsilon+h}$. That is

$$K_{\varepsilon+h}(\theta) \simeq K_\varepsilon(\theta) + \frac{\partial K_\varepsilon}{\partial \varepsilon}(\theta) \cdot h,\ \ f_{\varepsilon+h}(\theta) \simeq f_\varepsilon(\theta) + \frac{\partial f_\varepsilon}{\partial \varepsilon}(\theta) \cdot h, \tag{4.33}$$

where the variations $\frac{\partial K_\varepsilon}{\partial \varepsilon}(\theta)$ and $\frac{\partial f_\varepsilon}{\partial \varepsilon}(\theta)$ are to be computed in the following lines.

First, by deriving equation (4.31) with respect to parameter ε, we obtain

$$\mathrm{D}F_\varepsilon(K_\varepsilon(\theta))\frac{\partial K_\varepsilon}{\partial \varepsilon}(\theta) - \mathrm{D}K_\varepsilon(f_\varepsilon(\theta))\frac{\partial f_\varepsilon}{\partial \varepsilon}(\theta) - \frac{\partial K_\varepsilon}{\partial \varepsilon}(f_\varepsilon(\theta)) = -E(\theta),$$

where

$$E(\theta) = \frac{\partial F_\varepsilon}{\partial \varepsilon}(K_\varepsilon(\theta)).$$

Then, by writing the variations of K_ε and f_ε in the adapted frame $P_\varepsilon = \begin{pmatrix} \mathrm{D}K_\varepsilon & N_\varepsilon \end{pmatrix}$,

$$\frac{\partial K_\varepsilon}{\partial \varepsilon}(\theta) = P_\varepsilon(\theta)\xi(\theta), \frac{\partial f_\varepsilon}{\partial \varepsilon}(\theta) = \Delta f(\theta), \tag{4.34}$$

we reach the cohomology equation

$$\eta(\theta) = \Lambda_\varepsilon(\theta)\xi(\theta) - \xi(f_\varepsilon(\theta)) - \begin{pmatrix} \Delta f(\theta) \\ 0 \end{pmatrix},$$

where

$$\eta(\theta) = -(P_\varepsilon(f_\varepsilon(\theta)))^{-1}E(\theta). \tag{4.35}$$

As we learnt from Section 4.2.1, this cohomological equation have infinitely many solutions, and the solution we choose is

$$\Delta f(\theta) = -\eta^L(\theta)$$

and

$$\xi(\theta) = \begin{pmatrix} 0 \\ \xi^N(\theta) \end{pmatrix}$$

where ξ^N is the solution of

$$\eta^N(\theta) = \Lambda_{N\varepsilon}(\theta)\xi^N(\theta) - \xi^N(f_\varepsilon(\theta)). \tag{4.36}$$

This equation is solved by splitting into stable and unstable components, and using the contracting mapping principle.

Summing-up, we take as seeds of the Newton method for parameter $\varepsilon + h$

$$\begin{aligned} K^0_{\varepsilon+h}(\theta) &= K_\varepsilon(\theta) + N_\varepsilon(\theta)\xi^N(\theta) \cdot h, \\ f^0_{\varepsilon+h}(\theta) &= f_\varepsilon(\theta) - \eta^L(\theta) \cdot h. \end{aligned}$$

Remark 4.7 *In principle, to improve the seeds for computing $N_{\varepsilon+h}$ and $\Lambda_{N\varepsilon+h}$, we could do an analogous computation as in this section, but in any case, we will follow the procedures as in substep 2 of the method. However, our numerical experiments does not have shown special gain, especially where the torus is about to break.*

Remark 4.8 *Smooth dependence on parameters has to do with (local) uniqueness of the solutions. Notice that as long as Equation* (4.31) *has one solution, it has infinitely many solutions (by changing coordinates on the torus), which represents the same object. Then, if there are not extra constrains, one can abruptly tune the parameterizations to loose smoothness with respect to ε. This is also reflected in the infinitely many degrees of freedom one has to compute both the variations of K_ε and f_ε. But particular solutions are specified by the particular elections made in the steps of Newton method and continuation algorithm.*

4.3 Some guidelines for the implementations

In the following subsections we will present some examples of computations of normally hyperbolic invariant one-dimensional tori. The first step in the implementation of the parameterization method for the computation of invariant manifolds is choosing a method for numerically approximate them. Here, we will discuss some general ideas.

4.3.1 Modeling of tori

Developing methods and algorithms for the mathematical description of shapes is the object of geometric modeling. This area is so wide and has so many applications in science and engineering that we can only grasp here the tip of the iceberg. We refer to the excellent survey [61] on higher dimensional continuation methods, that includes a discussion on several methods from computational geometry to represent manifolds as simplicial complexes. Our purpose is much more modest. We consider here the computation of invariant tori given by periodic functions, hence, we have to deal with numerical approximations of periodic functions.

It is natural to discretize a model torus $\Theta = \mathbb{T}^d$ in a *regular* grid, of sizes $(N_1, \ldots, N_d)$, say a set of points

$$\theta_j^* := (\theta_{j_1}^*, \ldots, \theta_{j_d}^*) = \left(\frac{j_1}{N_1}, \ldots, \frac{j_d}{N_d} \right) \tag{4.37}$$

where $j = (j_1, \ldots, j_d)$, with $0 \leq j_r < N_r$ and $1 \leq r \leq d$. This defines a d-dimensional array $\{\varphi_j\}$ with $\varphi_j = \varphi(\theta_j^*)$, for some $\varphi : \mathbb{T}^d \to \mathbb{R}$.

The grid space (for periodic functions) is the set of all possible discretizations, i.e. $\mathbb{R}^{N_1} \times \cdots \times \mathbb{R}^{N_d}$. In order to approximate the function φ from its grid values φ_j, we can use interpolation. There are many interpolation methods available. In this chapter, we have considered piecewise Lagrange interpolation and trigonometric interpolation (using Fast Fourier Transform), but other methods such as spline polynomial interpolation can also be implemented. In general, one produces a (linear) map from the grid space $\mathbb{R}^{N_1} \times \cdots \times \mathbb{R}^{N_d}$ to a coefficient space $\mathbb{R}^{N_1 + \cdots + N_d}$ of the same dimension, producing coefficients $\bar{\varphi}_j$ from grid values. Notice that, while piecewise Lagrange interpolation is a "local" method, since the value of φ at a point $\theta \in \mathbb{T}^d$ is estimated from neighboring grid points, both trigonometric and spline interpolation are "global" methods, since the corresponding interpolating functions are computed from *all* the grid points.

Recall that, the d-dimensional tori $\mathcal{K}$ we consider in this chapter are immersed in $\mathbb{T}^d \times \mathbb{R}^n$ by means of parameterizations $K : \mathbb{T}^d \to \mathbb{T}^d \times \mathbb{R}^n$ of the form

$$K(\theta) = \begin{pmatrix} \theta \\ 0 \end{pmatrix} + K_p(\theta),$$

where $K_p : \mathbb{T}^d \to \mathbb{R}^d \times \mathbb{T}^n$ is 1-periodic in the θ-variable. See Section 1.3 for this setting. Hence, the $d + n$ components of K_p are periodic functions, that can be discretized in regular grids or approximated by trigonometric polynomials.

Remark 4.9 *Notice that a torus $\mathcal{K}$ immersed in $\mathbb{R}^m$ is parameterized by a periodic map $K : \mathbb{T}^d \to \mathbb{R}^m$, and the formulation is slightly simpler.*

Even though the grid points in the model torus $\mathbb{T}^d$ are equidistributed, one can adapt the grid values of the parameterization of the torus $\mathcal{K} = K(\mathbb{T}^d)$ to its particular shape. This adaptiveness is a manifestation of the versatility of the parameterization method, since one can choose representations of the torus for which computations are more numerically stable. For example, one can accumulate the grid values in the regions of larger curvature of the torus. The choice in [84, 85] is using an arc-length parameterization in the case of invariant curves and a conformal parameterization in the case of two dimensional invariant tori.

Let us give some details of the implementation of the piecewise Lagrangian interpolation method to approximate periodic functions. Fourier methods are profusely considered in Chapter 3.

Piecewise Lagrangian interpolation Let us consider the discretization of a 1-periodic function $\varphi : \mathbb{T}^d \to \mathbb{R}$ at the regular grid of sizes $N = (N_1, \dots, N_d)$. We denote $\varphi_j = \varphi(\theta_j^*)$ for $j \in \mathbb{Z}^d$, the value of φ at the grid point $\theta_j^* = j/N := \left(\frac{j_1}{N_1}, \dots, \frac{j_d}{N_d}\right)$ (notice that $\varphi_{j+N} = \varphi_j$). Given $\ell = (\ell_1, \dots, \ell_d)$, in order to estimate $\varphi(\theta)$ for $\theta \in \mathbb{T}^d$, we consider the neighboring points from the grid given by the indices $j \in [i-\ell, i+\ell+1] = \{j = (j_1, \dots, j_d) \mid i_r - \ell_r \le j_r \le i_r + \ell_r + 1\}$, where $i = [N\theta] = ([N_1\theta_1], \dots, [N_d\theta_d])$, and use the Lagrange interpolation formula

$$\tilde{\varphi}(\theta) = \sum_{j \in [i-\ell, i+\ell+1]} \varphi_j \; L_{i,j}(\theta) = \sum_{j_1 = i_1 - \ell_1}^{i_1+\ell_1+1} \cdots \sum_{j_d = i_d - \ell_d}^{i_d+\ell_d+1} \varphi_j \; L_{i_1,j_1}(\theta_1) \dots L_{i_d,j_d}(\theta_d) \tag{4.38}$$

where we define

$$L_{i,j}(\theta) = L_{i_1,j_1}(\theta_1) \dots L_{i_d,j_d}(\theta_d)$$

with

$$L_{i_r,j_r}(\theta) = \prod_{k_r = i_r - \ell_r, k_r \neq j_r}^{i_r+\ell_r+1} \frac{N_r\theta_r - k_r}{j_r - k_r}. \tag{4.39}$$

Notice that, since $L_{i,j}(\theta) = L_{0,j-i}(\theta - \theta_i^*)$, one could only store the coefficients of the Lagrangian polynomials corresponding to $i = 0$.

A suitable norm to produce estimates is the sup-norm on the grid space:

$$\|\tilde{\varphi}\|_L = \max_{i \in [0,N]} |\varphi_i|.$$

Information about the accuracy can be obtained by computing the sup-norm on a finer grid (by using interpolation).

Derivatives at the grid points are estimated by using finite difference formulas, which are provided by differentiating interpolation polynomials.

4.3.2 Manipulation of functions

The purpose of the algorithm discussed in this chapter is to compute a normally hyperbolic invariant torus, param3terized by $K = (\mathrm{id}, 0) + K_p : \mathbb{T}^d \to \mathbb{T}^d \times \mathbb{R}^n$, given by a smooth map $F = (A, 0) + F_p : \mathbb{T}^d \times \mathbb{R}^n \to \mathbb{T}^d \times \mathbb{R}^n$, and the corresponding internal dynamics, $f = A + f_p : \mathbb{T}^d \to \mathbb{T}^d$. Here, A is a unimodular matrix. See Section 1.3 for this setting. An outgrowth of the algorithm is the invariant normal bundle, described by a matrix valued map $N : \mathbb{T}^d \to \mathbb{R}^{m \times n}$, where $m = n + d$, for which the linearized dynamics is conjugate to $\Lambda_N : \mathbb{T}^d \to \mathbb{R}^{n \times n}$. Hence, in the numerical implementations of the algorithms one has to deal with the numerical approximations of the components of $K_p(\theta)$, $f_p(\theta)$, $N(\theta)$ and $\Lambda_N(\theta)$, which are periodic functions.

There are several basic routines which we have to implement in the algorithms explained along this chapter. Let us first consider the two terms of the invariance equation $F \circ K = K \circ f$. Both compositions require very different computational tools, since in the left hand side F is given "explicitly" (e.g. by an explicit formula, an algorithm, or as a result of an integration of a vector field), and in the right hand side both K and f are modeled. Notice that

$$F \circ K(\theta) = \begin{pmatrix} A\theta \\ 0 \end{pmatrix} + \underbrace{\begin{pmatrix} AK_p^x(\theta) \\ 0 \end{pmatrix} + F_p \begin{pmatrix} \theta + K_p^x(\theta) \\ K_p^y(\theta) \end{pmatrix}}_{(F \circ K)_p(\theta)}$$

and

$$K \circ f(\theta) = \begin{pmatrix} A\theta \\ 0 \end{pmatrix} + \underbrace{\begin{pmatrix} f_p(\theta) \\ 0 \end{pmatrix} + K_p(A\theta + f_p(\theta))}_{(K \circ f)_p(\theta)} .$$

From the computational point of view, we have to represent these periodic components $(F \circ K)_p$ and $(K \circ f)_p$. Notice that we store the grid values $\{K_{p,j}\}$ and $\{f_j\}$ of the periodic components K_p and f_p, respectively, and that our purpose is computing the grid values $\{(F \circ K)_{p,j}\}$ and $\{(K \circ f)_{p,j}\}$ of $(F \circ K)_p$ and $(K \circ f)_p$, respectively. The grid values $\{(F \circ K)_{p,j}\}$ are computed by evaluating F_p using the grid values $\{K_{p,j}\}$, since F is given. The grid values $\{(K_p \circ f)_j\}$ can be provided by piecewise interpolation, estimating $K_p(f(\theta_i))$ by interpolating K_p at neighboring grid points of $f(\theta_i) = A\theta_i + f_i$.

Manipulation of matrix valued maps, with entries given by periodic functions, are also easily handled in grid space. The computation of the inverse function of f, $g = f^-$, is another of the basic routines we need for the implementation of the algorithm. We can compute the periodic part g_p at the grid points θ_i by solving equation $f(A^{-1}\theta_i + g_i) = \theta_i$, e.g. using Newton method (in the examples of this chapter, for which $d = 1$, we use secant method). See section 4.2.4 to recall how to use continuation to compute the inverse.

Remark 4.10 *It is sometimes useful to keep track of both grid and Fourier representations, and then be able to choose the most efficient representation for each computation. While operations and compositions with functions are easily performed in grid space (with the aid of Lagrangian interpolation), computations of derivatives and compositions with rotations are more efficient in Fourier space.*

4.3.3 Grid point methods versus spectral methods: a digression

In general, *grid point methods* describe functions and objects by using their grid values (i.e., the values in a given grid). Then, we produce estimates of the function at a given point by using interpolation with neighboring grid points, where the accuracy of the computations depends on the diameter of the grid. These methods are potentially useful to represent *any* manifold, by using appropriate *triangularizations* and refinement algorithms. See e.g. [61] for a survey of simplicial methods. Such refinements are satisfactory to increase the resolution of the objects. Derivatives of functions can be estimated by using finite-difference formulas and interpolation formulas. In particular, these formulas are useful to compute tangent vectors to a parameterized manifold. Due to the local nature of grid point methods, they seem to be suitable to handle non-trivial bundles. Notice that the *regular* grid points is considered on the model manifolds, hence considering suitable parameterizations producing *regular* grid points on the immersed manifolds can result in numerical stability of the implementations.

On the other hand, spectral methods consist of describing functions as a superposition of basis functions. The name comes from the fact that, for a compact Riemannian manifold, we can construct an orthonormal basis of eigenfunctions for the Laplace-Beltrami operator, and then decompose the functions using this basis set producing series expansions. In numerical applications, we truncate these series expansions. Of course, Fourier methods correspond to the particular case of considering the (flat) torus. For example,

spherical harmonics are the appropriate basis of functions for the sphere. The accuracy of the computations has to do with the truncation order of the series. Derivatives of functions can be estimated by differentiating the corresponding series expansions. In particular, the tangent vectors to an immersed manifold can be computed by differentiating the series expansions of the corresponding parameterization. Spectral methods do not seem to be appropriate for dealing with non-trivial bundles.

Remark 4.11 *In general, transformations from grid space to spectral space are computationally demanding. Finding Fast Transforms (forward and backwards) between grid space and spectral space is a subject of great importance in applications. For periodic functions, these are the famous Fast Fourier Transforms, that were already known by Gauss, and reinvented and popularized by Cooley and Tukey in the sixties [28]. There is very efficient software implementing FFT, in any dimension, such as the awarded FFTW [48]. For the sphere, Fast Spherical Harmonics Transforms are very recent [81].*

4.4 Example 6: Continuation of attracting tori in a 2D-Fattened Arnold Family

In this section, we consider the so-called 2-dimensional Fattened Arnold Family (2D-FAF) [12]. It is a family of dissipative maps $F_{a,\varepsilon} : \mathbb{T}^1 \times \mathbb{R} \to \mathbb{T}^1 \times \mathbb{R}$ defined by:

$$F_{a,\varepsilon}\begin{pmatrix} x \\ y \end{pmatrix} = \begin{pmatrix} x + a + \frac{\varepsilon}{2\pi}(\sin(2\pi x) + y) \\ b(\sin(2\pi x) + y) \end{pmatrix}, \tag{4.40}$$

where $b \in]0, 1[$ is the Jacobian determinant of the family (which is fixed), $a \in \mathbb{T}^1$ is the rotation parameter and $\varepsilon \in \mathbb{R}$ is the perturbation parameter. A profuse study of the local and global bifurcations in this family is carried out in [12].

The family (4.40) displays many of the behaviors of its ancestor, the Arnold family of circle maps. In particular, there are regions in the parameter plane (a, ε), known as Arnold tongues, $\mathcal{R}_{p/q}$, defined as

$$(a, \varepsilon) \in \mathcal{R}_{p/q} \Leftrightarrow \exists (x, y) \in \mathbb{R}^2 \text{ such that } F^p_{a,\varepsilon}(x, y) = (x + q, y),$$

for which $F_{a,\varepsilon}$ has periodic orbits. The boundaries of these Arnold tongues correspond to saddle-node bifurcations of periodic orbits.

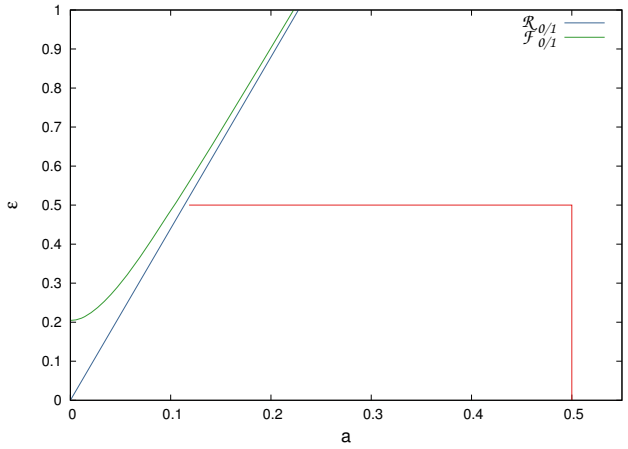

FIGURE 4.1: Regions $\mathcal{R}_{0/1}$ and $\mathcal{F}_{0/1}$ for $b = 0.3$ in the 2D-FAF given in (4.40). We include, in red, the continuation path for the example 10.

For example, the tongue

$$\mathcal{R}_{0/1} = \{(a, \varepsilon) \mid |2\pi a(1-b)| \leq |\varepsilon|\}$$

corresponds to the main resonance $0/1$, which matches to the existence of a couple of fixed points, one attracting and the other of saddle type. Inside this tongue, either the attracting fixed point is a node or a focus. The second case happens in the region

$$\mathcal{F}_{0/1} = \{(a, \varepsilon) \in R_{0/1} \mid (1-\sqrt{b})^4+(2\pi a(1-b))^2 < \varepsilon^2 < (1+\sqrt{b})^4+(2\pi a(1-b))^2\},$$

which is already inside $\mathcal{R}_{0/1}$.

In this section we are interested in the computation of normally hyperbolic invariant tori. As we are dealing with a 2-dimensional dissipative system, $\det F_{a,\varepsilon} = b < 1$, with $d = 1$, we are looking for invariant attracting circles of (4.40). We will perform the computation of the parameterizations of the invariant curves, $K_{a,\varepsilon}$, and their internal dynamics, $f_{a,\varepsilon}$ using the method explained in section 4.2. The corresponding internal dynamics generates a new family of circle maps. Hence, it is quite natural to expect that this family exhibits the same features of the paradigmatic Arnold family of circle maps. We emphasize that the normally hyperbolic (and attracting) invariant curve can not exist, for example, inside the region $\mathcal{F}_{0/1}$ mentioned above. In fact, one of the mechanisms of destruction of invariant curves is the transition of attracting periodic points from node type to focus type, where the curve survive only as a continuous curve, $\mathcal{C}^0$, with finite length. So, we can use

the boundary of this region to get bounds of parameters for which tori are destroyed.

In order to test the versatility of the algorithm, we will continue invariant circles and their internal dynamics in the (a, ε)-parameter plane, crossing resonances. Having the previous lines in mind, the continuation path in the (a, ε)-parameter plane has to start away from the resonance zone $\mathcal{R}_{0/1}$.

The numerical experiment we propose in this section is done for the fixed dissipative parameter $b = 0.3$. Figure 4.1 shows the boundaries of the regions $\mathcal{F}_{0/1}$ and $\mathcal{R}_{0/1}$ for $b = 0.3$ together with the continuation line in red.

4.4.1 The unperturbed case

Look first what happens for the unperturbed case $\varepsilon = 0$. In that case, the system (4.40) is simply a skew product over a rotation, $f_{a,0}(x) = x + a$. This skew product has an attracting invariant graph, given explicitly by

$$K_{a,0}(\theta) = \begin{pmatrix} \theta \\ \varphi_a(\theta) \end{pmatrix}, \tag{4.41}$$

where

$$\varphi_a(\theta) = \sum_{k=1}^{\infty} b^k \sin(2\pi(\theta - ka)) = -S(a,b)\ \cos(2\pi\theta) + (C(a,b) - 1)\ \sin(2\pi\theta), \tag{4.42}$$

being

$$C(a,b) = \frac{1 - b\cos(2\pi a)}{1 - 2b\cos(2\pi a) + b^2},\ S(a,b) = \frac{b\sin(2\pi a)}{1 - 2b\cos(2\pi a) + b^2}. \tag{4.43}$$

That is, $K_{a,0}$ and $f_{a,0}$ meet the invariance equation

$$F_{a,0} \circ K_{a,0} = K_{a,0} \circ f_{a,0},$$

and the unperturbed torus is analytic.

Then, the vertical bundle parameterized by $N : \mathbb{T}^1 \to \mathbb{R}^{2\times 1}$ with

$$N(\theta) = \begin{pmatrix} 0 \\ 1 \end{pmatrix},$$

is invariant under $\mathrm{D}F_{a,0}$. In particular, the linearized dynamics $\mathrm{D}F_{a,0}$ around the invariant circle on the adapted frame $P_{a,0}$ will be

$$P_{a,0}^{-1}(\theta + a)\mathrm{D}F_{a,0}(K_{a,0}(\theta))P_{a,0}(\theta) = \Lambda_{a,0}(\theta),$$

with

$$P_{a,0}(\theta) = \begin{pmatrix} 1 & 0 \\ \varphi_a'(\theta) & 1 \end{pmatrix}$$

and

$$\Lambda_{a,0}(\theta) = \begin{pmatrix} 1 & 0 \\ 0 & b \end{pmatrix}.$$

Since $b \in]0,1[$, the torus is normally hyperbolic, and attracting. By normal hyperbolicity, this invariant attracting circle persists for small perturbation of parameters a or ε.

Remark 4.12 *The invariant torus has a very different dynamics depending if the parameter $a \in \mathbb{Q}$ or $a \in \mathbb{R}/\mathbb{Q}$. In the first case all the orbits are periodic, while in the second case all the orbits are dense. Notice, however, that even though the torus persists for small values of ε, the internal dynamics can be quite different.*

Remark 4.13 *When the internal dynamics is a fixed parameter ω which is also* Diophantine*, we use a parameterization method that involves normal hyperbolicity and a KAM scheme to continue with respect to ε a family of invariant tori with fixed frequency ω by tuning parameter $a = a(\varepsilon)$, with $a(0) = \omega$. See Chapters 2 and 3 and reference [19]. There is also a tailored version for conformally symplectic systems (here, the determinant of the differential is constant b), which also works to the limit $b = 1$ [16].*

4.4.2 Computations far from the perturbative regime

In this example, we want to focus our attention on the resonance crossings of the internal dynamics when continuing an attracting invariant curve with respect to the parameters of the 2-dimensional Fattened Arnold map (4.40). In the same way as in the Arnold map, the phenomenon of the resonances is more apparent for big values of ε, i.e. far from the perturbative regime. In this numerical example, we have taken $\varepsilon = 0.5$ to observe it. We perform a continuation process with respect to parameter a starting at $a = 0.5$, which is far away from the main resonance $\mathcal{R}_{0/1}$, by decreasing its value. We follow two continuation paths (see Figure 4.1 in red):

(1) Continuation with respect to ε: $a = 0.5$ fixed, $\varepsilon = 0.0$ until 0.5, to fall in a zone where the resonances are apparent enough. Recall that for $\varepsilon = 0$ we have explicit formulae for $K_{a,0}$ and $f_{a,0}$, (4.41).

(2) Continuation with respect to a: $\varepsilon = 0.5$ fixed, $a = 0.5$ until 0.1184258179, to observe the phenomenon of the resonances until the algorithm stops.

Our interest falls on the second continuation path, which is displayed in Table 4.1.

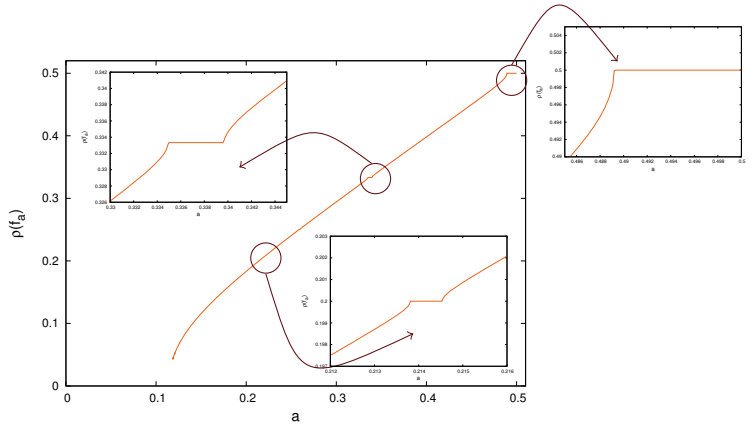

FIGURE 4.2: Rotation number for the internal dynamics of 2D-FAF, for $b = 0.3$ and $\varepsilon = 0.5$ fixed. Magnifications near the frequencies $\rho(f_a) = \frac{1}{2}, \frac{1}{3}, \frac{1}{5}$.

Since the algorithm computes the internal dynamics on the invariant curve, so it is given by a circle map, we can compute its rotation number. To compute the rotation number, we use the algorithm proposed in [96] to our function of the internal dynamics of the torus obtained during our computations. Note that the rotation number is a continuous function with respect to the parameters. Figure 4.2 shows the rotation number as a function of a, exhibiting the familiar devil staircase. The multiple plateaus correspond to the existence of periodic orbits on the invariant curve, for which the rotation number is rational, and their boundaries correspond to saddle-node bifurcations. In fact, we can see in Table 4.1 the corresponding rotation numbers for the continuation parameter a, where we highlight some resonances.

USING FOURIER DISCRETIZATION						
a	$\rho(f_a)$	N_{F}	E	E^N_{red}	E_{inv}	TAIL
0.5000000000	$\frac{1}{2}$	256	2.1e-11	7.9e-11	5.7e-15	7.5e-14
0.4904000000	$\frac{1}{2}$	256	1.5e-11	9.1e-11	1.2e-14	1.9e-15
0.4500000000	0.44997815	256	8.9e-11	1.0e-10	2.4e-15	4.3e-15
0.4017000000	$\frac{2}{5}$	256	9.1e-11	5.8e-11	9.6e-15	6.9e-15
0.4000000000	0.39819393	256	9.1e-11	5.7e-11	3.1e-15	4.1e-15
0.3500000000	0.34631620	256	1.1e-11	9.3e-12	1.5e-14	4.7e-15
0.3377000000	$\frac{1}{3}$	256	1.4e-11	1.0e-11	8.1e-15	4.8e-15
0.3000000000	0.29428313	256	1.1e-11	1.0e-11	1.5e-14	1.1e-14
0.2590000000	$\frac{1}{4}$	256	2.6e-11	5.0e-12	7.1e-14	1.6e-14
0.2500000000	0.24047813	256	2.2e-11	5.6e-12	6.4e-15	1.4e-14
0.2142000000	$\frac{1}{5}$	256	3.7e-11	9.0e-12	2.4e-14	5.4e-14
0.2000000000	0.18322639	256	2.6e-11	1.2e-11	2.1e-13	2.9e-14
0.1866000000	$\frac{1}{6}$	256	4.5e-11	4.3e-11	3.1e-14	4.1e-14
0.1684000000	$\frac{1}{7}$	256	3.3e-11	3.6e-11	8.1e-13	5.9e-14
0.1560000000	$\frac{1}{8}$	256	6.0e-11	5.1e-11	2.3e-12	7.5e-14
0.1500000000	0.11576335	256	3.8e-11	2.1e-11	1.4e-12	7.5e-14
0.1471000000	$\frac{1}{9}$	256	5.1e-11	3.3e-11	8.9e-12	1.7e-13
0.1407000000	$\frac{1}{10}$	256	9.3e-11	9.8e-11	2.9e-11	3.7e-13
0.1359000000	$\frac{1}{11}$	256	9.4e-11	9.0e-11	1.9e-11	2.8e-13
0.1349937500	0.08907000	512	4.6e-11	6.8e-11	2.7e-12	8.1e-16
0.1294062500	$\frac{1}{13}$	512	9.8e-11	4.6e-10	4.4e-11	5.3e-14
0.1280000000	0.07350508	512	1.0e-12	1.4e-09	1.9e-09	1.4e-13
0.1271656250	$\frac{1}{14}$	512	8.6e-11	6.3e-10	1.3e-09	3.3e-13
0.1270000000	0.07098623	1024	1.4e-11	2.1e-10	6.3e-11	4.4e-14
0.1259825195	0.06831106	8192	6.3e-11	2.3e-10	7.0e-09	1.1e-13
USING LOCAL INTERPOLATION						
a	$\rho(f_a)$	N	E	E^N_{red}	–	–
0.1259825195	0.06831106	16384	1.1e-11	1.3e-10	–	–
0.1183555167	0.04242959	65536	3.2e-11	1.1e-09	–	–
0.1162158902	0.03094355	524288	6.3e-11	8.8e-09	–	–

TABLE 4.1: Continuation with respect to a for $b = 0.3$ and $\varepsilon = 0.5$ fixed in the 2D-FAF. For each value a we show several quantities associated with it: the rotation number $\rho(f_a)$, the error in the invariance equation E, the error in the normal component of the reducibility equation E^N_{red}, the error in the computation of the inverse of the adapted frame E_{inv} and the maximum norm of the last Fourier terms TAIL. In gray it appears a values corresponding to rational frequencies, while in dark gray the ones for which we show the plots in this example (Figures 4.3 and 4.4).

Notice that we are able to catch out different resonant regions by studying the internal dynamics. In particular, Figure 4.3 shows invariant tori for values $a = 0.4904$, $a = 0.3377$ and $a = 0.2142$, for which the rotation number are $\frac{1}{2}$, $\frac{1}{3}$ and $\frac{1}{5}$ respectively. Their internal dynamics are displayed on the right of the Figure 4.3, where it is seen as a graph of the circle map. Indeed, there are couples of attracting-repelling 2, 3 and 5 periodic orbits inside the curves, which are plotted over each corresponding torus. Note that internal attracting periodic orbits correspond to attracting periodic orbits of the whole system, while internal repelling periodic orbits correspond to saddle period orbits. We emphasize that at the resonances during the continuation

process, the attracting periodic orbits are stable nodes.

Otherwise, in Figure 4.4, we can observe how varies the normal (stable) bundle for the same a parameters corresponding to the previous rational frequencies. In the right of this figure we see its corresponding dynamics over the bundles (i.e. the Λ_L, Λ_S functions).

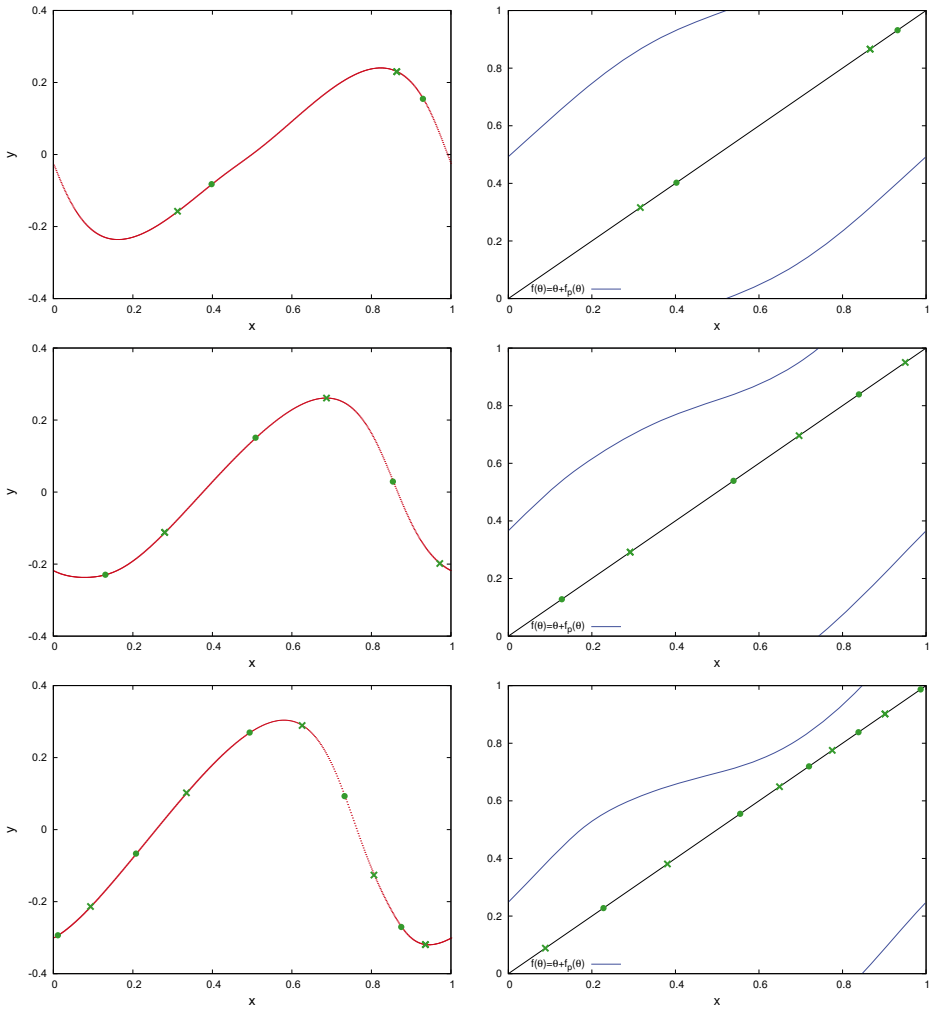

FIGURE 4.3: Left: invariant attracting circles with their two internal attracting-repelling periodic orbits, represented by green dots and crosses respectively. Right: internal dynamics over the torus, in blue, with the line of the fixed points in black. Figures for parameters $a = 0.4904$, $a = 0.3377$ and $a = 0.2142$ respectively, for $\varepsilon = 0.5$ and $b = 0.3$ fixed.

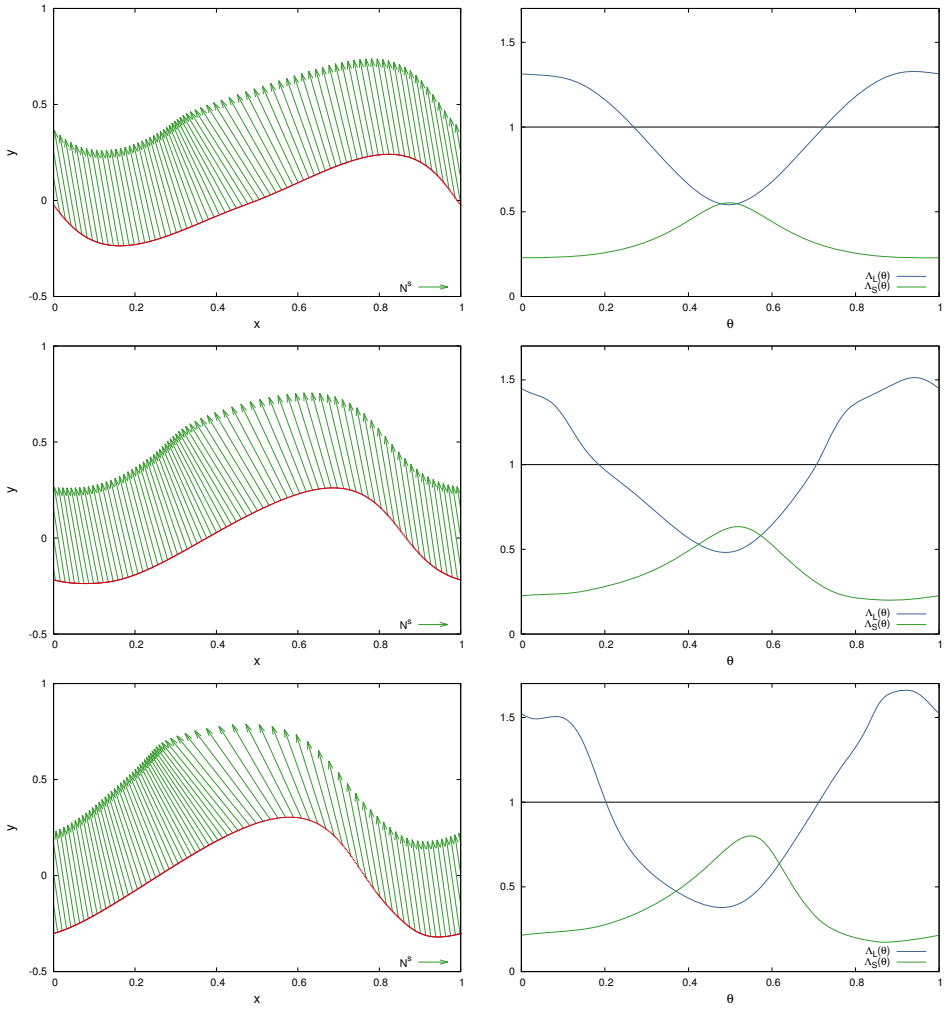

FIGURE 4.4: Left: invariant normal (stable) bundle of each circle. Right: linearized dynamics over the bundles. Figures for parameters $a = 0.4904$, $a = 0.3377$ and $a = 0.2142$ respectively, for $\varepsilon = 0.5$ and $b = 0.3$ fixed.

We can observe that during this crossing resonance path, we proceed with the same error tolerance on the invariant equation, $||E|| < 10^{-10}$, and without the necessity to increase the number of Fourier modes of the trigonometric approximations of the objects for almost all a values. The computation run into some troubles when crossing "big" resonances, that are overcome by increasing the number of the Fourier modes. This is much more apparent when we are close to the main resonance. As we explain in section 4.3.3, the speed of the algorithm is dominated by the computation time of the

composition of functions, which is a hard work in the Fourier space. So, when we are dealing with a high number of Fourier modes, we turn the periodic functions into functions discretized by local interpolation, and then we follow the continuation process using this kind of discretization.

The continuation process stops when we reach the value

$$a_{\text{last}} = 0.1162158902.$$

This is because the continuation step is very small, say smaller than 10^{-7}, since the Newton method does not converge. However, it is expected that the curve persists, and that the internal dynamics exhibits a saddle-node bifurcation of fixed points at

$$a_{\text{sn}} \simeq 0.1136821022.$$

Notice that this value corresponds to the boundary of the resonance region $\mathcal{R}_{0/1}$. After the bifurcation, the circle has an attracting (node) and a saddle fixed point, and the invariant curve is generated by the unstable manifold of the saddle point. Moreover, there is a node-focus transition of the attracting fixed point at

$$a_{\text{nf}} \simeq 0.1037332330,$$

when we touch the boundary of the region $\mathcal{F}_{0/1}$. As we know, inside this region we cannot have a (smooth) normally hyperbolic invariant circle, so a_{nf} is a lower bound for the existence of invariant attracting circles for the parameters $\varepsilon = 0.5$ and $b = 0.3$.

When our method stops, we can observe that the minimum angle between bundles decreases up to the value α_{last} =0.0129160145 (see Figure 4.5 top). This behavior suggests that the breakdown of the torus is not due to a node-focus transition nor to a bundle collision. In a node-focus transition, the stable node turns to a focus. Hence, if the breakdown is due to this transition, the angle between bundles at the fixed point has to be zero at the moment of the collision of the two real eigenvalues. Other sophisticated scenarios of bundle collision in the context of quasi-periodic invariant tori can be seen in [19, 56, 59, 18].

However, it is already known that other possible scenarios of destruction involving global phenomena related with homoclinic bifurcations can occur. In fact, it could happen before the creation of a focus, as a *cubic tangency* between invariant manifolds. In that case, the unstable manifold, $\mathcal{W}^U$, that generates the invariant curve, has a cubic tangency with some leaves of the stable foliation of the invariant curve. After these tangencies, the torus is

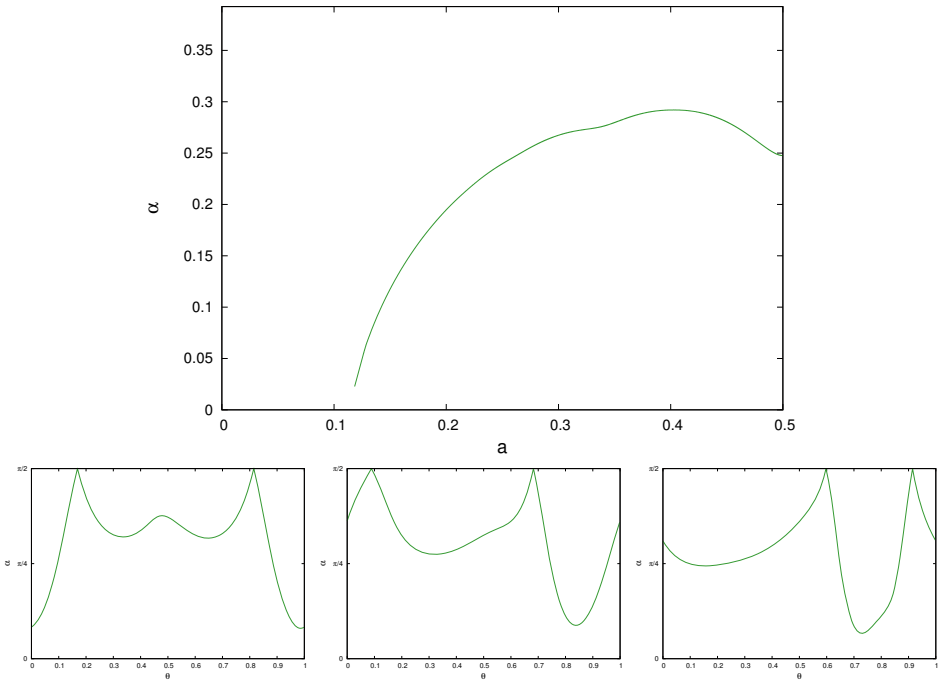

FIGURE 4.5: Top: Minimum angle between tangent and stable bundle for each parameter a during the continuation process, for $\varepsilon = 0.5$ and $b = 0.3$ fixed. Bottom: Minimum angle between tangent and stable bundle for fixed parameters $a = 0.4904$, $a = 0.3377$ and $a = 0.2142$ respectively.

destroyed (in the sense of a normally hyperbolic invariant circle), and persists only as a continuous curve. A sudden loss of regularity of the curve occurs, from $\mathcal{C}^r$ to $\mathcal{C}^0$. See [1, 34, 12, 51] for more details.

We expect that is what occurs in our example. Using algorithms to compute higher order invariant manifolds of fixed points, see e.g. [99, 53], we can compute the invariant curve. We pick several a values after the saddle-node creation but before the node-focus transition, and then we compute the unstable manifold of the saddle, which meets to the invariant circle, and the strong stable manifold of the node, $\mathcal{W}^{SS}$, which coincides with the leave of the stable foliation in the node. We observe that for some parameters there are transversal crossings between the unstable manifold of the saddle and the strong stable manifold of the node. Indeed, before these crossings there is a value a_{qt} for which we have a *quadratic tangency*:

$$a_{\text{qt}} \approx 0.1130118205.$$

This transition is showed at bottom of Figure 4.6. It is known (see [12]) that before a quadratic tangency there is a cubic tangency for a certain parameter

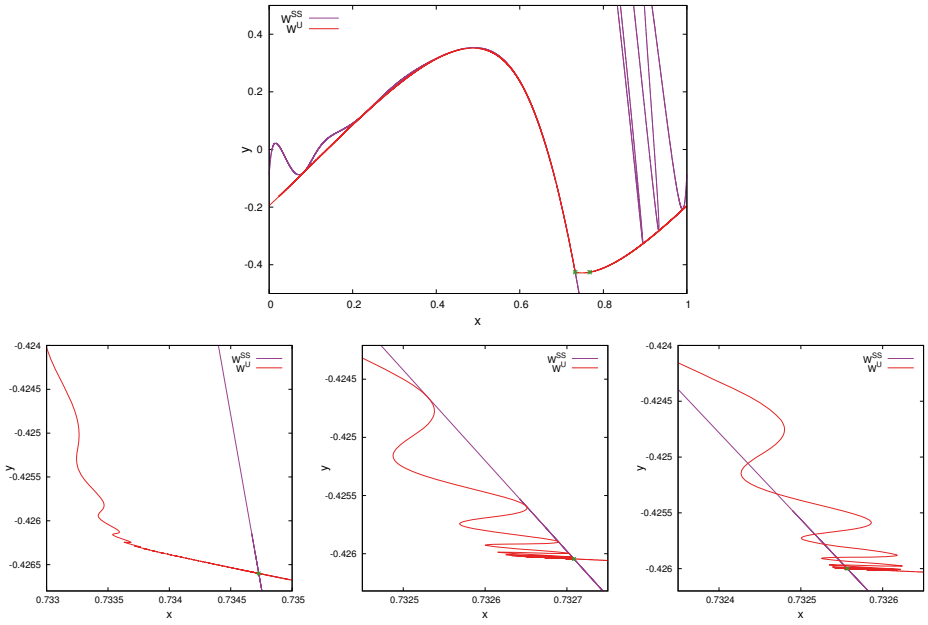

FIGURE 4.6: Top: Quadratic tangency between a leave of the stable foliation of the strong-stable manifold of the node, $\mathcal{W}^{SS}$, and the unstable manifold of the saddle $\mathcal{W}^{U}$ (which corresponds to the circle), for $a = 0.71007421$. Bottom: Transition through the quadratic tangency (from left to right): before the tangency ($a = 0.1131591645$), at the quadratic tangency ($a_{\rm qt} = 0.1130118205$) which is in fact a magnification near the attracting node of the figure of the top, and after the tangency ($a = 0.1130000096$), when there is transversal crossing.

value $a_{\rm ct}$ between the stable foliation and the invariant circle. Then, we can upgrade the lower bound of the destruction of our torus to the value $a_{\rm qt}$, in which we know that the torus is already broken.

In summary, we obtain a cascade of phenomena at parameters

$$a_{\rm nf} \simeq 0.1037 < a_{\rm qt} \simeq 0.1130 < a_{\rm ct} \leq a_{\rm sn} \simeq 0.1137 < a_{\rm last} \simeq 0.1162,$$

that happens in a short range in parameter space a. Notice that the algorithm breaks down at parameter $a_{\rm last}$ relatively close to the torus breakdown at the critical parameter $a_{\rm ct}$.

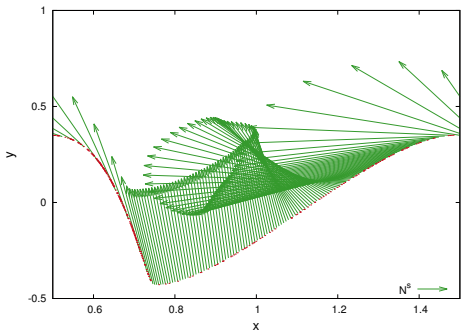

FIGURE 4.7: Invariant circle and its stable bundle for the last parameter we can compute, $a_{\text{last}} = 0.1162158902$, for $b = 0.3$ and $\varepsilon = 0.5$ fixed. x-axis is moved $+0.5$.

4.5 Example 7: Continuation of saddle tori in a 3D-Fattened Arnold Family

In this section we consider a 3 dimensional Fattened Arnold Family (3D-FAF), a family of maps $F_{a,\varepsilon} : \mathbb{T}^1 \times \mathbb{R}^2 \to \mathbb{T}^1 \times \mathbb{R}^2$ defined by :

$$F_{a,\varepsilon} \begin{pmatrix} x \\ y \\ z \end{pmatrix} = \begin{pmatrix} x + a + \frac{\varepsilon}{2\pi}(\sin(2\pi x) + y + z/2) \\ b(\sin(2\pi x) + y) \\ c(\sin(2\pi x) + y + z) \end{pmatrix} \tag{4.44}$$

where b, $c \in \mathbb{R}$ are fixed parameters, $a \in \mathbb{T}^1$ is the rotation parameter and $\varepsilon \in \mathbb{R}$ is the perturbation parameter. The Jacobian determinant is constant and equal to bc. We consider parameters $0 < b < 1 < c$ with $bc < 1$, hence a dissipative case. The family (4.44) was introduced in [11, 8] as a perfect ground to test algorithms of computation of normally hyperbolic invariant curves of saddle type (in fact, (4.44) is a rescaled version). This is the precisely the problem we consider in this section.

As the family (4.40) of the previous example, this new family (4.44) displays many of the behavior of the Arnold family of circle maps. In this case, the main resonance $0/1$ is

$$\mathcal{R}_{0/1} = \left\{ (a, \varepsilon) \mid \left| \frac{-2\pi a(1-b)(2-2c)}{2-c} \right| \leq |\varepsilon| \right\},$$

which corresponds to the region where there exist a couple of fixed points of saddle type with different stability indices: a saddle with stability index 2 (i.e., with a 2D stable manifold), which is either a saddle-node and a saddle-focus (inside the region $\mathcal{F}_{0/1}$), and a saddle-node with stability index

1 (i.e., with a 1D stable manifold). These saddles are born in a saddle-node bifurcation for parameters in the boundary of $\mathcal{R}_{0/1}$.

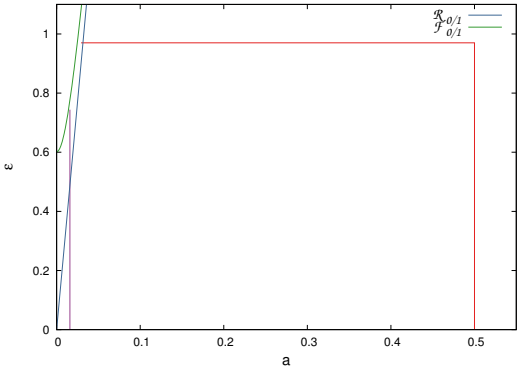

FIGURE 4.8: Curves $\mathcal{R}_{0/1}$ and $\mathcal{F}_{0/1}$ for $b = 0.3$ and $c = 2.4$ in the 3D-FAF given in (4.44). We include the two continuation paths for the example 11.

In this example, we are again interested in the computation of normally hyperbolic invariant tori. Now, we are dealing with a 3-dimensional dissipative system with $d = 1$, so then we are in fact looking for invariant circles of saddle type of the family (4.44). Recall that the normally hyperbolic (saddle) invariant curve, with such a saddle-focus on it, can not exist inside this region $\mathcal{F}_{0/1}$. In fact, a mechanism of breakdown of the saddle invariant curve corresponds to a node-focus transition. This is a transition on the saddle type invariant curve from a saddle-node type periodic point to a saddle-focus type periodic point (inside the invariant curve), where the torus losses of its regularity from $\mathcal{C}^r$ to $\mathcal{C}^0$, and persists only as a continuous curve. We will use the boundary values of $\mathcal{F}_{0/1}$ as an upper bound of the persistence of the invariant saddle circle of (4.44). However, as we see in the previous examples and in previous mentioned references, there could be other global mechanisms of breakdown of the invariant torus. The phenomenon deserves further study. To best of our knowledge, this is still not well-understood.

In this implementation we want to show the efficiency of the method explained in section 4.2 by computing not only parameterizations of attracting invariant tori but of saddle type, $K_{a,\varepsilon}$ and its internal dynamics $f_{a,\varepsilon}$. Numerical computations have been done for parameters $b = 0.3$ and $c = 2.4$ fixed, so that the constant Jacobian for this example is $\mathrm{D}F_{a,\varepsilon} = 0.72 < 1$. We have performed two different continuations through the parameter space (a, ε). In the first case, we do a continuation under the same point of view as in example 10, and we start the continuation in the (a, ε)-parameter space

far away from the resonance zone $\mathcal{R}_{0/1}$. So, by doing the continuation by the "rotation" parameter a, we focus our attention in the crossing resonances phenomena. In the other case, we start the continuation near the boundary of the main resonance $\mathcal{R}_{0/1}$ and we carry out the continuation with respect to the perturbation parameter ε, so proceeding near the main resonance and entering in it. Figure 4.8 shows the boundaries of regions $\mathcal{F}_{0/1}$ and $\mathcal{R}_{0/1}$ for the family (4.44), together with the two continuation paths of saddle NHIT we have performed in this section (one in red and the other in purple).

4.5.1 The unperturbed case

The analysis of the unperturbed case is, again, straightforward, and we can find explicit expressions for the parameterizations of the invariant curves and their bundles. For $\varepsilon = 0$, for each a, (4.44) is an skew-product system with a saddle invariant torus parameterized by

$$K_{a,0}(\theta) = \begin{pmatrix} \theta \\ \varphi_a(\theta) \\ \psi_a(\theta) \end{pmatrix},$$

where φ_a is given by (4.42) and

$$\begin{aligned} \psi_a(\theta) &= -\sum_{k=0}^{\infty} c^{-k} \left(\sin(2\pi(\theta + ka)) + \varphi_a(\theta + ka)\right) \\ &= \frac{c}{b}\left(S(a,b)(C(-a,c^{-1}) - 1) + (C(a,b) - 1)S(-a,c^{-1})\right)\cos(2\pi\theta) \\ &\quad - \frac{c}{b}\left((C(a,b) - 1)(C(-a,c^{-1}) - 1) - S(a,b)S(-a,c^{-1})\right)\sin(2\pi\theta), \end{aligned} \tag{4.45}$$

see (4.43) for the definition of the coefficients C, S. The dynamics on the torus is given by the rotation $f_{a,0}(\theta) = \theta + a$. That is, $K_{a,0}$ and $f_{a,0}$ meet the invariance equation.

$$F_{a,0} \circ K_{a,0} = K_{a,0} \circ f_{a,0}.$$

Moreover,

$$P_{a,0}^{-1}(\theta + a)\mathrm{D}F_{a,0}(K_{a,0}(\theta))P_{a,0}(\theta) = \Lambda_{a,0}(\theta),$$

with

$$P_{a,0}(\theta) = \begin{pmatrix} 1 & 0 & 0 \\ \varphi_a'(\theta) & 1 & 0 \\ \psi_a'(\theta) & \frac{c}{b-c} & 1 \end{pmatrix}$$

and

$$\Lambda_{a,0}(\theta) = \begin{pmatrix} 1 & 0 & 0 \\ 0 & b & 0 \\ 0 & 0 & c \end{pmatrix}.$$

Since $0 < b < 1 < c$, the torus is normally hyperbolic and saddle-type. The invariant stable and unstable bundles are parameterized by

$$N^S_{a,0}(\theta) = \begin{pmatrix} 0 \\ 1 \\ \frac{c}{b-c} \end{pmatrix}, \; N^U_{a,0}(\theta) = \begin{pmatrix} 0 \\ 0 \\ 1 \end{pmatrix},$$

respectively, the last two columns of $P_{a,0}$.

By normal hyperbolicity this invariant saddle circle persists for small perturbation of parameters a or ε.

4.5.2 Continuation far from the perturbative regime

In this first continuation, we want to focus on the resonance crossings of the internal dynamics when continuing a saddle invariant curve with respect to the parameters of the 3-dimensional Fattened Arnold map (4.44). Resonance tongues are more viewable for big values of ε, so that we pick a big perturbative parameter $\varepsilon = 0.97$. Then, we perform the continuation with respect to parameter a, starting at $a = 0.5$, which is far enough to the main resonance, and decreasing its value. The continuation path through the (a, ε)-parameter space is split up into two subpaths (see Figure 4.8 in red):

(1) Continuation with respect to ε: $a = 0.5$ fixed, $\varepsilon = 0.0$ until 0.97. Recall that for $\varepsilon = 0$ we have explicit formulae for $K_{a,0}$ and $f_{a,0}$, (4.42) and (4.45).

(2) Continuation with respect to a: $\varepsilon = 0.97$ fixed, $a = 0.5$ until 0.0293044529, to observe the phenomenon of the resonances until the algorithm stops.

Indeed, our interest is only on the second subpath (horizontal red line in Figure 4.8), which is displayed in Table 4.2. Figure 4.9 shows the rotation number as a function of a, which is computed from the internal dynamics $f_{a,\varepsilon}$. The internal dynamics have exhibited multiple saddle-node bifurcations of periodic orbits at different resonances, for which the rotation number is rational, and it also has taken irrational rotation numbers. Even though in a first look we only see the 1/2 resonance, doing magnifications on the graph of the rotation number we can see many plateaus of the devil staircase,

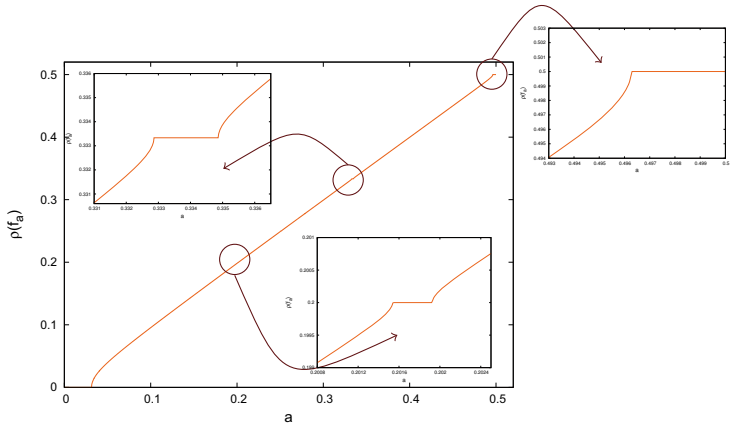

FIGURE 4.9: Rotation number for the internal dynamics of 3D-FAF, for $b = 0.3$, $c = 2.4$ and $\varepsilon = 0.97$ fixed. Magnifications near the frequencies $\rho(f_a) = \frac{1}{2}, \frac{1}{3}, \frac{1}{5}$.

corresponding to regions with periodic orbits. In Table 4.2 we show several a values with their corresponding rotation numbers, where we have highlighted the corresponding to rational rotation number.

We have selected three different parameter values corresponding to different rational rotation numbers and we study them. Figure 4.10 shows the saddle-type invariant tori and their corresponding internal dynamics of (4.44) for fixed values $a = 0.4978$, $a = 0.3348$ and $a = 0.2017089258$, for which the rotation number is $\frac{1}{2}$, $\frac{1}{3}$ and $\frac{1}{5}$ respectively. So that, there are couples of attracting-repelling periodic orbits, of period 2, 3 and 5 respectively, inside the curves, which are drawn with dots and crosses, respectively. Note that these attracting and repelling internal periodic orbits are saddle periodic orbits of index 2 and 1, respectively, for the whole system. Recall that our algorithm computes also the invariant bundles and their corresponding linearized dynamics. The stable and unstable bundles of these three tori appear in Figure 4.11. We also display the dynamics over the invariant bundles (i.e. the Λ_L, Λ_S, Λ_U functions).

Using Fourier discretization						
a	$\rho(f_a)$	N_{F}	E	E^N_{red}	E_{inv}	Tail
0.5000000000	$\frac{1}{2}$	64	5.1e-11	1.6e-10	1.1e-13	1.9e-11
0.4978000000	$\frac{1}{2}$	64	4.8e-11	7.9e-11	3.7e-14	1.2e-11
0.4500000000	0.45000748	64	3.5e-11	2.3e-11	1.1e-14	5.5e-13
0.4002000000	$\frac{2}{5}$	64	2.3e-11	2.1e-11	6.1e-15	4.4e-13
0.4000000000	0.39979773	64	2.3e-11	2.2e-11	3.2e-15	4.3e-13
0.3500000000	0.34951896	64	2.9e-11	1.8e-11	2.3e-14	1.1e-12
0.3348000000	$\frac{1}{3}$	64	5.4e-11	5.0e-11	3.6e-14	2.8e-12
0.3000000000	0.29928372	64	6.9e-11	1.5e-10	2.5e-13	5.1e-12
0.2788000000	0.27792300	64	9.6e-11	1.3e-10	6.9e-13	5.8e-12
0.2787937500	0.27791670	128	3.8e-11	1.4e-10	1.3e-14	1.7e-15
0.2510989257	$\frac{1}{4}$	128	2.2e-11	1.2e-11	1.2e-14	4.6e-15
0.2500989258	0.24904881	128	2.3e-11	1.1e-11	1.3e-14	6.3e-15
0.2017089258	$\frac{1}{5}$	128	5.5e-11	1.7e-10	9.9e-15	1.7e-14
0.2000989258	0.19835414	128	2.1e-11	2.2e-11	1.7e-14	3.6e-15
0.1689989258	$\frac{1}{6}$	128	1.9e-11	3.0e-11	2.6e-14	1.1e-14
0.1500989258	0.14733728	128	2.1e-11	2.4e-11	1.9e-14	2.8e-14
0.1457989258	$\frac{1}{7}$	128	2.0e-11	2.4e-11	1.5e-14	8.7e-15
0.1300989257	0.12675684	128	2.3e-11	2.9e-11	4.1e-14	1.2e-14
0.1283989258	$\frac{1}{8}$	128	2.4e-11	3.2e-11	5.6e-14	1.6e-14
0.1200989258	0.11640626	128	2.9e-11	5.8e-11	6.5e-14	7.0e-15
0.1149989258	$\frac{1}{9}$	128	3.2e-11	5.8e-11	3.6e-14	2.3e-14
0.1000989258	0.09551729	128	5.6e-11	2.3e-10	3.6e-14	8.7e-15
0.0885989258	$\frac{1}{12}$	128	5.7e-11	4.6e-10	2.9e-14	7.2e-15
0.0800989258	0.07419206	128	5.5e-11	5.4e-10	3.4e-14	7.7e-15
0.0700989258	0.06321529	128	2.3e-11	8.9e-10	5.4e-14	2.8e-14
0.0600989258	0.05183550	128	4.8e-11	5.4e-10	1.0e-12	5.4e-13
0.0533715820	0.05183550	256	1.1e-11	5.4e-11	1.3e-13	3.9e-15
0.0531083084	$\frac{13}{300}$	256	5.7e-11	7.3e-10	1.8e-13	5.1e-15
0.0500083084	0.03955723	256	2.9e-11	4.8e-10	2.0e-13	4.1e-15
0.0406536209	0.02641140	512	2.2e-11	1.1e-10	3.8e-13	3.6e-15
0.0344499724	0.01441782	1024	2.4e-11	2.4e-10	2.2e-11	1.2e-14
0.0332879345	0.01110032	2048	1.5e-11	1.1e-10	1.2e-10	1.1e-14
0.0327502148	0.00921540	4096	2.3e-11	2.0e-10	2.1e-10	8.5e-15
0.0327211468	0.00910343	8192	7.9e-11	1.2e-09	9.6e-09	1.1e-13
0.0327205964	0.00910130	16384	8.9e-11	1.7e-09	5.9e-09	6.7e-14
Using Local Interpolation						
a	$\rho(f_a)$	N	E	E^N_{red}	E_{inv}	–
0.0327205964	0.00910130	32768	3.7e-11	1.2e-09	2.4e-07	–
0.0315061826	0.00000000	32768	5.5e-11	2.3e-10	1.1e-06	–
0.0300000000	0.00000000	32768	6.1e-11	1.6e-08	1.5e-06	–
0.0297750000	0.00000000	65536	1.4e-11	4.6e-10	1.3e-08	–
0.0296695313	0.00000000	131072	9.1e-12	4.7e-10	2.0e-08	–
0.0294519505	0.00000000	262144	1.4e-11	3.5e-10	8.4e-08	–
0.0293044529	0.00000000	524288	1.2e-11	0.1e-10	2.4e-06	–

Table 4.2: Continuation with respect to a for $b = 0.3$, $c = 2.4$ and $\varepsilon = 0.97$ fixed in the 3D-FAF. For each value a we show several quantities associated with it: the rotation number $\rho(f_a)$, the error in the invariance equation E, the error in the normal component of the reducibility equation E^N_{red}, the error in the computation of the inverse of the adapted frame E_{inv} and the maximum norm of the last Fourier terms Tail. In gray it appears a values corresponding to rational frequencies, while in dark gray the ones for which we show the plots in this example.

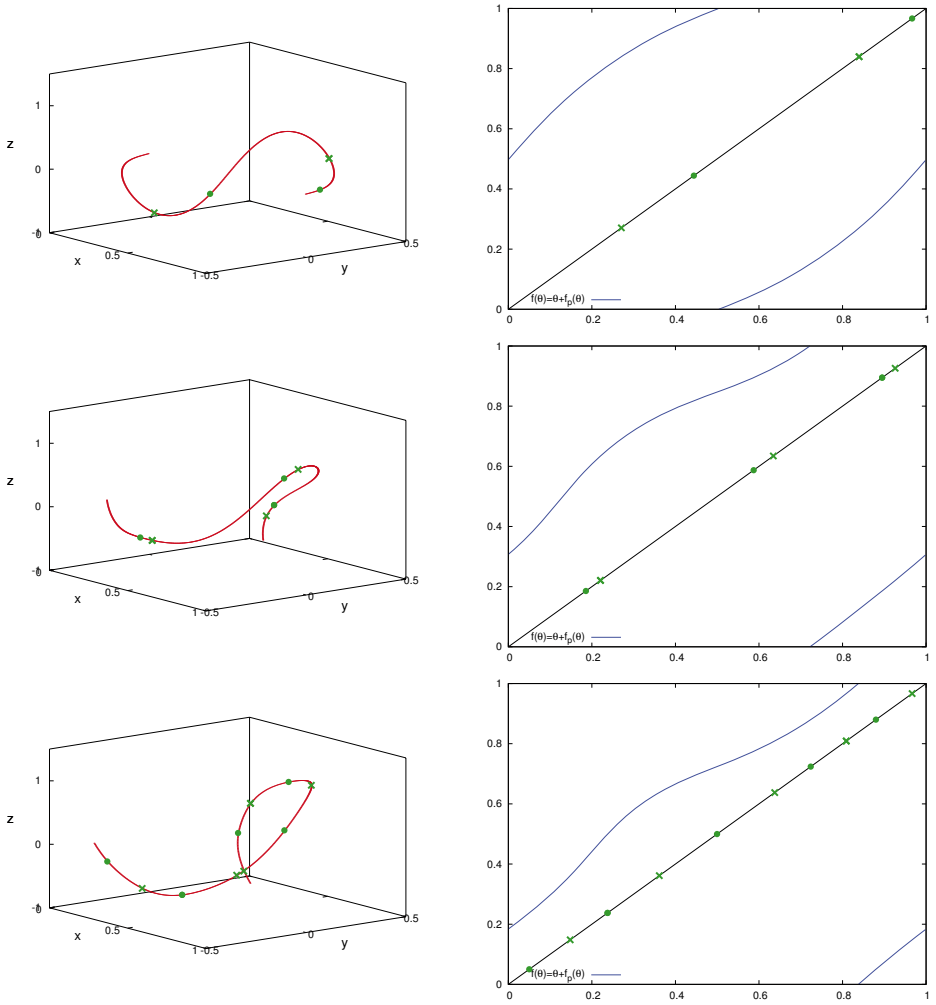

FIGURE 4.10: Left: Invariant saddle-type tori with their two internal attracting-repelling periodic orbits, represented by green dots and crosses respectively. Right: internal dynamics over the torus, in blue, with the line of the fixed points in black. Figures for parameters $a = 0.4978$, $a = 0.3348$ and $a = 0.2017089258$ respectively, for $b = 0.3$, $c = 2.4$ and $\varepsilon = 0.97$ fixed.

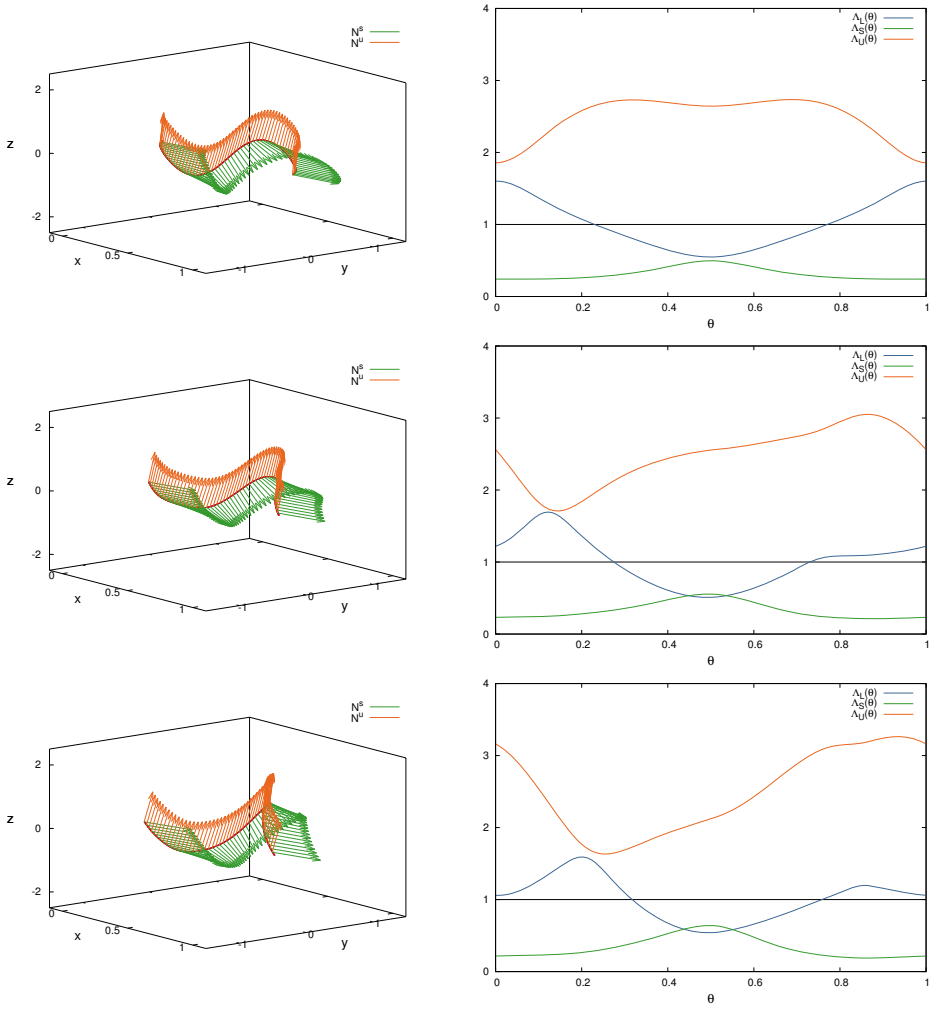

FIGURE 4.11: Left: Invariant stable and unstable bundles of each curve. Right: linearized dynamics over the bundles. Figures for parameters $a = 0.4978$, $a = 0.3348$ and $a = 0.2017089258$ respectively, for $b = 0.3$, $c = 2.4$ and $\varepsilon = 0.97$ fixed.

We observe that during the continuation process we cross many resonances with error tolerance $||E|| < 10^{-10}$ and keeping a relatively small number of Fourier modes in order to approximate the objects, using $N_F \leq 256$. As in the previous example, the computation has some difficulties when we approach the main resonance $\mathcal{R}_{0/1}$. Then, it is needed to increase the number of Fourier modes to well approximate our objects and to be able to continue the computations.

The internal dynamics exhibits a saddle-node bifurcation of fixed points at

$$a_{\text{sn}} = 0.0315061826,$$

when entering in the Arnold tongue $\mathcal{R}_{0/1}$. So that, in this example we can observe the two saddle fixed points inside our invariant torus. The index 2 saddle fixed point corresponds to the attracting fixed point for the internal dynamics, while the index 1 saddle fixed point corresponds to the repelling fixed point for the internal dynamics. When we are close to the parameter a_{sn}, the number of Fourier modes is too high to make the computations fast enough. At that moment, we change the discretization type of our objects from the Fourier approximation to a local piecewise interpolation type. Then, we can proceed the continuation process in a faster way. See Section 4.3.3 for the details between spectral and grid points approximations.

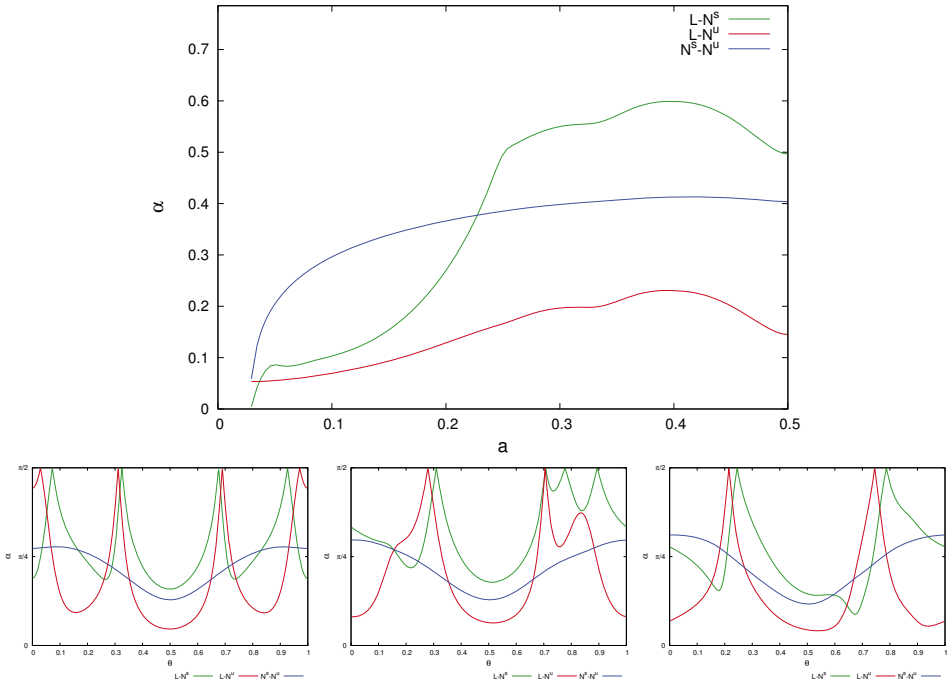

FIGURE 4.12: Top: Minimum angle between all bundles for each parameter a during the continuation process, for $\varepsilon = 0.97$, $b = 0.3$ and $c = 2.4$ fixed. Bottom: Minimum angle between bundles for fixed parameters $a = 0.4978$, $a = 0.3348$ and $a = 0.2017089258$ respectively.

Our computation stops when we reach the parameter

$$a_{\text{last}} = 0.0293044529,$$

when the continuation step is smaller than 10^{-7} and we need too many points in the mesh to represent the torus. However, our computation stops before getting the parameter corresponding to the node-focus transition of the index 2 saddle fixed point

$$a_{\mathrm{nf}} \simeq 0.0247053794,$$

which corresponds to the boundary of $\mathcal{F}_{0/1}$ for our fixed parameters $b = 0.3$, $c = 2.4$ and $\varepsilon = 0.97$. Recall that this value a_{nf} is a lower bound of the critical value, a_{c}, of the destruction of the curve.

In this example, when the method stops, the minimum angle between bundles corresponds to the minimum angle between the tangent and the stable bundles, which has a value $\alpha_{\mathrm{last}}(L - N^S) = 0.0044193874$ (see Figure 4.12 top). We know that at the moment of the node-focus transition this angle has to be exactly zero, because both stable eigenvalues of the saddle fixed point of index 2 collide, and so the corresponding eigenspaces. Even that this value α_{last} is relatively small, from the results and arguments we carried out in example 10, it makes us suspect that the breakdown due to some other global phenomena, such as tangencies between invariant manifolds or foliations, which can occurs prior to the node-focus transitions. The study of the breakdown of saddle-type invariant curve deserves further study. Note that the transition to the breakdown of the torus occurs in a short range in parameter space a, through a cascade of phenomena at parameters

$$a_{\mathrm{nf}} \simeq 0.0247 \leq a_{\mathrm{c}} < a_{\mathrm{last}} \simeq 0.0293 < a_{\mathrm{sn}} \simeq 0.0315.$$

4.5.3 Continuation starting close to the main resonance $\mathcal{R}_{0/1}$

In this subsection, we select a low value of a, $2\pi a = 0.1$, $b = 0.3$ and $c = 2.4$ fixed, and perform the continuation with respect to the perturbation parameter ε, starting from $\varepsilon = 0$. These are, in particular, the parameters used in [11, 8], in which parameter a is rescaled modulus 2π. The continuation path of the invariant saddle curve for these parameters appears in purple in Figure 4.8. Notice that the continuation starts extremely close to the main resonance $\mathcal{R}_{0/1}$ and crosses it at the parameter

$$\varepsilon_{\mathrm{sn}} = 0.49,$$

when there is a saddle-node bifurcation. Inside the region $\mathcal{R}_{0/1}$, the saddle-type curve has two saddle points with different stability indices until the

torus breaks down at some critical parameter ε_{c}. An upper bound of ε_{c} is given by

$$\varepsilon_{\mathrm{nf}} \simeq 0.7761816294,$$

for which there is a node-focus transition. This corresponds to the boundary of $\mathcal{F}_{0/1}$ for the fixed parameters of this implementation.

	Local Interpolation			Fourier Expansions		
ε	N	E	E^N_{red}	N_{F}	E	E^N_{red}
0.0000000000	2048	4.8e-12	4.4e-16	64	1.5e-14	2.7e-14
0.2000000000	2048	8.1e-11	2.1e-10	64	3.0e-11	8.3e-11
0.4000000000	2048	2.5e-11	2.9e-10	64	4.8e-11	7.9e-11
0.4900000000	2048	6.7e-11	2.0e-09	64	7.1e-11	1.7e-10
0.6000000000	2048	7.6e-11	7.1e-08	256	2.2e-11	1.6e-11
0.7000000000	16384	2.6e-11	1.5e-10	8192	9.1e-11	1.3e-09
0.7181951181	65536	5.0e-11	1.9e-08	32768	8.5e-09	4.5e-08
0.7200000000	65536	4.9e-11	8.3e-09	–	–	–
0.7440768923	524288	9.9e-09	7.0e-08	–	–	–

TABLE 4.3: Continuation with respect to ε for $a = 0.1/2\pi$, $b = 0.3$ and $c = 2.4$ fixed in the 3D-FAF. For each ε value we show: the error in the invariance equation, E, and the error in the normal component of the reducibility equation, E^N_{red}. We compare both errors using the two different discretization types: by piecewise Lagrangian interpolation (with an N grid) and by using Fourier expansions (with N_{F} Fourier modes).

In this subsection, we use both discretization methods explained in Section 4.3 to approximate the objects: a grid method based on a cubic local interpolation and a Fourier method. The results are displayed in Table 4.3. For the grid method, we start the continuation with an initial grid of $N = 2^8 = 256$ nodes for the first approximation. We do the continuation with respect to ε and each time that the program runs into troubles to well approximate the objects, we increase the grid. We can do the computations up to parameter $\varepsilon_{\mathrm{last,G}} = 0.7440768923$, for which we have needed a grid of $N = 2^{19} = 524288$ points. On the other hand, for the Fourier method, we start with an initial approximation given by $N_{\mathrm{F}} = 64$ Fourier modes. We do the continuation with respect to ε, and we stops the method when we have had to add too many Fourier modes, for $\varepsilon_{\mathrm{last,F}} = 0.7181951181$ we have needed $N_{\mathrm{F}} = 32768$). As mentioned in Section 4.3.3, Fourier method suffers in computing composition $K \circ f$, and such a number of modes N_F is too high to continue the computations in a reasonable time. In particular, until we reach $\varepsilon = 0.7$, we proceed with an error tolerance $||E|| < 10^{-10}$. Up to there, we only ask for an error tolerance $||E|| < 10^{-8}$, for both discretization cases.

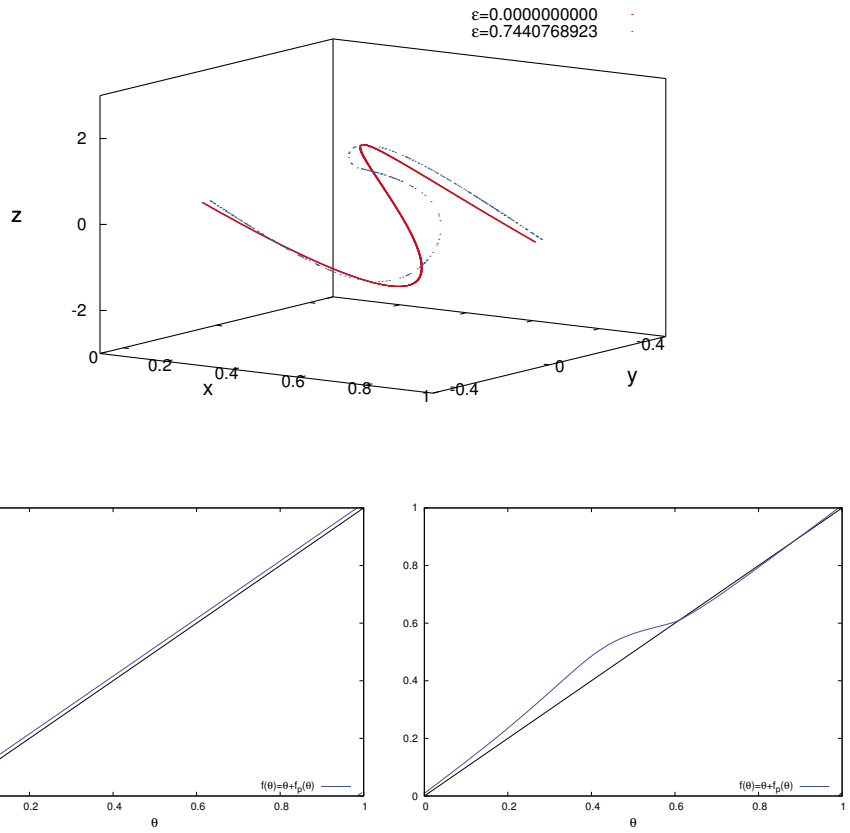

FIGURE 4.13: Top: Variation of the invariant saddle torus, from $\varepsilon = 0$, in red, up to the last NHIT we can compute, in blue. Bottom: The internal dynamics for the unperturbed case (left) and the last computed saddle torus (right).

In Figure 4.13, we observe the invariant saddle type curve for $\varepsilon_{\text{last,G}}$ (in blue), which is heavily deformed with respect to the unperturbed one (in red). On the bottom of this Figure 4.13, we can see how the internal dynamics oscillates with respect the initial one. While for the unperturbed case, the internal dynamics is a rigid rotation of angle $a = 0.1/2\pi$, for the last computed torus the internal dynamics exhibits fixed attracting-repelling fixed points.

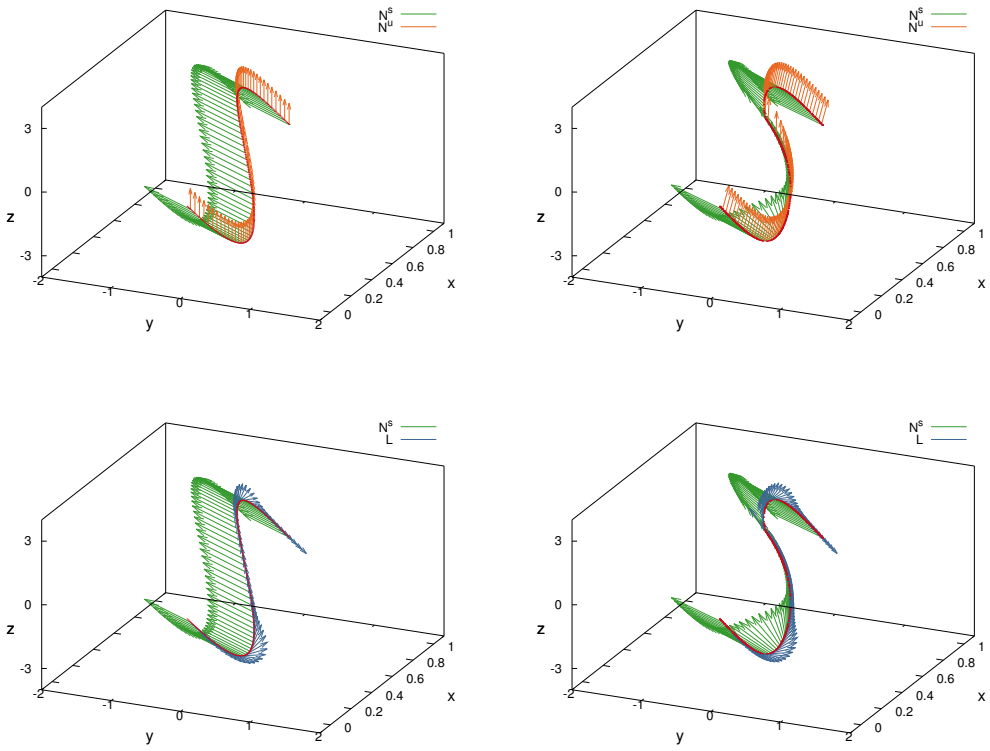

FIGURE 4.14: Right: Invariant bundles for the unperturbed torus. Left: Invariant bundles for the last computed saddle torus.

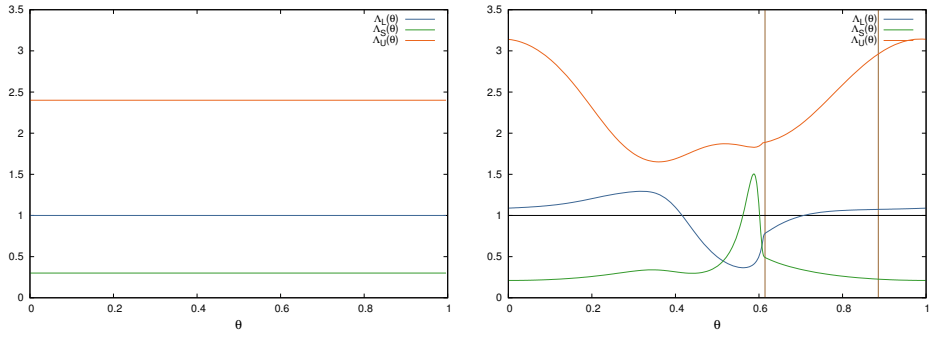

FIGURE 4.15: Linearized dynamics on the tangent, stable and unstable bundles for the unperturbed case and for the last computed torus, respectively. In the perturbed case (right), the two vertical lines point out to the θ-angle position where there are the two saddle points.

The information about the bundles is showed in Figures 4.14 and 4.15. Figure 4.14 shows the invariant bundles for $\varepsilon = 0$ and $\varepsilon_{\text{last,G}}$. Notice that while tangent (in blue) and stable bundles (in green) seems to be approaching, the unstable bundle (in orange) does not change so much. Otherwise, Figure 4.15 shows the dynamics over the bundles (i.e.: Λ_L, Λ_S, Λ_U), which provide us a quantitative measure of the quality of the hyperbolicity condition. We observe that Λ_S, the "stable dynamics", is not always less than 1. In fact, near the "dangerous" saddle point (printed in the left vertical line) the stable dynamics has a large peak and it overpasses the tangent dynamics. However, notice that the normal hyperbolicity conditions on Λ_L, Λ_S and Λ_U have to be satisfied in average.

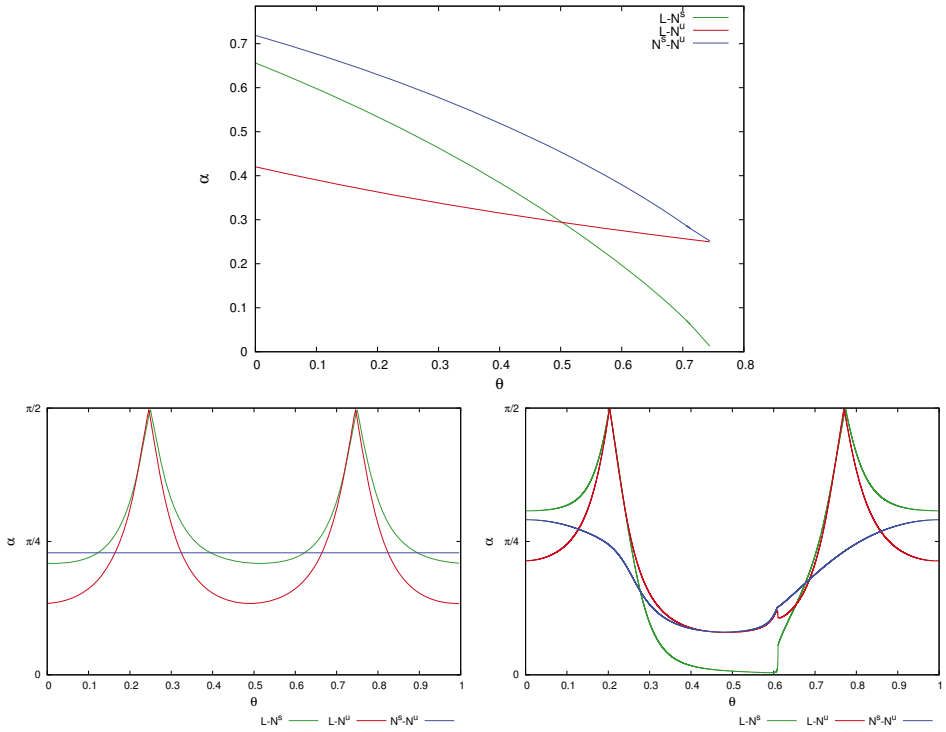

FIGURE 4.16: Top: Minimum angle between all bundles for each parameter ε during the continuation process, for $a = 0.1/2\pi$, $b = 0.3$, $c = 2.4$ fixed in the 3D-FAF. Bottom: Minimum angle between bundles for the unperturbed saddle torus and the last computed torus, respectively.

Another measure of the quality of the normal hyperbolicity property is provided by the angles between the invariant bundles, see Figure 4.16. We observe that the minimum angle between the tangent and stable bundles decreases to $\alpha_{\text{last}}(L - N^S) = 0.012666821$ when we increment the parameter ε up to the value $\varepsilon_{\text{last,G}} = 0.7440768923$. As we explain at the beginning of

this example, we have an upper bound of the critical parameter in which the torus is broken, $\varepsilon_{\text{nf}} \simeq 0.7761816294$, and obviously our method do not exceed this value. From our computations, we cannot claim that the breakdown is produced at the node-focus transition. As we argue in previous examples, there could be some global mechanisms of breakdown, such as tangencies between invariant manifolds or foliations of the torus. With all this information, we cannot conclude what is the mechanism of destruction of that torus. We leave this study of saddle torus breakdown as an open problem in which we will continue working.

4.6 Example 8: Computation of a normally hyperbolic invariant cylinder

In this section we illustrate the applicability of the Newton method described in Section 4.2 to compute an invariant cylinder, in a higher dimensional phase space. We consider the Froeschlé map (see [49]), which consists in two coupled standard maps with fixed parameters κ_1, κ_2, and a coupling parameter ε, in the following slightly different formulation:

$$\begin{array}{rcl} F_\varepsilon : \mathbb{T}\times\mathbb{R}\times\mathbb{R}^2 & \longrightarrow & \mathbb{T}\times\mathbb{R}\times\mathbb{R}^2 \\ \begin{pmatrix} x_1 \\ y_1 \\ x_2 \\ y_2 \end{pmatrix} & \longrightarrow & \begin{pmatrix} x_1 + y_1 - \frac{\kappa_1}{2\pi}\sin(2\pi x_1) - \frac{\varepsilon}{2\pi}\sin(2\pi(x_1+x_2)) \\ y_1 - \frac{\kappa_1}{2\pi}\sin(2\pi x_1) - \frac{\varepsilon}{2\pi}\sin(2\pi(x_1+x_2)) \\ x_2 + y_2 - \frac{\kappa_2}{2\pi}\sin(2\pi x_2) - \frac{\varepsilon}{2\pi}\sin(2\pi(x_1+x_2)) \\ y_2 - \frac{\kappa_2}{2\pi}\sin(2\pi x_2) - \frac{\varepsilon}{2\pi}\sin(2\pi(x_1+x_2)) \end{pmatrix}. \end{array} \tag{4.46}$$

This is a family of 4 dimensional symplectic maps, $F_\varepsilon^* \boldsymbol{\omega} = \boldsymbol{\omega}$, with

$$\boldsymbol{\omega} = \mathrm{d}y_1 \wedge \mathrm{d}x_1 + \mathrm{d}y_2 \wedge \mathrm{d}x_2. \tag{4.47}$$

This family has been extensively studied in the literature as a model to understand instability channels [74, 78], which are very related with the phenomenon of Arnold's diffusion [3], namely the drift of the action variables, for a priori unstable nearly integrable Hamiltonian systems [27]. Remarkably, the relatively recent discovery in [32] (see also [33]) of the role of normally hyperbolic invariant manifolds (in fact, cylinders) in some mechanisms that lead to Arnold's diffusion has revolutionized the area. Our goal is much more modest, and we will illustrate some preliminary computations of a normally hyperbolic cylinder, a first step to compute their invariant manifolds and the internal invariant foliations (although we compute their linearizations), their homoclinic intersections and the corresponding scattering map, that

are important for describing a geometric mechanism of Arnold's diffusion [32].

In the present example notice that for $\varepsilon = 0$ the system is uncoupled. Moreover, the cylinder

$$\mathcal{C}_0 = \{(x_1, y_1, \frac{1}{2}, 0) \mid (x_1, y_1) \in \mathbb{T} \times \mathbb{R}\}$$

is invariant, and the internal dynamics on $\mathcal{C}_0$ is a standard map with parameter κ_1. Notice that the model manifold is $\mathbb{T} \times \mathbb{R}$. If κ_2 is large enough, the hyperbolicity of the saddle fixed point $(\frac{1}{2}, 0)$ for the corresponding standard map dominates the internal dynamics of $\mathcal{C}_0$, and the cylinder is a normally hyperbolic invariant manifold. A particular case is $\kappa_1 = 0$ and $\kappa_2 > 0$, for which the internal dynamics is integrable, and the system is said to be *a priori* unstable. Even if there is available a theory of persistence of non-compact normally hyperbolic manifolds [6, 41], we can apply the classical theory [63, 43] to assert the persistence of $\mathcal{C}_0$ for small values of the coupling parameter ε, that is the existence of a F_ε-invariant cylinder $\mathcal{C}_\varepsilon$ close to $\mathcal{C}_0$. The trick for the argument (and for the numerical computation performed in this section) is that we can think of F_ε as defined in $\mathbb{T} \times \mathbb{T} \times \mathbb{R}^2$ and the model manifold to be $\mathbb{T}^2$.

In a more functional parlance, by writing $z_1 = (x_1, y_1)$ and $z_2 = (x_2, y_2)$, the Froeschlé map (4.46) is a map $F : \mathbb{T} \times \mathbb{R} \times \mathbb{R}^2 \to \mathbb{T} \times \mathbb{R} \times \mathbb{R}^2$ of the form

$$F \begin{pmatrix} z_1 \\ z_2 \end{pmatrix} = \begin{pmatrix} Az_1 \\ 0 \end{pmatrix} + F_p \begin{pmatrix} z_1 \\ z_2 \end{pmatrix},$$

where

$$A = \begin{pmatrix} 1 & 1 \\ 0 & 1 \end{pmatrix}$$

and $F_p(z_1, z_2)$ is 1-periodic in z_1. Our goal is finding a 2-dimensional F-invariant cylinder $\mathcal{C}$ parameterized by $C : \mathbb{T} \times \mathbb{R} \to \mathbb{T} \times \mathbb{R} \times \mathbb{R}^2$, of the form

$$C(\theta) = \begin{pmatrix} \theta \\ 0 \end{pmatrix} + C_p(\theta),$$

where $C_p(\theta)$ is 1-periodic in $\theta = (\theta_1, \theta_2)$. The dynamics on the cylinder $\mathcal{C}$, parameterized by C, is then a map $f : \mathbb{T} \times \mathbb{R} \to \mathbb{T} \times \mathbb{R}$ of the form

$$f(\theta) = A\theta + f_p(\theta),$$

where f_p is 1-periodic in θ. The fact that homotopy classes of F, C and f has to match lead to an error function

$$E(\theta) = \begin{pmatrix} AC_p^{z_1}(\theta) \\ 0 \end{pmatrix} + F_p \begin{pmatrix} \theta + C_p^{z_1}(\theta) \\ C_p^{z_2}(\theta) \end{pmatrix} - \begin{pmatrix} f_p(\theta) \\ 0 \end{pmatrix} - \begin{pmatrix} C_p^{z_1}(A\theta + f_p(\theta)) \\ C_p^{z_2}(A\theta + f_p(\theta)) \end{pmatrix},$$

in which only appear 1-periodic functions. Therefore, we can directly apply the methods described in this chapter.

Remark 4.14 *In this example, the main assumption is the periodicity of F_p with respect to x_1 and y_1 (and of C_p with respect to θ_1 and θ_2). In the absence of the periodicity property of F_p with respect to y_1 (and of C_p with respect to θ_2), the method described here can be easily implemented with a few modifications to compute truncated invariant cylinders. In the present example, dynamics helps and invariant rotational curves around a truncated cylinder prevent the orbits to escape. In higher dimensional examples, (for instance, a 4 dimensional cylinder for a 6 dimensional symplectic map), the diffusion in the cylinder can be very small since there are many obstructions that prevent orbits to escape in practical times.*

Geometrical properties of the F_ε-invariant cylinder $\mathcal{C}_\varepsilon$ follow from the invariance equation

$$F_\varepsilon \circ C_\varepsilon = C_\varepsilon \circ f_\varepsilon. \tag{4.48}$$

In particular, since

$$f_\varepsilon^*(C_\varepsilon^* \boldsymbol{\omega}) = C_\varepsilon^* \boldsymbol{\omega}, \tag{4.49}$$

the internal dynamics f_ε is symplectic with respect to the reduced symplectic form. The fact that the reduced 2-form $\boldsymbol{\omega}_{C_\varepsilon} = C_\varepsilon^* \boldsymbol{\omega}$ is non-degenerate (and then it is symplectic) follows from the following perturbative argument: since $\boldsymbol{\omega}_{C_0} = \mathrm{d}\theta_2 \wedge \mathrm{d}\theta_1$ is non-degenerate, then $\boldsymbol{\omega}_{C_\varepsilon}$ is also non-degenerate for ε small. This is in contrast with KAM tori, for which the restricted symplectic form vanishes. For that reason, we observe, inside the cylinder, the same structures that appear in area preserving maps, such as periodic orbits, islands, rotational invariant curves or chaotic orbits close to separatrices (see Figure 4.17).

For the numerical computation we present in this section, we have taken $\kappa_1 = 0.1$ and $\kappa_2 = 1.5$. Notice that for $\varepsilon = 0$, we have an uncoupled system, so that the invariant cylinder $\mathcal{C}_0$ has an internal dynamics given by a standard map with parameter $\kappa_1 = 0.1$. Particularly, this unperturbed cylinder $\mathcal{C}_0$ has two fixed points, $P_1 = (0, 0, 1/2, 0) = C_0(0, 0)$ and $P_2 = (1/2, 0, 1/2, 0) = C_0(1/2, 0)$. The first one is elliptic on the manifold (and elliptic-hyperbolic on the whole space, also called *center*$\times$*saddle* in the Hamiltonian context) whereas the second one is hyperbolic on the manifold (and hyperbolic-hyperbolic on the whole phase space, also called *saddle*$\times$*saddle* in the Hamiltonian context).

By increasing parameter ε, we perturb this initial invariant cylinder, which, by normally hyperbolic theory, will persists for small ε. In this example, we

ε	E	E_{red}	e
0.00	2.96e-17	6.07e-18	4.39e-18
0.05	4.63e-10	4.36e-07	4.59e-10
0.10	4.46e-10	9.96e-08	1.77e-10
0.15	5.47e-10	6.55e-07	3.28e-10
0.20	5.46e-10	9.93e-07	9.24e-10
0.25	5.60e-09	9.90e-06	4.20e-09
0.30	8.52e-09	1.55e-05	8.16e-08
0.35	6.40e-09	6.12e-05	3.24e-06

Table 4.4: Continuation with respect to ε for $\kappa_1 = 0.1$, $\kappa_2 = 1.5$ fixed in the Froeschlé map. For each ε value we show: the error in the invariance equation, E, the error in the reducibility equation, E_{red}, and the error in the invertibility equation, e.

have used a 2 dimensional grid with 512×512 points and have performed interpolations with 8×8 neighboring points. This is a good enough choice, see errors in Table 4.4. Notice that the error on the invariance equation is getting worst as we increase the ε value. When the numerical computation does not pass our quality control, we stop the computations. In this example, it happens when $\varepsilon = 0.35$. We can refine the computations by increasing the grid points to 1024×1024, or even finer, at the expense of much larger computing times.

As in previous examples, we compute the internal dynamics of the object, which is now a 2 dimensional function. First interesting thing we can observe on the system is the presence of bifurcations inside the cylinder. By inspecting the internal dynamics for different ε values, see Figure 4.17, we can easily see how the role of the fixed points inside the cylinder changes as we increase the ε value. In fact, for $\varepsilon \approx 0.0938$, there is a bifurcation on the tangent eigenvalues of the fixed point $P_2 = (1/2, 0, 1/2, 0) = C_\varepsilon(1/2, 0)$ where this hyperbolic fixed point turns into an elliptic one, so that we have a NHIM with two elliptic fixed points inside it. After a while, near $\varepsilon \approx 0.1071$, there is another bifurcation in which the elliptic fixed point $P_1 = (0, 0, 1/2, 0) = C_\varepsilon(0, 0)$ turns into an hyperbolic one, so then the fixed points of the cylinder has exchanged their character from the unperturbed initial cylinder. This phenomenon is immediately observable by the behavior of the orbits around these two fixed points. Figure 4.18 shows the bifurcation diagram of the eigenvalues of fixed points P_1 (in red) and P_2 (in blue) inside the cylinder, with a marked light green zone corresponding to the ε values for this concrete example. Observe that we can continue this invariant cylinder $\mathcal{C}_\varepsilon$ through that bifurcations. This is because the tangent eigenvalues (inside the cylinder) are always dominated by the normal eigenvalues (in the normal directions to the cylinder), so that the normal hyperbolicity condition is always satisfied on the fixed point, where the behavior of the internal dynamics is influential.

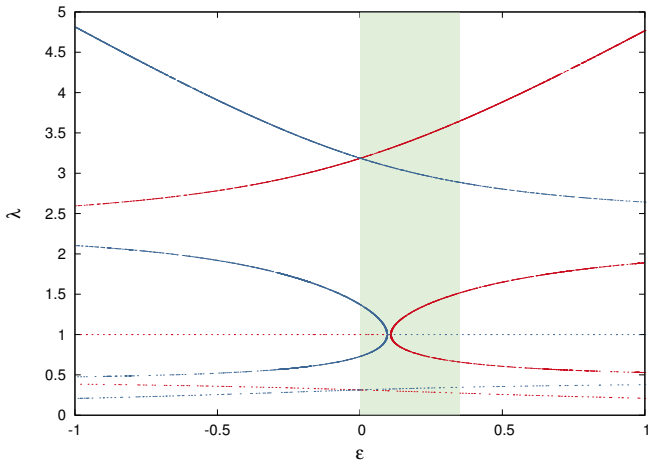

FIGURE 4.18: Bifurcation diagram for ε of the eigenvalues of the fixed points $P_1 = (0, 0, 1/2, 0) = C_\varepsilon(0, 0)$ (in red) and $P_2 = (1/2, 0, 1/2, 0) = C_\varepsilon(1/2, 0)$ (in blue) of the cylinder $\mathcal{C}_\varepsilon$.

In order to represent the invariant cylinder, a 2D object inside a 4D phase

space, we consider the map $R = (X, Y, Z) : \mathbb{T} \times \mathbb{R} \times \mathbb{R}^2 \to \mathbb{R}^3$:

$$\begin{aligned} X(x_1, y_1, x_2, y_2) &= \sqrt{x_2^2 + y_2^2}\ \sin(2\pi x_1), \\ Y(x_1, y_1, x_2, y_2) &= \sqrt{x_2^2 + y_2^2}\ \cos(2\pi x_1), \\ Z(x_1, y_1, x_2, y_2) &= y_1. \end{aligned}$$

We use these coordinates to show the cylinder, parameterized by $R \circ C$, and the internal dynamics (see Figure 4.19 and Figure 4.21). Notice that the cylinder is slightly deformed during the continuation with respect to parameter ε.

Furthermore, from the internal dynamics we obtain more information of the objects. We can compute the rotation number inside the manifold, so that we can inspect the different dynamics on it. For example, Figure 4.20 shows the rotation number inside the cylinder $\mathcal{C}_\varepsilon$ for $\varepsilon = 0.35$, for each θ_2 value and fixed $\theta_1 = 0.5$, observing the familiar devil staircase. Moreover, as we already know the rotation number for all orbits through $(0.5, \theta_2)$, for all $\theta_2 \in \mathbb{T}$, we can elaborate the inverse process: select a desired rotation number and then compute its corresponding orbit. For instance, we have done it for the golden mean number, and we compute the golden invariant curve inside all the invariant cylinders of our example, which is drawn in dark yellow in Figures 4.17, 4.19 and 4.21.

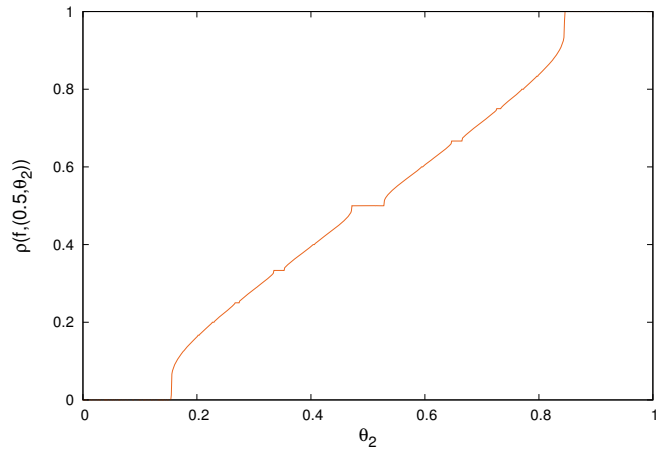

FIGURE 4.20: Rotation number of the internal dynamics for the cylinder $\mathcal{C}_\varepsilon$, $\varepsilon = 0.35$, for the fixed coordinate $\theta_1 = 0.5$.

Once we have obtained a curve inside the cylinder (in our case the golden curve), we could refine it by using the internal dynamics of the cylinder, by

using the methodology exposed in [30, 52], since it is a KAM torus for the internal dynamics. We emphasize that, since the symplectic form on the cylinder is not the standard one, the methodology in [30, 52] is very appropriate. In particular, the "global" dynamics is now the internal dynamics on the cylinder $f : \mathbb{T} \times \mathbb{R} \to \mathbb{T} \times \mathbb{R}$, the invariant curve parameterized by a map $k : \mathbb{T} \to \mathbb{T} \times \mathbb{R}$ is just the curve inside the invariant cylinder (in our case the golden curve), and the internal dynamics on the curve is a quasi-periodic motion given by the rotation number ω of that curve on the cylinder:

$$f(k(\theta)) - k(\theta + \omega) = 0. \tag{4.50}$$

Moreover, invariant curves inside the cylinder are in fact *one dimensional partially hyperbolic invariant curves* in the total 4 dimensional space, so the methodology in [66, 67] could be also used. In that case, the invariant curve with fixed frequency ω (e.g. the golden curve), $\mathcal{K}$, is now considered as an embedding on the total 4 dimensional space, $K : \mathbb{T} \to \mathbb{T}\times\mathbb{R}\times\mathbb{R}^2$ and satisfies the invariance equation

$$F(K(\theta)) - K(\theta + \omega) = 0, \tag{4.51}$$

for the global 4 dimensional dynamics (4.46). Notice that, $K = C \circ k$.

In addition, we could compute parameterizations $W_{\mathcal{K}}^{S,U} : \mathbb{T}\times\mathbb{R} \to \mathbb{T}\times\mathbb{R}\times\mathbb{R}^2$, of the stable and unstable invariant manifold of $\mathcal{K}$, $\mathcal{W}_{\mathcal{K}}^{S,U}$, the *whiskers*, that satisfy an invariance equation of the form

$$F(W(\theta, s)) - W(\theta + \omega, \lambda s) = 0, \tag{4.52}$$

where $\theta \in \mathbb{T}$ is the *angle variable* moved by a rigid rotation ω, and $s \in \mathbb{R}$ is the *normal variable* moved in the direction along the stable (or unstable) invariant bundle which contracts (or expands) in a factor λ. These manifolds $\mathcal{W}_{\mathcal{K}}^{S,U}$ are, in fact, invariant submanifolds of the stable and unstable manifolds of the whole cylinder $\mathcal{C}$, $\mathcal{W}_{\mathcal{C}}^{S,U}$, for which we have already computed their linearizations, the invariant normal bundles $\mathcal{N}^{S,U}$.

The mechanisms of breakdown of this object are still unknown to us. This is a challenging project since the heavy computations make very difficult the continuation of the invariant cylinder up to larger values of the perturbation parameter ε. The fact is that using 2 dimensional interpolation, we cannot increment the mesh grid as much as we have done for 1 dimensional invariant tori in previous examples, $N = 524288$. Notice that, now, it is converted into a grid formed by $N = 524288 \times 524288 = 2^{38}$ points, so that the computations cannot be done with a common desktop computer, the machine used for the computations in this section. At this point, parallelizing the grid

routines and the use of adaptive grids seem to be a possibility to improve the performance of the method. Further work on these techniques could be an aid to improve the numerical computations and understand the destruction of these normally hyperbolic invariant manifolds.

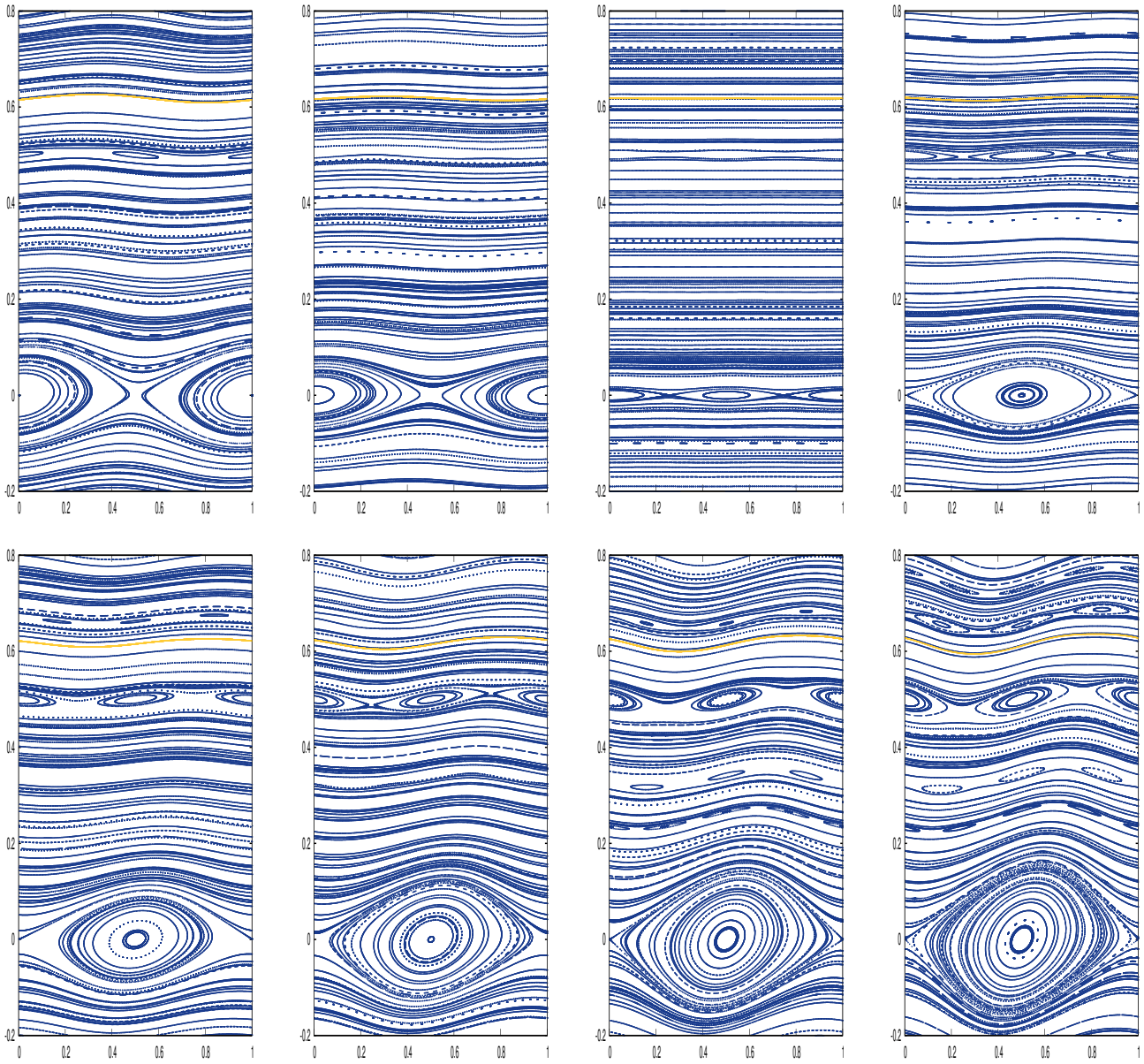

FIGURE 4.17: Internal dynamics on the normally hyperbolic invariant cylinder, for $\kappa_1 = 0.1$, $\kappa_2 = 1.5$, and (from top-left to bottom-right) $\varepsilon = 0.00, 0.05, 0.10, 0.15, 0.20, 0.25, 0.30, 0.35$.

.

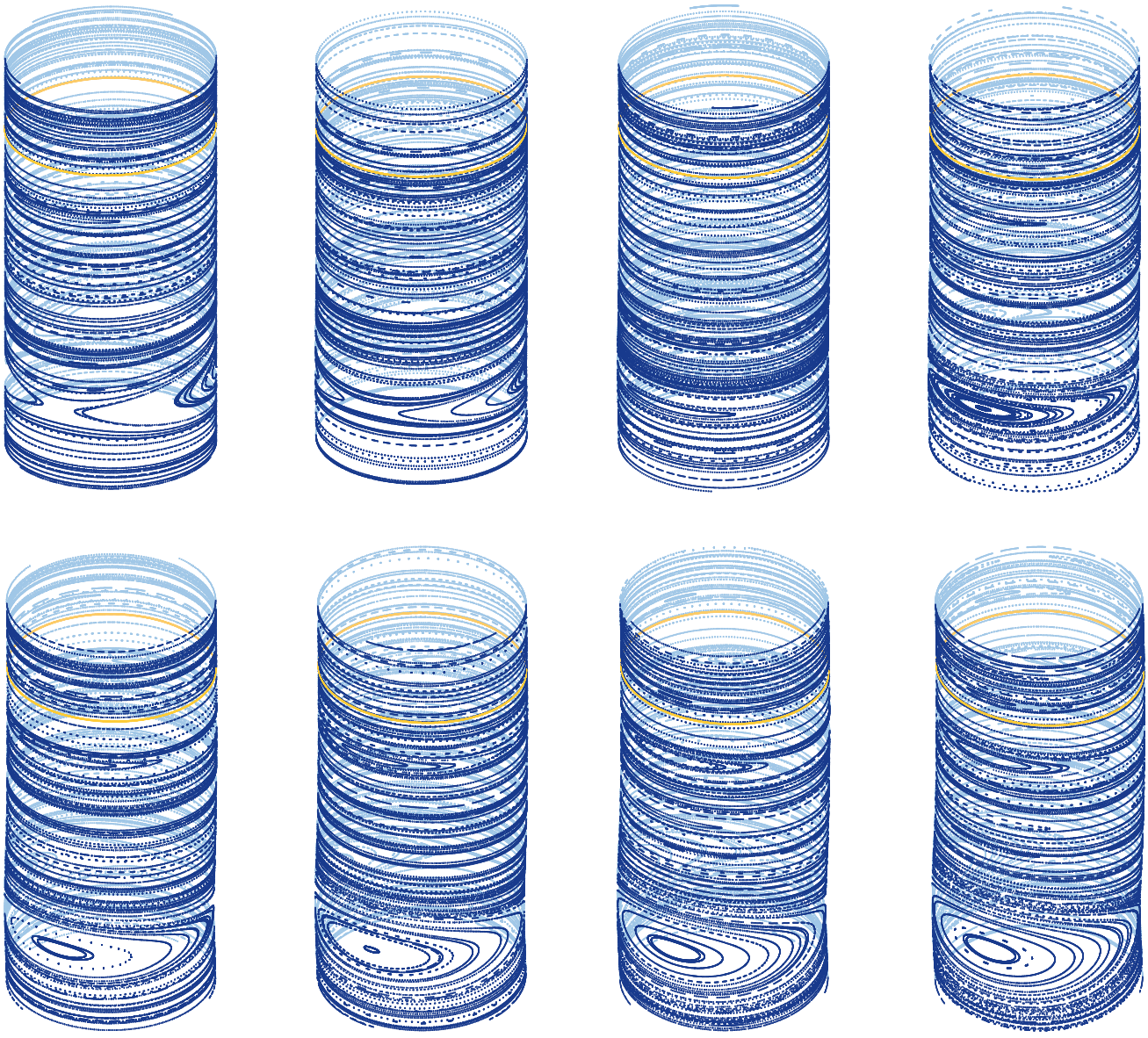

Figure 4.19: Representation of the normally hyperbolic invariant cylinder, for $\kappa_1 = 0.1$, $\kappa_2 = 1.5$, and (from top-left to bottom-right) $\varepsilon = 0.00, 0.05, 0.10, 0.15, 0.20, 0.25, 0.30, 0.35$.

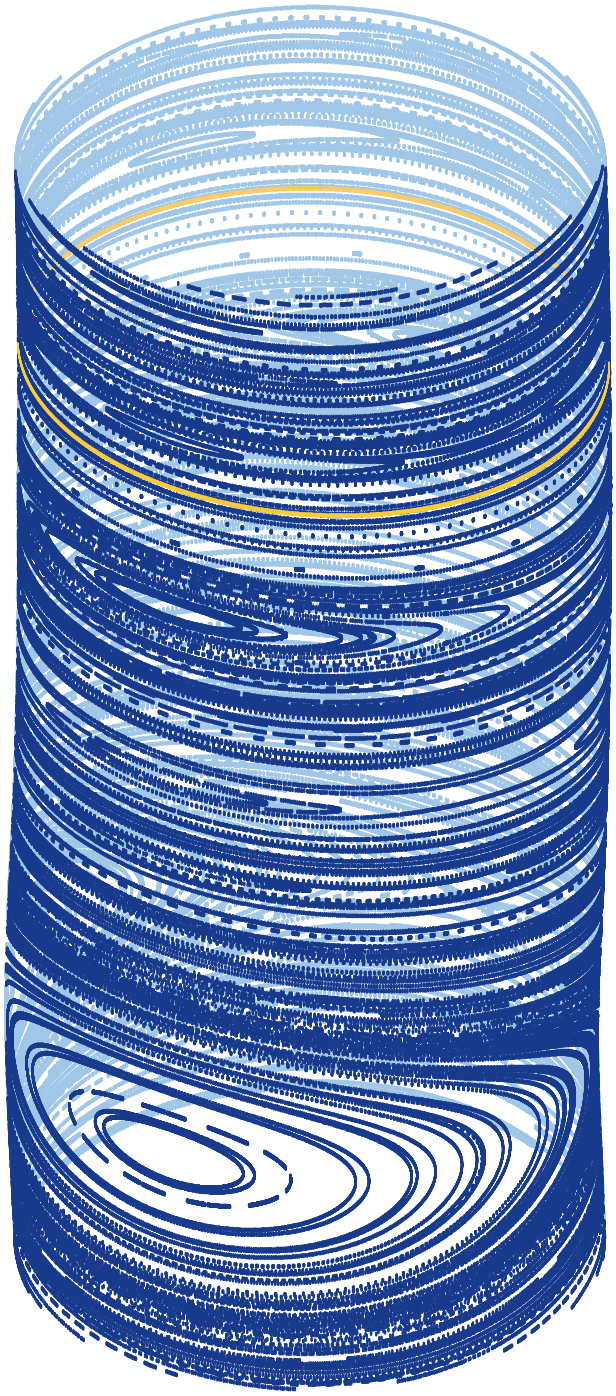

FIGURE 4.21: Representation of the normally hyperbolic invariant cylinder, for $\kappa_1 = 0.1$, $\kappa_2 = 1.5$ and $\varepsilon = 0.35$.

Chapter 5

Conclusions and future work

The main goal of this thesis has been the development of the rigorous and numerical techniques for the computation of normally hyperbolic invariant tori and the study of a general dynamical system by using these tools. The aim of the algorithms is to compute the parameterization of the invariant torus, the corresponding internal dynamics (or the adjusting parameter in the quasi-periodic case) and the parameterizations of the associated stable and unstable bundles. Hence, we avoid the need for a separate algorithm to compute the invariant torus as the intersection of its stable and unstable manifolds, which is the main drawback of graph transform methods.

The methods explained on this thesis follows the idea of the parameterization method to solve the invariance equation. The key point of this methodology is the avoidance of *large matrix methods* and a better representation of the invariance equations, leading to a lower level the discretization of them. Concretely, we also did the computations of the method for NHIT with an unknown dynamics by using a large system matrix method, and we observe that they went wrong to compute the internal dynamics near the places in which some obstructions happens to the torus. The inconclusion results has not been included in this thesis.

We should emphasize that our continuation methods uses to stop *before* the breakdown of the torus. This is due to the fact that the parameterization method algorithms rely in dynamical properties of the torus and then "feels" when these dynamical properties degenerate. In contrast, large matrix method uses to stop after the breakdown of the torus. A paradigmatic example is the approximation of invariant tori by periodic orbits, a standard practice in KAM computations. The reason is that the algorithms solve

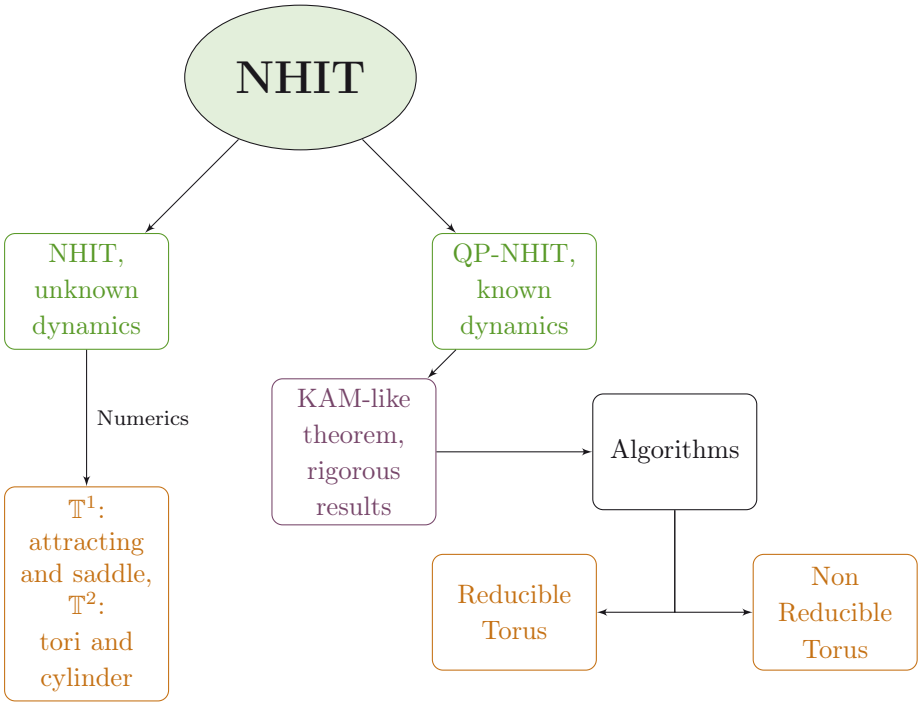

FIGURE 5.1: Outline of the achievements of this thesis.

equations that are close to the initial ones. Moreover, by monitoring several observables of dynamical and regularity properties we can detect how hyperbolicity properties degenerate and extrapolate the parameter values in which the torus is destroyed.

The theoretical results of this thesis give us rigorous results of the existence of quasi-periodic tori. We should mention that, even that similar KAM-like theorems in "a-posteriori" format have been stated in previous works, such as [16, 30, 52, 53] our Theorem 2.21 is well-founded for a general case of families of Diffeomorphisms and leads to efficient numerical algorithms and (in the near future) to computer assisted proofs.

First of all we should comment the new results we obtain in the continuation of quasi-periodic tori. The numerical algorithms are well settled in our previous rigorous result. Our implementations, give us information about different breakdown and bifurcation mechanisms in quasi-periodic tori. In an scenario with a smooth bundle collision between the slow and fast subbundles, in which also the Lyapunov multipliers collide, we have observed how the torus is not destroyed nor losses the reducibility. This is an example of transitions from *node-torus* to *focus-torus*, in which there is only the loss

of the completely reducibility property. This phenomenon has been observed in Example 4 of Chapter 3. Smooth collisions leading to period-halving bifurcations, in which the eigenvalues associated to the smooth bundles crosses 1 has also been observed, see Example 5 of Chapter 3. There are also several mechanisms in which bundles collide non-smoothly, to which we referred to as *bundle merging scenarios*, see [56, 59]. When the collision is between bundles with different stability properties, such a collision produces the destruction of the torus. In the literature, destruction due to non-smooth collision between tangent and stable bundles for attracting quasi-periodic torus (1 dimensional torus in a 2 dimensional phase space) in conformally symplectic maps, see [18], and between stable and unstable bundles for saddle type tori in skew products, see [56, 59], has been seen. We observe the same bundle merging scenario leading to destruction tori, with a bundle collision while the Lyapunov multipliers are separate, for saddle-type tori in a 3 dimensional family of diffeomorphisms in Examples 1, 2 and 3 and for attracting torus in Example 4. Concretely, the collision observed in Example 3, a triple bundle collision where all bundles collide together, and the collision between the tangent and the two dimensional stable bundle in Example 4 are new phenomena observed on quasi-periodic tori. This phenomenon of bundle merging can also do not destroy the torus. This case is showed in Example 5, where the torus only losses the reducibility, without being be destroyed, but is the prelude of the breakdown of the torus. We should emphasize that this study of the different bundle merging scenarios, carried out really close to breakdown of the torus, has only been possible due to the efficient methods we perform. The careful numerical computations lead to several conjectures, see Conjectures 3.12 and 3.14 in Chapter 3, on the behavior of the observables, which give us information about the breakdown. We hope that these conjectures stimulate future research.

The numerical results for the general case give us the internal dynamics of the torus, which is the newness in the computation of normally hyperbolic invariant tori. Then, using our algorithms we are able to cross resonances and study the different dynamics that appears during the continuation of an invariant tori. The computation of normally hyperbolic invariant curves of attracting and saddle type has been already done in the literature, see e.g. [8, 11, 38], but without the computation of the internal dynamics. Our results, by computing also the internal dynamics of the torus, improve the quality of their computations. However, the computation of a higher dimensional normally hyperbolic invariant cylinder is newest in this sense, see Example 8 of Chapter 4. The main interest of this example is that inside the cylinder, from which we know its internal dynamics, we can find KAM quasi-

periodic curves as well as periodic orbits, and their expressions are given well defined. Moreover, this example is closely related to Arnold diffusion, so further work in this direction is one of our forthcoming targets. Additional work on these techniques, such as the use of parallel computing and the implementation to other higher dimensional normally hyperbolic invariant manifolds, could be an aid to improve the numerical computations and comprehend the destruction of these bigger normally hyperbolic invariant manifolds.

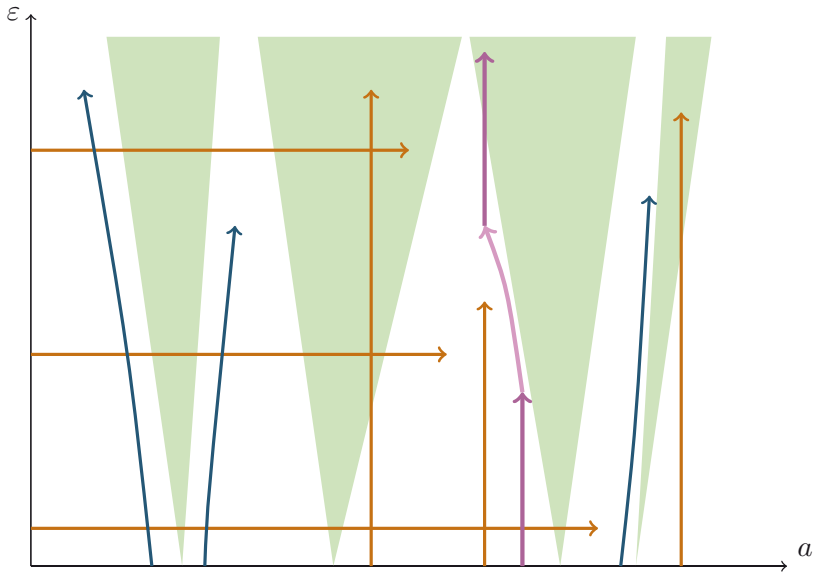

FIGURE 5.2: Pictorial representation of the different continuations of normally hyperbolic invariant tori, in the parameter space (a, ε), we have done on this thesis. Blue lines represent the continuations of quasi-periodic tori, whereas orange lines represent the continuations of invariant tori regardless its internal dynamics, so crossing resonances (represented in green). In purple it appears the continuation by using a mixture of both algorithms.

We should remark that with our algorithms we obtain the bundles of the torus, which are in fact the linear approximations of the stable an unstable manifolds of it. But are even more, with the computation of the invariant bundles we obtain the approximations of the corresponding foliation (up to lineal order). Our closest interest is to globalize it to obtain the invariant manifolds of the invariant torus. A (possible) step is first computing higher order expansions of invariant manifolds. I have already developed several numerical algorithms for computing higher order expansions of whiskers of quasi-periodic tori in 4-dimensional symplectic maps, following [46, 67].

Another interesting point of our work is that we almost cover the whole phase space of a map in which there are normally hyperbolic invariant tori.

To get an idea look the Figure 5.2. With the algorithms for computing quasi-periodic tori, we can continue any torus of a Diophantine frequency, represented as blue lines. We emphasize that these quasi-periodic tori are analytic. On the other hand, we can do continuations by fixing one of the parameters, so crossing resonances in the vertical directions and in the horizontal direction. In these resonances, tori are only finitely differentiable. Then, by mixing both algorithms, when a torus with an unknown dynamics is destroyed, or closely to be destroyed, we can fix parameters and use the quasi-periodic method to continue it. At some desired point, e.g, desired parameter, we can use again the algorithm for the unknown dynamics and continue the continuation. Doing this mixture of both methods, we can use the continuation path as highways to travel around the whole phase space. In particular, the method for computing quasi-periodic tori also works empirically for elliptic tori.

Other future work closely in our mind, is to adapt our general method for other discretization methods, for instance splines or Chebyshev polynomials. We emphasize that higher order level routines are independent on the method.

Bibliography

[1] V. S. Afraĭmovich and L. P. Shil′nikov, *Invariant two-dimensional tori, their breakdown and stochasticity*, Methods of the qualitative theory of differential equations, Gor′kov. Gos. Univ., Gorki, 1983, pp. 3–26, 164.

[2] R. Aris, I. G. Kevrekidis, S. Pelikan, and L. D. Schmidt, *Numerical computation of invariant circles of maps*, Phys. D **16** (1985), no. 2, 243–251.

[3] V. I. Arnold, *Instability of dynamical systems with many degrees of freedom*, Dokl. Akad. Nauk SSSR **156** (1964), 9–12. MR 0163026 (29 #329)

[4] V.I. Arnold, *Proof of a theorem of A. N. Kolmogorov on the preservation of conditionally periodic motions under a small perturbation of the Hamiltonian*, Uspehi Mat. Nauk **18** (1963), no. 5 (113), 13–40.

[5] ———, *Small denominators and problems of stability of motion in classical and celestial mechanics*, Russ. Math. Surveys **18** (1963), 85–192.

[6] P.W. Bates, K. Lu, and C. Zeng, *Existence and persistence of invariant manifolds for semiflows in Banach space*, Mem. Amer. Math. Soc. **135** (1998), no. 645, viii+129.

[7] J.B. Bost, *Tores invariants des systèmes dynamiques hamiltoniens (d'après Kolmogorov, Arnold, Moser, Rüssmann, Zehnder, Herman, Pöschel,...)*, Astérisque (1986), no. 133-134, 113–157, Seminar Bourbaki, Vol. 1984/85.

[8] H.W. Broer, A. Hagen, and G. Vegter, *Numerical continuation of normally hyperbolic invariant manifolds*, Nonlinearity **20** (2007), no. 6, 1499–1534.

[9] H.W. Broer, G.B. Huitema, and M.B. Sevryuk, *Quasi-periodic motions in families of dynamical systems. Order amidst chaos*, Lecture Notes in Math., Vol 1645, Springer-Verlag, Berlin, 1996.

[10] H.W. Broer, G.B. Huitema, F. Takens, and B.L.J. Braaksma, *Unfoldings and bifurcations of quasi-periodic tori.*, Mem. Am. Math. Soc. **421** (1990), 175 p. (English).

[11] H.W. Broer, H.M. Osinga, and G. Vegter, *Algorithms for computing normally hyperbolic invariant manifolds*, Z. Angew. Math. Phys. **48** (1997), no. 3, 480–524.

[12] H.W. Broer, C. Simó, and J.-C. Tatjer, *Towards global models near homoclinic tangencies of dissipative diffeomorphisms*, Nonlinearity **11** (1998), 667–770.

[13] X. Cabré, E. Fontich, and R. de la Llave, *The parameterization method for invariant manifolds. I. Manifolds associated to non-resonant subspaces*, Indiana Univ. Math. J. **52** (2003), no. 2, 283–328.

[14] ———, *The parameterization method for invariant manifolds. II. Regularity with respect to parameters*, Indiana Univ. Math. J. **52** (2003), no. 2, 329–360.

[15] ———, *The parameterization method for invariant manifolds. III. Overview and applications*, J. Differential Equations **218** (2005), no. 2, 444–515.

[16] R. Calleja, A. Celletti, and R. de la Llave, *A KAM theory for conformally symplectic systems: efficient algorithms and their validation*, J. Differential Equations **255** (2013), no. 5, 978–1049.

[17] R. Calleja and R. de la Llave, *Fast numerical computation of quasi-periodic equilibrium states in 1D statistical mechanics, including twist maps*, Nonlinearity **22** (2009), no. 6, 1311–1336.

[18] R. Calleja and J.-Ll. Figueras, *Collision of invariant bundles of quasi-periodic attractors in the dissipative standard map*, Chaos: An Interdisciplinary Journal of Nonlinear Science **22** (2012), no. 3, –.

[19] M. Canadell and A. Haro, *Parameterization method for computing quasi-periodic reducible normally hyperbolic invariant tori*, Accepted in SEMA-SIMAI series (Proceedings CEDYA 2013). Preprint available electronically at `http://www.maia.ub.es/~marta`.

[20] Maciej J. Capinski and Piotr Zgliczynski, *Transition tori in the planar restricted elliptic three-body problem*, Nonlinearity **24** (2011), 1395–1432.

[21] M.J. Capiński, *Covering relations and the existence of topologically normally hyperbolic invariant sets*, Discrete Contin. Dyn. Syst. **23** (2009), no. 3, 705–725.

[22] M.J. Capiński and C. Simó, *Computer assisted proof for normally hyperbolic invariant manifolds*, Nonlinearity **25** (2012), 1997–2026.

[23] Enric Castellà and Àngel Jorba, *On the vertical families of two-dimensional tori near the triangular points of the bicircular problem*, Celestial Mech. Dynam. Astronom. **76** (2000), no. 1, 35–54.

[24] T.N. Chan, *Numerical bifurcation analysis of simple dynamical systems*, Ph.D. thesis, Concordia University, Montreal, Canada, September 1983.

[25] A. Chenciner and G. Iooss, *Bifurcations de tores invariants*, Arch. Rational Mech. Anal. **69** (1979), no. 2, 109–198.

[26] ———, *Persistance et bifurcation de tores invariants*, Arch. Rational Mech. Anal. **71** (1979), no. 4, 301–306. MR 81h:58045

[27] L. Chierchia and G. Gallavotti, *Drift and diffusion in phase space*, Ann. Inst. H. Poincaré Phys. Théor. **60** (1994), no. 1, 144. MR 1259103 (95b:58056)

[28] J. W. Cooley and J. W. Tukey, *An algorithm for the machine calculation of complex Fourier series*, Mathematics of Computation **19** (1965), no. 90, 297–301.

[29] R. de la Llave, *A tutorial on KAM theory*, Smooth ergodic theory and its applications (Seattle, WA, 1999), Proc. Sympos. Pure Math., vol. 69, Amer. Math. Soc., Providence, RI, 2001, pp. 175–292.

[30] R. de la Llave, A. González, À. Jorba, and J. Villanueva, *KAM theory without action-angle variables*, Nonlinearity **18** (2005), no. 2, 855–895.

[31] R. de la Llave and A. Luque, *Differentiability at the tip of Arnold tongues for Diophantine rotations: numerical studies and renormalization group explanations*, J. Stat. Phys. **143** (2011), no. 6, 1154–1188.

[32] A. Delshams, R. de la Llave, and T. M. Seara, *A geometric mechanism for diffusion in Hamiltonian systems overcoming the large gap problem: heuristics and rigorous verification on a model*, Mem. Amer. Math. Soc. **179** (2006), no. 844, viii+141. MR 2184276 (2009m:37170)

[33] A. Delshams and G. Huguet, *Geography of resonances and Arnold diffusion in a priori unstable Hamiltonian systems*, Nonlinearity **22** (2009), no. 8, 1997–2077. MR 2525822 (2010h:37136)

[34] Lorenzo J. Díaz, Isabel L. Rios, and Marcelo Viana, *The intermittency route to chaotic dynamics*, Global analysis of dynamical systems, Inst. Phys., Bristol, 2001, pp. 309–327.

[35] L. Dieci and G. Bader, *Solution of the systems associated with invariant tori approximation. II. Multigrid methods*, SIAM J. Sci. Comput. **15** (1994), no. 6, 1375–1400.

[36] L. Dieci and J. Lorenz, *Block M-matrices and computation of invariant tori*, SIAM J. Sci. Statist. Comput. **13** (1992), no. 4, 885–903.

[37] ———, *Computation of invariant tori by the method of characteristics*, SIAM J. Numer. Anal. **32** (1995), no. 5, 1436–1474.

[38] L. Dieci, J. Lorenz, and R.D. Russell, *Numerical calculation of invariant tori*, SIAM J. Sci. Statist. Comput. **12** (1991), no. 3, 607–647.

[39] C. Díez, À. Jorba, and C. Simó, *A dynamical equivalent to the equilateral libration points of the real Earth-Moon system*, Celestial Mech. **50** (1991), no. 1, 13–29.

[40] K.D. Edoh, R.D. Russell, and W. Sun, *Computation of invariant tori by orthogonal collocation*, Appl. Numer. Math. **32** (2000), no. 3, 273–289.

[41] J. Eldering, *Normally hyperbolic invariant manifolds*, Atlantis Studies in Dynamical Systems, vol. 2, Atlantis Press, Paris, 2013, The non-compact case. MR 3098498

[42] L. H. Eliasson, *Almost reducibility of linear quasi-periodic systems*, Smooth ergodic theory and its applications (Seattle, WA, 1999), Proc. Sympos. Pure Math., vol. 69, Amer. Math. Soc., Providence, RI, 2001, pp. 679–705. MR 1858550 (2003a:34064)

[43] N. Fenichel, *Persistence and smoothness of invariant manifolds for flows*, Indiana Univ. Math. J. **21** (1971/1972), 193–226.

[44] J.-Ll. Figueras, *Fiberwise Hyperbolic Invariant Tori in quasiperiodically skew product systems*, Ph.D. thesis, Universitat de Barcelona, Barcelona, Spain, May 2011.

[45] J.-Ll. Figueras and A. Haro, *Reliable computation of robust response tori on the verge of breakdown*, SIAM J. Appl. Dyn. Syst. **11** (2012), 597–628.

[46] E. Fontich, R. de la Llave, and Y. Sire, *Construction of invariant whiskered tori by a parameterization method. I. Maps and flows in finite dimensions*, J. Differential Equations **246** (2009), no. 8, 3136–3213.

[47] A. M. Fox and J. D. Meiss, *Critical invariant circles in asymmetric and multiharmonic generalized standard maps*, Commun. Nonlinear Sci. Numer. Simul. **19** (2014), no. 4, 1004–1026. MR 3119277

[48] M. Frigo and S.G. Johnson, *The design and implementation of FFTW3*, Proceedings of the IEEE **93** (2005), no. 2, 216–231, Special issue on "Program Generation, Optimization, and Platform Adaptation".

[49] C. Froeschè, *Numerical study of a four-dimensional mapping*, Astron. Astrophys. **16** (1972), 172–189.

[50] T. Ge and A.Y.T. Leung, *Construction of invariant torus using Toeplitz Jacobian matrices/fast Fourier transform approach*, Nonlinear Dynam. **15** (1998), no. 3, 283–305.

[51] S.V. Gonchenko, C. Simó, and A. Vieiro, *Richness of dynamics and global bifurcations in systems with a homoclinic figure-eight*, Nonlinearity **26** (2013), no. 3, 621–678.

[52] A. González, A. Haro, and R. de la Llave, *Singularity theory for non-twist KAM tori*, Mem. Amer. Math. Soc. **227** (2014), no. 1067, vi+115.

[53] A. Haro, M. Canadell, J-LL. Figueras, A. Luque, and J-M. Mondelo, *The parameterization method for invariant manifolds: from theory to effective computations*, `http://www.maia.ub.es/~alex`, 2014.

[54] A. Haro and R. de la Llave, *Persistence of normally hyperbolic invariant manifolds*, In progress.

[55] ———, *Spectral theory and dynamical systems*, ftp://ftp.ma.utexas.edu/pub/papers/llave/spectrum-dynamics.pdf.

[56] ———, *Manifolds on the verge of a hyperbolicity breakdown*, Chaos **16** (2006), no. 1, 013120, 8.

[57] ———, *A parameterization method for the computation of invariant tori and their whiskers in quasi-periodic maps: numerical algorithms*, Discrete Contin. Dyn. Syst. Ser. B **6** (2006), no. 6, 1261–1300.

[58] ———, *A parameterization method for the computation of invariant tori and their whiskers in quasi-periodic maps: rigorous results*, J. Differential Equations **228** (2006), no. 2, 530–579.

[59] ———, *A parameterization method for the computation of invariant tori and their whiskers in quasi-periodic maps: explorations and mechanisms for the breakdown of hyperbolicity*, SIAM J. Appl. Dyn. Syst. **6** (2007), no. 1, 142–207 (electronic).

[60] A. Haro and C. Simó, *To be or not to be a SNA: That is the question*, 2005, http://www.maia.ub.es/dsg/2005/0503haro.pdf.

[61] M.E. Henderson, *Computing invariant manifolds by integrating fat trajectories*, SIAM J. Appl. Dyn. Syst. **4** (2005), no. 4, 832–882 (electronic).

[62] ———, *Flow box tiling methods for compact invariant manifolds*, SIAM J. Appl. Dyn. Syst. **10** (2011), no. 3, 1154–1176.

[63] M.W. Hirsch, C.C. Pugh, and M. Shub, *Invariant manifolds*, Lecture Notes in Mathematics, Vol. 583, Springer-Verlag, Berlin, 1977.

[64] M. Huang, T. Küpper, and N. Masbaum, *Computation of invariant tori by the Fourier methods*, SIAM J. Sci. Comput. **18** (1997), no. 3, 918–942.

[65] G. Huguet and R. de la Llave, *Computation of limit cycles and their isochrons: Fast algorithms and their convergence*, SIAM J. Appl. Dyn. Syst. **12** (2013), no. 4, 1763–1802.

[66] G. Huguet, R. de la Llave, and Y. Sire, *Computation of whiskered invariant tori and their associated manifolds: new fast algorithms*, Discrete Contin. Dyn. Syst. **32** (2012), no. 4, 1309–1353.

[67] ———, *Fast iteration of cocycles over rotations and computation of hyperbolic bundles*, Discrete Contin. Dyn. Syst. S (2013), 323–333, Issue special.

[68] À. Jorba, *Numerical computation of the normal behaviour of invariant curves of n-dimensional maps*, Nonlinearity **14** (2001), no. 5, 943–976.

[69] À. Jorba and M. Ollé, *Invariant curves near Hamiltonian-Hopf bifurcations of four-dimensional symplectic maps*, Nonlinearity **17** (2004), no. 2, 691–710.

[70] À. Jorba and C. Simó, *On the reducibility of linear differential equations with quasiperiodic coefficients*, J. Differential Equations **98** (1992), no. 1, 111–124.

[71] ———, *On quasi-periodic perturbations of elliptic equilibrium points*, SIAM J. Math. Anal. **27** (1996), no. 6, 1704–1737.

[72] K. Kaneko, *Fractalization of torus*, Progr. Theoret. Phys. **71** (1984), no. 5, 1112–1115.

[73] ———, *Collapse of tori and genesis of chaos in dissipative systems*, World Scientific Publishing Co., Singapore, 1986.

[74] K. Kaneko and R. Bagley, *Arnold diffusion, ergodicity and intermittency in a coupled standard mapping*, Physics Letters A **110** (1985), no. 9, 435–440.

[75] A.N. Kolmogorov, *On conservation of conditionally periodic motions for a small change in Hamilton's function*, Dokl. Akad. Nauk SSSR (N.S.) **98** (1954), 527–530, Translated in p. 51–56 of *Stochastic Behavior in Classical and Quantum Hamiltonian Systems, Como 1977* (eds. G. Casati and J. Ford) Lect. Notes Phys. 93, Springer, Berlin, 1979.

[76] B. Krauskopf, H. M. Osinga, and J. Galán-Vioque (eds.), *Numerical continuation methods for dynamical systems*, Understanding Complex Systems, Springer, Dordrecht, 2007, Path following and boundary value problems, Dedicated to Eusebius J. Doedel for his 60th birthday.

[77] J. Lorenz and A. Morlet, *Numerical solution of a functional equation on a circle*, SIAM J. Numer. Anal. **29** (1992), no. 6, 1741–1768.

[78] R.S. MacKay, J.D. Meiss, and J. Stark, *Converse KAM theory for symplectic twist maps*, Nonlinearity **2** (1989), no. 4, 555–570.

[79] R. Mañé, *Persistent manifolds are normally hyperbolic*, Trans. Amer. Math. Soc. **246** (1978), 261–283.

[80] J.N. Mather, *Characterization of Anosov diffeomorphisms*, Nederl. Akad. Wetensch. Proc. Ser. A 71 = Indag. Math. **30** (1968), 479–483.

[81] M.J. Mohlenkamp, *A fast transform for spherical harmonics*, J. Fourier Anal. Appl. **5** (1999), no. 2-3, 159–184.

[82] J.M. Mondelo, E. Barrabés, G. Gómez, and M. Ollé, *Numerical parametrisations of libration point trajectories and their invariant manifolds*, AAS/AIAA Astrodynamics Specialists Conference, AAS, 2007.

[83] J.M. Mondelo, E. Barrabés, G. Gómez, and M. Ollé, *Fast numerical computation of Lissajous and quasi-halo libration point trajectories and their invariant manifolds*, Paper IAC-12, C1, 6, 9, x14982. 63rd International Astronautical Congress, Naples, Italy, 2012.

[84] G. Moore, *Computation and parametrization of periodic and connecting orbits*, IMA J. Numer. Anal. **15** (1995), no. 2, 245–263.

[85] ———, *Computation and parameterisation of invariant curves and tori*, SIAM J. Numer. Anal. **33** (1996), no. 6, 2333–2358.

[86] J. Moser, *On invariant curves of area-preserving mappings of an annulus*, Nachr. Akad. Wiss. Göttingen Math.-Phys. Kl. II **1962** (1962), 1–20.

[87] ———, *A rapidly convergent iteration method and non-linear differential equations. II*, Ann. Scuola Norm. Sup. Pisa (3) **20** (1966), 499–535.

[88] ———, *A rapidly convergent iteration method and non-linear partial differential equations. I*, Ann. Scuola Norm. Sup. Pisa (3) **20** (1966), 265–315.

[89] ———, *Convergent series expansions for quasi-periodic motions*, Math. Ann. **169** (1967), 136–176.

[90] B.B. Peckham and F. Schilder, *Computing Arnol′d tongue scenarios*, J. Comput. Phys. **220** (2007), no. 2, 932–951. MR 2284332 (2008f:37195)

[91] Yakov B. Pesin, *Lectures on partial hyperbolicity and stable ergodicity*, Zurich Lectures in Advanced Mathematics, European Mathematical Society (EMS), Zürich, 2004. MR 2068774 (2005j:37039)

[92] B. Rasmussen and L. Dieci, *A geometrical method for the approximation of invariant tori*, J. Comput. Appl. Math. **216** (2008), no. 2, 388–412.

[93] V. Reichelt, *Computing invariant tori and circles in dynamical systems*, Numerical methods for bifurcation problems and large-scale dynamical systems (Minneapolis, MN, 1997), IMA Vol. Math. Appl., vol. 119, Springer, New York, 2000, pp. 407–437.

[94] H. Rüssmann, *On a new proof of Moser's twist mapping theorem*, Proceedings of the Fifth Conference on Mathematical Methods in Celestial Mechanics (Oberwolfach, 1975), Part I. Celestial Mech., 14(1):19–31, 1976.

[95] ———, *On optimal estimates for the solutions of linear difference equations on the circle*, Proceedings of the Fifth Conference on Mathematical Methods in Celestial Mechanics (Oberwolfach, 1975), Part I. Celestial Mech., vol. 14, 1976.

[96] J. Sánchez, M. Net, and C. Simó, *Computation of invariant tori by Newton-Krylov methods in large-scale dissipative systems*, Phys. D **239** (2010), no. 3-4, 123–133.

[97] F. Schilder, H.M. Osinga, and W. Vogt, *Continuation of quasi-periodic invariant tori*, SIAM J. Appl. Dyn. Syst. **4** (2005), no. 3, 459–488 (electronic).

[98] F. Schilder, W. Vogt, S. Schreiber, and H.M. Osinga, *Fourier methods for quasi-periodic oscillations*, Internat. J. Numer. Methods Engrg. **67** (2006), no. 5, 629–671.

[99] C. Simó, *On the Analytical and Numerical Approximation of Invariant Manifolds*, Modern Methods in Celestial Mechanics, Comptes Rendus de la 13ieme Ecole Printemps d'Astrophysique de Goutelas (France), 24-29 Avril, 1989. Edited by Daniel Benest and Claude Froeschlé. Gif-sur-Yvette: Editions Frontieres, 1990., p.285 (1990), 285–32.

[100] R. Swanson, *The spectral characterization of normal hyperbolicity*, Proc. Amer. Math. Soc. **89** (1983), no. 3, 503–509.

[101] M.R. Trummer, *Spectral methods in computing invariant tori*, Appl. Numer. Math. **34** (2000), no. 2-3, 275–292, Auckland numerical ordinary differential equations (Auckland, 1998).

[102] M. van Veldhuizen, *A new algorithm for the numerical approximation of an invariant curve*, SIAM J. Sci. Stat. Comput. **8** (1987), no. 6, 951–962.